VIBRATION-BASED STRUCTURAL HEALTH MONITORING OF COMPOSITE STRUCTURES

A thesis submitted to

The University of Manchester

For the degree of

Doctor of Philosophy (PhD)

in the Faculty of Engineering and Physical Sciences

2011

Israr Ullah

School of Mechanical, Aerospace and Civil Engineering

(This page is intentionally left blank)

TABLE OF CONTENTS

LIST OF FIGURES

LIST OF TABLES

NOMENCLATURE

Notation	Description
f	frequency
ρ	Density
E	Young's modulus
G	Modulus of rigidity
N	Total number of data points
μ	Poisson's ratio
Ku	Kurtosis
Sk	Skewness
RMS	Root Mean Square
CF	Crest Factor
σ	Variance
FFT	Fast Fourier Transform

LIST OF ABBREVIATIONS

DA	Derivative of acceleration
DDA	Double derivative of acceleration
DDDA	Derivative of Double derivative of acceleration
CFRP	Carbon fibre-reinforced polymer composite material
FBG	Fibre Brag grating
FE	Finite element
FEA	Finite element analysis
FEM	Finite element modelling
FRC	Fibre-reinforced composite material
NSH	Normalised summation of harmonics
CNSH	Cumulative Normalised summation of harmonics
STFT	Short time FFT
SH	Summation of Harmonics
FRF	Frequency Response Function
IPV	Inner product vector
CDM	Continuum damage mechanics
PZT	Lead Zirconium Titanium
PVDF	Polyvinylidene fluoride
AE	Acoustic emission
ASE	Amplified spontaneous emission
ESPI	Electronic Speckle Pattern Interferometry
STMR	Single-transmission –multi-receiver
MTMR	Multi-transmission –multi-receiver
MFC	Macro fibre composite

LIST OF PUBLICATIONS

Peer Reviewed Journal Publications

1. *I. Ullah, J.K. Sinha, A. Pinkerton, "Vibration-based Delamination Detection in a Composite Plate", Mechanics* of Advanced Materials & Structures*, (In Press).*

2. *I. Ullah, J.K. Sinha, "Dynamics of Composite Plate by Experiment and Finite Element Analysis"*, European Journal of Scientific Research*, (In Press).*

3. *I. Ullah, J.K. Sinha, "Experimental Vibration Study on the Healthy and Delaminated Composite Plates"*, Journal of Physics Conference Series (JPCS)*, Proceedings of the 9th International Conference on Damage Assessment of Structures, IOP 11-13July 2011), (In Press).*

4. *I. Ullah, J.K. Sinha, "Vibration based delamination localization in composite structure"*, The Journal of Structural Control and Health Monitoring*, (Revision Submitted).*

5. *I. Ullah, J.K. Sinha, "Simple Reference-Free Method for Delamination Detection in Composite",* The Journal of Sound & Vibration*, (Under Preparation).*

Conference Publications

1. *I. Ullah, J.K. Sinha, "Dynamic behaviour of delaminated composite beam", The Fifth International Conference on Condition Monitoring and Machinery Failure Prevention Technologies-CM/MFPT 15 Jul 2008 - 18 Jul 2008, Edinburgh*

2. *I. Ullah, J.K. Sinha, "Dynamic Study of a Composite Plate with Delamination", 3rd International Conference on Integrity, Reliability and Failure, Porto/Portugal, 20-24 July 2009, Porto*

3. *I. Ullah, J.K. Sinha, "Vibration Based Method To Detect Delamination In Composite", ICCS/16, At the University of Porto, Porto, Portugal, 28-30 June 2011), (In Press).*

4. *I. Ullah, J.K. Sinha, "Experimental Vibration Study on the Healthy and Delaminated Composite Plates", Proceedings of the 9th International Conference on Damage Assessment of Structures, IOP 11-13July 2011), (In Press), Oxford*

ABSTRACT

Composite materials are in use in several applications, for example, aircraft structural components, because of their light weight and high strength. However the delamination which is one of the serious defects often develops and propagates due to vibration during the service of the structure. The presence of this defect warrants the design life of the structure and the safety. Hence the presence of such defect has to be detected in time to plan the remedial action well in advance. There are a number of methods in the literature for damage detection. They are either “baseline free/reference free method” or using the data from the healthy structure for damage detection. However very limited vibration-based methods are available in the literature for delamination detection in composite structures. Many of these methods are just simulated studies without experimental validation.

Grossly 2 kinds of the approaches have been suggested in the literature, one related to low frequency methods and other high frequency methods. In low frequency approaches, the change in the modal parameters, curvatures, etc. is compared with the healthy structure as the reference, however in the high frequency approaches, excitation of structures at higher modes of the order of few kHz or more needed with distributed sensors to map the deflection for identification of delamination. Use of high frequency methods imposes the limitations on the use of the conventional electromagnetic shaker and vibration sensors, whereas the low frequency methods may not be feasible for practical purpose because it often requires data from the healthy state which may not be available for old structures.

Hence the objective of this research is to develop a novel reference-free method which can just use the vibration responses at a few lower modes using a conventional shaker and vibration sensors (accelerometers/laser vibrometers). It is believed that the delaminated layers will interact nonlinearly when excited externally. Hence this mechanism has been utilised in the numerical simulations and the experiments on the healthy and delaminated composite plates. Two methods have been developed here – first method can quickly identify the presence of the delamination when excited at just few lower modes and other method identify the location once the presence of the delamination is confirmed. In the first approach an averaged normalised RMS has been suggested and experimentally validated for this purpose. Latter the vibration data have then been analysed further to identify the location of delamination and its size. Initially, the measured acceleration responses from the composite plates have been differentiated twice to amplify the nonlinear interaction clearly in case of delaminated plate and then kurtosis was calculated at each measured location to identify the delamination location. The method has further been simplified by just using the harmonics in the measured responses to identify the location. The thesis presents the process of the development of the novel methods, details of analysis, observations and results.

DECLARATION

I hereby declare that no portion the work referred to in the thesis has been submitted in support of an application for another degree or qualification of this or any other university or other institute of learning.

COPYRIGHT STATEMENT

I. The author of this thesis (including any appendices and/or schedules to this thesis) owns certain copyright or related rights in it (the "Copyright") and s/he has given The University of Manchester certain rights to use such Copyright, including for administrative purposes.

II. Copies of this thesis, either in full or in extracts and whether in hard or electronic copy, may be made **only** in accordance with the Copyright, Designs and Patents Act 1988 (as amended) and regulations issued under it or, where appropriate, in accordance with licensing agreements which the University has from time to time. This page must form part of any such copies made.

III. The ownership of certain Copyright, patents, designs, trademarks and other intellectual property (the "Intellectual Property") and any reproductions of copyright works in the thesis, for example graphs and tables ("Reproductions"), which may be described in this thesis, may not be owned by the author and may be owned by third parties. Such Intellectual Property and Reproductions cannot and must not be made available for use without the prior written permission of the owner(s) of the relevant Intellectual Property and/or Reproductions.

IV. Further information on the conditions under which disclosure, publication and commercialisation of this thesis, the Copyright and any Intellectual Property and/or Reproductions described in it may take place is available in the University IP Policy (see http://www.campus.manchester.ac.uk/medialibrary/policies/intellectual-property.pdf), in any relevant Thesis restriction declarations deposited in the University Library, The University Library's regulations (see http://www.manchester.ac.uk/library/aboutus/regulations) and in The University's policy on presentation of Theses.

ACKNOWLEDGMENTS

I would like to thank my supervisor Dr. **Jyoti K. Sinha** for his continuous support, guidance, and encouragement throughout the period of this research study.

Special thanks to Prof. Paul J Hogg and Dr. Payam Jamshidi from the NorthWest Composites Centre, The University of Manchester for their kind effort to prepare the test composite plate samples with and without delamination for the present study. I also acknowledge the assistance provided by the PhD fellows Mr. Abdul Latef Badri, Mr. Elbahbah Keri, and George A Vadakkel during the experiments. I also appreciate the assistance of Paul Townsend, Technical Coordinator, the Pariser Building, for preparing Aluminium samples for the verification of nonlinear interaction due to delamination.

DEDICATION

I dedicate this work to my late father who encouraged me to proceed for this Ph.D. study.

CHAPTER 1
INTRODUCTION

1.1 Overview

Internal damage in composite structures can cause abrupt failure during its operation and this in turn can lead to catastrophic consequences. Importance of the delamination detection and localization can be accessed from the practical incidents occurred in the past. American Airlines Flight 587 crashed in to the streets of Belle Harbor on November 12, 2001. Aviation experts declared that the major cause of the accident was the failure of the laminate bond that keeps the tails structure intact [1].

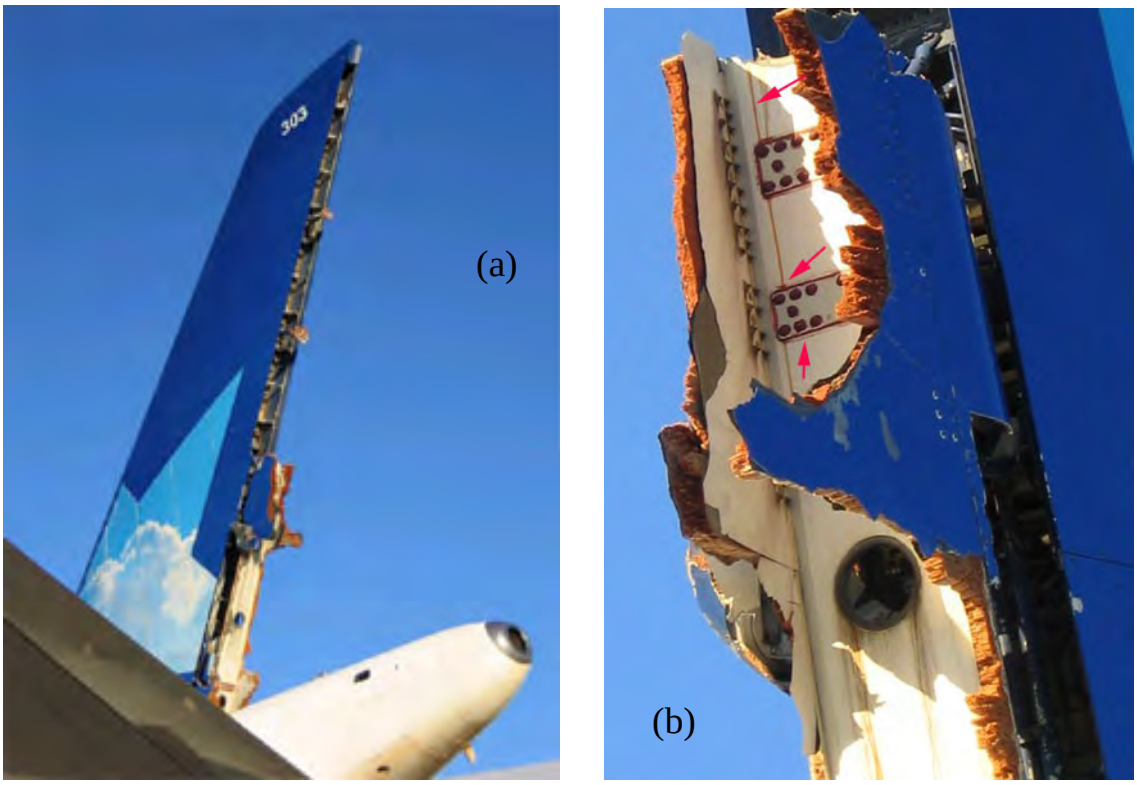

Figure 1.1 (a-b) Rudder failure of Air Transat Airbus A310-308 [2]

Air Transat Flight 961, had an accident of its rudder, as shown in Figure 1.1, fallen in the ocean during the flight on March 06, 2005 [2]. Canadian Transportation Safety Board believe that the failure was caused by the laminate debonding that occurred during the flight [1]. Massive hull failures in Bertram Yachts can be seen in Figure 1.2 [3]

(a)

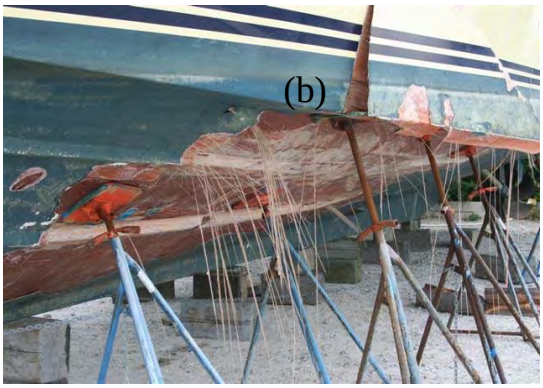

(b)

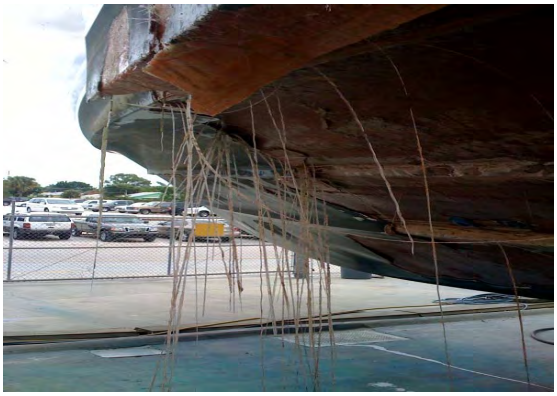

Figure 1.2 (a-b) shows the composite delamination failure [3]

Figures 1.1 and 1.2 show excellent examples of composite failures due to de-bonds in the structure.

Composite laminates are lighter and stronger and hence these are used in aircrafts interiors and fuselage. Although composite laminates are believed to be lightweight and stronger and has greater strength to weight ratio, it has the intrinsic problem of

delamination development due to various reasons. Once the delamination, which is by definition the internal debonding of the adjoining layers, onsets it grows unnoticed till there is a great fall of performance in the structure. Figures 1.1 and 1.2 are excellent examples of the damage caused by internal delaminations in engineering structures. Hence there is need for the early diagnosis of the delamination. Once the delamination onset is detected measures can be taken to stop the further growth of the delamination. These limitations provided inspiration for developing new techniques based on the excitation of the first few modes and using advanced signal processing and statistical techniques.

1.2 Objectives

The main aim of this research is to develop delamination detection technique based on the first few modes of vibration. In the proposed technique nonlinear interaction due to delamination has been used to detect and measure the presence of fault (delamination) in the composite structure under study.

Objective 1:

The finite element (FE) modelling of the sample composite plates with and without delaminations (of different sizes and at different locations) using FE code (ABAQUS) to understand the dynamics of the delaminated and healthy composite plates

Objective 2:

Experimental verifications of the objective 1

Objective 3:

Detection of the presence of delamination in the composite plates, using vibration response data, by exciting the plate in several modes without the use of the vibration data from the healthy composite plate ("baseline-free damage detection" or "referenced-free damage detection" method)

Objective 4:

Explore the possibility to locate the delamination in much simplified approach initially on simulations and then by experiments on composite plates.

1.3 Thesis structure

The present Chapter 1 highlights the overview of this research work, the major objectives and the structure of the thesis break-up.

- Chapter 2 is dedicated to the literature review. This chapter provides, in detail, major research work so far accomplished in the non-destructive testing and structural health monitoring related to the title of this research.

- Chapter 3 summarises the experimental set-ups and layouts used in this research work.

- Chapter 4 is on the delamination detection (Objective 1) using nonlinear interaction between the delaminated layers. In this chapter numerical experiments on carbon fibre composite plate have been discussed. The results have been compared with previous research studies. Experiments have been performed on Aluminium plates to verify part of the results.

- Chapter 5 presents the dynamic analysis of composite plate by experiment and Finite Element Analysis in detail. The performance of the different types of elements from the ABAQUS Explicit library generally used in literature for the composite plate modelling have been compared with the experimental responses (Objective 2).

- Chapter 6 presents the statistical parameters study on the vibration responses for delamination detection (Objectives 1 & 2) in composite plates.
- Chapter 7 gives in detail the research work on the localisation of the delamination (Objective 3). In this chapter vibration response data (acceleration) has been differentiated twice and then the statistical parameter, kurtosis of the double differentiated plotted for the measurement grid of the delaminated plate. The plots clearly show the delaminated location**.**
- Chapter 8 presents further study to develop a new simpler method (Objective 4) based on the harmonics of the modes at which the plate is excited. The method is superior to the one developed in chapter 7 as this method can work with velocity measurements which are easier to do as compared to acceleration measurements.

- Chapter 9 is the summary of the results and new techniques developed in this research study. The chapter also mentions how the work can be further extended (future work)**.**

CHAPTER 2
LITERATURE REVIEW

This chapter covers an overview of the structural health monitoring and different techniques, used so far, to diagnose, locate, and find the extent of the damage in the form of cracks and delaminations in composite structures. Various techniques have been developed and practised, depending on various factors like feasibility, cost, and ease of use. Techniques like ultrasonic, fibre optic, laser, thermography etc. are generally reviewed but mainly vibration based techniques have been discussed in the following sections.

2.1 Overview of Structural Health Monitoring

All dynamic structures degrade with the passage of time due to various reasons like environmental conditions, operational variations, accidental events, and probably imperfect design. Whatever is the reason for degradation, there is need to assess the useful remaining life of the structure. Visual inspection of structural parts has been the first and most common procedure. Depending on the type of the structure, its cost of maintenance, and the cost of changing worn-out parts various methods have been adopted over time. Non-destructive testing at specified intervals has been common practice for damage detection in power plants. Structural health monitoring is an advanced type of continuous online inspection of the complicated structure. Figure 2.1 is the idea of a central nervous system installed in a modern commercial airline [4]. Figure 2.1 shows the concept of online structural health monitoring system. Mufti [5] has given a layout of the structural health monitoring system of the Taylor Bridge as

explained in Figure 2.2. Balageas et al. [6] have given a comprehensive schematic presentation of the structural health monitoring as shown in Figure 2.3. Conventional health monitoring is often termed as non-destructive testing (NDT) and is usually done offline. NDT include dye penetrant testing, radiography, ultrasonic testing, infrared thermography, eddy current and X-ray tomography [7]. Structural health monitoring (SHM) is generally implemented online while the structure is in operation. Together the two (NDT and SHM) are often called non-destructive evaluation (NDE). Adams [8] has explained comparison between NDT and SHM in Figure 2.4.

Figure 2.1 Structural health monitoring ‘nervous’ system [4]

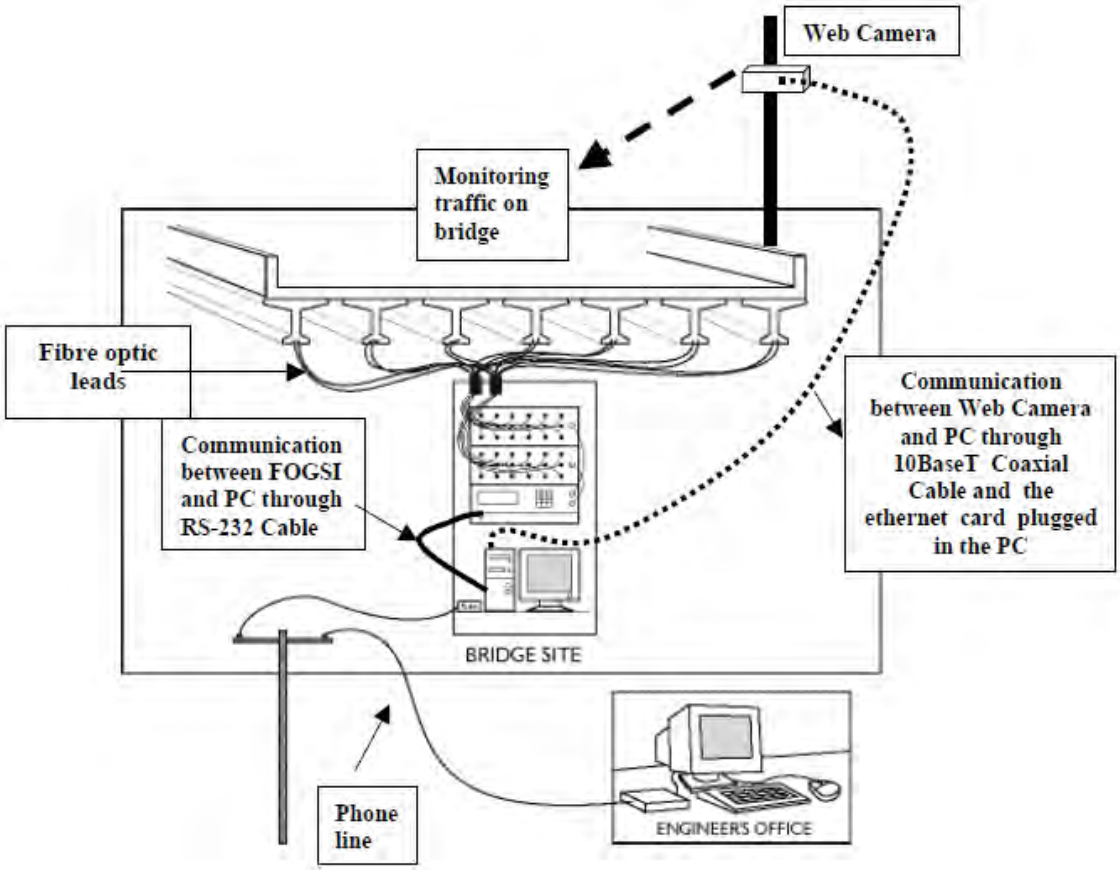

Figure 2.2 Layout of SHM systems in a bridge [5]

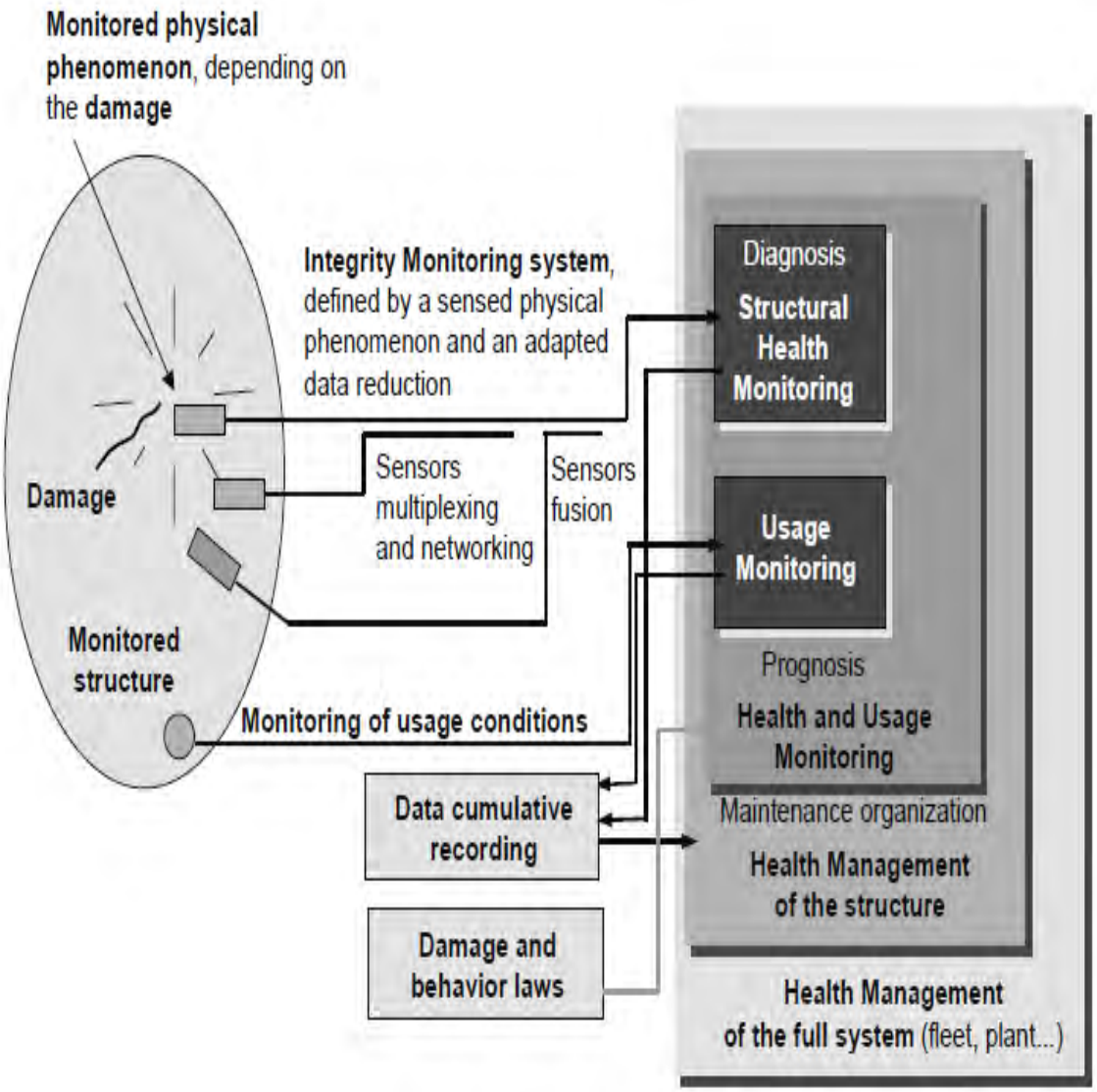

Figure 2.3 Principle and organization of a SHM system [6]

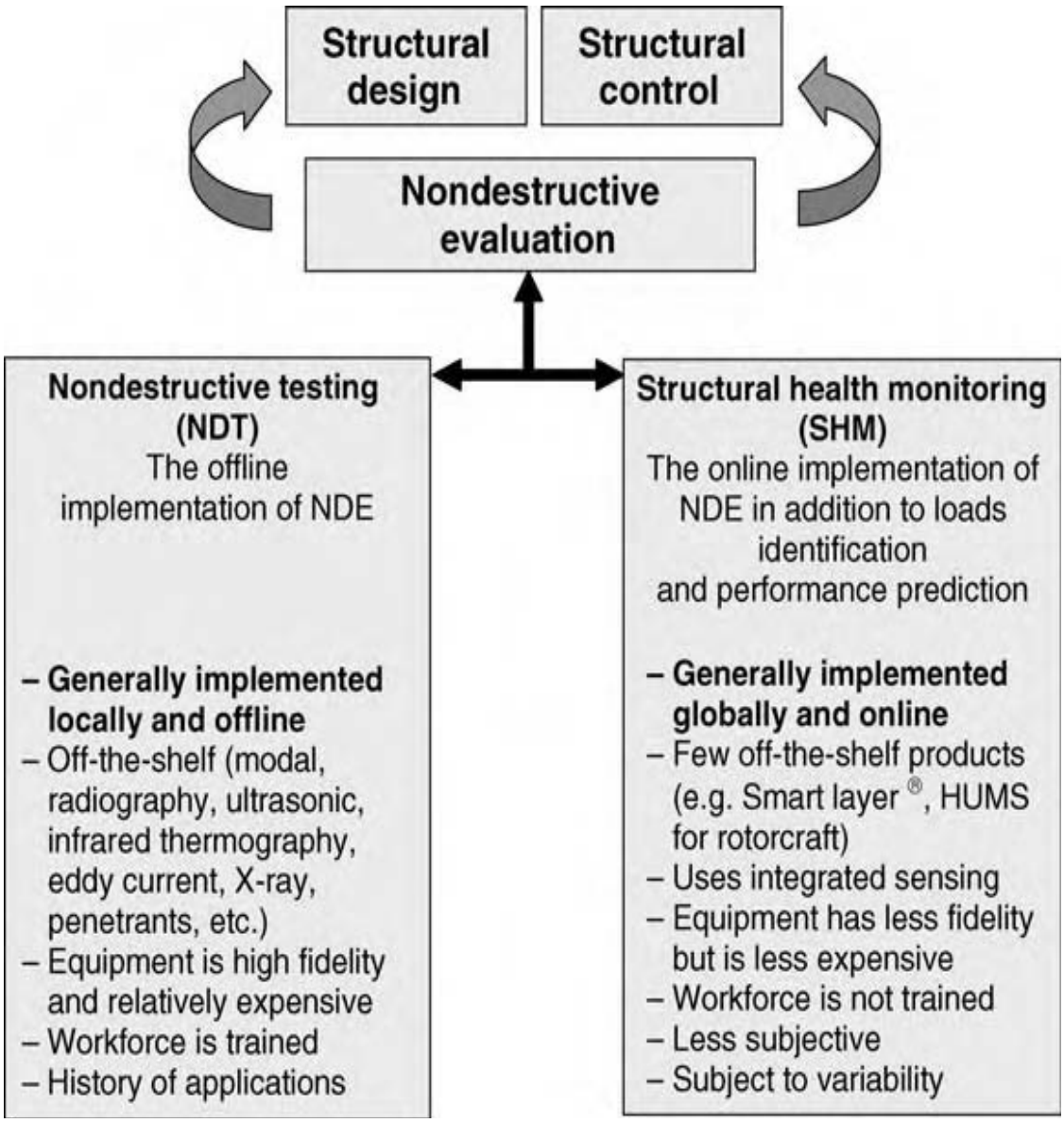

Figure 2.4 Comparison of NDT and health monitoring technologies [8]

2.2 Non Destructive Testing (NDT) Techniques

All composite structures are inspected for the presence of defects mostly caused by the continuous operation of these structures. The easiest and most commonly used method of inspection is visual. Radiography is generally used to analyze bond-line defects.

Shearography and thermography are the other common NDT techniques for damage diagnosis of fibre discontinuities, honeycomb core defects and adhesive voids. Ultrasonic techniques are used to attenuate the sound wave energy to detect damage in the composite structures. Acoustic emissions are another type of common NDT used for the damage detection of thin structures. Comparison of the common NDT techniques is presented in Table 2.1 [9].

Table 2.1 NDT capability matrix [9]

	Defect/anomaly type				Operation consideration		
Test type	Porosity	Voids	Adhesion	Impact	Skill	Cost	Coverage
Acoustic (tap test)		✓	✓	✓	Low	Low	Single point
Sonic (Resonance)		✓	✓	✓	Low	Med	Single point
Shearography		✓	✓		High	Med.	Large area
Thermography			✓	✓	Med.	Med.	Large area
Ultrasonic: A-scan	✓	✓	✓	✓	Low	Low	Single point
Ultrasonic: C-scan	✓	✓	✓	✓	Med. to high	Low to med.	Large area
Visual	✓		✓	✓	Low	Low	N/A

2.2.1 Thermal NDT

According to Dutton [10] thermography can be used for condition monitoring of the composite structures. Dutton [10] used infrared thermography with external source of radiation to excite temperature differences at the surface of the sample composite plates for the detection of air-filled voids and foreign bodies as shown in Figure 2.5. Genest et al. [11] used pulse thermography (PT) and thermographic signal processing (TSR) with

derivative processing for the detection of disbands in composite bonded repairs. Avdelidis et al. [12] used transient thermal NDT for the damage assessment of aircraft composite structures. They applied the techniques to various types of damages in composite specimens. The method has been shown to be effective in large structures. The method has limitation of a certain amount of depth and size of damage below it fails to diagnose the defect. So it is not suitable for small delaminations in small structures. Meola et al. [13] used optical lock-in thermography to disclose the artificial damages created in the carbon fibre reinforced polymer specimens. Figure 2.6 shows the lock-in thermography set-up used in the experiments in this research work. Thermographic techniques can be harmful for the sensitive surface being tested and are not well suited for online structure health monitoring.

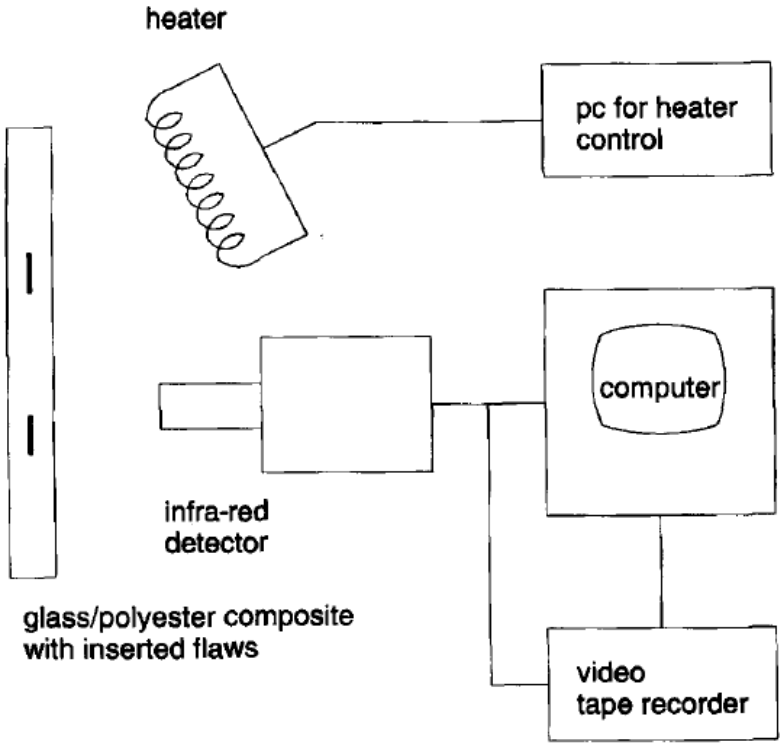

Figure 2.5 Experimental sketch for thermography [10]

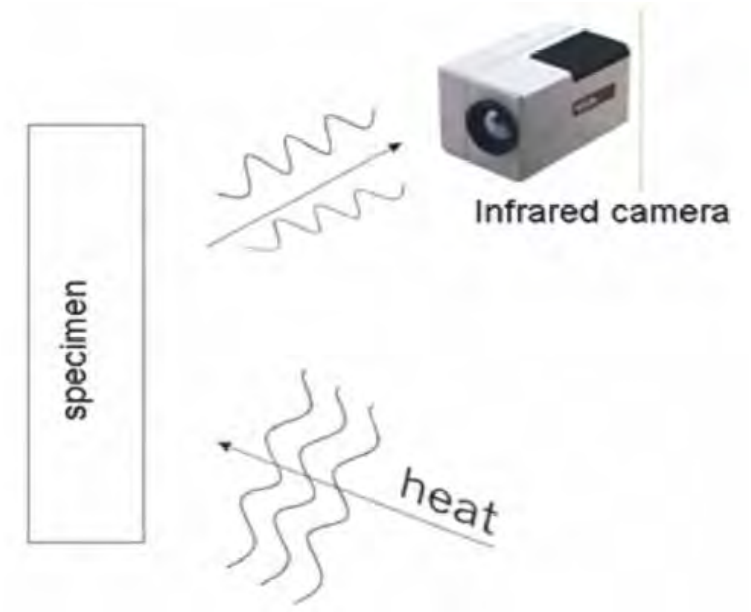

Figure 2.6 Lock-in thermography setup [13]

2.2.2 Tomography and C-scanning Methods

Hocheng et al. [14] developed a method to effectively use computerised tomography for the delamination evaluation caused by drilling operations on composite materials. They compared the results with the results from the well established C-scan method of damage detection. Figure 2.7 shows the schematics of computerised tomography and ultrasonic C-scans used in the experiments. Shin et al. [15] inserted a 100 micron triangular-shaped artificial plate in a silicon carbide (SiC) composite plate and applied ultrasonic test (UT) method based on computerized tomography to examine the sensitivity limit of the UT method. They used frequencies in the range of 50 MHz to 80 MHz. The layout of the C-scan is shown in Figure 2.8. The method used is not suitable for online structural health monitoring and is dedicated for drilling-induced delamination detection only.

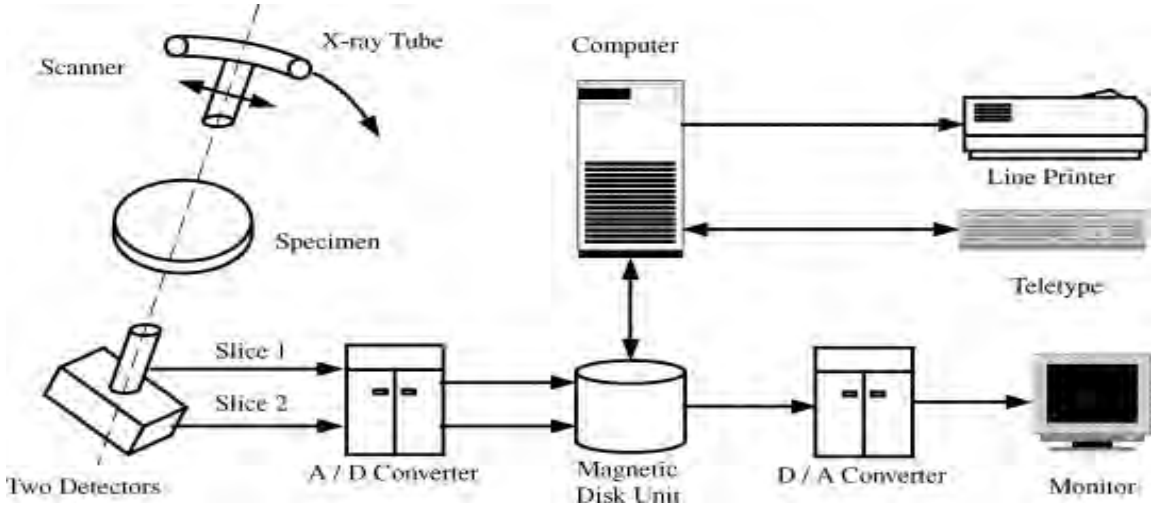

Figure 2.7 Layout of X-ray tomography [14]

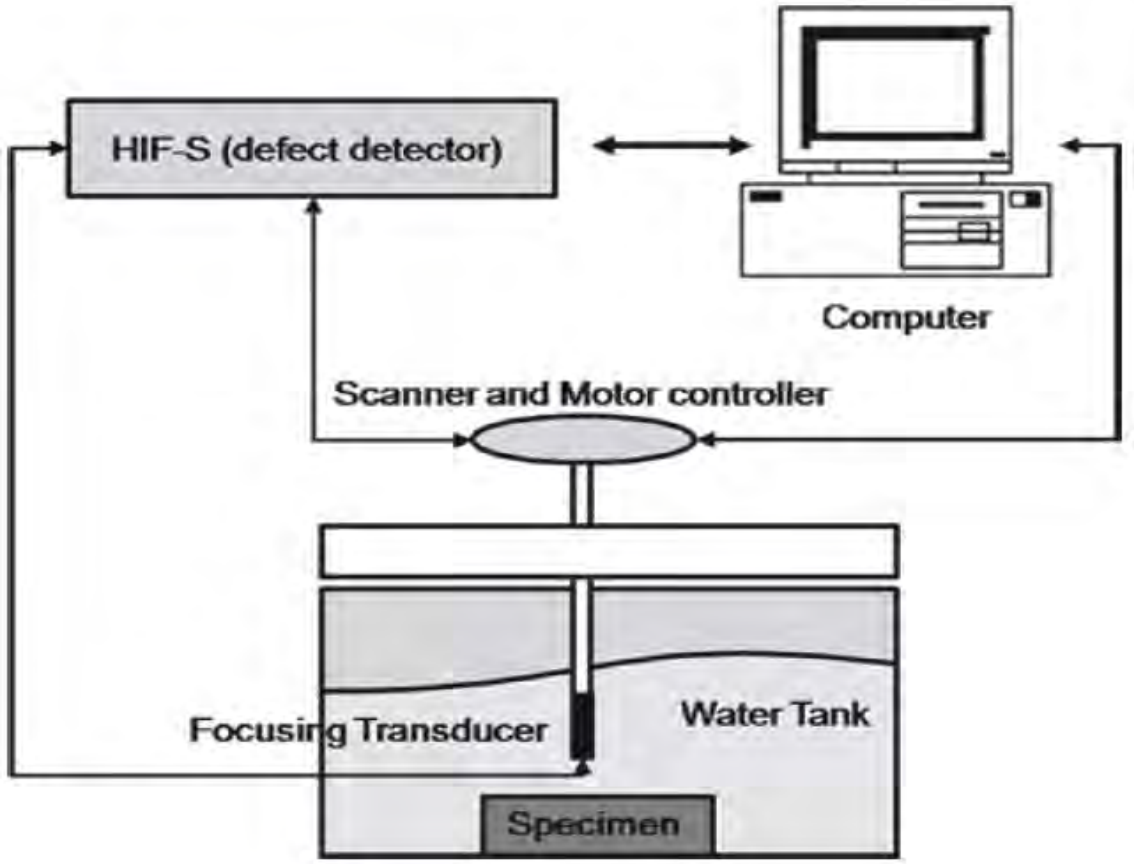

Figure 2.8 Layout of ultrasonic C-scan [15]

2.2.3 Radiography

Albuquerque et al. [16] studied radiographic images of the composite plates subjected to drilling which have created delamination in these plates. They have used four drill geometries with different combinations of feed rates. The research involved relationship between delamination size and various option of drill geometry and feed rate. In fact they have proposed a novel method of image analysis based on neural networks to detect and quantize the damage. The study can be useful for drilling practices causing minimum delamination. The technique is restricted to drilling based delamination detection and quantification and requires lengthy procedure. Concept layout of their experimental work is shown in Figure 2.9 below.

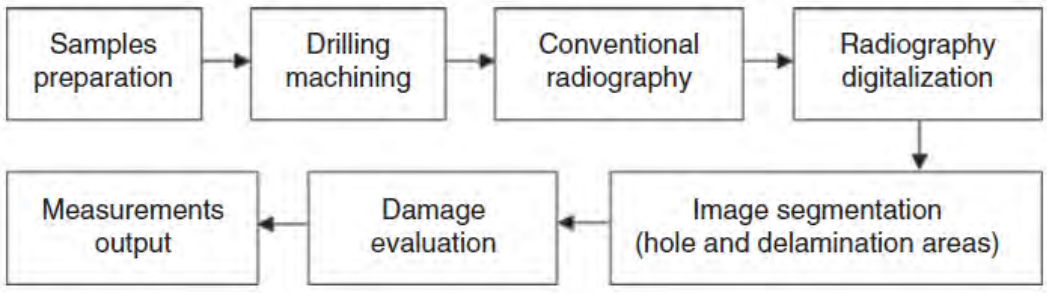

Figure 2.9 Block diagram of the experimental work [16]

2.2.4 Electrical Resistance Methods

Ueda et al. [17] used two-staged electrical potential change method (EPCM) to locate and quantify the delaminations in the damaged beam structure. The method is complicated and needs lots of experiments. Todoroki [18] used a modified electrical resistance change method (ERCM) to diagnose the delamination in the Carbon Fibre Reinforced Polymer (CFRP) laminates. The method has the merit of not requiring expensive equipments. Lots of electrodes need to be mounted in the experiment using

electrical resistance change method. In the present work a modified technique has been developed based on ERCM and the author has termed it as Multi-Probe Electrical Method (MPEM). The new method does not require lots of electrodes to be mounted during experiment for the delamination detection.

2.2.5 Acoustic Emissions

Hatta et al. [19] studied Acoustic Emissions (AE) using Electronic Speckle Pattern Interferometry (ESPI) (as shown in Figure 2.10), and Super Conducting Quantum Interference Device (SQUID) (as shown in Figure 2.11) current mapping to examine the damage process of carbon/carbon (C/C) composites subjected to compact tension and having notches. They found that AE technique was successful in indentifying the fracture steps; ESPI was able to diagnose delamination, whereas ESPI proved useful to detect fibre failure. Figure 2.12 shows the application of acoustic emission in a composite structure [4]. These methods are generally not suitable for online structural health monitoring.

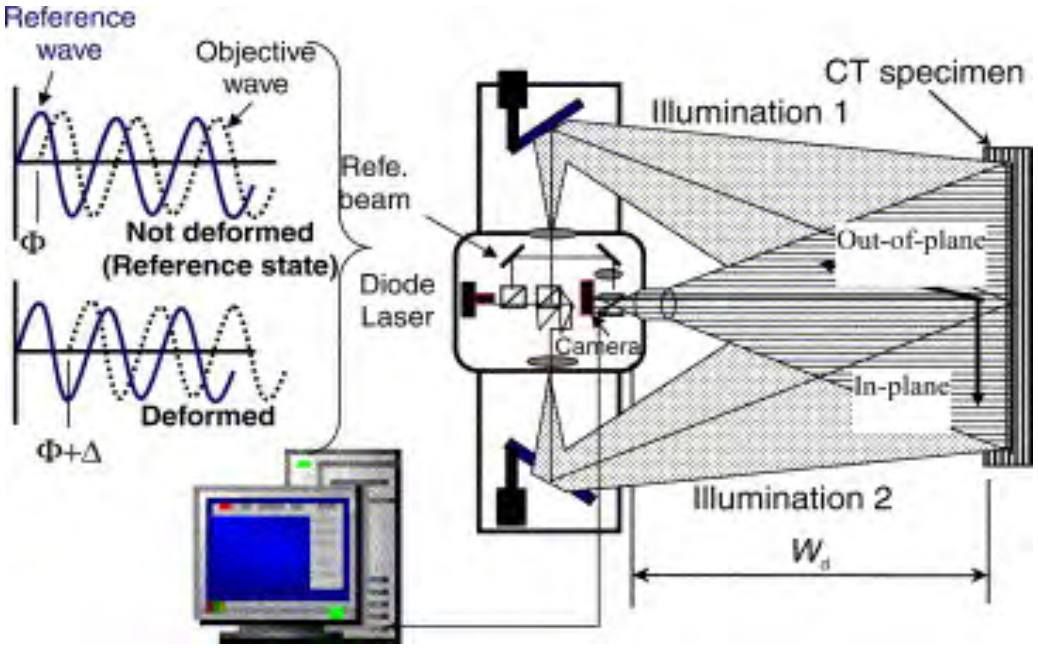

Figure 2.10 Schematics of 3D ESPI system [19]

Figure 2.11 Composite structure with acoustic emission sensors [4]

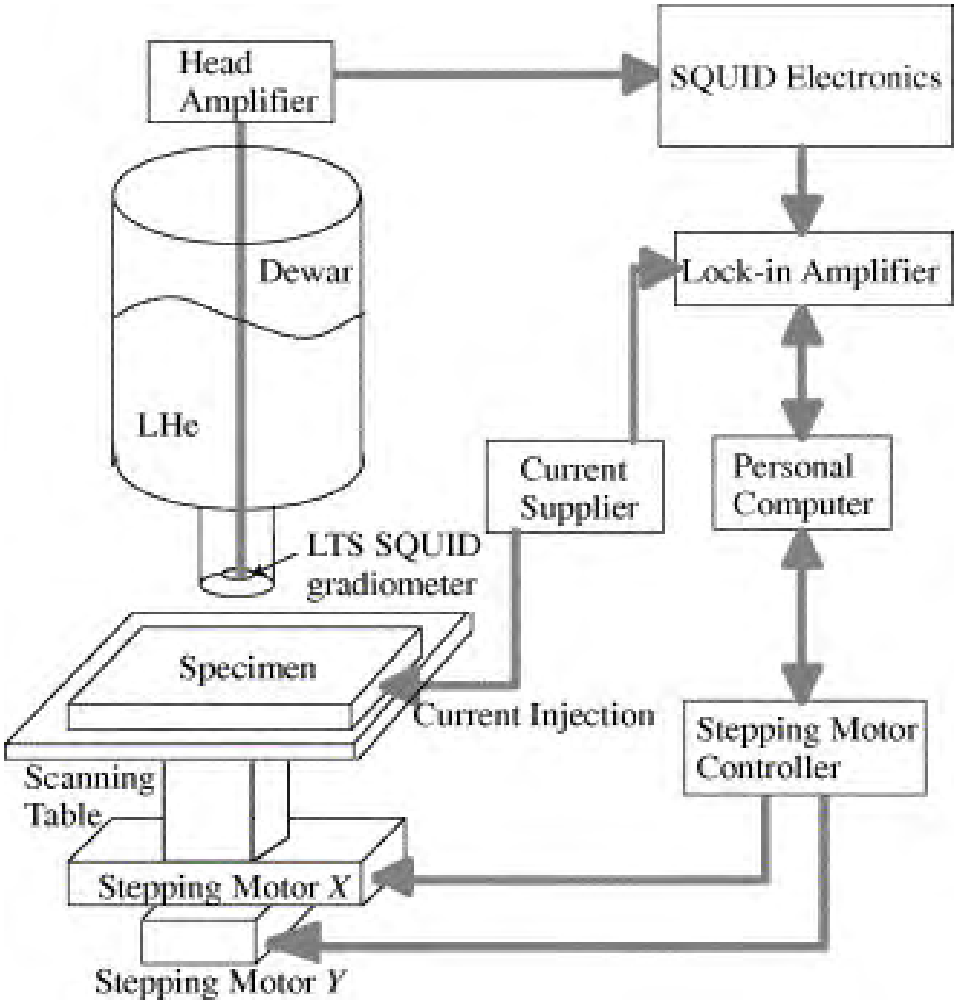

Figure 2.12 Schematics of SQUID NDE system [19]

2.2.6 Other Non-vibration-based Methods

Visual inspection is the most common and first type of NDT step [20]. Using magnifying glasses and fibre optic cameras visual inspection can be very useful to detection the surface cracks of larger sizes. Another method named as eddy currents technique is also used for damage detection. In this method electricity is passed through the structure under investigation and the differences in the flow of current in the structure, are measured [21]. Chattopadhay et al. [22] analysed dynamic strain for smart

composite plates with and without delamination and worked out a new approach for delamination detection using root mean square (RMS) values of the plates. They calculated the RMS values of the nodal displacements after applying 127 volts to the piezo-actuators to both the healthy and through-width delaminated plates. They found that RMS values of the nodal displacements are higher for delaminated plate as compared to healthy plate. The method is based on comparison of the healthy and damaged structures and the work is purely numerical and has not been verified by experiments.

Tan et al. [23] developed a mathematical model for magnetostrictive layer (ML) attached to the beam with internal delamination. They used integrated ML (IML) and distributed ML (DML) for their numerical experiment. They found from their numerical results that the concept can detect, localize, and quantify the internal damage in a composite beam. The concept of DML is shown in Figure 2.13. The method is not experimentally verified so far.

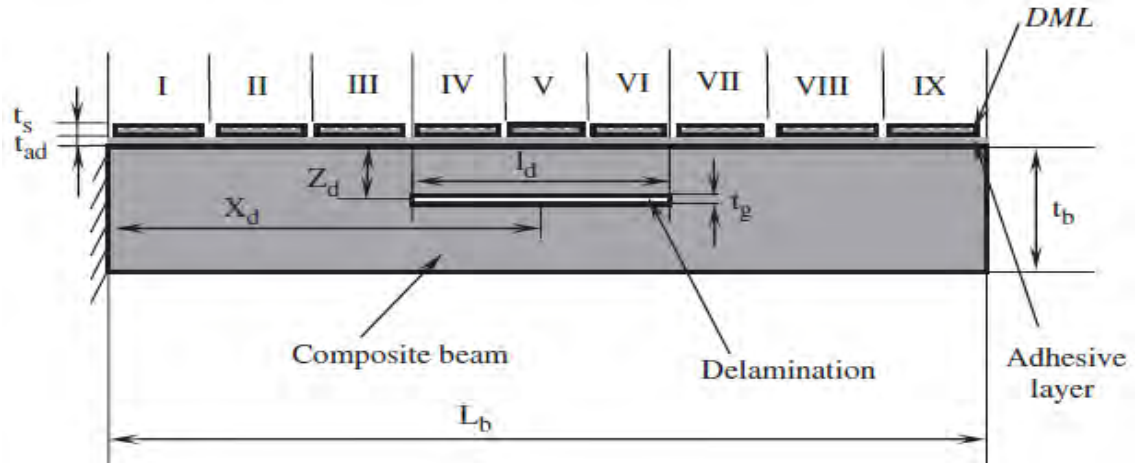

Figure 2.13 Layout of delaminated composite beam bonded with DML [23]

Comparative vacuum monitoring (CVM) systems and sensors are other types of health monitoring techniques that can be utilised to monitor damage in metallic and composite structures. Applications range from simple systems used to improve the efficiency of QA/QC testing of automotive components through to complicated installations for the aerospace industry. The operating principle is simple, requiring small sensor pockets to be created in a region where damage is expected. When damage develops in the structure, a leakage path is formed between the vacuum and ambient pockets creating a measurable vacuum change [24]. The method is mainly suited for cracks in joints and void pockets in the structures.

2.3 Vibration Based Methods

2.3.1 Laser Techniques

Cheong et al. [25] used laser techniques to indentify damage in composite structures. They used ESPI and shearographics system to detect damages in delaminated composites, debonded honeycomb structures and adhesive joints. Shang et al. [26] used a scanning laser vibrometer, a lead zirconate titanate (PZT) and a polyvinylidene fluoride (PVDF) to conduct experimental modal testing as shown in Figure 2.14. They used higher order finite element model and Mindlin plate theory while interlaminar delamination has been modelled using continuum damage mechanics (CDM) formulation. Exciting frequency of 1 to 1000 Hz (swept sine) has been used to excite the plate through PZT actuator. They found that the subset selection analysis using modal parameters was capable to detect and localise the damage/multiple damages in the composite plate. Higher excitation frequency range is required for the experiment to achieve required results.

Higher excitation frequency range is required for the experiment to achieve required results.

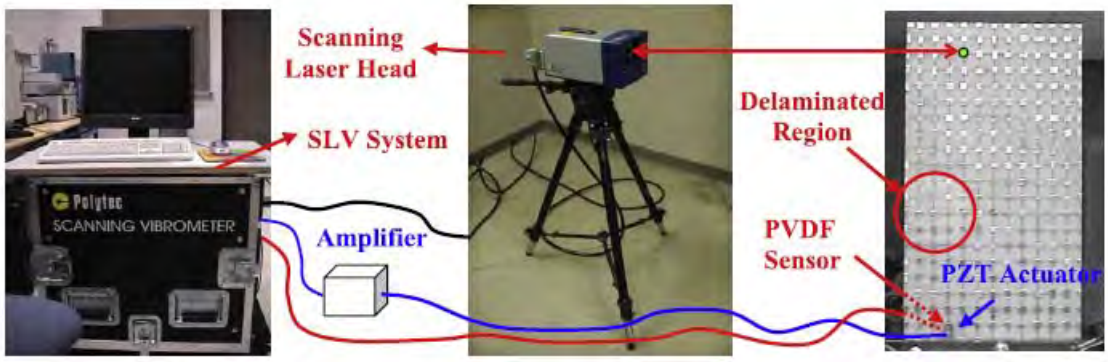

Figure 2.14 Test set-up for experimental modal testing using SLV and PZT-PVDF system [26]

2.3.2 Statistical-Based Methods

Hadjileontiadis and Douka [27] have developed a statistical method (kurtosis) using first few modes of vibration for a thin isotropic rectangular plate with crack parallel to one of its edges. The kurtosis analysis has been able to diagnose, locate and quantify the crack in the rectangular plate. The method worked in the presence of the added noise as well. The method has not been verified by experiments yet and is limited to cracks evaluations only. Yang et al. [28] used cross correlation function of the measured vibration signatures to develop a new technique of inner product vector (IPV) which has been successful to locate the damage in the composite beam. The IPV is a weighted summation of the modal parameters in terms of the vibration response (displacements). Detection of the damage is based on the difference between the normalised IPVs of healthy and damaged (D_{IPV}) beams. In fact the double differentiation of the D_{IPV} gives the location of the damage in the composite beam. The method requires vibration responses from random excitation and the sensors should be closely located to the

damage. The method has yet to be verified by experiments. Wang et al. [29] extended the IPV technique to be valid for general structures as well. They have checked the application of the method for shear frame structures, honeycomb sandwich beam, and stiffened panel structure and found it useful for the damage detection and location in all the three cases. The method still needs experimental verification and has the common drawback for the healthy structure data.

2.3.3 Optical-Fibre Techniques

Mackenzie et al. [30] used an array of fibre Bragg grating strain sensors (FBG) to monitor crack propagation and delamination under a bonded repair. They used a 500 kN MTS uni-axial hydraulic testing machine to conduct the tests. The damage was measured using a portable Zetec eddy-current instrument, with a 50–500 kHz differential probe. They verified the experimental observations by thermo-elastic scan of the patch and finite element analysis as well. Takeda et al. [31] found relationship between the spectrum, obtained from the data processed from the FBG sensors, and the delamination size of the delaminated CFRP laminate. The set up of the experiment is shown in Figure 2.15. Amplified spontaneous emission (ASE) light source (Ando Electric Co. Ltd, AQ-4310) of more than 40 nm wavelength range was used to illuminate the optical fibre. Takeda et al. [32] used fibre Bragg grating strain sensors for the delamination detection of the carbon fibre reinforced plastic laminates under cyclic loading. They found that the spectrum obtained from the processing of the FBG data changes with the size and location of the edge delamination. Figure 2.17 shows how a small diameter FBG sensor was embedded into a CFRP quasi-isotropic laminate. Cyclic load of 0 to 440 MPa was applied to the specimen at a frequency of 5 Hz in the experiment. The problem with the technique is that the sensor has to be near the

delamination location. Also the fabrication of the laminate with embedded FBG becomes challenging.

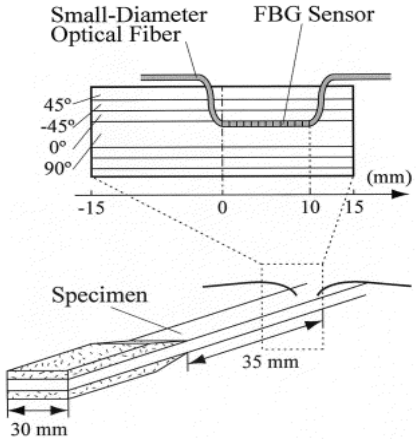

Figure 2.15 CFRP specimen with FBG sensor embedded [31]

Grouve et al. [33] showed that fibre Bragg grating sensors can be used to get the resonant frequencies of a vibrating anisotropic beam structure. In their research work on the subject, they introduced delaminations in the laminated plate by placing a 16 micron foil of polyimide between two plies prior to consolidation. During the fabrication they also inserted two FBG strips. They observed that the modal parameters have direct relationship with delamination and conversely delamination can be detected by the changes in the modal parameters. Xu et al. [34] used fibre-optic interferometric arrangement to compare the integral strain versus load position curve for both healthy and damaged beams to find the delamination presence and location. They have verified their numerical results through experiments. Ihn et al. [35] presented two active sensing methods which the authors have termed as pitch-catch methods. The first one is a damage index method, using a pair of actuator-sensor, which can quantify damage at a known location and the second one, is imaging method using multiple pairs of actuators-sensors and lamb waves can detect location and size of the damage. All the

fibre optic techniques so far mentioned need FBG embedded inside the structure which is not a welcome feature in online structure health monitoring technique.

2.3.4 Lamb-Wave Based Techniques

Wavelet analysis is used for processing the dynamic signals in damage detection of composite structures. Mal et al. [36] combined vibration (modal) and wave propagation (lamb waves) data in their technique that require minimum user intervention. The damage index they calculated from the modal data was used for delamination detection whereas the broadband excitation (0.1-2.5MHz) has been employed for the location and size of the delamination. They used two types of delaminations in their samples viz., internal delamination caused by impact and delamination caused by drilling holes in the plates. Quaegebeur et al. [37] have used lamb waves to develop a technique for delamination detection in composite structure. They studied first low frequency behaviour (<300 kHz) both numerically and experimentally and then high frequency behaviour (>300 kHz). They found that detection was more successful at higher excitation frequency and independent of the piezoceramic equipment spacing and other characteristics. They concluded that excitation at higher frequency level is more suited for interlaminar delamination detection. Su and Ye [38] studied the propagation characteristics of the lamb waves in the delaminated composite plate. They used PZT actuators and applied 0.1MHz to 1.5MHz as sweep frequency and collected the data with PZT sensors at a step of 50 Hz in their experiments. They also developed an active online diagnosis system based on their work as shown in Figure 2.16.

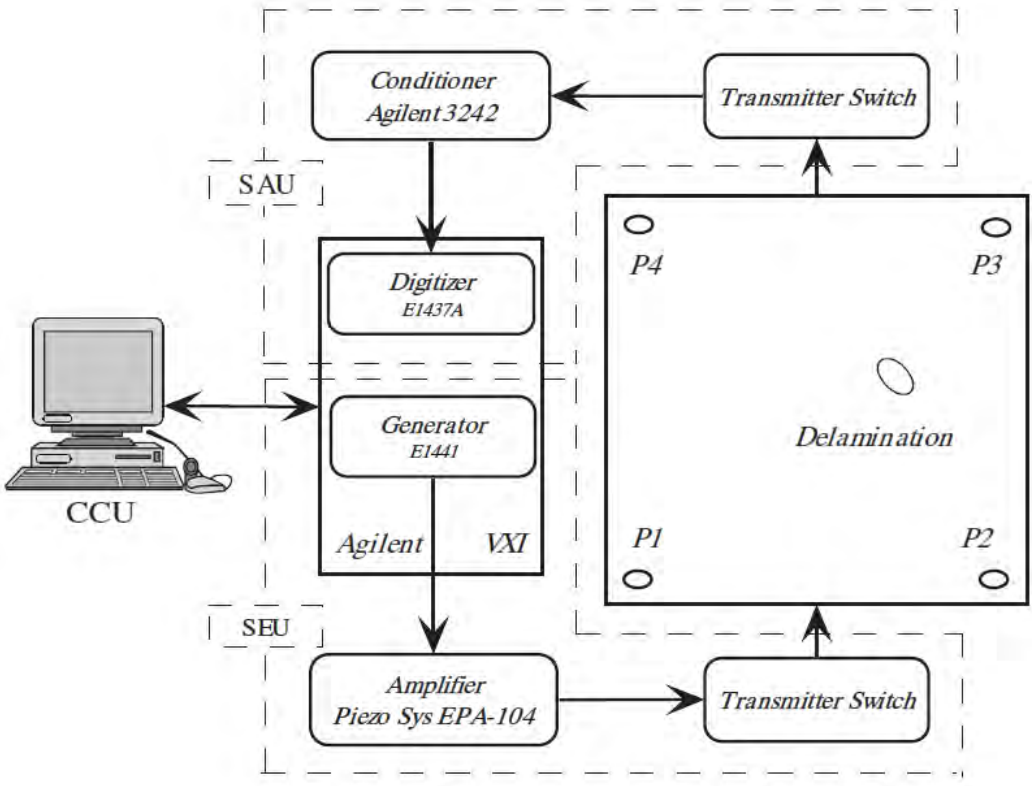

Figure 2.16 Configuration of diagnosis system using piezoelectric network [38]

Balasubramaniam et al. [39] worked on three techniques viz., multi-transmitter-multi receiver (MTMR) combined with tomographic technique for data processing, single-transmitter-multi-receiver (STMR), and the third one a linear array of sensors installed across a stiffener for the damage detection. They generated ultrasonic lamb waves (with central frequency of 500 kHz) to explore their structural health monitoring techniques. Using tomography with lamb waves complicates the experiment.

Kudela and Ostachowicz [40] developed beam and plate spectral elements with delamination. They have performed study on the relationship between the size and location of the delamination and the reflected waves. The work is only numerical and has not been verified by experiments. Hu et al. [41] have studied the influence of the excitation frequencies (10kHz to 120kHz) of Lamb waves on the power of the reflected waves from a delaminated composite plate. They have found that the optimal excitation

frequencies are close to the natural frequencies of the local delaminated regions corresponding to the pure bending modes. Pohl and Mook [42] have investigated the utility of impedance spectroscopy and lamb wave (in the range of 10kHz) techniques for delamination detection on carbon fibre reinforced polymers. They found that impedance spectroscopy is useful for self monitoring and its surrounding while lamb waves are suited for large areas. Wang et al. [43] found that the correlation-based algorithm in combination with virtual sensing paths (VSPs) proved to be a good tool for diagnosis of damage in the v-notched aluminium plate. They used central frequencies of excitation to vary from 250 kHz to 350 kHz and sampling rate of 20.48 MHz for data collection. Okabe et al. [44] worked out an ultrasonic propagation system using actuator made of macro fibre composite (MFC) and sensors made of fibre Bragg grating. The new technique of delamination detection and localization is based on the change in the dispersion characteristics of the lamb waves. Although the above mentioned actuators and sensors are smaller in size and effective but it needs expensive hardware and broadband excitation to work effectively.

Wandowski et al. [45] used pulse-echo method to excite the structure with guided waves and receive it using a circular array of sensors as shown in Figure 2.17 installed on the structure. Rathod and Mahapatra [46] used circular array of sensors similar to the one used by Wandowski et al. [45] for localisation of damage. Both of these research works has the limitation of number of sensors, due to the finite size of the sensor itself, for small structures. An et al. [47] developed a technique to normalise the data from the guided wave signals such that the effect of ambient variations like temperature are avoided.

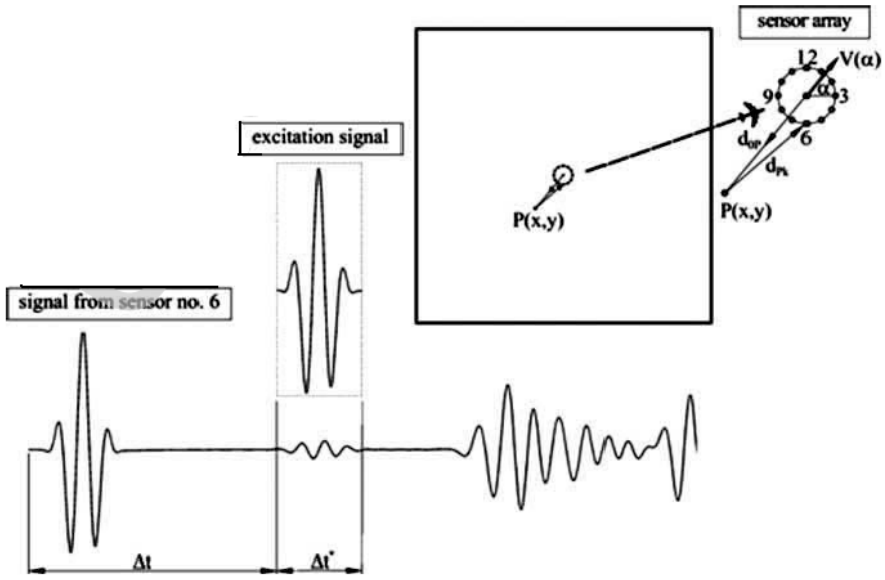

Figure 2.17 Principles of damage localisation algorithm in a composite plate [45]

They validated their work by experiments. The technique is still under development but can be useful where temperature variations are quite large. Bhalla et al. [48] have used array of surface bonded piezoceramics (PZT) to diagnose and locate the damage in structures by wave-propagation based method. They used frequency range of 100-150 kHz to invoke high sensitivity. The experimental structure is shown in Figure 2.18. All the work so far mentioned in this section uses broadband signals to localize the damage whether the guided waves are used directly or indirectly. Khodei and Aliabadi [49] used piezoelectric patches as both sensors and actuators to identify damage in the aluminium plate. The excitation frequency of 350 kHz has been applied for the usage of Lamb waves in the numerical experiment.

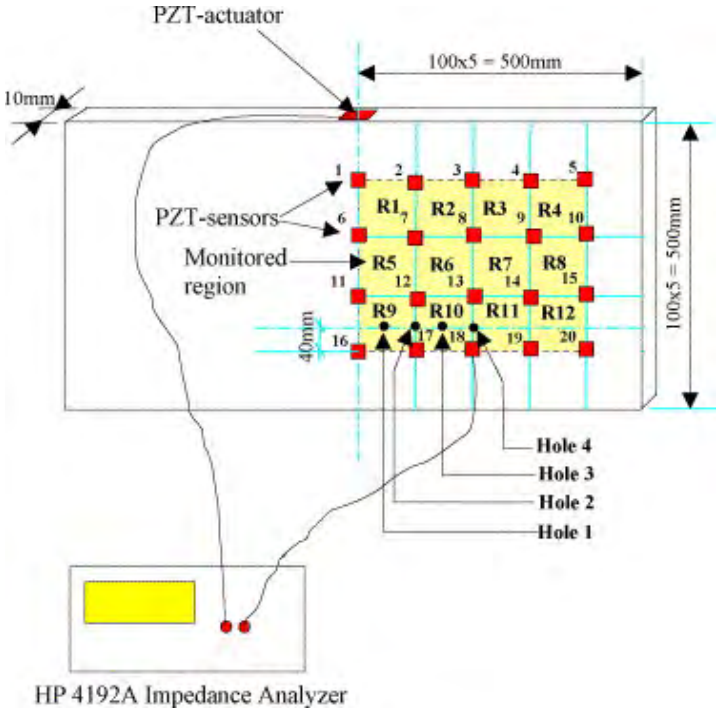

Figure 2.18 Experimental structure showing actuator and sensors [48]

2.3.5 Frequency-based damage detection

Changes in natural frequencies and mode shapes due to delaminations in composite structures were the first indicators which researchers have used for the detection of debonding damages. Paolozzi and Peroni [50] observed frequency shifts against the order of the mode when the damage percentage was increased. They noticed increasing shift with increasing damage percentage concluding that both delamination detection and its extent can be seen from the frequency variations in composite plate. The method depends on the natural frequencies and both the delaminated and healthy structures and gives only qualitative assessment of the damage.

Salawu [51] reviewed the investigations on the relationship between changes in natural frequencies and artificial damages in structure. The author concluded that changes in natural frequencies could characterize damage in the structure. Zhu et al. [52] used neural networks and sensivity analysis for the detection of damages in structures based

on natural frequency variations. They verified their work by experiments. The techniques require both healthy and damaged data to be compared for damage detection. Cerri and Vestroni [53] studied a beam with a diffuse crack for possibility of crack detection based on frequency changes due to damage in the beam. They compared numerical results with the corresponding experimental results and analysed the error between the two sets of data. The method needs data from the healthy beam.

Kim [54] developed a technique to process the frequency response functions (FRF) of the damaged and intact composite structures such the residual FRF provides information of the damage presence in the delaminated structure. The reconstructed FRFs not only provide information regarding damage presence but these also give the location and size of the delamination as well. Figure 2.19 shows the experimental setup of the Kim et al. experiment for FRF measurements. Gorl and Link [55] applied modal updating technique to the modal parameters for damage localisation and size approximation. A steel frame structure was used for the analysis and the work is purely numerical. Kim and Ywang [56] observed the extent of the delamination can be identified in terms of the natural frequencies and damping ratios of the de-bonded beams. They verified their theoretical models by experiments. The method is not a direct technique for delamination detection and localisation.

Yam et al. [57] found that using measured modal damping change and computed modal strain energy the location of the internal delamination can be estimated in multilayer composite plate. The work is based on the comparison of healthy and delaminated plates. Yam et al. [58] found that changes in natural frequencies of the damaged plates, as compared to healthy plate, increase with increase of delamination sizes and vary with mode numbers. They verified their numerical results through experiments on

honeycomb sandwich plates as well as multilayer composite plates with internal delaminations.

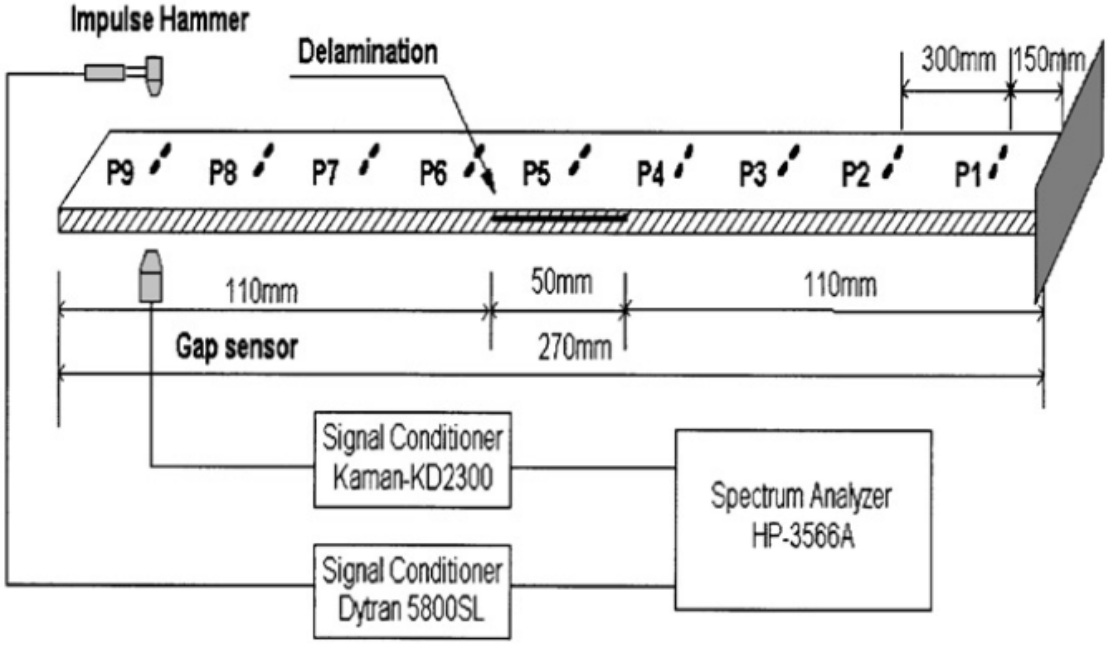

Figure 2.19 Experimental set-up for vibration testing [54]

2.3.6 Mode shape-based damage detection

Abdo and Hori [59] employed variations in mode shapes by rotations to indentify the damage in the structure. They showed that the technique was able enough to detect, locate, and quantify the damage size in the structures. The work done was numerically verified and no experiments were done.

Hamey et al. [60] used smart piezoelectric materials (sensors) to map the curvature mode shapes of a structure. The method used the data from healthy and damaged plates. They calculated Absolute Difference Method, Curvature Damage Factor, Damage Index, and FRF Curvature Method all depending on the curvature mode shapes of

healthy and damaged plates. The method is dependent on the data from healthy plate. Santos et al.[61] used double pulse TV holography and acoustic excitation to acquire mode shape data of the composite plates with delamination. The method is based on mode shape curvature. The method is expensive hardware dependent and also dependent on the accuracy of the modes.

Yoon et al. [62] used the Operating Deflection Shape (ODS) obtained from experiments to detect and localise the damage in beams and plates. The method employs the global fitting method (GFM) to get the Curvature Operation Shapes (COS). The Curvature Operation Shapes are then numerically processed to calculate the Structural Irregularity Index (SII) for each mode. These Structural Irregularity Indices are further processed to locate the damage. The method does not need data from healthy beam/plate. The method uses FRF data to calculate the above mentioned indices and is presently restricted to 1D and 2D structures.

Minak et al. [63] used the first six natural frequencies by pattern recognition technique to detect, localise and find the extent of the delamination in composite beam. The method has been used for a beam type structure and need the data from healthy beam to detect the damage. Yan et al. [64] summarised damaged detection techniques based on vibration. They have categorised the techniques to traditional type damage detection methods (TTDD) and modern-type damage detection methods. Qiao et al. [65] used a combined static/dynamic technique for the diagnosis of the damage in the composite structure. A preset static compressive force help the dynamic measurements of mode shape data to result in an easy and smooth way to detect damage. In fact the presence of static force magnifies the effect of the presence of damage. Uniform load surface (ULS) equations are used to process the first three modes and provide inputs for the Simplified

Gapped Smoothing (GSM) and Generalised Fractal Dimension (GFD) to further process the data for damage localisation. Gherlone et al. [66] have used the higher mode shapes to identify, localise, and quantify delamination in the delaminated composite plates. They computed mode shapes from mode 1 to mode 50 and used modes 31 to 50 to find the delamination location and extent in the composite plate. The benefit of the higher modes gave an edge over the conventional mode shape methods that the delamination localisation did not require data from the healthy plates. The disadvantage is that it's not practically feasible to measure higher modes. The work is purely numerical and has not been verified by experiments. Qiao et al. [67] utilized simplified gapped smoothing method (GSM), generalized fractal dimension (GFD), and strain energy method (SEM) to diagnose, locate, and quantify the delamination present in the composite plate using the experimental and numerical curvature mode shape data and uniform load surface (ULS) curvatures. They used three consecutive mode curvatures (modes 3–5) to compute the three damage detection techniques viz., GSM, GFD and SEM. Akhtar et al. [68] have employed pulsed Electronic Speckle Pattern Interferometry (Pulsed-ESPI) on a carbon fibre reinforced plastic (CFRP) laminate plates with different types and sizes of delaminations at the centre of the specimen, based on mode shape characteristics. A plate structure with delamination sizes are shown in Figure 2.22. Figure 2.23 shows the setup used for experiment. Ghoshal et al. [69] used Vibration Deflection shapes (VDS) to detect and locate the damage in the composite material structures. Vibration Deflection shapes are in fact the vibration patterns of the composite structure under study subject to steady state vibrations. They used Scanning Laser Doppler Vibrometer (SLDV) to measure the vibration response and piezoelectric actuators in their experiments. They found the VDS method can detect and localise the damage in large composite structure. All the work so far mentioned in this section need modal analysis

and or mode shape data of the damaged and or healthy structures. Mode shape data is very sensitive to changes and can result in wrong results.

Amraoui and Lieven [70] used multilayer perception neural networks with SLDV as a sensor and piezoceramics patches as actuators to identify and locate multiple delaminations in glass/epoxy composite structures. They found the superficial delaminations are easily and successfully located by using the compressed data of the measured FRFs but failed to locate the deep delaminations in the experiment. Choi et al. [71] investigated the relationship between the changes in the natural frequencies and mode shapes due to the simulated faults in the structure.

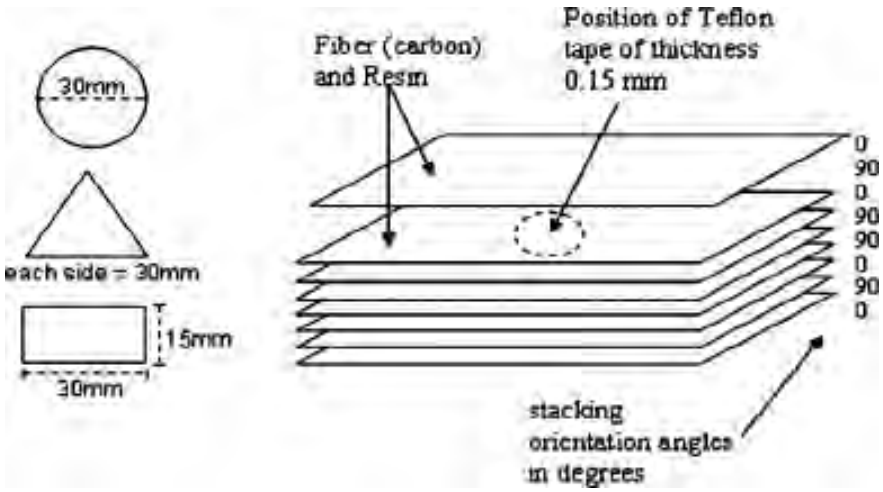

Figure 2.20 CFRP specimen with various sizes of artificial defects [68]

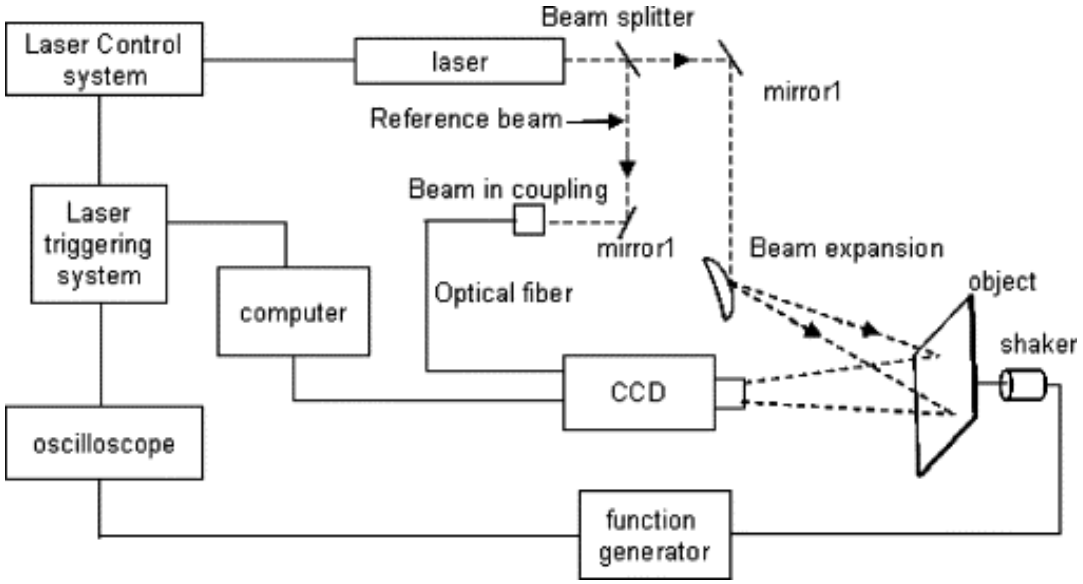

Figure 2.21 The layout of experimental set-up [68]

In fact they derived a new damage index. The methodology was based on changes in modal strain energy and natural frequencies and was capable to find damage locations and sizes in the damaged plate structure. The work was purely numerical and requires data from both healthy and damaged structures.

2.4 Summary

- Overview of different NDT and SHM methods for damage detection has been discussed.
- Different SHM techniques used for composite structures have also been discussed in this review of literature chapter.
- Conventional NDT is time consuming and not suitable for online structural health monitoring.

- Vibration-based methods can identify the delamination quickly as compared to conventional NDT.

- However most of the conventional vibration-based methods require healthy data (baseline based method) and some require excitation at very high frequency. This limits the use of conventional electromagnetic shaker and accelerometers for practical applications.

- Hence in the present research methods using lower vibration modes have been attempted for delamination detection and location.

CHAPTER 3
EXPERIMENTAL SETUP

3.1 Overview

In this research study two different types of plates have been used. One is composite Aluminium plates and the other type is glass fibre composite plates. Details of the Aluminium plates are given in Section 3.2 while the detail of glass fibre plates is explained in Section 3.3. An ISI-SYS Piezo-shaker was used to apply a harmonic excitation load, set of accelerometers (PCB) were used to measure data, National Instruments (NI) data acquisition card was used to convert the data received from accelerometers to computer, and the Labview based data collection software, Vibration Monitor was used to capture the data . For the modal analysis a PCB instrumented hammer was also used in addition to the Piezo-shaker.

3.2 Experimental Setup for Aluminium Plates

Experimental setup for the Aluminium plates is shown in Figure 3.1. The plate in the experiment is fixed on one edge as shown in Figure 3.1(a). Figure 3.1(b) shows the photograph of the experimental setup.

Figure 3.1 Schematic of Experiments, (a) Plate with shaker and accelerometer, (b) Experimental setup

3.2.1 Aluminium Plates

Two Aluminium plates of sizes 190 mm x 190 mm x 1.15 mm and 190 mm x 190 mm x 3.15 mm glued together leaving a square pocket of 50 mm x 50 mm in the centre have are prepared to simulate the delamination condition so that the effect of the nonlinear interaction between the layers during the vibration experiment can be observed. The two-piece Aluminium plate with a piezo-shaker, accelerometer and a fixed end are shown in Figure 3.2. Another set of identical Aluminium plates were glued together without leaving a square pocket (healthy set) to compare the response of the delaminated set with healthy set. Glued mass of the Aluminium plates was 419 grams.

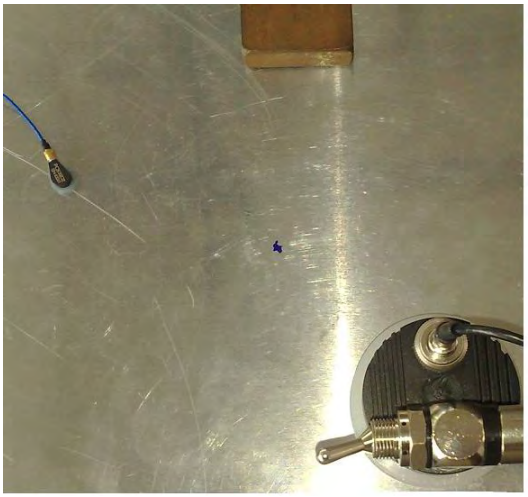

Figure 3.2 Composite Aluminium plate 190 mm x 190 mm x 4.3 mm

3.2.2 Shaker & Amplifier

A piezo-electric shaker (Model PS-X03, M/s ISI-SYS) and a dual channel bipolar amplifier, as shown in Figure 3.2, have been used to excite the plate. Weight of the piezoelectric shaker is 234 grams. Amplifier shown in Figure 3.2(b) provides a suction force to keep the shaker in place while the latter is in operation to apply the excitation load to the composite plate under testing.

Figure 3.3 (a) Piezo-shaker, (b) Dual channel bipolar amplifier

The ISI-SYS Piezo-shakers are specifically developed for very low to high frequencies (frequency range 0- 50 kHz) broadband excitation.

3.2.3 PCB Hammer

The instrumental hammer used for modal analysis is shown in Figure 3.4. The sensitivity of the instrumented hammer, used in the experiments, is 2.25mV/N at room temperature. Its mass is 160 grams and its length is 216 mm. it is connected with data acquisition card via power amplifier through standard BNC jack connector.

Figure 3.4 M/s PCB hammer used in the experiments

3.2.4 Data Acquisition

The data were recorded on the Laptop using 16-bit 8-channel data acquisition Analogue to Digital card. The data acquisition card is shown in Figure 3.5. It is called NI USB 6221BNC and is 16-Bit, 250 kS/s M Series.

Figure 3.5 Data acquisition card used in the experiments

3.2.5 PCB Accelerometer

Accelerometers (Model 352C22, M/s PCB) as shown in Figure 3.6 are used to measure the vibration response in terms of acceleration. Model 352C22 accelerometers are lightweight (0.5 grams) and is capable of measuring frequencies in the range of 1 to 10000 Hz. It has sensitivity of 10mV/g.

Figure 3.6 Accelerometer Model 352C22

3.2.6 Data collection

All the data collected in the experiments are done using the Labview-based Vibration Monitor software developed by Austin Consultants (UK). A vibration monitor is designed to collect the data through the data acquisition card. Figure 3.7 shows snapshot of online data collection by the Vibration Monitor during the experiment. The software allows selection of sampling rate and voltage limits for each channel in use.

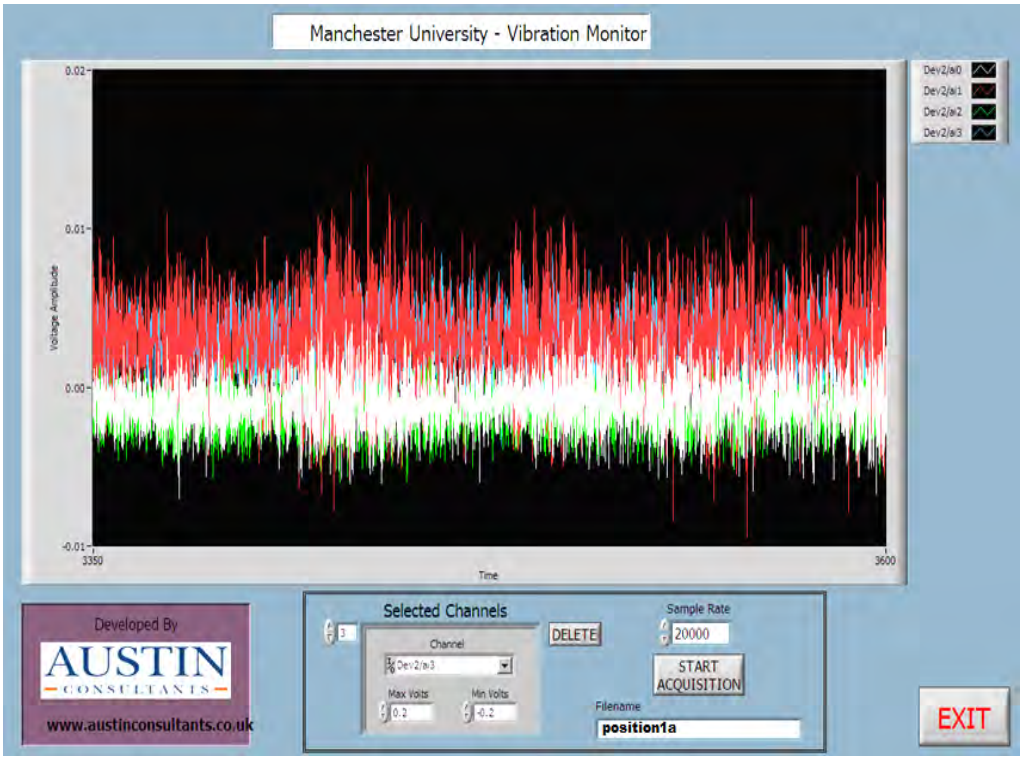

Figure 3.7 Vibrator Monitor Interface and Data acquisition

3.3 Experimental Set-up for glass fibre plates

Experimental setup for the glass fibre composite plates is shown in Figure 3.8 (a-b).

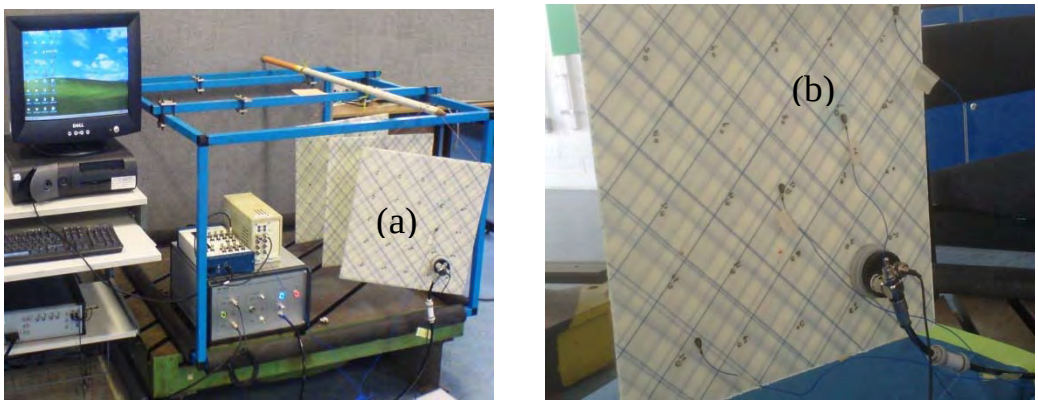

Figure 3.8 (a) The experimental test setup, (b) Shaker mounting

The test plate made of E-glass fibre and epoxy resins has been used here. It has a total of 8 layers of equal thickness which are arranged as [0^o /90^o/0^o /90^o/90^o /0^o /90^o/0^o] as shown in Figure 3.9. The size of the test plate is 400 mm x 400 mm and total thickness 3.5mm. Total mass of the composite plate is 664 grams. The inter-laminar delamination (Teflon tape of 20 microns) was introduced between 3rd and 4th layers, during the pre-preg process, in order to create a discontinuity in strains. Healthy plate used in the experiments is shown in Figure 3.10 (a) whereas the plate with off-centre delamination is shown in Figure 3.10 (b). The delamination location is shown in Figure 3.10(b).

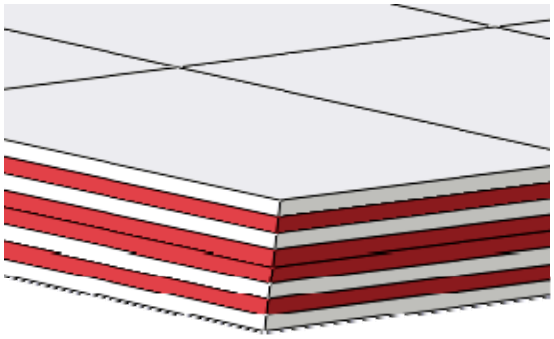

Figure 3.9 Arrangement of 8 layers in the test plates

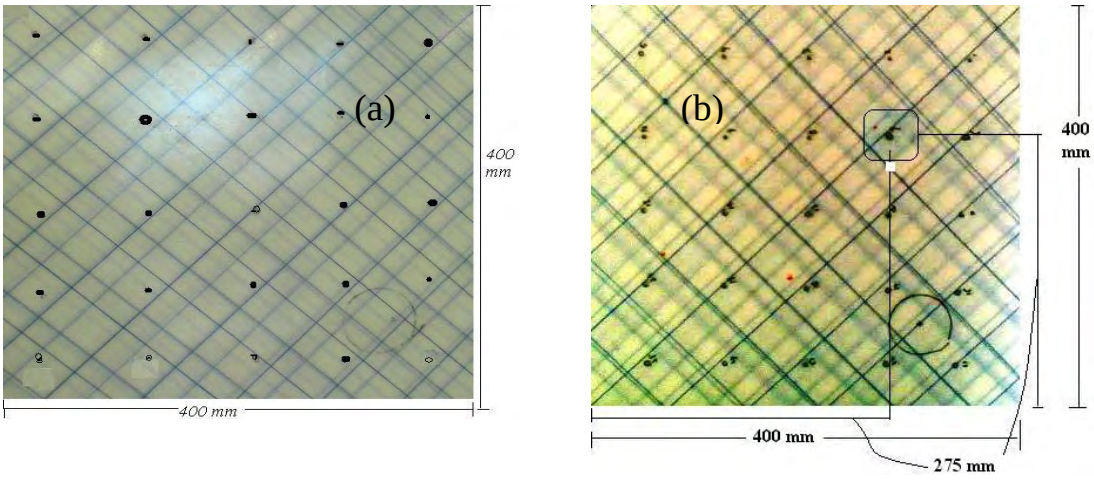

Figure 3.10 Typical test plates of E-glass fibre, (a) no delamination, (b) delamination at coordinate location (275mm, 275mm)

3.3.1 Shaker with Excitation positions

Figure 3.11(a-c) show three different positions of excitations and the measurement locations (5 x 5 grids) used during the experiments. Three different positions of excitations have been used during the experiments. All the three plates mentioned in section 3.2 were excited at the three different positions shown in the following figures.

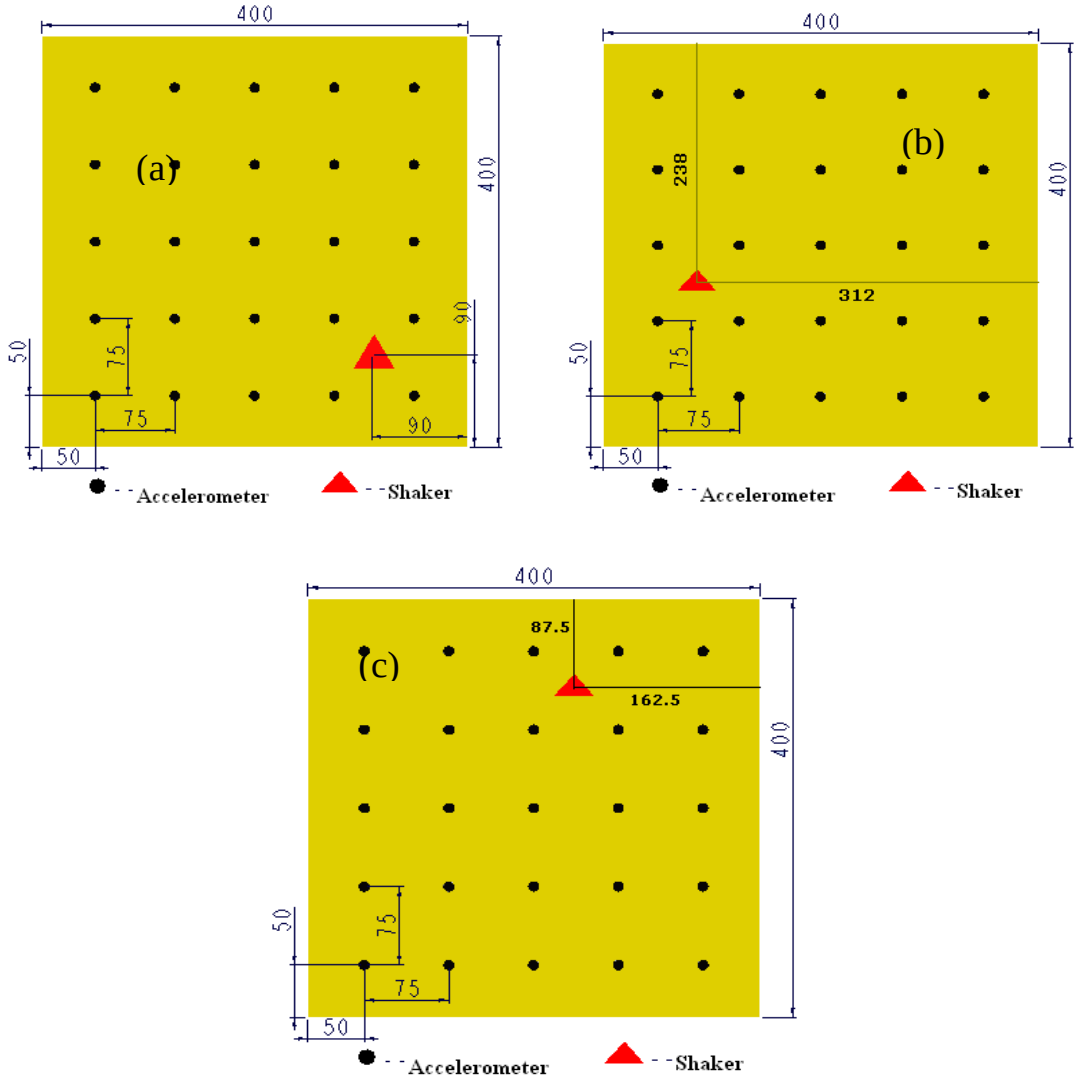

Figure 3.11 Composite plate of E-glass fibre with (a) Shaker location 1(b) Shaker location 2(c) Shaker location 3

CHAPTER 4
NONLINEAR INTERACTION BETWEEN DELAMINATION LAYERS IN COMPOSITE PLATES

4.1 Introduction

The dynamic behaviour of the delaminated composite plate based on the numerically simulated experiments has been studied in this chapter. The possibility of delamination detection using the nonlinear interaction feature in the delaminated region has been explored when excited the plate through a shaker. A composite plate with 3 cases of the delamination has been considered first in the simulated examples. Initially the experiments on simple aluminium plates with and without delamination have also been carried out which confirms the existence of the nonlinear interaction between the delaminated layers used in the simulated studies and then the results of the simulated examples were also compared with the earlier published experimental results on the composite plates. The results and observations of the study which can be used for the delamination detection in the composite structures have been discussed.

In the present approach, the structural response due to the nonlinear interaction between the layers in the delamination region, when the structure is excited externally, has been utilised. It has been believed that such nonlinear interaction response will travel all along the surface and can be measured at any location. The proposed concept has further been demonstrated on a simple cantilever beam made of steel where delamination has been introduced by dividing the width of beam cross-section in two parts of small length of the beam [72]. It has been observed that the delaminated beam shows number of harmonics in their acceleration responses when excited at different

modes [72]. Now the concept has further been extended here on a carbon fibre plate with delamination. The acceleration responses were estimated at 3 randomly selected measurement locations when excited at number of modes from 1 to mode 20. The proposed analysis has been applied to a composite plate with 3 cases of the delamination in the numerically simulated examples. These are the cases where a small size delamination has been assumed which resulted in insignificant change in the natural frequencies at low modes but the nonlinear interaction between the delaminated layers shows promising results to detect the delamination at early stage. The observations have been summarised here which shows the possibility of the delamination detection in much economical way. Simple experiments have also been carried out on aluminium plates with and without delamination which confirms the existence of the nonlinear interaction between the delaminated layers used in the simulated studies and then the results of the simulated examples have further been compared with the earlier published experimental results on the composite plates[73]. The results and observations of the study which can be used for the delamination detection in the composite structures have been discussed in this chapter.

4.2 Example of a Composite Plate

A composite plate of multi-layer carbon fibre-reinforced epoxy material has been chosen for the present study. The plate is made of 8 lamina layers and 225.5mm x 225.5mm square plate with 2.05mm overall thickness. The composite plate ply orientations are $[0^0/90^0/0^0/90^0]_s$ and the material properties for the lamina are; Density, ρ =1813.9 kg/m^{3,} the elasticity constants, $E_1 = 37.78\,\text{GPa}$, $E_2 = E_3 = 10.9\,\text{GPa}$,

$G_{12} = G_{13} = 4.91\,\text{GPa}$, $G_{23} = 3.838\,\text{GPa}$, and the Poisson ratios, $\mu_{12} = \mu_{13} = 0.33$, $\mu_{23} = 0.42$

Three cases have been considered, Case A – healthy plate (no delamination) and however the other two cases named B, and C have delaminations with area 60 mm x 60 mm (Figure 4.1), and 30 mm x 30 mm (Figure 4.2) respectively. The delamination has been introduced between the 3rd layer from top and 5th layer from bottom and the centre of the delamination region i.e., the location (165.37mm x 165.37mm) is shown in Figure 4.1. The mathematical model of the plate has been modelled using eight-node rectangular solid elements (C3D8I) in the Finite element (FE) code ABAQUS. The FE model for the plate without delamination (Case A) is shown in Figure 4.1. A total of 900 elements of size 7.51667mm x 7.51667mm x 0.25625mm were used for each layer. Delamination in the composite plate was also introduced in the FE model for other two Cases B and C with delamination of 60mm x 60mm and 30mm x 30mm (Figure 4.2) respectively. The upper and lower layers in the delamination region have also been modelled using 8-noded rectangular solid elements (C3D8I). The nodes on the upper and lower layers have been created such that they have same *x* and *y* location in the delaminated region but not connected to each other. In Figure 4.3, the node 5705 (also marked as circle in Figure 4.1) is the node at the centre of the delamination on the top layer of the composite plate and the node 15705 is the node (not shown) that is exactly at the same location as 5705 but on the bottom layer. Figure 4.3 also shows the measurement locations (Accelerometers) and the location of the external excitation which has been used latter in Section 2.1 on the simulated experiments.

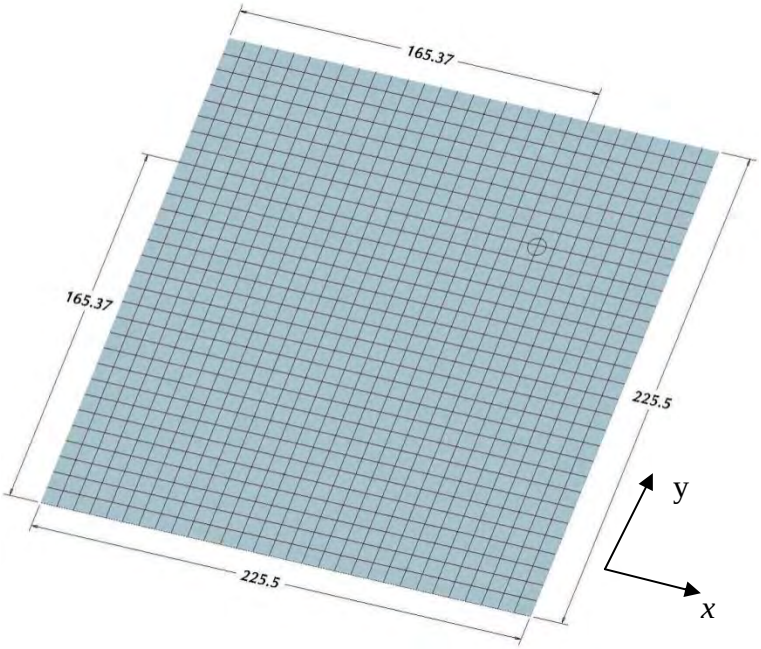

Figure 4.1 A typical FE model of the Composite plate without delamination (Case A), centre (165.37mm x 165.37mm) of assumed delamination for Cases B and C shown as a Node with circle.

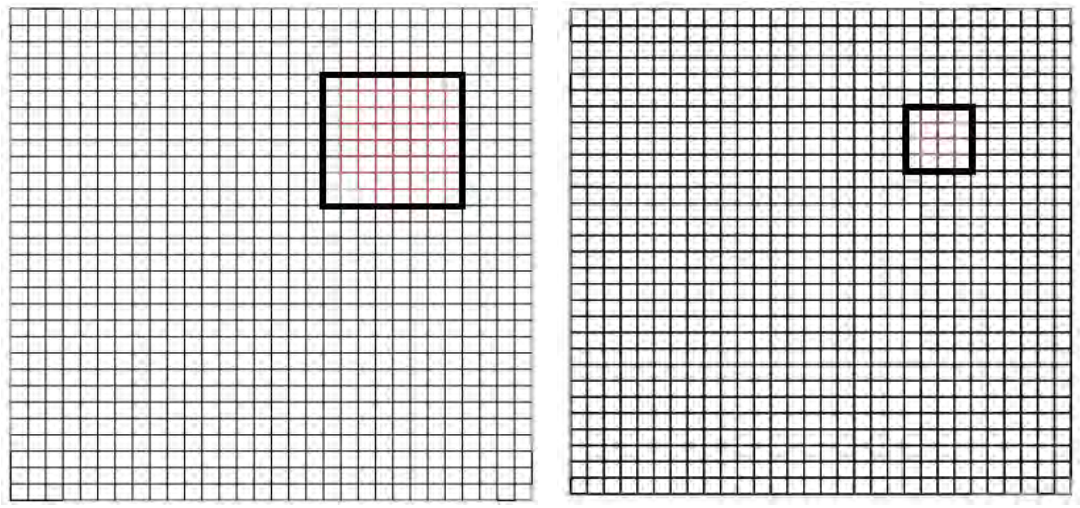

Figure 4.2 (a) FE mesh of the Composite plate for Case B (delamination size 60mm x 60mm), (b) Cases C (delamination size 30mm x30mm)

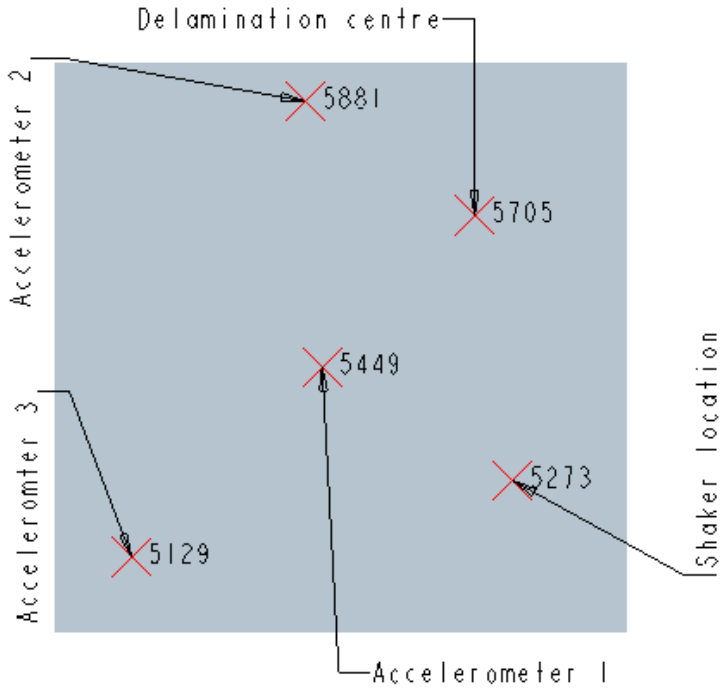

Figure 4.3 Composite plate showing the shaker and accelerometer locations used in the simulated experiments

The modal analysis has been carried out for the FE models for all the 3 cases to estimate the natural frequencies and the mode shapes. The free boundary condition has been assumed for all the 4 edges in all the three cases and then the forty modes have been computed. The comparisons of the calculated natural frequencies up to 40 modes for the Cases A, B and C are shown in Figure 4.4. From Figure 4.4, it can be seen that at lower modes there is no significant change in the Eigen-values for the three cases until mode 15. After mode 15 the changes are visible for the larger delamination area (Case B) and there is very little change in the frequencies between laminated plate (Case A) and the delaminated plate with smaller delamination region (Case C). It is also important to note that the estimated natural frequencies for Cases B and C assumed the upper and lower layers in the delamination region are completely separate, however in practice the

resonance frequencies are expected to nearly same or slightly higher depending on the level of excitation which results in the nonlinear interaction (open and close behaviour) between the delaminated layers during the vibration. The open behaviour means that both delaminated layers move independently and move together during the closed behaviour. Few typical computed mode shapes and their natural frequencies are also shown in Figure 4.5 for Case B during the open condition. The separation between the delamination nodes 5705 and 15705 at Modes 1 and 2 is not clearly visible from their mode shapes shown in Figure 4.5, however higher modes like modes 21 and 26 do show a good separation between top and bottom layers in the delamination region in their mode shapes. This separation is clearly visible in their mode shapes when the wireframe diagram of the plate is used which are shown in Figure 4.6 where the pair of nodes 7505 and 15705 shows separation. The separation between the centre of nodes 5705 and 15705 at each mode up to 40 modes in their mode shapes along the thickness of the plate for the Cases B and C is shown in Figure 4.7. Case B with larger delamination area of 60mm x60mm shows good separation after mode 6, however nearly negligible separation observed for the Case C with small delamination area 30mm x 30mm.

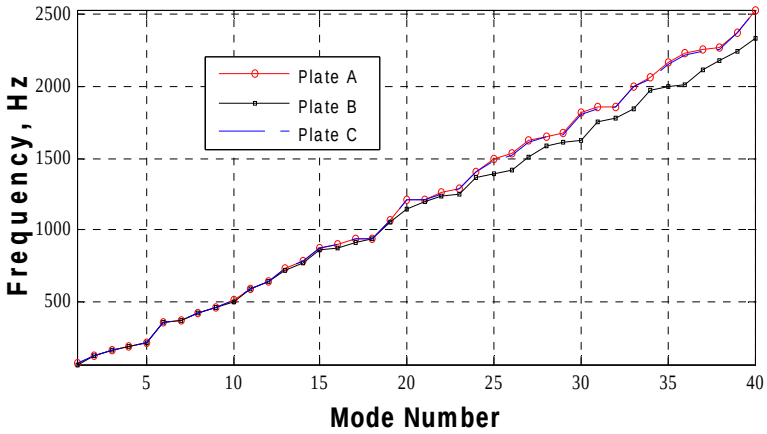

Figure 4.4 Natural frequencies with mode number for Cases A, B and C of the composite plate

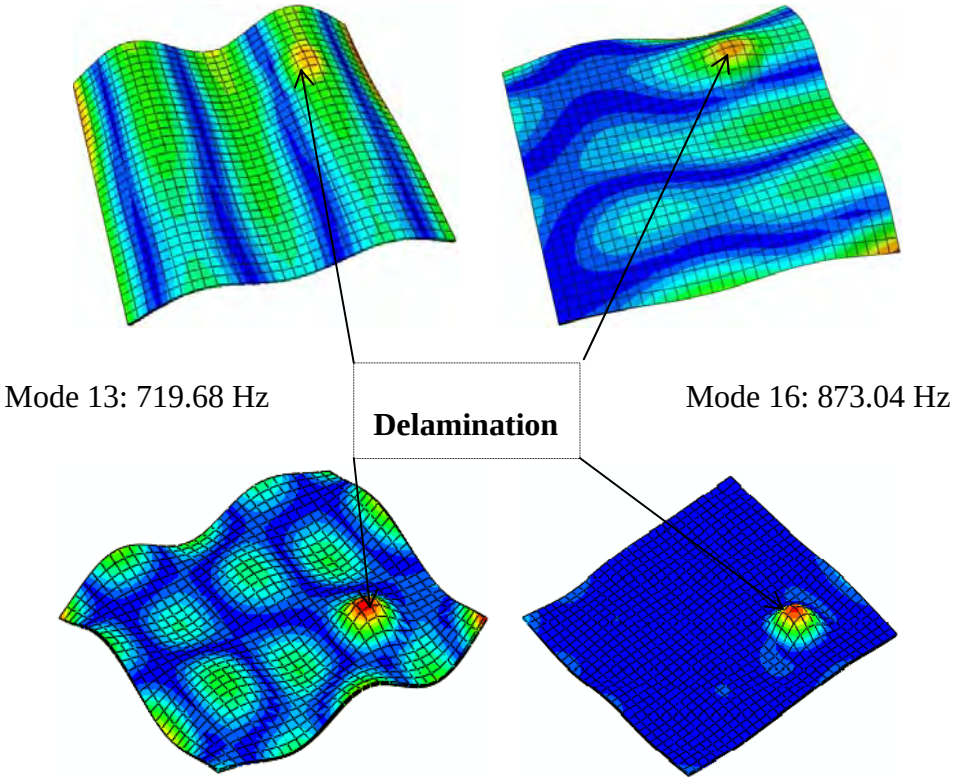

Figure 4.5 Few typical mode shape plots of the delaminated plate for Case B

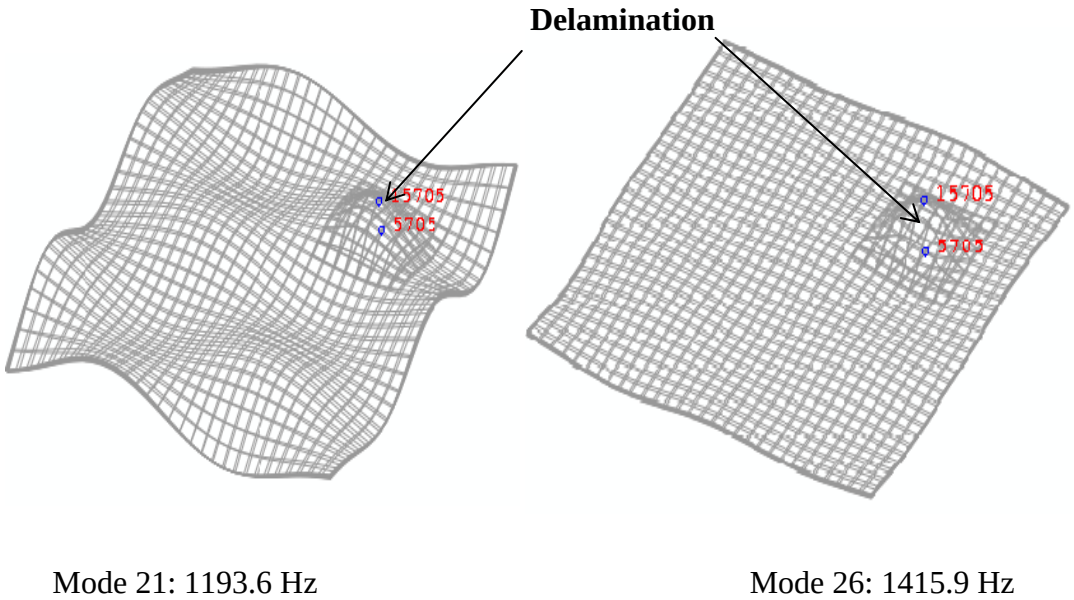

Figure 4.6 Mode shape using wireframe plots for the delaminated plate for Case B

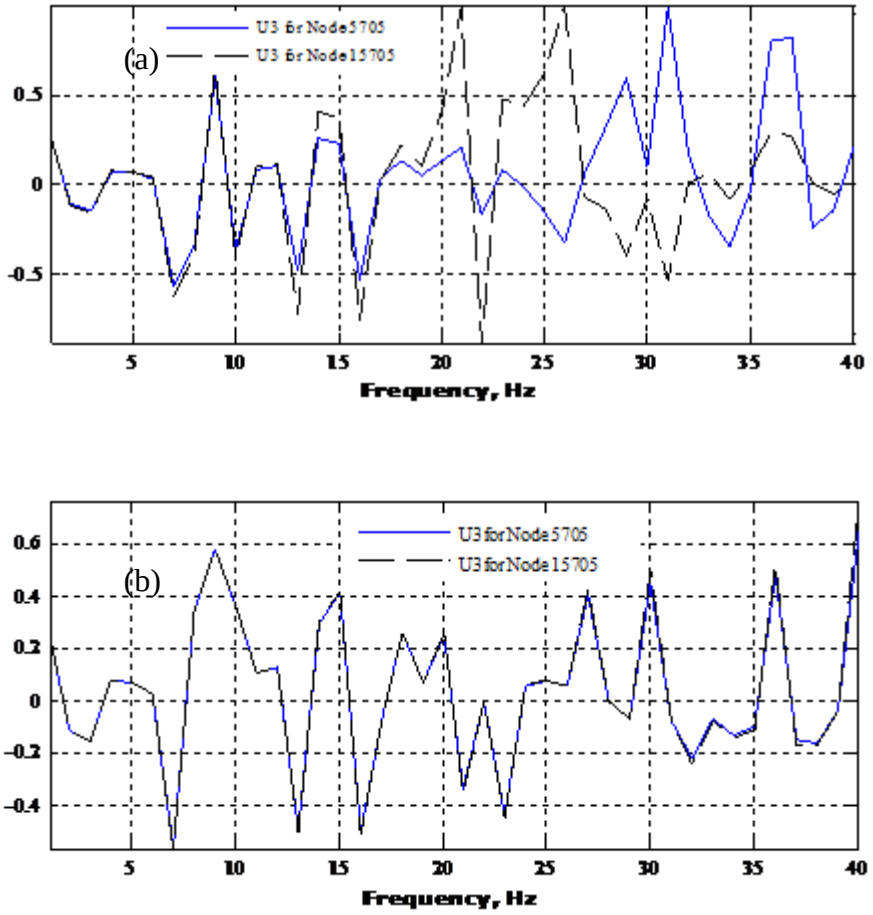

Figure 4.7 Mode shape deflection for the nodes 5705 and 15705 (pair of nodes at delamination centre) along the z- direction with the mode number for the delaminated plates, (a) Case B and (b) Case C.

4.3 Simulated Experiments

The composite structure with delamination is expected to show nonlinear interaction in the delamination region when excited externally. Such responses may get amplified when excited at the natural frequencies. Hence the acceleration responses have been computed at the randomly assumed measurement locations shown in Figure 4.3 when the linear chirp-sine excitation was applied at each mode up to 20 modes. The assumed measurement locations and the shaker location for the simulated study are shown in

Figure 4.3. The linear chirp-sine excitation was given in the frequency band of $f_r \pm 10$ Hz with the chirp rate of 4 Hz/s for all the modes, where f_r is the r^{th} natural frequency (Hz). The banded frequency excitation was given to account for the change in the natural frequency for the delaminated plate due to the nonlinear interaction between the delaminated layers during the vibration of the delaminated plate. The time step for the response computation was kept equal to $1\,\mu s$. It was difficult to simulate the nonlinear interaction between the pair of nodes in the delamination region in the ABAQUS FE code, hence the mode-superposition method was slightly modified to allow the nonlinear interaction and then responses were estimated separately in a Matlab code developed for this analysis which has been explained here.

In the Mode-superposition method, the dynamic equation in the modal domain in Equation (4.1) has been used to estimate the modal responses.

$$\ddot{\mathbf{p}}_r(t) + 2\zeta_r\omega_r\dot{\mathbf{p}}_r(t) + \omega_r^2\mathbf{p}_r(t) = \boldsymbol{\varphi}_r^T\mathbf{F}(t)\,, \quad \text{.....(4.1)}$$

where $\omega_r = 2\pi f_r$, ζ_r is damping ratio at r^{th} mode, $\boldsymbol{\varphi}_r$ is the vectors of the r^{th} mode shape, $\mathbf{p}_r(t)$ is the modal responses at r^{th} mode and $\mathbf{F}(t)$ is applied force. The responses (displacement, velocity and acceleration) have then been estimated as $\mathbf{x}(t) = \boldsymbol{\varphi}\mathbf{p}(t)$, $\mathbf{v}(t) = \boldsymbol{\varphi}\dot{\mathbf{p}}(t)$ and $\mathbf{a}(t) = \boldsymbol{\varphi}\ddot{\mathbf{p}}(t)$ respectively, where $\boldsymbol{\varphi}$ is the mode shape matrix which is equal to $\begin{bmatrix}\boldsymbol{\varphi}_1 & \boldsymbol{\varphi}_2 & \cdots & \boldsymbol{\varphi}_n\end{bmatrix}$ and the modal response vectors, $\mathbf{p}(t) = \begin{bmatrix}\mathbf{p}_1(t) & \mathbf{p}_2(t) & \mathbf{p}_3(t) & \cdots & \mathbf{p}_n(t)\end{bmatrix}^T$ for the 1st to n^{th} mode respectively. However

for the present study the modal parameters – the natural frequencies, $\mathbf{f}_n = [f_1 \quad f_2 \quad \cdots \quad f_r \quad \cdots \quad f_n]^T$ and the corresponding mode shape vectors, $\boldsymbol{\varphi}$ would not be constant with time due to the nonlinear interaction. Hence the 2 sets of modal parameters, Set (1) ($\mathbf{f}_{n\_d}$ and $\boldsymbol{\varphi}_d$) for the delamination case and Set (2) ($\mathbf{f}_{n\_nd}$ and $\boldsymbol{\varphi}_{nd}$) for the perfectly laminated (no delamination) case, computed from the FE models developed in the ABAQUS (version 6.6) have been used for this purpose. The set (1) data were used in Equation (4.1) and the responses estimated when the nodal displacement, $w_i(t) > w_j(t)$ in the *z*-direction of thickness of the plate and the set (2) when $w_i(t) \le w_j(t)$, where $\boldsymbol{i}$ denotes a set of nodes in the upper delamination region and $\boldsymbol{j}$ denotes a set of nodes in the lower delamination region that were paired with the corresponding $\boldsymbol{i}$ nodes. It is because the later condition is more like the plate without delamination. The impact energy between the delaminated layers during the nonlinear interaction was assumed to be small for the small size delamination considered here and hence this affect has been neglected in the response estimation. Figure 4.8 explains a simple understanding of the nonlinear interaction adopted in the response computation. Hence a computational programme has been developed based on the proposed scheme in the Matlab software code to estimate the responses using the 2 sets of the modal data from the FE model (with and without delamination) developed in the ABAQUS code.

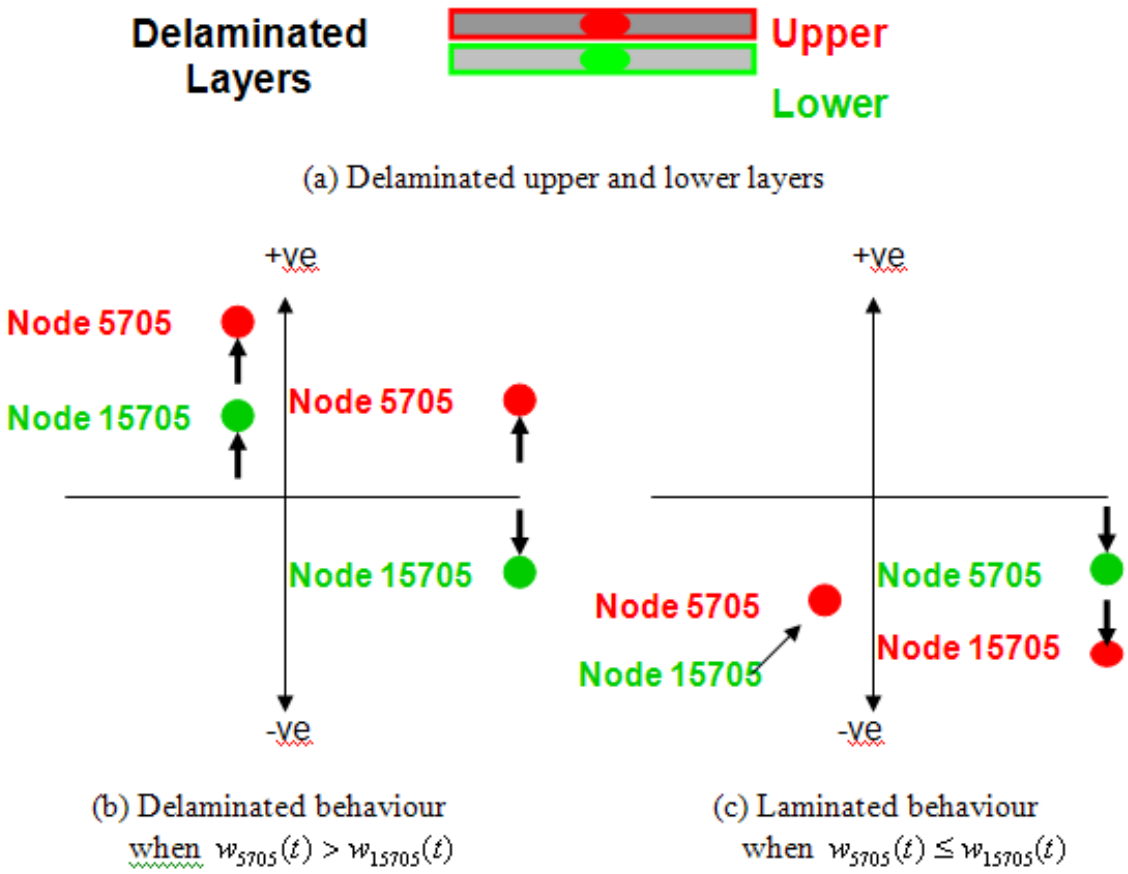

Figure 4.8 The scheme adopted for the nonlinear interaction between the delaminated layers

The Newmark-β method was used for solving Equation (4.1). It is also important to note that if the excitation is at the r^{th} mode, f_r, generally the r^{th} modal response is computed in Equation (4.1) to the estimate nodal responses based on the assumption that the response from other modes may be negligible due to the orthogonality condition. However, the composite structure is generally non-isotropic material due to the direction dependent material properties for each lamina in the composite structure and it is very much expected that the some modes may be coupled to each-other. Hence a total of 20 modes have been used in the response estimation so the influence of the other modes in the response can be observed even when excited at a mode. The computed measured acceleration responses and the displacement responses at the pair of

nodes were then down sampled by 10 and low-pass filtered at 49 kHz to remove the high frequencies noise components likely to occur due to the time step used in the computation. Few typical displacement responses for the nodes 5705 and 15705 in the z-direction are shown in Figure 4.9 for Case B delaminated plate. The displacement responses clearly show the nonlinear interaction in the delamination region even at the lower modes where the separation between the nodes 5705 and 15705 is clearly visible in the mode shape (Figure 4.7). It is also encouraging to observe a similar behaviour for Case C where delamination area is just one fourth of Case B and the change in natural frequencies when compared with the plate without delamination (Case A) nearly negligible for several lower modes (Figure 4.4). Few typical displacement responses for Case C at the nodes 5705 and 15705 at Modes 10 and 18 are also shown in Figure 4.9 which do not show the nonlinear interaction clearly, however the difference of the displacement between these 2 nodes clearly indicates the presence of the nonlinear interaction which is shown in Figure 4.11.

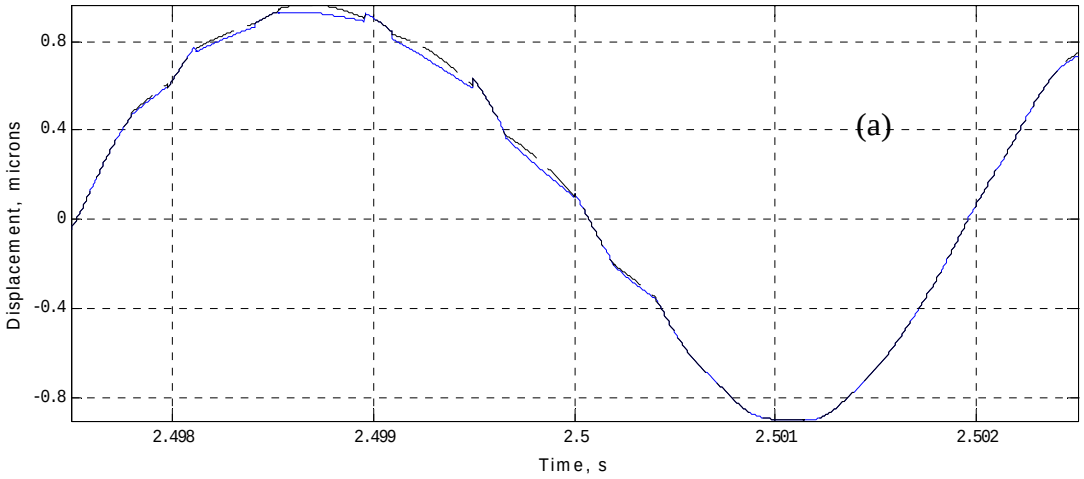

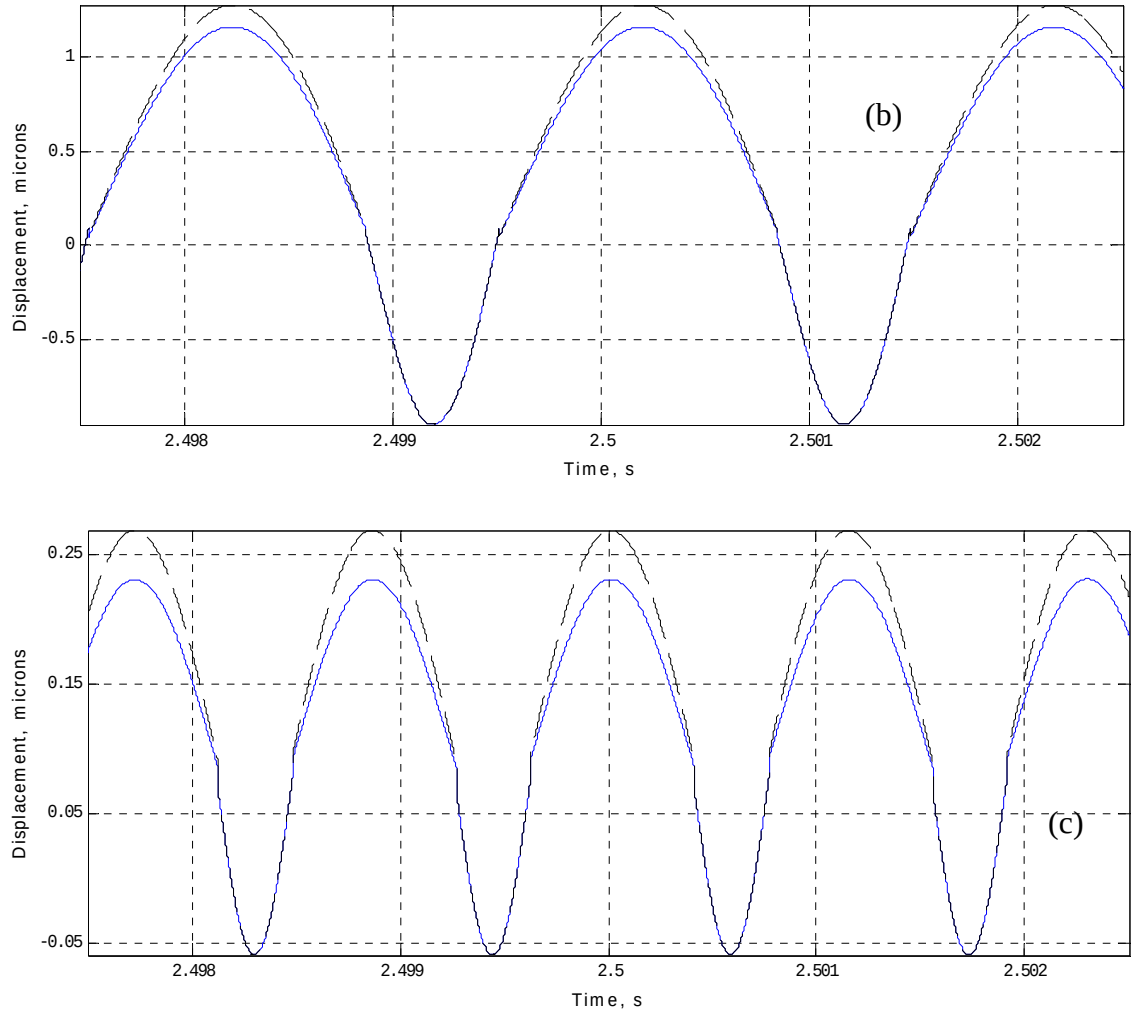

Figure 4.9 The displacement responses along the z-direction of nodes 5705(solid line) and 15705 (dashed line) for Case B (a) Mode 5:218 Hz, (b) Mode 10: 508 Hz, (c) Mode 16:874 Hz

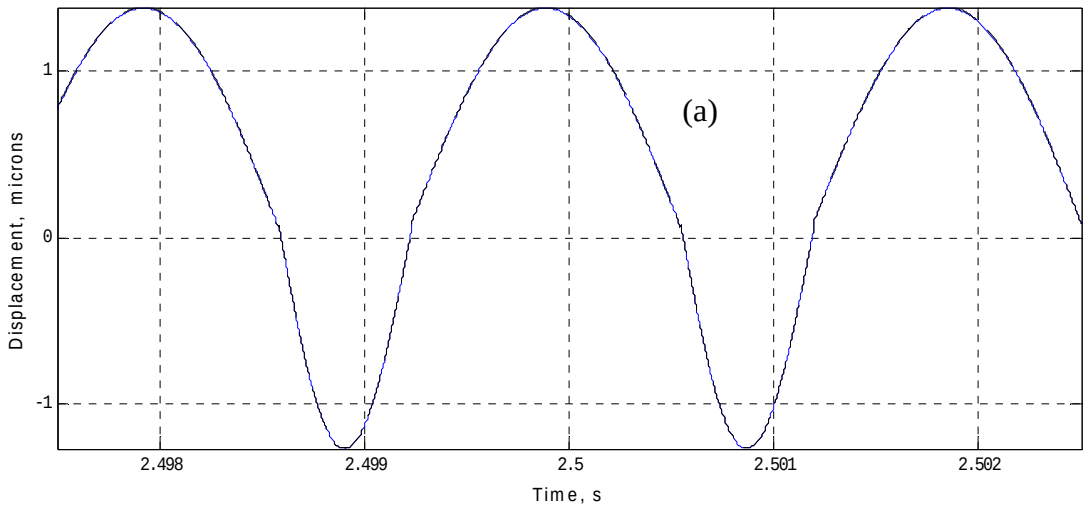

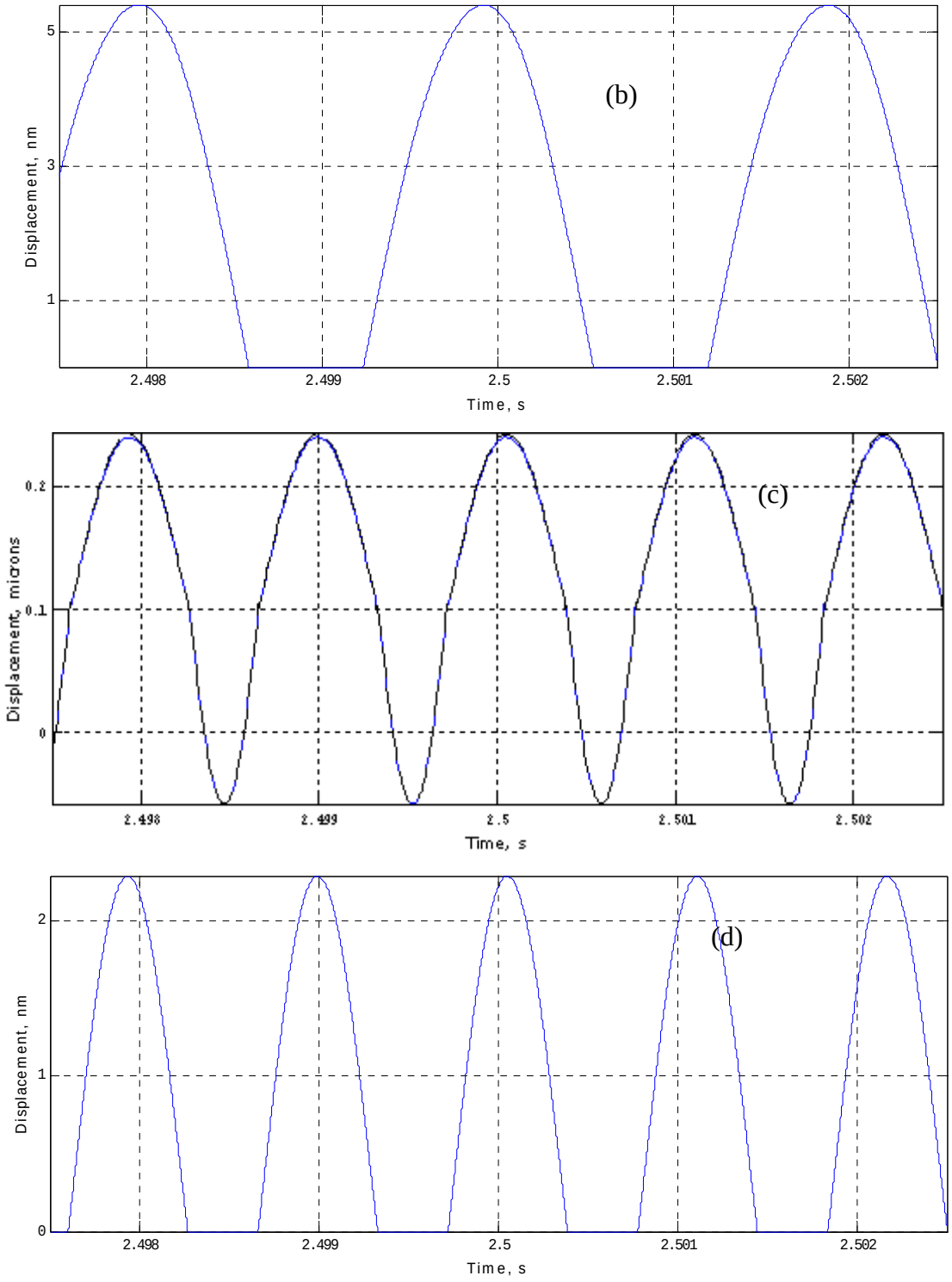

Figure 4.10 (a) & (c) are the displacement responses along the z-direction of nodes 5705(solid line) and 15705 (dashed line) for Case C , Modes 10 & 18; (b) &(d) are the difference of displacements respectively.

4.4 Data Analysis and Results

Since the simulated experimental responses were initially computed at the time step of 1 μs and then down sampled the response data by 10 so that the sampling frequency ($f_{sampling}$) becomes equal to 100 ksamples/s for the responses. The averaged spectra have been estimated for all the simulated measured acceleration responses data keeping the frequency resolution, Δf = 3.052 Hz by using the number data points, N= 32768 for the sampling frequency ($f_{sampling}$) with data overlap of 40%. No window was used for this analysis. Since the excitation frequency band for each mode was the linear chirp-sine excitation, hence ordered spectra were estimated for averaging and the order axis was then converted to the frequency axis by multiplying the order 1 by the excited natural frequency. Total 5s data around the resonance response were used for this calculation. The results are summarised in Table 4.1 and few typical acceleration amplitude spectra in Figures 4.11-4.13 for Case C of the delaminated plate where delamination area is small.

Table 4.1 Summary of the observations for the delaminated plate for Case C

Excitation Mode	Observation made at the measured locations	Figures
1-3, 8-10, 12,17-18, 20	Excited mode and its higher harmonics	Figure 4.11
4, 5, 14	Excited mode, higher harmonics and sub-harmonics	Figure 4.12
6, 7, 11, 13, 15, 16, 19	Excited mode with side bands and their harmonics.	Figure 4.13

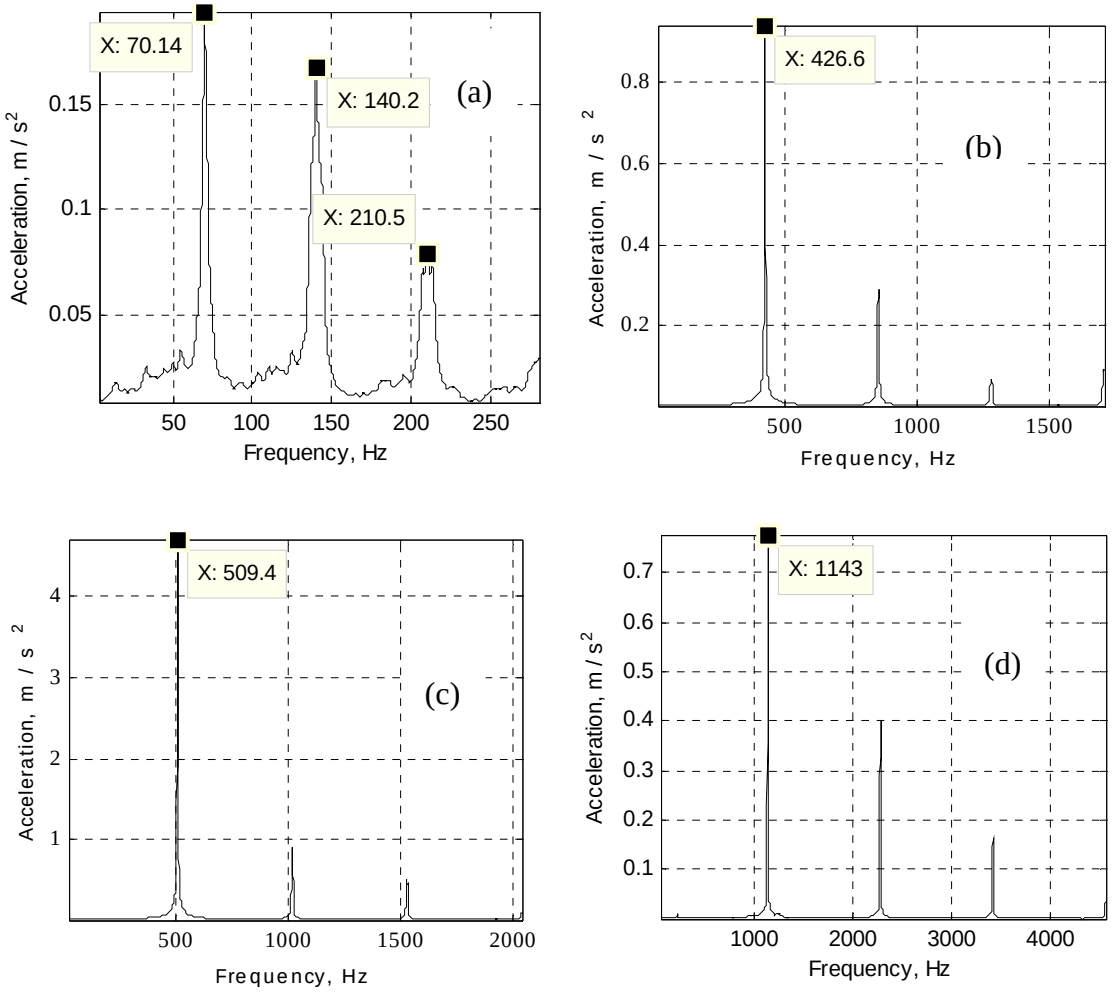

Figure 4.11 Amplitude acceleration spectra at the measurement location 1 for Case C, (a) Mode 1: 70 Hz (b) Mode 8: 427 Hz (c) Mode 10: 509 Hz (d) Mode 20: 1143 Hz

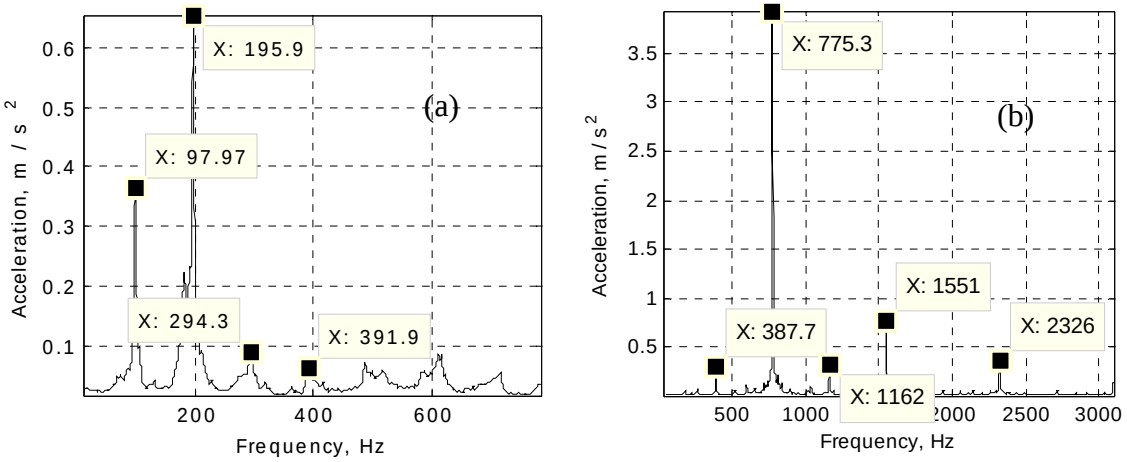

Figure 4.12 Amplitude response spectra at the measurement location 1 for Case C, (a) Mode 4: 196 Hz (b) Mode 14: 775 Hz

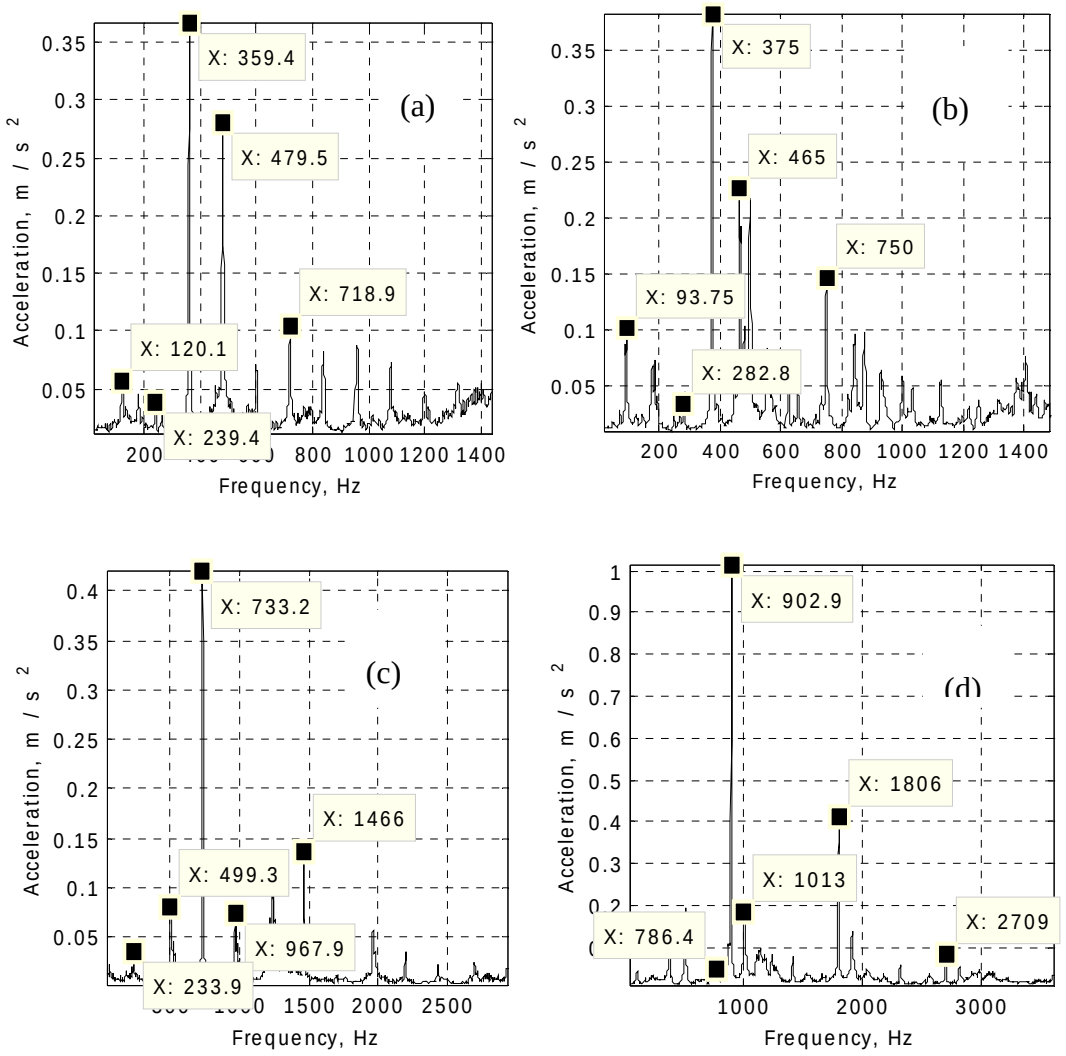

Figure 4.13 Amplitude response spectra at the measurement location 1 for Case C, (a) Mode 6: 359 Hz (b) Mode 7: 375 Hz (c) Mode 13: 733 Hz (d) Mode 16: 903 Hz

It has been observed from Figures 4.11-13 that the harmonics, sub-harmonics or modulation at the excited natural frequencies have been observed clearly in their spectra even for small delamination in Case C. Figure 4.11 shows the presence of the exciting frequency (1x) and its higher multiples (2x, 3x, etc.) which is nothing but higher harmonics of the exciting frequency. For example, the exciting frequency is the 1st mode in Figure 4.11(a) showing the presence of 70.14Hz (1x), 140.20Hz (2x) and

210.50Hz (3x). However the number of other modes shows the appearance of the sub-harmonics and harmonics (0.5x, 1x, 1.5x, 2x, 2.5x, etc.) of the exciting frequency as shown in Figure 4.12. For example, when the plate was excited at Mode 4, the response contain the frequency peaks at 97.97Hz (0.5x), 195.9Hz (the exciting frequency 1x), 294.3Hz (1.5x), 391.9Hz (2x), etc. in Figure 4.12(a). In addition, the 3rd category of the responses has also been observed when excited at some other modes and few typical examples are shown in Figure 4.13. In this category, the appearance of the exciting mode (1x) and its higher harmonics (2x, 3x, etc.) together with the multiple side band frequencies at 1x, 2x, etc. showing modulation with other natural frequency of the delaminated plate. For example, in Figure 4.13(a), the presence of the peak at the exciting Mode 6: 359.4Hz (1x) along with its higher harmonics at the frequencies 718.9Hz (2x), 1078Hz (3x), etc. have been observed together with side band frequencies of 239.4Hz and 479.5Hz at 1x. This indicates the side band frequencies are approximately at equidistant of the frequency120Hz on either side of the frequency peak at 359Hz. The frequency of 120Hz is close to Mode 2 which confirms that the Mode 2 gets modulated with Mode 6 when the delaminated plate has been excited at the Mode 6 due to the nonlinear interaction. All the 3 kinds of the responses have also been observed for the Case B as well. Often the isotropic material shows the appearance of the higher harmonics of the exciting frequency is very common if there is some of kind of nonlinearity exists in the system, e.g., the breathing of a crack in a steel beam [74]. However, the other kinds of the responses seen in the delaminated composite plate could be due to the non-isotropic material properties of the composite structure.

The responses were also estimated for the plate without delamination (Case A). Few typical acceleration spectra for the composite plate without delamination are shown in

Figure 4.14 which shows the response at the excited mode only. It can be seen that there is no harmonic, sub-harmonic or side band when there is no delamination in the composite plate as compared to the delaminated plates.

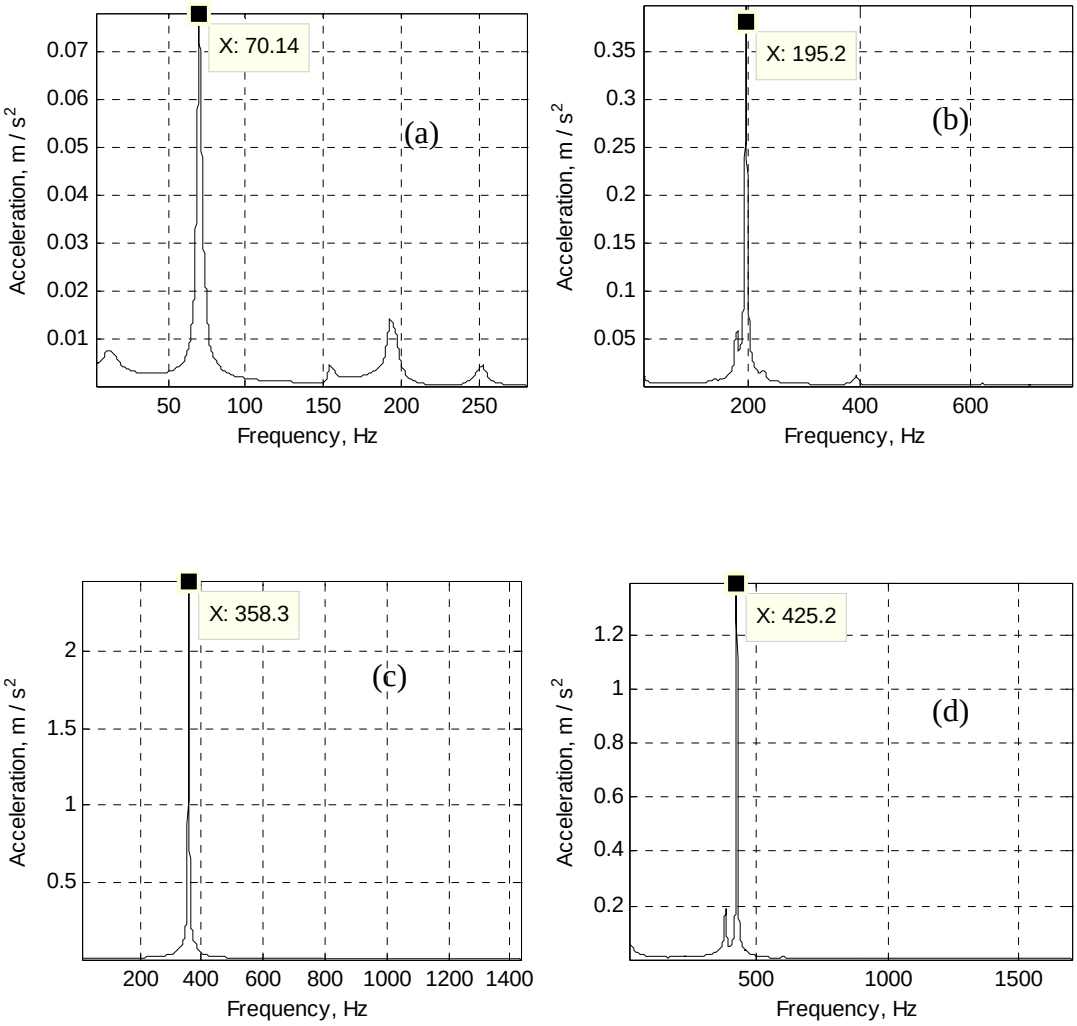

Figure 4.14 Amplitude spectra at the measurement location 1 for Case A (a) Mode 1: 70 Hz, (b) Mode 4: 196 Hz, (c) Mode 6: 359 Hz, (d) Mode 8: 425 Hz,

4.5 Delamination at the centre of the plate

In this case the effect of delamination position has been studied. Here the delamination has been induced at the centre of the composite plate. The delamination layer in the z-direction was assumed same as before (3rd layer from top and 5th layer from bottom). This example has been referred as Case D. Here the pair of nodes at the delamination centre are 5481 and 15481. The delamination area has been kept as 30mm x 30mm similar to plate C. The comparison of the computed natural frequencies of the Case D with Case A (Healthy condition) is shown in Figure 4.15. No significant change in the natural frequencies has been observed.

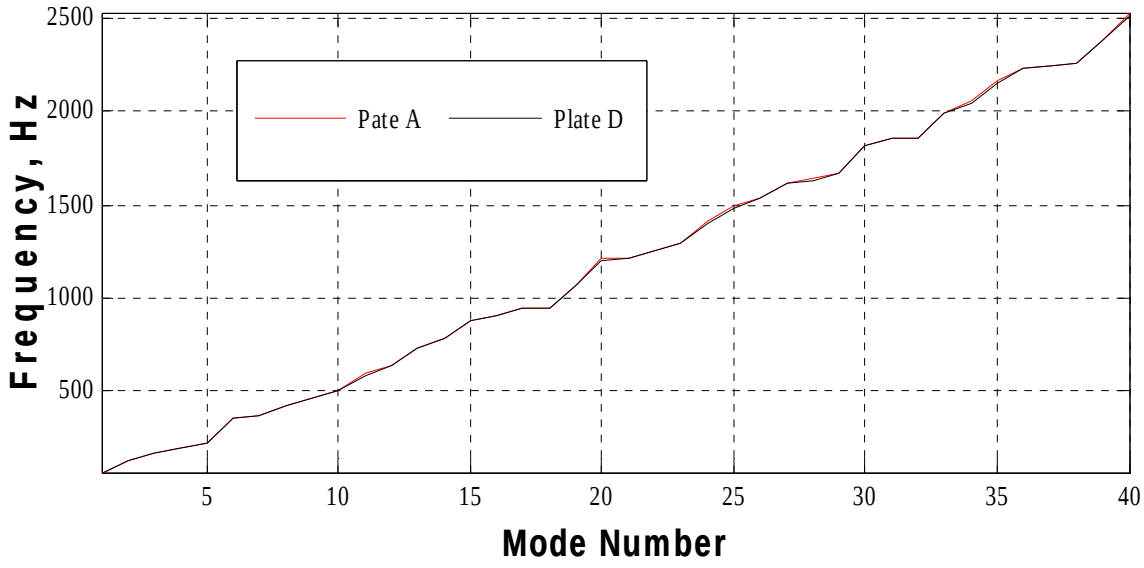

Figure 4.15 Natural frequencies with mode number for Cases A and D of the composite plate

4.6 Observations

The simulated measured acceleration responses have been estimated upto mode 20 exactly similar to the simulated experiments in Section 2.1 i.e., no change in the

excitation and measurement locations and the computational parameters. The results are summarised in Table 4.2 and few typical acceleration amplitude spectra in Figures 4.16-18.

Table 4.2 Summary of the observations for Case D (delamination at the centre)

Excitation Mode	Observation made at the measured locations	Figures
1-7,9-10, 14-19	Excited mode and its higher harmonics	Figure 16
8, 12	Excited mode, higher harmonics and sub-harmonics	Figure 17
11,13, 20	Excited mode with side bands and their harmonics.	Figure 18

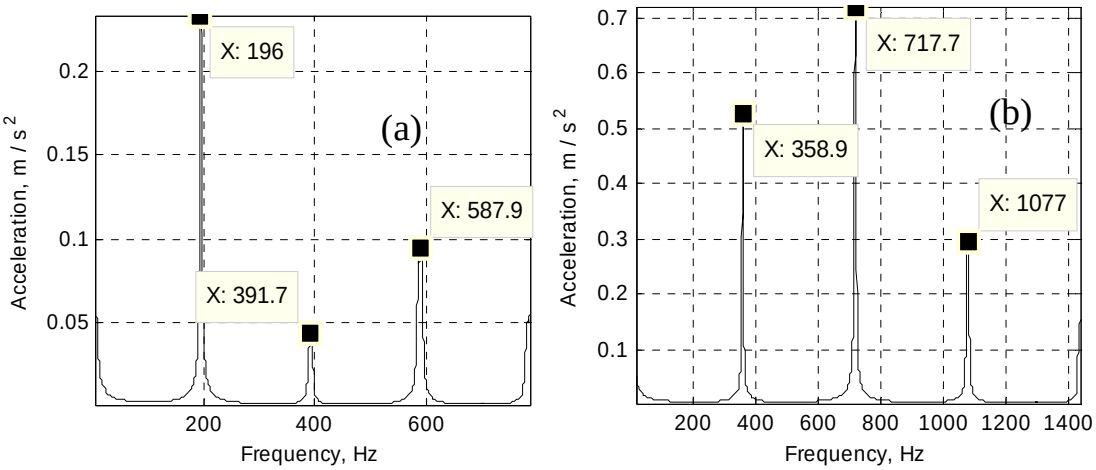

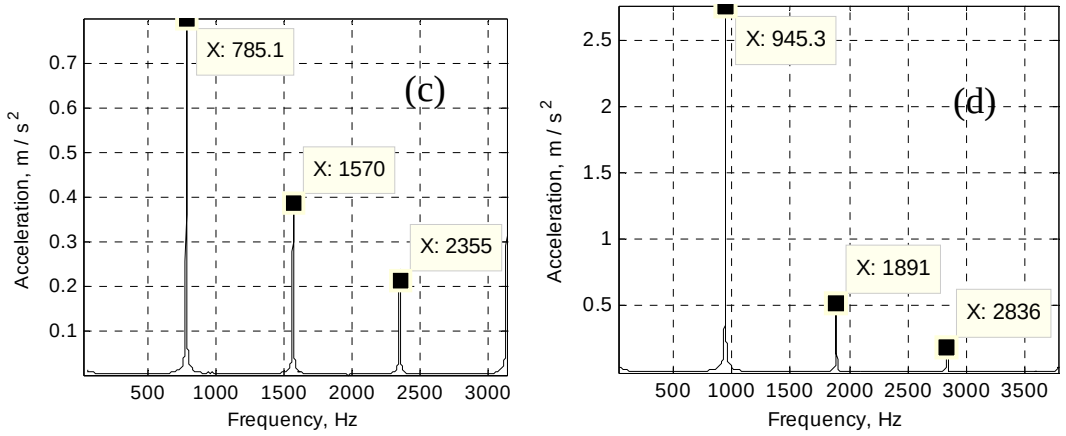

Figure 4.16 Amplitude spectra at the measurement location 1 for Case D, (a) Mode 4: 196 Hz, (b) Mode 6: 359 Hz, (c) Mode 14: 785 Hz, (d) Mode 18: 945 Hz

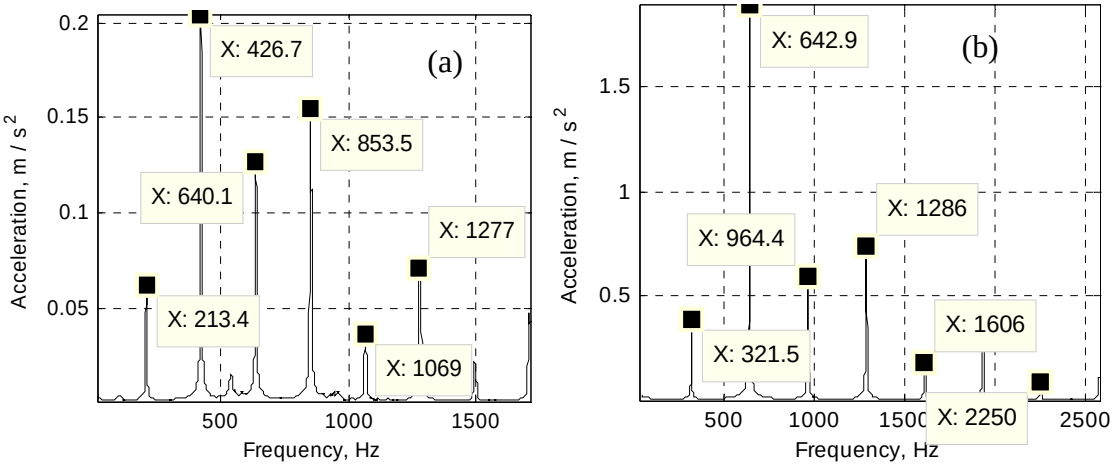

Figure 4.17 Amplitude spectra at the measurement location 1 for Case D (a) Mode 8: 427 Hz, (b) Mode 12: 643 Hz

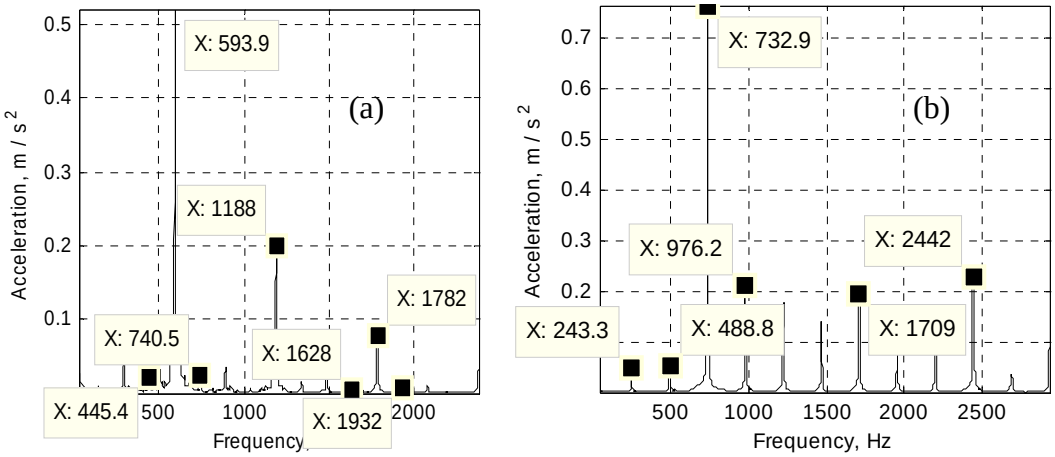

Figure 4.18 Amplitude spectra at the measurement location 1 for Case D, (a) Mode 11: 594 Hz, (b) Mode13: 732 Hz

4.7 Discussion

It has been observed that there is no significant change in natural frequencies for small delamination area as in Cases of C and D irrespective of their delamination position in the plate. However the acceleration responses at all the measured locations show nearly common features like harmonics, sub-harmonics and/or modulation at the excited mode for all delaminated Cases –B to D. These observations are summarised in Table 4.3. Hence these 3 kinds of features in the measured responses can be used to detect the presence of the delamination in the composite structure.

Table 4.3 Summary of the observations for all Cases of the composite plate

Measured Acceleration Responses	Excited Modes			
	Case A	Case B	Case C	Case D
Harmonics only	Response at Excited Modes only	1-7, 9-11, 13, 14, 18, 19	1-3, 8-10, 12,17-18, 20	1-7,9-10, 14-19
Sub-harmonics and harmonics		20	4, 5, 14	8, 12
Side Bands at excited mode and their harmonics		8, 12, 17	6, 7, 11, 13, 15, 16, 19	11,13, 20

4.8 Experimental Example

In the absence of composite plates with delamination, a very simple experiment has been conducted on Aluminium plates with and without delamination to confirm and understand the existence of the nonlinear interaction between delaminated layers that was assumed in the simulated examples. Experimental setup is shown in Figure 3.1. Figure 3.1 shows the Aluminium sample (glued plate) is fixed on one edge. The data were analysed online using a 2-channel FFT analyser and also recorded on a Laptop computer using a 16-bit, 8-channel data acquisition Analogy-to-Digital card. The data were recorded at a sampling frequency of 100ksamples/s. In the initial experiments, the impulse-response modal test [28] was carried out using an instrumented hammer (Model 086C03, M/s PCB) to find the natural frequencies. Then sine excitation was applied at the few experimentally identified modes. A few typical acceleration amplitude spectra are shown in Figure 4.19 for the delaminated plate. The higher harmonics of the excited modes can be seen in the acceleration amplitude spectra. However, no harmonic components can be observed in the acceleration spectra for the plate without delamination (Figure 4.20). This observation confirms the presence of the nonlinear interaction in the delaminated region in the delaminated plate. The experimental observations made here are same as the authors' earlier study using a simple simulated example of a cantilever beam made of steel with a small delamination, in which the presence of the exciting frequency and its higher harmonics were observed [72]. However, the other two phenomena revealed in this study, namely the presence of the sub-harmonic components and the modulation, must be related to the anisotropic material properties of the composite structure. These are further investigated in Section 4.9.

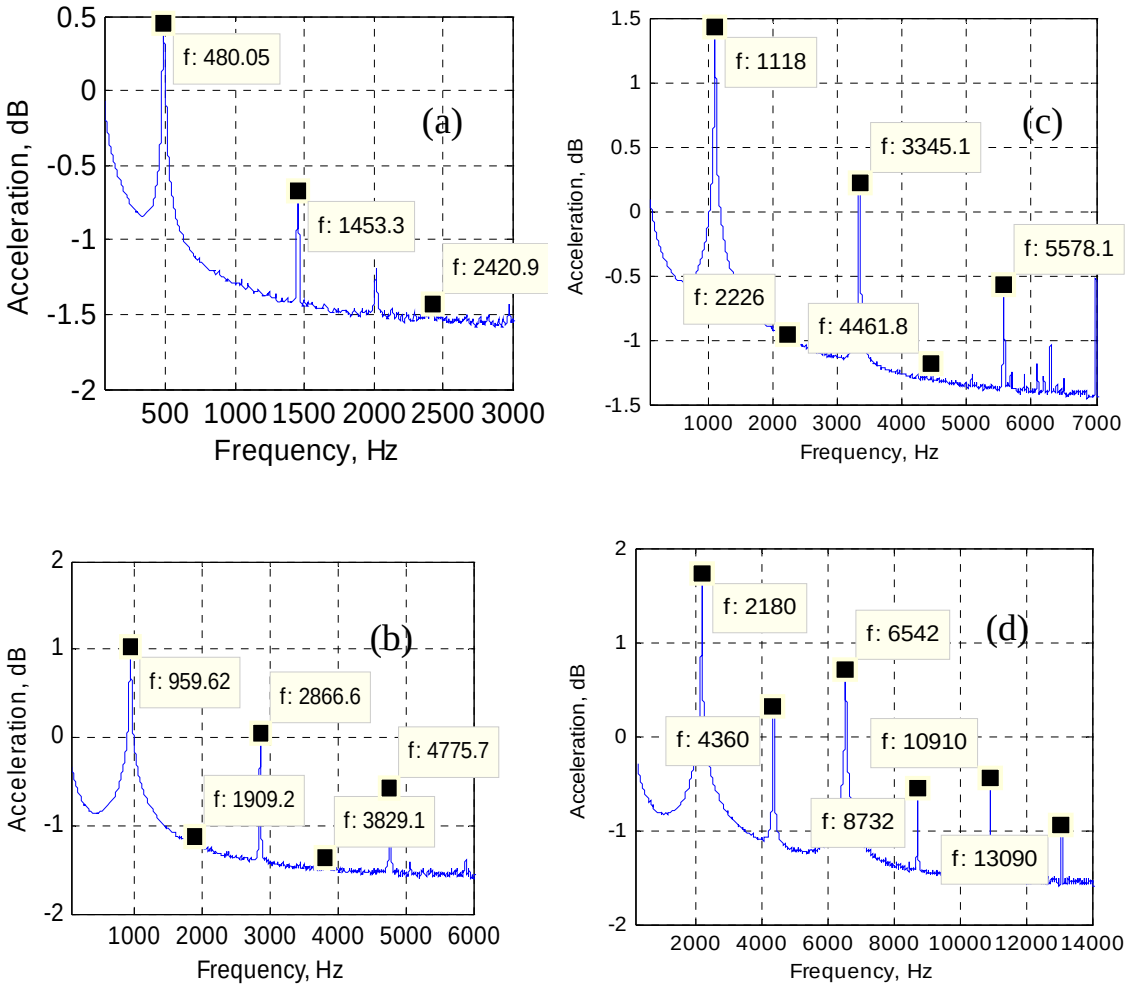

Figure 4.19 Typical measured acceleration amplitude spectra of the delaminated aluminium plate when excited at (a) 480 Hz, (b) 960 Hz, (c) 1118 Hz, (d) 2180 Hz

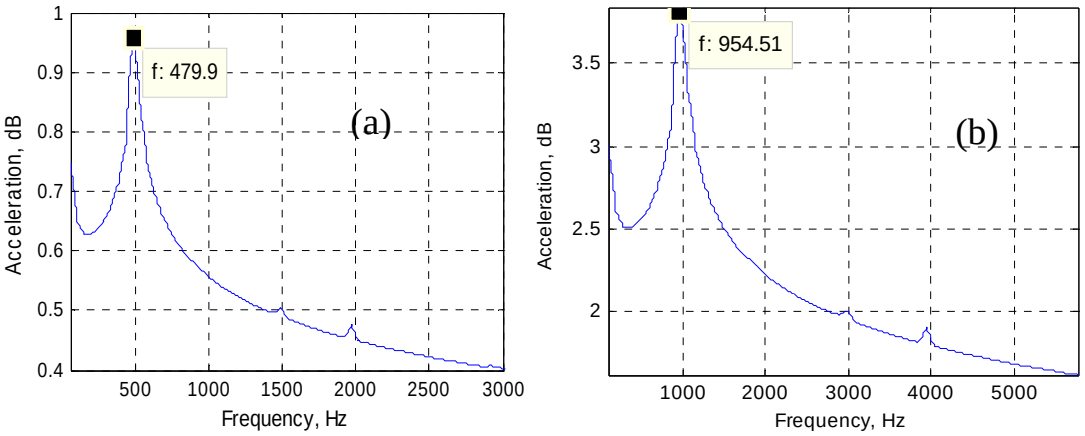

Figure 4.20 Typical measured acceleration amplitude spectra of the healthy aluminium plate when excited at (a) 480 Hz, (b) 960 Hz

4.9 Comparison with the earlier published results

Section 4.8 confirms the presence of the nonlinear interaction between the delaminated layers, but could not produce all the 3 features, presence of (a) higher harmonics, (b) harmonics and (c) modulated response for the delaminated plate, as observed in the simulated examples. However the experimental results on the delaminated composite plates by Polimeno *et al.* [75], Meo *et al.* [76], and Solodov *et al.* [77] shows the presence of all these features which are shown in Figures 4.21-4.23. Figure 22 [75] shows the presence of higher harmonics, the presence of the modulated response in Figure 23 . [76] for the delaminated carbon/epoxy plate and the presence of subharmonic component in Figure 24 [77] for the delaminated C/C-SiC composite plate with increasing amplitude of vibration during the experiments. Hence, the experimental observations shown in Figures 4.21-4.23 validate the observation made on the simulated examples on the delaminated plates.

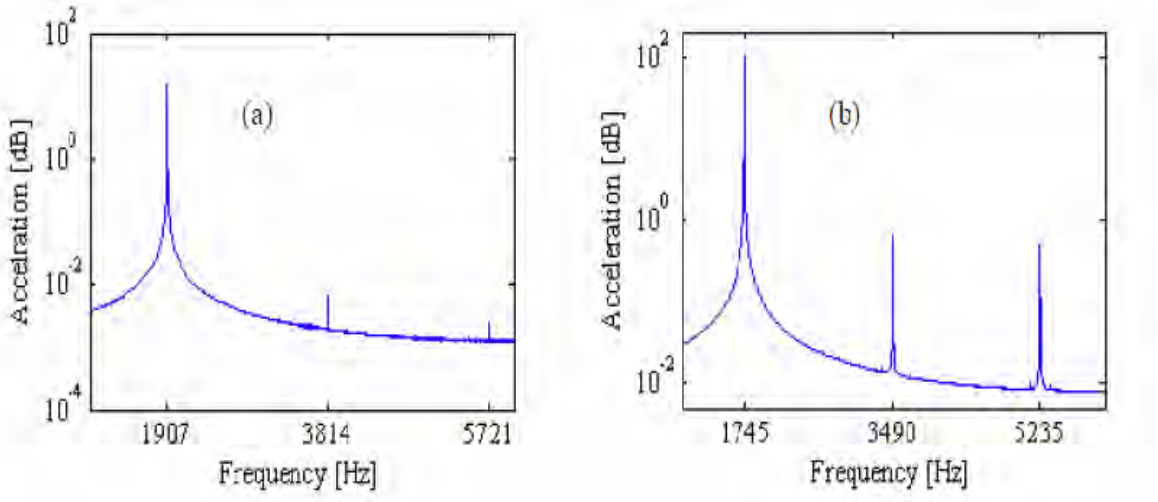

Figure 4.21 Typical experimental spectrum for the delaminated plate showing presence of higher harmonics **[75]**

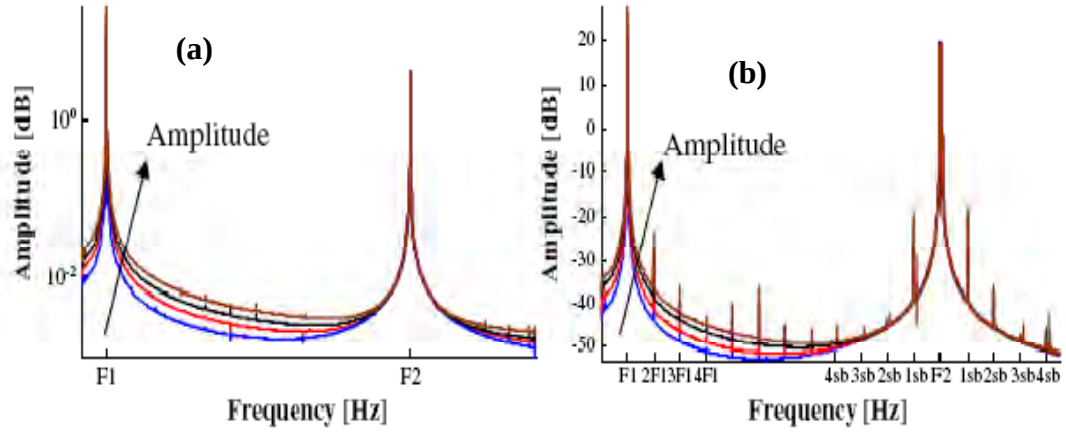

Figure 4.22 Typical experimental spectra for the composite plate, (a) the healthy plate, (b) delaminated plate showing presence of modulated response **[76]**

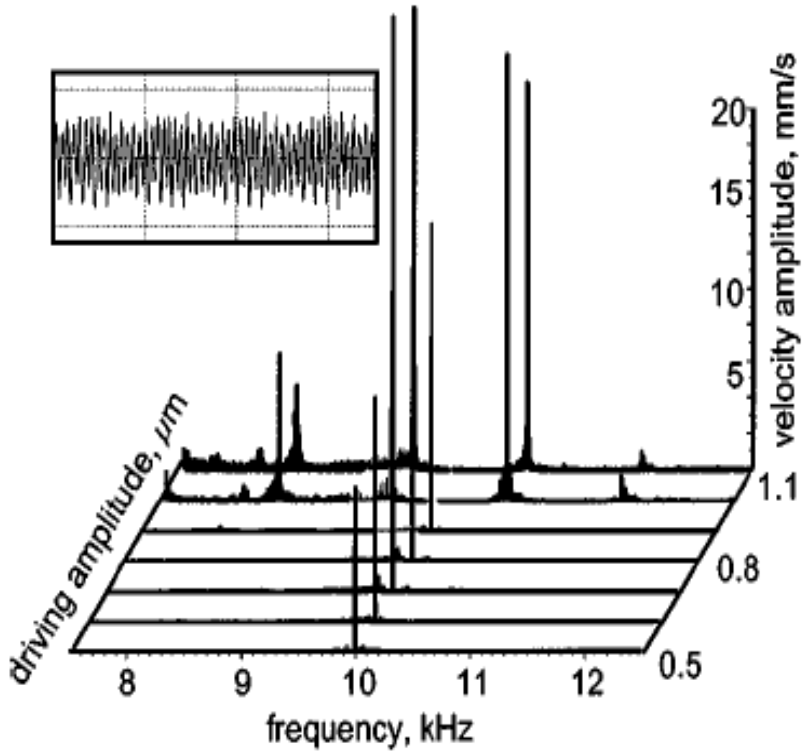

Figure 4.23 Typical experimental spectrum for the delaminated plate showing presence of sub-harmonic component **[77]**

4.10 Summary

The dynamics of the composite plate with 3 different cases of the delamination have been discussed. FE models of the chosen carbon fibre composite plate with different size and location of delaminations have been developed and then the responses were estimated when excited at the number of modes using the mode-superposition method. The mode-superposition method was slightly modified to realise the nonlinear interaction between the delaminated layers. The 3 different features have been observed in their acceleration responses when excited at the number of modes. These features are the presence of the harmonics of the excited modes, the presence of the sub-harmonic and higher harmonics of the excited modes and the modulated response of the exiting modes with the other mode and their higher harmonics. In fact, the appearance of these 3 features is irrespective of the delamination size and location. Hence, these 3 features can be used to detect the presence of the delamination in the composite plate. A simple test on a composite plate made of aluminium with delamination have also confirmed the existence of the nonlinear interaction between the delaminated layers which resulted in the presence of higher harmonics when excited at number of modes. But the presence of the side bands or sub-harmonics has not been observed in the present experiments probably due to the fact that the isotropic material has been used in the experiment. Hence this needs further tests on the delaminated composite plates which are under preparation. The detection of the delamination location will also be explored when the experiment on the composite plate will be conducted.

CHAPTER 5
EVALUATING PERFORMANCE OF EIGHT TYPES OF FINITE ELEMENTS USING EXPERIMENTAL RESULTS

5.1 Introduction

To simulate nonlinear interaction between the delaminated layers explicit dynamic analysis is the best and fastest option due to very small time step [78] needed to solve the problem, as compared to implicit dynamic analysis. In chapter 4 the ABAQUS element C3D8I was used for modal analysis and the ABAQUS version used was 6.6. Element C3D8I was not available in ABAQUS Explicit library [78] and hence it was not possible to simulate the dynamics of composite plates using ABAQUS Explicit library. Modified mode superposition method was used in Matlab to simulate the nonlinear interaction. The method lacks in considering impact energy transfer which can occur due to the excitation of the composite plate. The element C3D8I was introduced into the ABAQUS Explicit library for the first time in ABAQUS 6.7 [78]. In this chapter dynamics of composite plates has been compared between the experimental results and the prediction by the finite element (FE) models using different element types in the ABAQUS FE code (version 6.9). Looking at the literature review of the ABAQUS finite elements used for the dynamic analysis of thin composite plates with and without delamination it was found that different researchers used different elements available in ABAQUS element library [79]. No proper guidelines were found in any research paper to date about a specific element used. This inspired the author of this thesis to work on all the elements, available so far in the ASBAQUS explicit element

library and examine the results, and dedicate this chapter to the discussion on different element usage and performance.

5.2 Finite Element Selection

There are a number of elements available in high performance FE (finite element) code ABAQUS for the dynamic analysis for thin composite plates. In the recent years a total of 8 different element types in the ABAQUS code have been used by the researchers to develop the FE model of composite structures in their studies. These elements are the 3D planar shell elements (S4R, S8R and S8R5), the 3D continuum shell (SC8R) and the solid elements (C3D8I, C3D8R, C3D20R, C3D8R). The details of the each element are listed in Table 5.1. It is important to note that the quadratic elements S8R, S8R5 and C3D20R and the linear S4R5 elements are not supported by the ABAQUS Explicit module; hence these 4 elements are only useful for the computation of natural frequencies. The advantage of the elements S4R and SC8R is that they have control over the numerical difficulty of hour-glassing, however the element C3D8I (added to ABAQUS Explicit recently) completely overcome this problem. In the earlier studies, these 8 elements have been used for the FE modelling for the composite structures and very limited studies compared the calculated natural frequencies with the experimentally identified modes. However the calculated dynamic responses by the FE models have not been compared with the experimentally measured responses in most of the earlier studies. Hence, in the present study, a total of 8 FE models have been developed and their predications have been compared with the experimental observations so the usefulness of the each FE model can be assessed.

Table 5.1 ABAQUS Element's details

Element Type	Description	Type/Behaviour	Explicit
S4R	4-node shell, reduced integration	Linear, hourglass control, finite membrane strains	Yes
S4R5	4-node shell, reduced integration	Linear, hourglass control, finite membrane strains	No
S8R	8-node shell, reduced integration	Quadratic, doubly curved thick	No
S8R5	8-node shell, reduced integration	Quadratic, doubly curved thin	No
SC8R	8-node quadrilateral in-plane general-purpose continuum shell	Linear, reduced integration with hourglass control, finite membrane strains.	Yes
C3D8I	8-node solid brick	Linear, incompatible modes	Yes
C3D8R	8-node solid brick, reduced integration	Linear, hourglass control	Yes
C3D20R	20-node solid brick, reduced integration	Quadratic, hourglass control	No

Initially the calculated natural frequencies and the acceleration responses when excited at first 4 modes by the FE models were compared the experimental results for a healthy composite plate (without delamination) and then for a composite plate with a small delamination. The paper presents the observations made on the 8 FE models.

5.3 Modal Testing

The modal tests were conducted for the composite plate using the sweep-sine excitation in the frequency band of 0 to 500 Hz initially and then the impulse-response modal test has been carried out using the instrumented hammer (Model 086C03, M/s PCB) to find out the natural frequencies. The measured data for both the tests were collected to the computer through an 8-channels 16-bit data acquisition card for the further analysis. The natural frequencies were then identified using the frequency response functions (FRFs) computed from the measured force and acceleration data. Typical impact force and the measured responses and their FRF plot are shown in Figures 5.1 and 5.2. The experimentally identified modes are listed in Table 5.2 and Table 5.3.

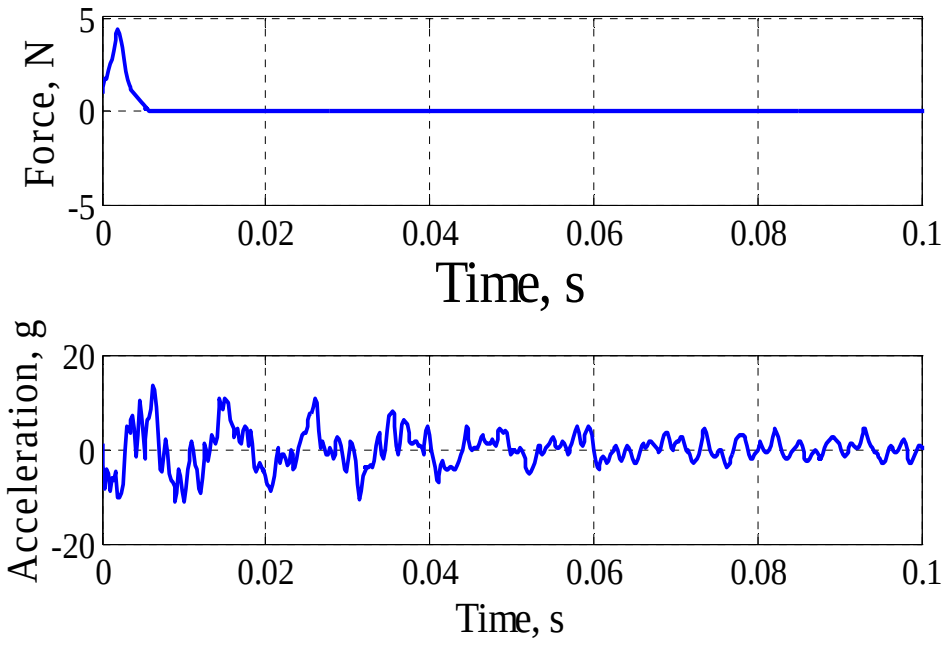

Figure 5.1 Typical applied impulsive load (a) and the measured acceleration response (b) during Impulse-Response Tests

5.4 Finite Element (FE) Models

The number of the FE models for the test composite plate has been constructed in the ABAQUS 6.10 FE code using the different elements used earlier in the literature for the modelling of the composite structures. This has been done to carry out the comparative study for all FE models with the experimental results. The different elements used are listed in Tables 5.2 and 5.3. An element size of 10 mm x 10 mm has been used for each layers resulting in 1600 elements in the case of 3D planar shell elements (S4R, S8R, and S8R5) and 12800 elements in case of 3D continuum shell (SC8R) or solid (C3D8I, C3D8R, C3D20R, C3D8R) for a plate. Hence, altogether 8 FE models have been constructed. A typical modelling mesh for all the FE models is shown in Figure 5.4. The boundary condition has been assumed to be free-free on all edges. The distribution of the mass of the portable shaker shown in Figure 3.2(a) has also been added to the appropriate nodes to each FE model so that the FE analysis can be directly compared with the experimental results.

The modal analysis for the FE models has been carried out. The calculated frequencies are also listed in Table 5.2 and compared with the experimental values. It can be seen that the calculated natural frequencies are nearly close to the experimental values except. First six mode shapes for the composite plate using most commonly used 3D planar shell element S4R are shown in Figure 5.3.

It has been observed that the pattern of mode shapes is similar using all elements except solid element C3D8R (for the same mesh size) which gives higher values due to hour-glass effect.

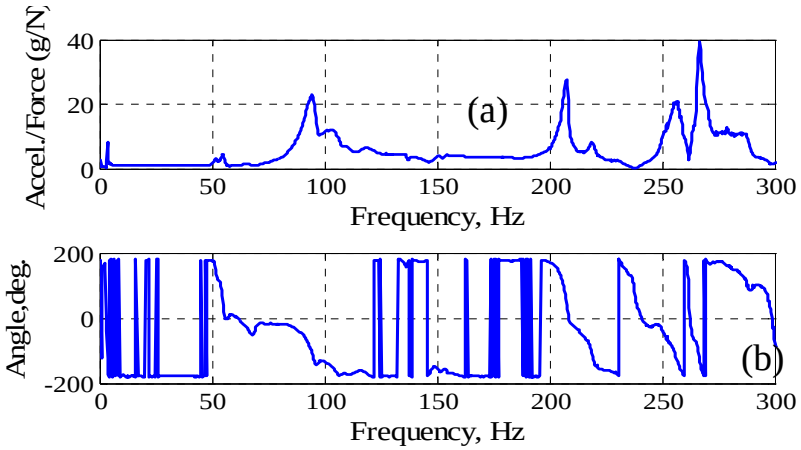

Figure 5.2 Typical FRF plot (a) FRF amplitude, (b) FRF phase

Table 5.2 Comparison of Natural Frequencies of FE models using different 3D planar shell elements with experimental values

Mode	Experimental	Element Type (using ABAQUS)			
		S4R	S4R5	S8R	S8R5
1	58.03Hz	47.24Hz	47.33Hz	47.16Hz	47.24Hz
2	94.54	100.796	100.797	100.704	100.717
3	130.27	133.974	133.976	133.849	133.863
4	141.44	143.118	143.318	142.867	143.045
5	160.27	166.673	166.844	166.43	166.589
6	211.12	219.878	220.073	219.405	219.418
7	263.55	265.968	266.477	265.367	265.85

Table 5.3 Comparison of Natural Frequencies of FE models using different 3D solid/continuum shell elements with experimental values

Mode	Experimental	Element Type(using ABAQUS)			
		C3D8R	C3D20R	SC8R	C3D8I
1	58.03 Hz	98.11 Hz	47.16 Hz	47.40 Hz	45.88 Hz
2	94.54	127.038	100.692	99.9688	99.35
3	130.27	188.616	133.826	130.693	127.74
4	137.44	258.641	142.855	142.539	142.52
5	153.27	316.63	166.426	161.741	158.97
6	211.12	404.19	219.019	241.233	220.40
7	263.55	451.947	265.404	264.923	265.51

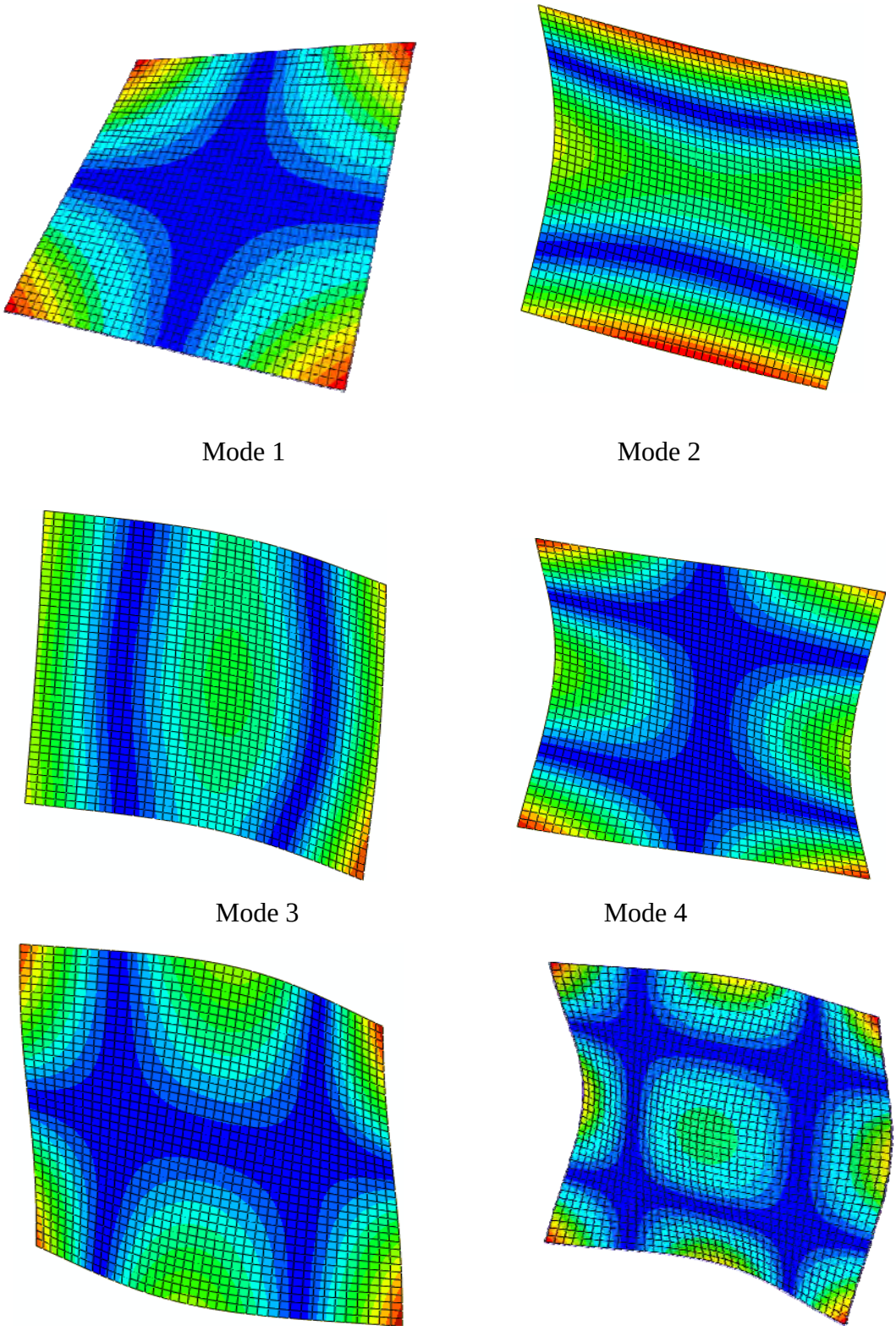

Figure 5.3 Numerical mode shapes of the few modes of the composite plate

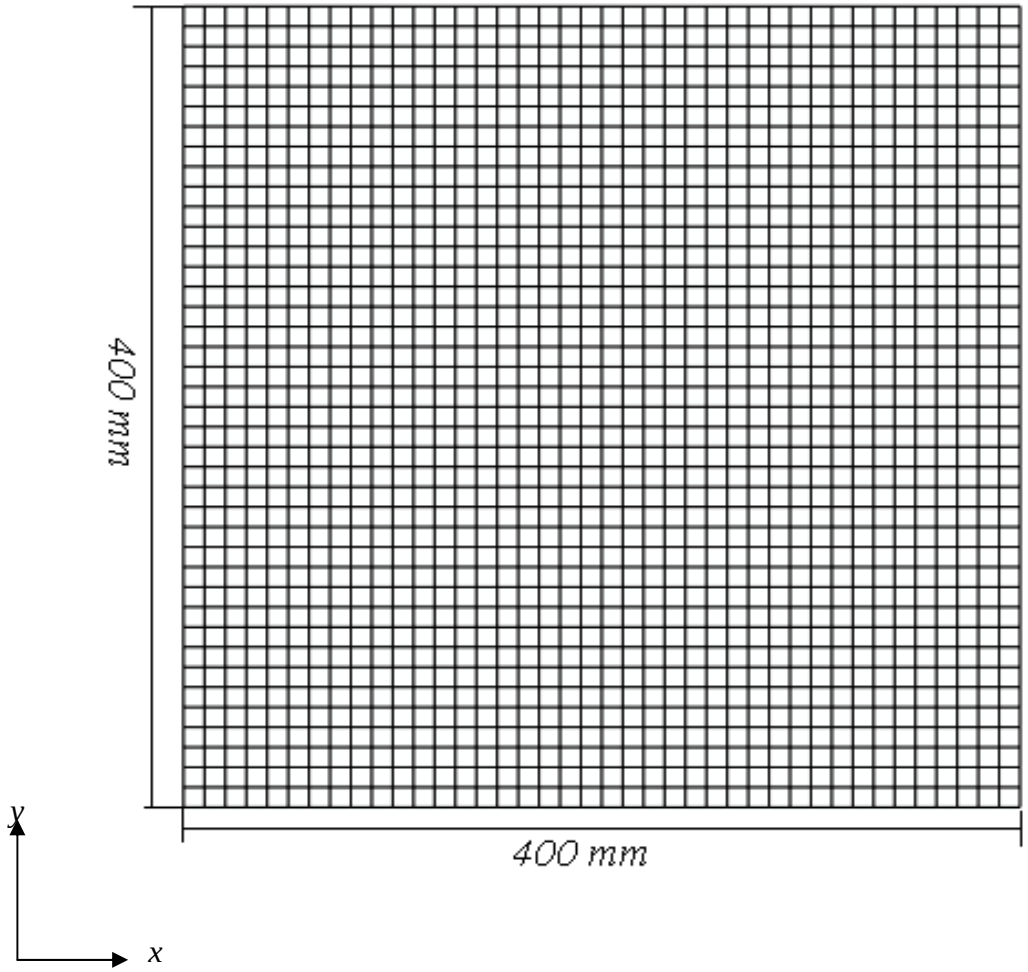

Figure 5.4 An FE model of the test composite sample E-glass fibre

Experimental mode shapes for few modes were also calculated from the acceleration response data of the 25 measuring points. Few typical experimental mode shapes are shown in Figure 5.5. It can be seen in both Table 5.2 and Table 5.3 that the computed natural frequencies by the FE model using C3D8R elements missed number of modes, however remaining 7 FE models produced nearly same natural frequencies as observed experimentally.

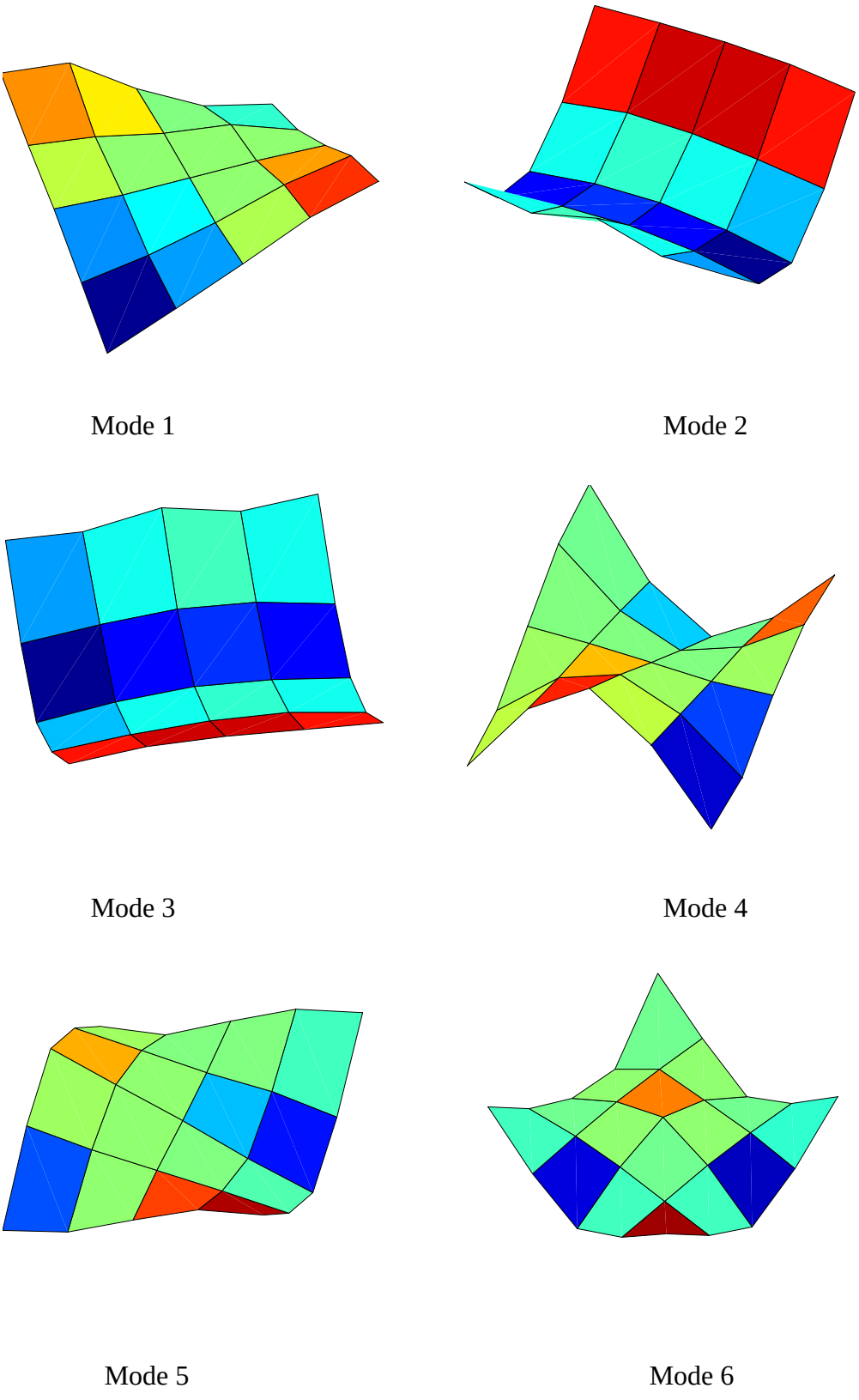

Figure 5.5 Experimental mode shapes of the few modes of the composite plate

The small difference between the computed natural frequencies and the experimental values except for the first mode may be either related to small manufacturing problem of the test sample especially prepared for this test or little error in the distribution of the shaker mass into the FE models. The relatively large error in the first mode seems to be consistent with the earlier observation made by [80]. They confirmed in their study that the free-free test may not fully realised the ideal free-free condition which results in slightly higher 1^{st} first natural frequency in the experiment compared to the computed one. Hence, it can be concluded that the remaining 7 FE models (except C3D8R FE model) can compute the accurate natural frequencies for the composite structures.

5.5 Comparison of the Measured and Computed Responses

The remaining 7 FE models were further examined by comparing the computed responses with the experimentally measured responses to understand which FE models are useful for the dynamic response estimation.

5.5.1 Response Measurement

In the experimental phase, the composite plate was excited through the piezo-electric shaker (Model PS-X03, M/s ISI-SYS) shown in Figure 2 at each mode. The steady state acceleration responses were then measured at the 25 locations of the composite plate as shown in Figure 3.10. The data were collected to the PC through the 16-bit 8-channels data acquisition device at the sampling frequency of 20 kHz. The data have then been analyzed to compute the amplitude spectra. Few typical measured acceleration amplitude spectra at the modes 1, 2 and 3 are shown in Figure 5.6. It has been observed that the number of modes appear in the spectra even when excited at a mode. For

example, Figure 5.6(a) shows the response at the Modes 3, 4, 7 and possible higher modes when excited only at the mode 1.

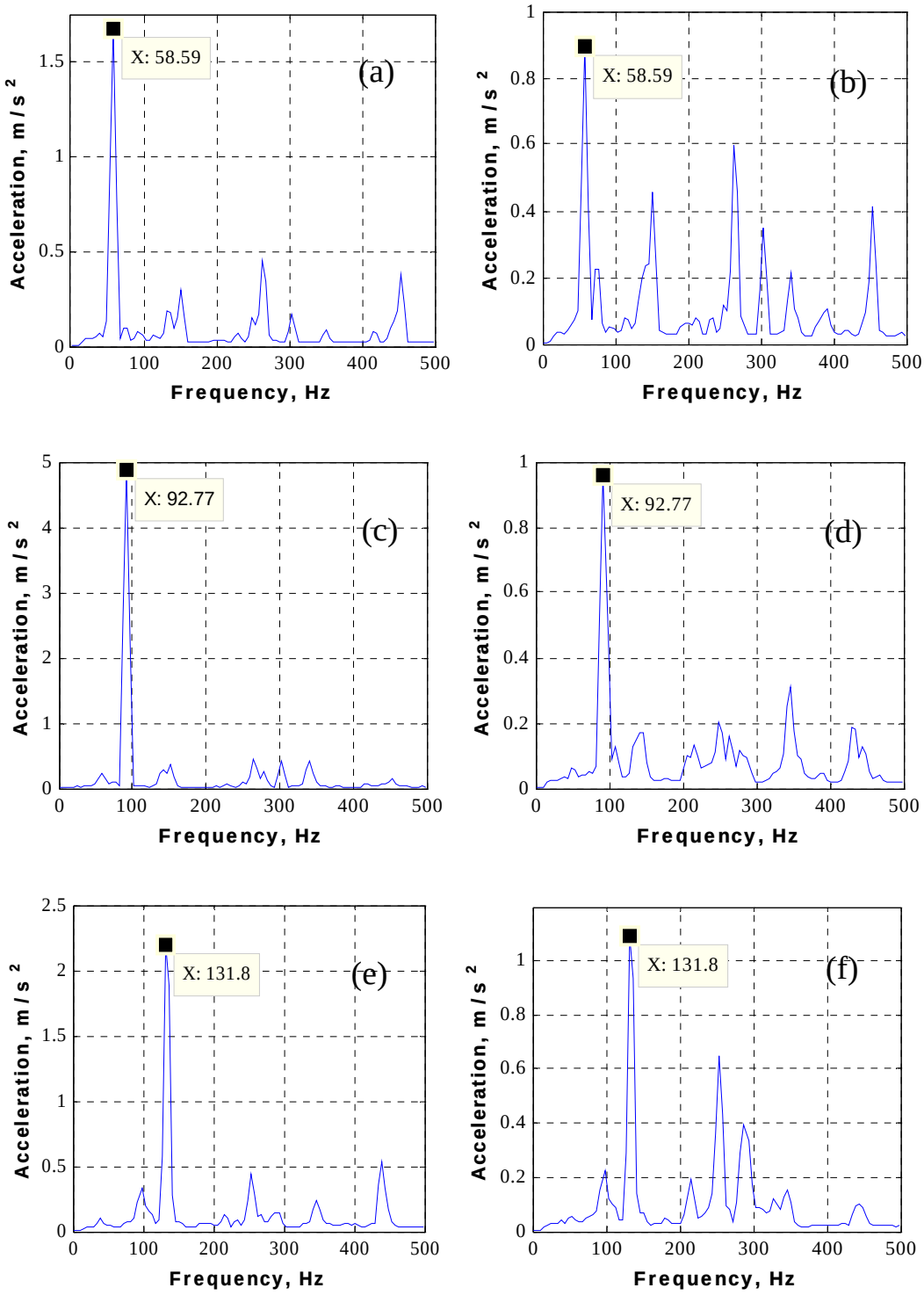

Figure 5.6 Measured acceleration spectra at coordinates (50mm, 50mm) and (150mm, 275mm), (a)-(b) for Mode 1, (c)-(d) for Mode 2 and (e)-(f) for Mode 3

5.5.2 Response Estimation by the FE Models

Similar to the experiment, the acceleration responses were computed from the FE models when sinusoidal input excitation was given to the shaker location at each mode. However it important to note that the out of the 7 remaining FE models, the 3 FE models using the quadratic elements S8R, S8R5 and C3D20R and the 1 FE model using the linear S4R5 elements don't support the explicit dynamic analysis as discussed in Table 5.1. Hence, the remaining 3 FE models using S4R, SC8R and C3D8I elements have further been examined by comparing the computed responses with the experimentally measured responses. The best fit proportional damping coefficients were calculated from the experimentally obtained damping values for each mode in the ABAQUS code for the computation of the responses. Table 5.4 compares initial step time used by ABAQUS and the computed time for 0.1 s response data and the element C3D8I relatively took more time due to the small stable time step used in the computation. All computation has been carried out on a 4x Intel Itanium2 Montecito Dual Core 1.6GHz/8MB cache (i.e. 8 cores per node) and 16GB RAM. The amplitude spectra for the computed acceleration responses from the 3 FE models have then been computed. Few Typical acceleration spectra are shown in Figures 5.7-5.9.

Table 5.4 Step time and CPU time for explicit analysis (0.1 second response)

Element Type	S4R	SC8R	C3D8I
Initial Step time (s)	1.229E-06	1.172E-07	5.789E-08
Computational time (Hours)	0.42	26.92	47.66

5.6 Comparison of Results

It has been observed that the laminated plates show the appearance of different modes even when excited at a mode similar to the experimental observations shown in Figure 5.6. However, the computed acceleration spectra by the FE models using SC8R and C3D8I elements match closely to the experiments compared to the FE model using S4R elements. This study confirms that the 2 FE models, one using SC8R elements and other C3D8I elements, are good for both the modal analysis and the dynamic analysis for the composite structures. Further study has also been carried to understand the use of these 2 FE models when a composite structure with delamination.

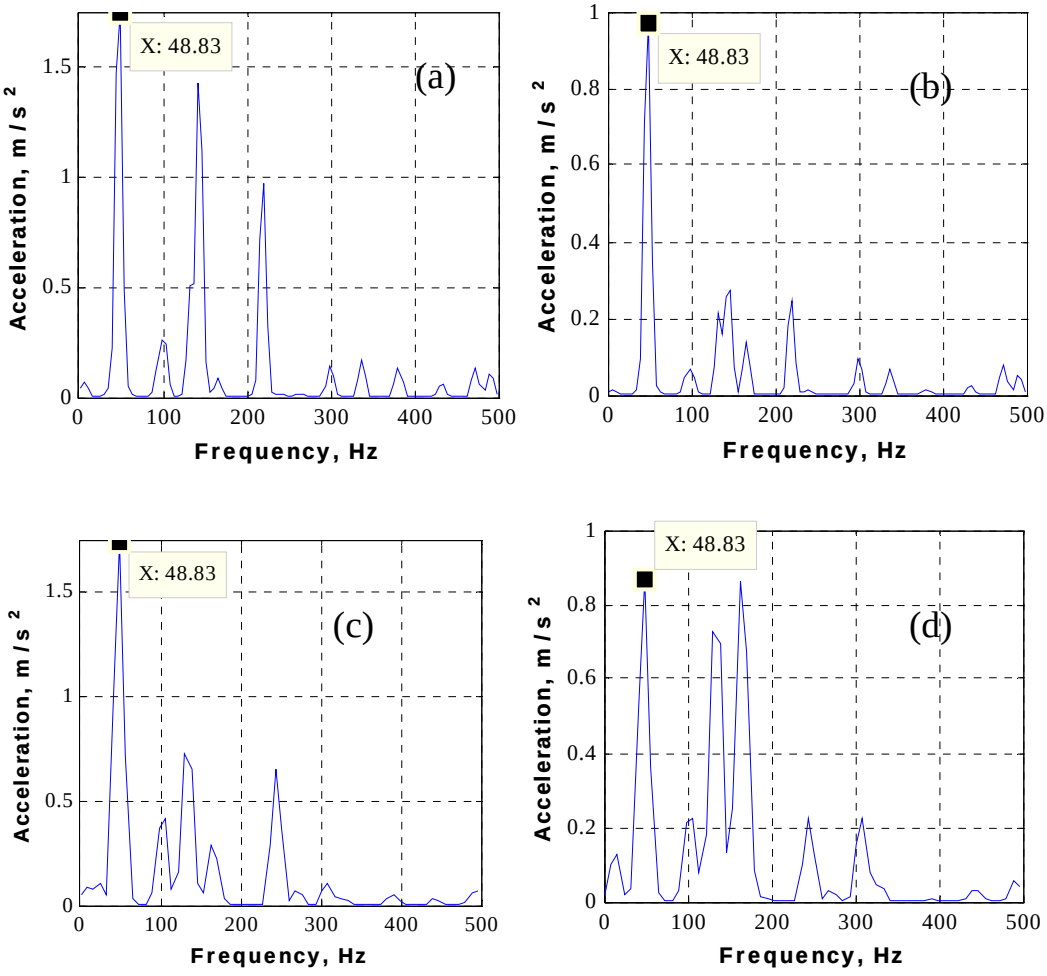

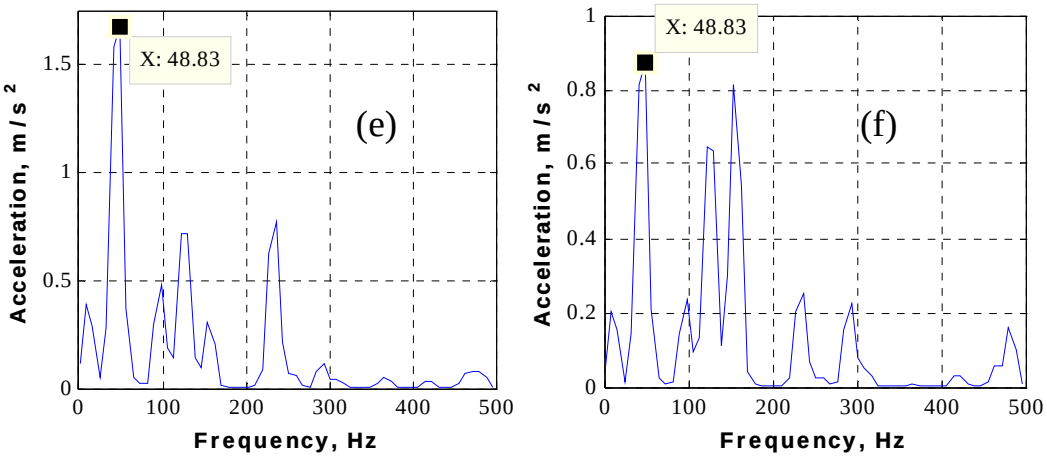

Figure 5.7 Estimated acceleration response spectra at mode 1 at coordinates (50mm, 50mm) and (150mm, 275mm), (a)-(b) S4R, (c)-(d) SC8R and (e)-(f) C3D8I

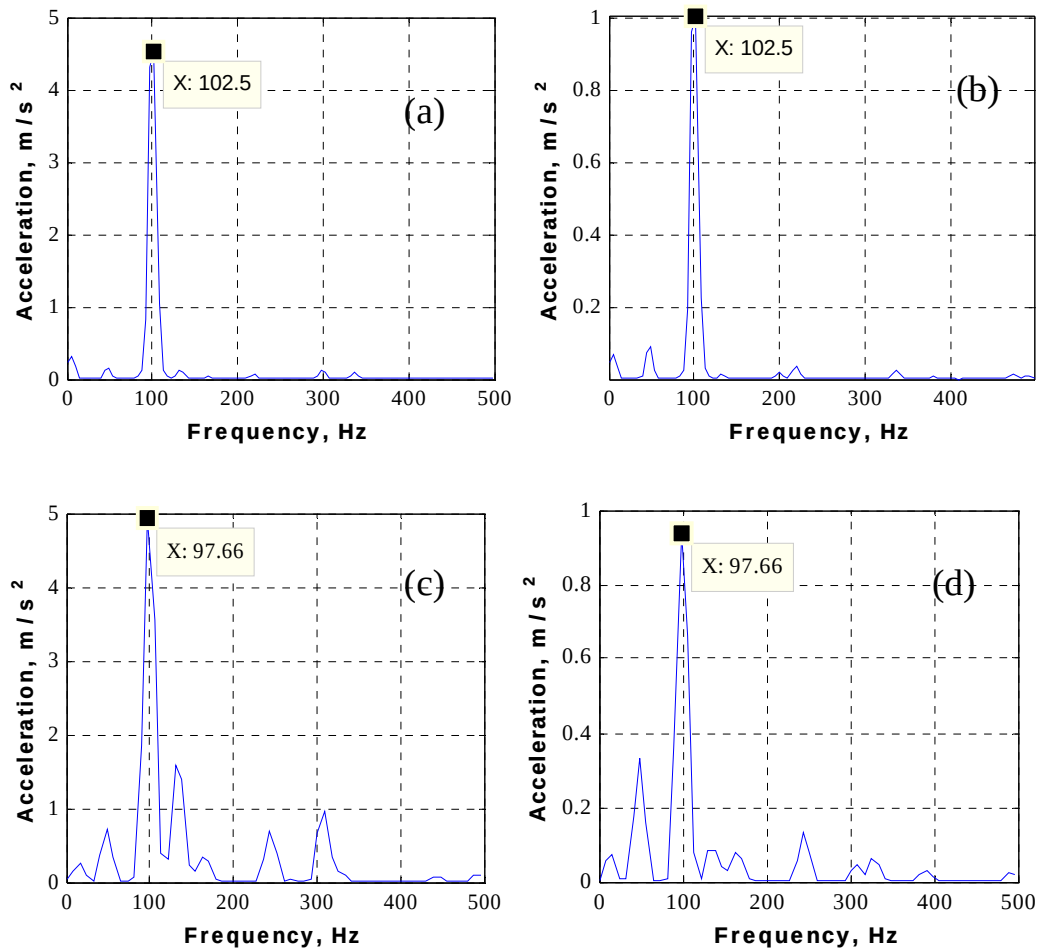

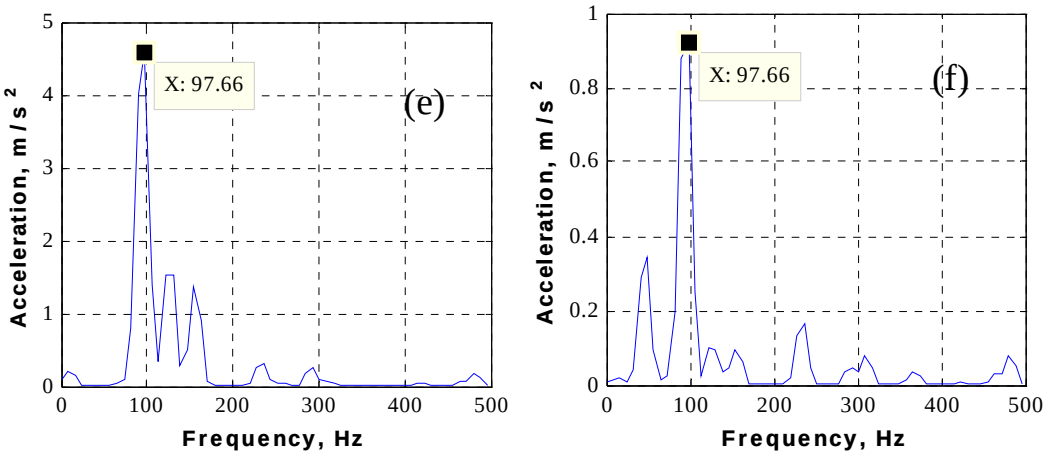

Figure 5.8 Estimated acceleration response spectra at mode 2 at coordinates (50mm, 50mm) and (150mm, 275mm), (a)-(b) S4R, (c)-(d) SC8R and (e)-(f) C3D8I

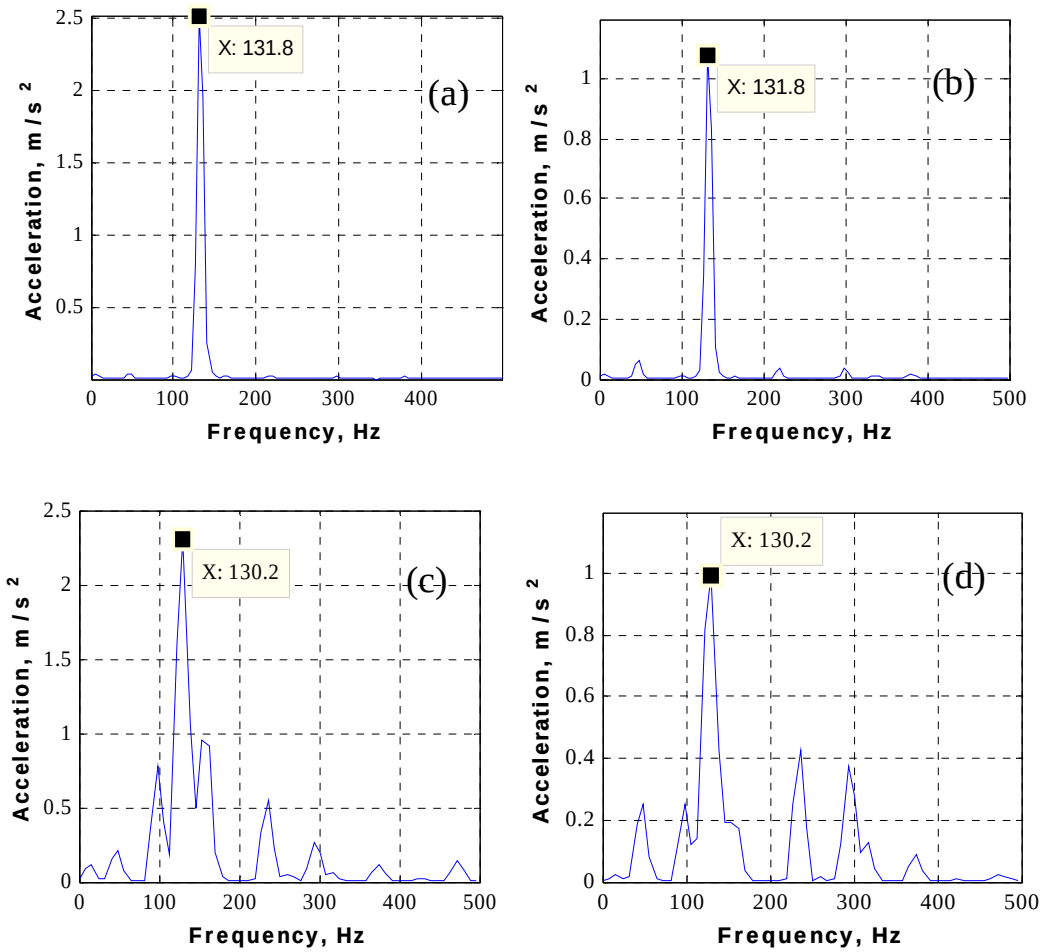

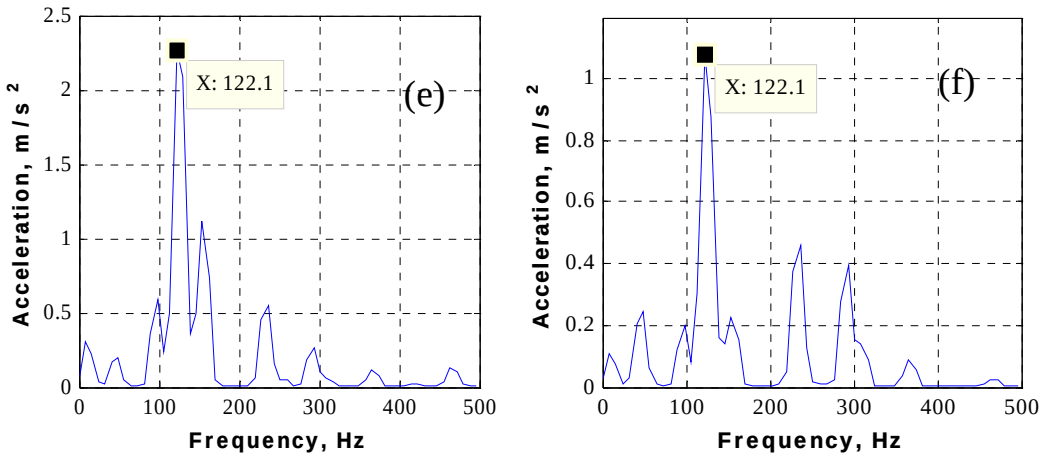

Figure 5.9 Estimated acceleration response spectra at mode 3 at coordinates (50mm, 50mm) and (150mm, 275mm), (a)-(b) S4R, (c)-(d) SC8R and (e)-(f) C3D8I

5.7 An Example of a Delaminated Plate

An another composite plate of same dimension and material properties as shown in Figure 3.8 has also been prepared with a embedded delamination of size 40mm x 40mm between the third and the fourth layer from top which is shown in Figure 3.8. Here again, the measurement scheme same as shown in Figure 3.9 has been adopted. Initially the modal testing has been done to identify the natural frequencies and then the responses were measured when excited at each mode. The frequencies 57.21 Hz, 92.45 Hz, 133.22 Hz, 140.40 Hz, 154.11 Hz, and 262.37 Hz have been identified as the first 7 modes. These values are closed to the healthy composite plate (Tables 5.2 and 5.3) as expected because such a small delamination may not influence the natural frequencies significantly. Few typical measured acceleration spectra are also shown in Figures 5.10.

The 2 FE models, one using SC8R elements and other C3D8I elements, have also been constructed for this delaminated plate. The element size was kept same as earlier for both FE models and the delamination region was modelled by creating duplicate nodes

at the delamination interface such that the coinciding nodes in the delaminated region have separate identity. The computed natural frequencies by both the FE models were observed to be closely matching with the experimentally identified modes. The dynamic responses were also computed when excited at each mode. However, during the response computation, the nonlinear between the delaminated layers was also included using the ABAQUS function explicit dynamic analysis together with the general contact analysis [11]. Figures 5.11 and 5.12 show the acceleration spectra of the estimated responses by both FE models at the measurement locations of coordinates (50mm, 50mm) and (150mm, 275mm) for the direct comparison with measured spectra in Figure 13. It can be observed that although the element C3D8I is computationally a bit more expensive than the element SC8R, the results from the former are more nearer to the measured ones.

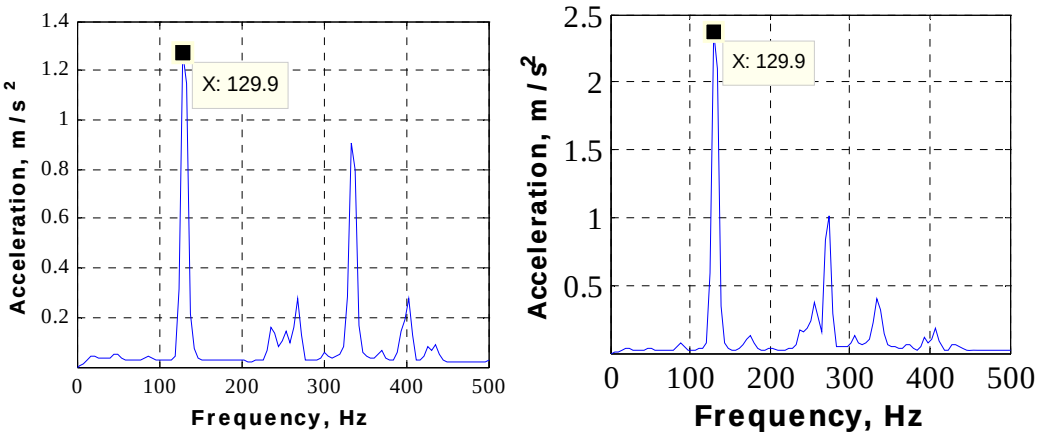

Figure 5.10 Measured acceleration spectra at Mode 3 at coordinates (a) (50mm, 50mm), (b) (150mm, 275mm)

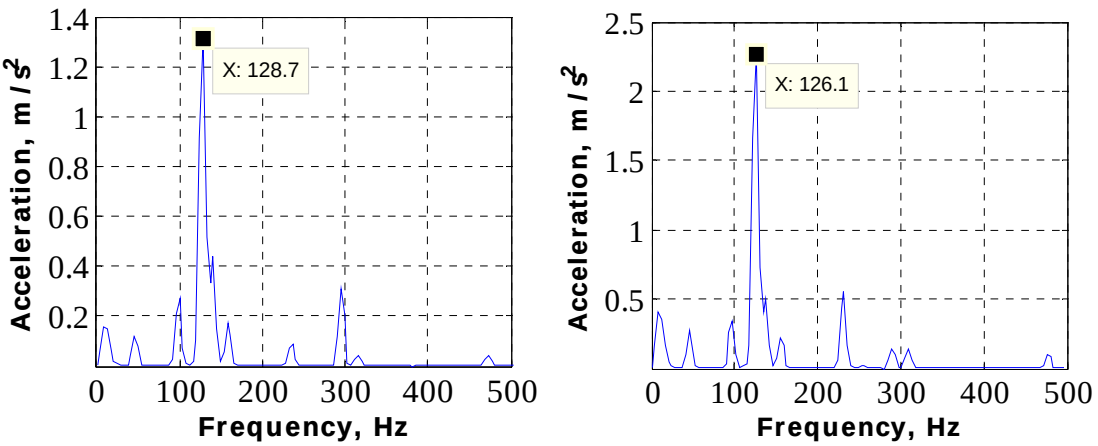

Figure 5.11 Estimated acceleration spectra at Mode 3 at coordinates (a) (50mm, 50mm), (b) (150mm, 275mm) using element SC8R

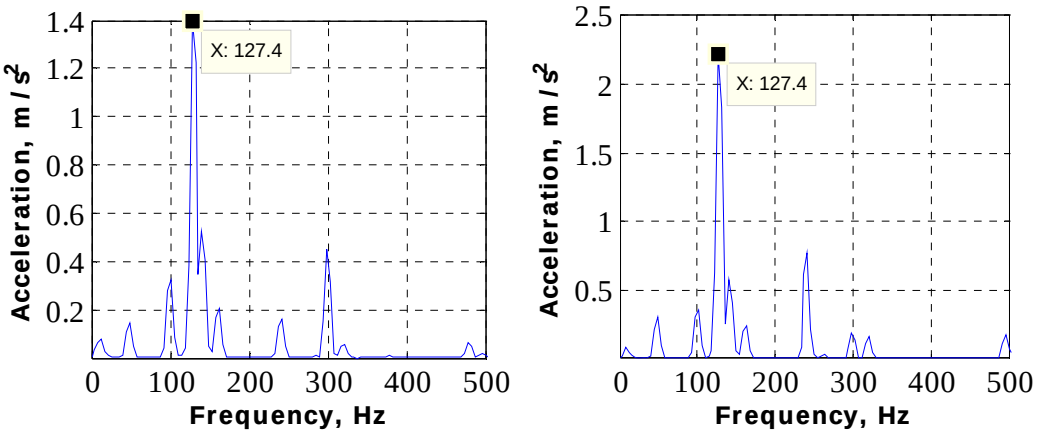

Figure 5.12 Estimated acceleration spectra at Mode 3 at coordinates (a) (50mm, 50mm), (b) (150mm, 275mm) using element C3D8I

5.8 Summary

A total of 8 FE models using the 8 different element types in the FE ABAQUS have models were then evaluated with the experimental results. Out of 8 models, 7 models found to be useful for the modal analysis except the FE model using element C3D8R. Of the remaining 7 FE models, only 2 FE models using the elements SC8R and C3D8I show good agreement with the experimentally measured responses for the healthy

composite plate. Further investigation on a composite plate with a small delamination confirms that the FE model using the element C3D8I is possibly an appropriate model for the simulation of the non-linear interaction between the delaminated layers and to predict the responses close to the experiments. Hence the FE model using the element type C3D8I seems to be suitable for modelling the thin composite structure with and without delamination for different dynamic analysis based on the observations from the present study.

CHAPTER 6
USE OF STATISTICAL PARAMETERS FOR DELAMINATION DETECTION IN COMPOSITE PLATES

6.1 Introduction

This chapter discusses the observations made on the measured vibration responses from both healthy and delaminated plates and the possibility of delamination detection from the use of statistical parameters obtained from the values of the experimental vibration data. Statistical parameters like kurtosis, crest factor, and root mean square (RMS) have been computed for the composite plates (healthy, off-centre, and in-centre delaminated plate) using vibration response (acceleration) data when excited at a few lower modes. The observations have also been compared for three different shaker locations (Figure 3.10) used for the excitation. It has been observed that the averaged normalised RMS provides a very good indicator for the delamination detection irrespective of the excitation location.

However it is important to note that the acceleration responses using accelerometer at large number of locations for any real structure may not be practically feasible, hence the method has further been tested on the measured velocity responses. It is because the laser vibrometer can be used to scan the large surface of any structure quickly which can remove the limitation of vibration measurement at number of locations using accelerometers. Hence the measured acceleration responses were converted to velocity response data and then the proposed method of the RMS has been applied. It has been observed that the results are once again consistent with the earlier observations made of

the acceleration data. The method has then been verified on the numerical simulations of both healthy and delaminated plates. The test plate made of E-glass fibre and epoxy resins has been used here. A piezo-electric shaker has been used to excite the plate and the acceleration responses were measured using the number of accelerometers (Figure 3.8). The chapter presents the methods, experimental results [79] and theoretical validation.

6.2 Modal Testing

The modal tests were conducted for all the plates (healthy & faulty). The natural frequencies were then identified using the frequency response functions (FRFs) computed from the measured force and acceleration data. The experimentally identified modes with shaker locations, shown in Figure 3.10(a-c), are listed in Tables 6.1-6.3

Table 6.1 Comparison of the experimental natural frequencies at shaker location 1

Mode	Healthy Plate	Faulty Plate (in-centre delamination)	Faulty Plate (off- centre delamination)
1	58.03 Hz	55.56 Hz	57.46 Hz
2	92.85 Hz	94.05 Hz	92.45 Hz
3	130.27 Hz	130.65 Hz	133.22 Hz
4	137.44 Hz	138.11 Hz	140.40 Hz
5	153.27 Hz	156.77 Hz	155.01 Hz
6	211.12 Hz	204.34 Hz	211.25 Hz

7	263.55 Hz	266.06 Hz	262.37 Hz
8	344.89 Hz	362.45 Hz	354.21 Hz

Table 6.2 Comparison of the experimental natural frequencies at shaker location 2

Mode	Healthy Plate	Faulty Plate (in-centre delamination)	Faulty Plate (off- centre delamination)
1	56.21 Hz	54.27 Hz	53.89 Hz
2	88.59 Hz	91.22 Hz	87.91 Hz
3	130.50 Hz	128.25 Hz	127.59 Hz
4	136.85 Hz	132.52 Hz	133.34 Hz
5	162.36 Hz	155.88 Hz	156.55 Hz
6	224.65 Hz	212.62 Hz	209.43 Hz
7	267.23 Hz	262.06 Hz	261.87 Hz
8	341.89 Hz	336.45 Hz	351.57 Hz

Table 6.3 Comparison of the experimental natural frequencies at shaker location 3

Modes	Healthy Plate	Faulty Plate (in-centre delamination)	Faulty Plate (off- centre delamination)
1	54.89Hz	55.56 Hz	52.91 Hz
2	95.21 Hz	87.66 Hz	86.87 Hz

3	127.66 Hz	130.65 Hz	126.49 Hz
4	138.32 Hz	135.11 Hz	133.55 Hz
5	157.26 Hz	156.77 Hz	152.54 Hz
6	218.06 Hz	204.34 Hz	207.77 Hz
7	265.11 Hz	262.06 Hz	260.44 Hz

6.3 Response Estimation

The steady state acceleration responses were collected from 25 locations. The data were collected to the PC through the 16-bit 8-channels data acquisition device at the sampling frequency of 20 kHz. The data have then been analyzed to compute the amplitude spectra. The amplitude spectra for the estimated acceleration responses when sinusoidal excitation was used for the first 8 modes have been computed and compared between the healthy and the delaminated plates. Several Typical acceleration spectra are shown in Figure 6.1. It has been observed that both healthy and delaminated plates show the appearance of different modes even when excited at one mode; however amplitude of vibration at the other modes when excited at the mode observed to be generally higher for the delaminated plate compared to the healthy plate.

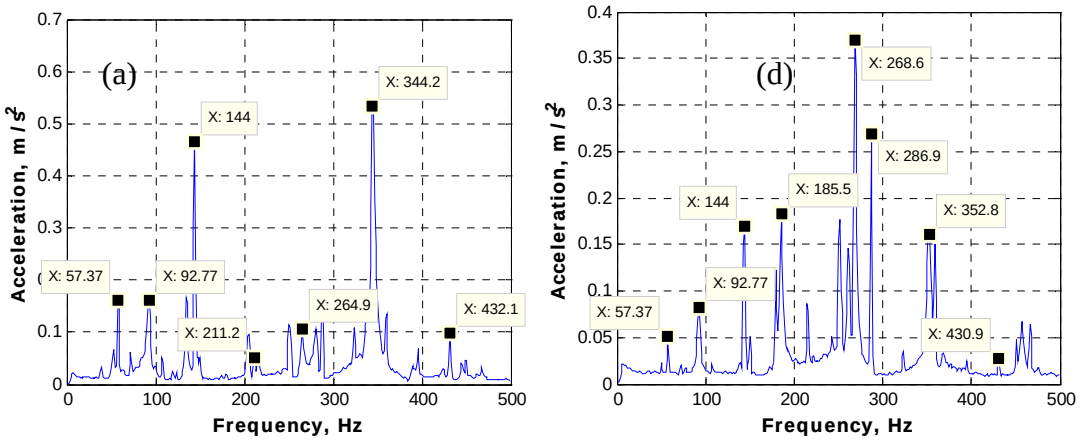

Mode 1 at the location (200mm, 200mm)

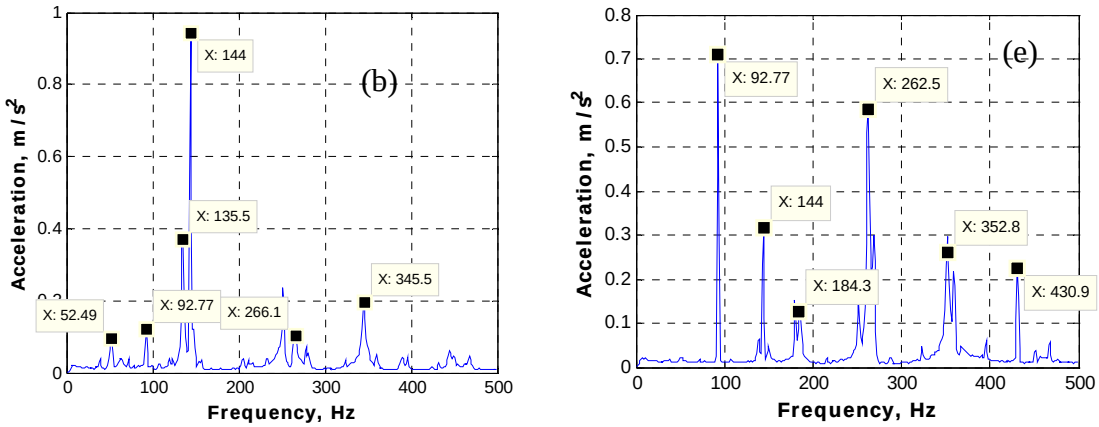

Mode 2 at the location (125mm, 200mm)

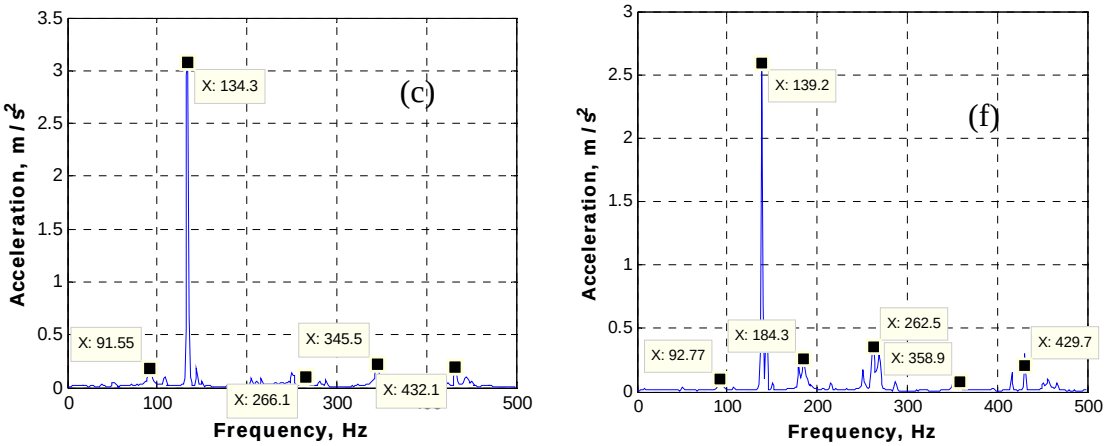

Mode 3 at the location (50mm, 275mm)

Figure 6.1 Typical measured acceleration amplitude spectra at first 3 modes, (a) to (c) for Healthy plate, (d) to (f) for Delaminated plate

6.4 Statistical Parameters

In an attempt to develop a method of delamination detection the acceleration response data were used to perform statistical analysis. The section is dedicated to some introduction to the different statistical parameters used in this research study. The non-dimensional statistical parameters like Kurtosis (*ku*), Crest Factor (CF), etc. and the root-mean square (RMS) value of any vibration signal have generally been used to detect the presence of impulsive nature in the signal [81]. The nonlinear interaction between the delaminated layers of the composite structures is also expected to show such signal in their responses when excited externally. Hence these parameters have been computed to explore the early detection of delamination. A brief description of these parameters and how these have used in the present study have been discussed here.

- **Kurtosis:** Let's assume that the measured vibration response at the location, *i* when excited at mode, *p* is $x_{i,p}(t)$. Kurtosis can then be calculated as

$$ku_{i,p} = \frac{M_{i,p}^{4}}{\left(M_{i,p}^{2}\right)^{2}} \tag{6.1}$$

where $M_{i,p}^{2}$ and $M_{i,p}^{4}$ are the 2nd and 4th moment of the signal, $x_{i,p}(t)$. The q^{th} moment of the signal, $x_{i,p}(t)$ is defined as

$$M_{i,p}^{q} = \frac{1}{N}\sum_{r=1}^{N}\left(x_{i,p}(t_r) - \bar{x}_{i,p}\right)^{q} \tag{6.2}$$

where $\bar{x}_{i,p}$ is the mean of the signal, $x_{i,p}(t)$ and $x_{i,p}(t_r)$ is the amplitude of the signal at time, t_r, where *r*= 1, 2, 3…., *N*. Let's assume that *m* is the total number of measurement locations, and then averaged kurtosis for the plate when excited at the p^{th} mode is calculated as

$$aku_p = \frac{1}{m}\sum_{i=1}^{m} ku_{i,p} \tag{6.3}$$

- **Crest Factor:** Crest Factor is the ratio of the peak value in the response data and RMS. Averaged normalised Crest Factor (aCF_p) is calculated by the following equation.

$$\mathrm{aCF_p} = \frac{1}{\mathrm{m}}\sum_{\mathrm{i=1}}^{\mathrm{m}} CF_{i,p} \tag{6.4}$$

where $CF_{i,p}$ is expressed as

$$CF_{i,p} = \frac{max(x_{i,p}(t_r))}{RMS_{i,p}} \tag{6.5}$$

- **Root Mean Square:** Similar to kurtosis the averaged normalised RMS ($anRMS_p$) for the plate when excited at the p^{th} mode is calculated as

$$\mathrm{anRMS_p} = \frac{1}{\mathrm{m}}\sum_{\mathrm{i=1}}^{\mathrm{m}} nRMS_{i,p} \tag{6.6}$$

where the normalised RMS at location, *i* when excited at *p*th mode ($nRMS_{i,p}$) is expressed as

$$nRMS_{i,p} = \sqrt{\frac{1}{N}\sum\left(\frac{x_{i,p}(t_r)}{max(x_{i,p}(t_r))}\right)^2} \tag{6.7}$$

It is important to note that the Kurtosis and CF are the non-dimensional parameters so they can be directly compared between the healthy and delaminated plate, however the RMS value is a dimensional parameter so it may becomes difficult to compare between two sets, hence amplitude of the all the measured responses has been converted into +/- unit value then RMS has been computed. This is named as the normalised RMS (Equation 6.7) and average of the normalised RMS for all measurement locations as "Averaged normalised RMS" (Equation 6.6).

6.5 Delamination Detection

Having observed the difference in the spectra between the healthy and delaminated plates (Figure 6.1), the vibration response data has been analyzed further so that the delamination detection process becomes simple. Initially the statistical parameters Crest Factor and Kurtosis discussed in Section 6.4 have been studies on the measured responses; however it was difficult to observe any good indicator for the delamination detection. It can be seen in Tables 6.4-6.5 for shaker location 1. The cumulative average for the CF and Kurtosis upto 8 modes for the 3 plates with 3 different shaker location positions are also shown graphically in Figures 6.2-6.3 respectively.

Table 6.4 Averaged Kurtosis values for acceleration responses at Shaker Locations 1

Mode	Healthy Plate	Faulty Plate (in-centre delamination)	Faulty Plate (off- centre delamination)
1	2.680	2.632	2.656

2	2.483	2.504	2.491
3	2.070	2.128	2.080
4	2.471	2.402	2.436
5	2.609	2.579	2.595
6	2.580	2.504	2.542
7	1.909	2.118	2.014
8	2.049	2.211	2.132
Average	**2.356**	**2.385**	**2.3705**

Table 6.5 Averaged Crest Factor values for acceleration responses at Shaker Locations 1

Mode	Healthy	Faulty Plate (off-centre delamination)	Faulty Plate (in- centre delamination)
1	1.3469	1.4978	1.463
2	1.4878	1.1102	1.345
3	1.6326	1.3125	1.478
4	1.6479	1.3014	1.461
5	1.4789	1.4013	1.447

6	1.4581	1.3998	1.392
7	1.3978	1.3210	1.391
8	1.5301	1.3987	1.398
Average	**1.498**	**1.343**	**1.422**

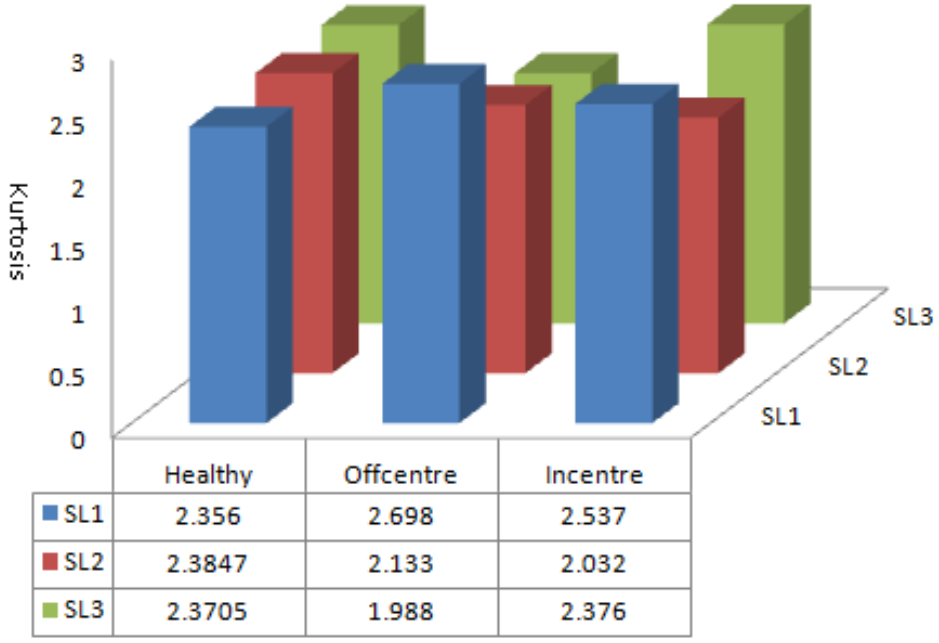

Figure 6.2 Average Kurtosis values for the 3 plates with 3 Shaker Locations (SL)

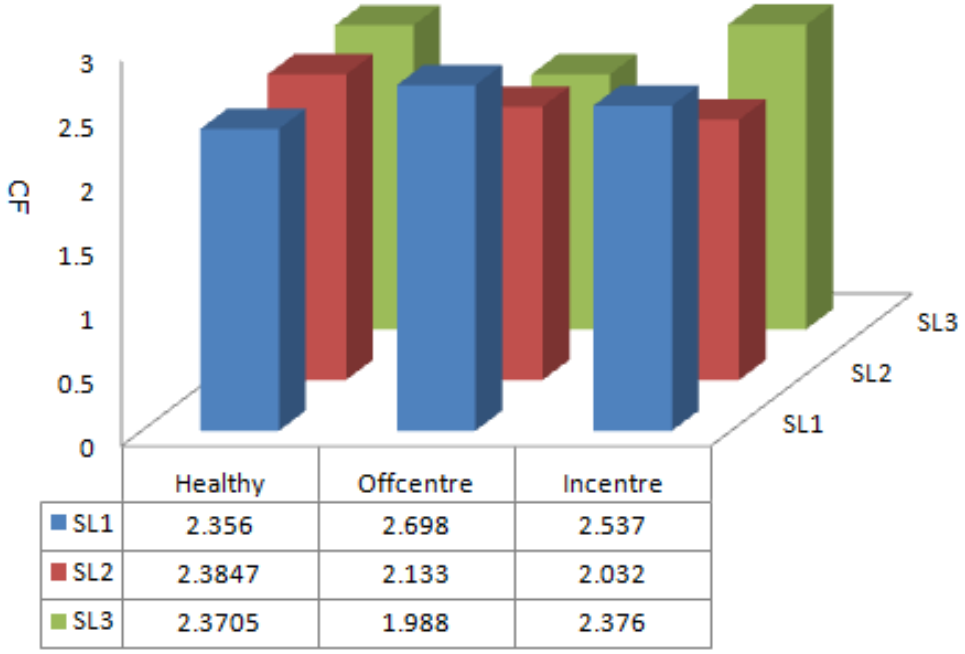

	Healthy	Offcentre	Incentre
SL1	2.356	2.698	2.537
SL2	2.3847	2.133	2.032
SL3	2.3705	1.988	2.376

Figure 6.3 Average CF values for the 3 plates with 3 Shaker Locations (SL)

The RMS (root mean square) value for the measured responses was also computed and encouraging observations have been made, hence this parameter has further been investigated. The measured acceleration responses generally have different overall amplitude (peak to peak) at different locations which make it difficult to compare the RMS values at different locations. Hence to unify the computation of the RMS at different measured locations, all the measured acceleration responses were normalised to ±1 amplitude and then the normalised RMS for the 25 measured locations of each plate at each mode of excitation have been computed first and then their average RMS value for each mode as per Equation 6.6). Table 6.6 gives the averaged normalised RMS values for 25 locations at each mode for one healthy and two faulty plates. Hence to unify the computation of the RMS at different measured locations, all the measured acceleration responses were normalised to ±1 amplitude and then the normalised RMS

for the 25 measured locations of each plate at each mode of excitation have been computed first and then their average RMS value for each mode as per Equation 6.6). Table 6.6 gives the averaged normalised RMS values for 25 locations at each mode for one healthy and two faulty plates. It has been observed that the averaged normalised RMS value at each mode for the healthy plates up to mode 8 shows small increase, however the increase in the averaged normalised RMS value for the acceleration responses observed to be more for the delaminated plates. Hence this parameter is good health indicator for the delamination detection.

Since it is not always practical to measure the acceleration response at the number of points on the large structure using accelerometers, the laser vibrometer is preferred option since this can easily and quickly scan the complete area at the desired number of points. Hence the acceleration data has been converted to velocity data and then again the averaged normalised RMS has been computed for each mode. Hence to unify the computation of the RMS at different measured locations, all the measured velocity responses were normalised to ±1 amplitude and then the normalised RMS for the 25 measured locations of each plate at each mode of excitation have been computed first and then their average RMS value for each mode. Tables 6.7 to Table 6.9 give the average normalised RMS (*anRMS*) values for 25 locations at each mode for one healthy and two faulty plates at three different excitation positions.

Table 6.6 Averaged normalised RMS (*anRMS*) values for the measured acceleration responses for Shaker Location 1

Mode #	Healthy	Faulty(Off centre)	Faulty (In centre)
1	0.2473	0.2442	0.2169

2	0.2770	0.2190	0.2212
3	0.3465	0.3943	0.2251
4	0.2793	0.4461	0.2799
5	0.2708	0.3009	0.3025
6	0.2793	0.4403	0.4614
7	0.3869	0.5239	0.3966
8	0.3807	0.4718	0.4132
Average	**0.3085**	**0.3801**	**0.3146**

It has been observed that the averaged normalised RMS value at each mode for the healthy plates up to mode 8 shows small increase, however the increase in the averaged normalised RMS value for the acceleration responses observed to be more for the delaminated plates. The cumulative average for the normalised RMS upto 8 modes for the 3 plates with 3 different shaker location positions are also shown graphically in Figures 6.4. Hence this parameter is good health indicator for the delamination detection.

Table 6.7 Averaged normalised RMS values for the experimental velocity responses at each mode at shaker location 1

Mode	Healthy	Faulty(Off-centre)	Faulty (In-centre)
1	0.3319	0.2888	0.2972

2	0.3421	0.3123	0.2784
3	0.3473	0.4085	0.2654
4	0.3128	0.4877	0.3595
5	0.3009	0.3175	0.3369
6	0.2962	0.4567	0.6194
7	0.3628	0.6225	0.5720
8	0.3836	0.6188	0.5819
Average	**0.3347**	**0.4391**	**0.4138**

Table 6.8 Averaged normalised RMS values for the experimental velocity responses at each mode at shaker location 2

Mode	Healthy	Faulty(Off centre)	Faulty (In centre)
1	0.3056	0.2902	0.3004
2	0.3247	0.3231	0.2964
3	0.3102	0.3992	0.3013
4	0.2897	0.4567	0.3661
5	0.3125	0.3698	0.3623
6	0.2964	0.4661	0.5991

7	0.3446	0.5950	0.5667
8	0.3781	0.5770	0.5908
Average	**0.3202**	**0.4346**	**0.4229**

Table 6.9 Averaged normalised RMS values for the experimental velocity responses at each mode at shaker location 3

Mode	Healthy	Faulty(Off centre)	Faulty (In centre)
1	0.3114	0.2892	0.2947
2	0.3316	0.3312	0.3012
3	0.3217	0.3987	0.3210
4	0.3059	0.4601	0.3552
5	0.3213	0.3732	0.3701
6	0.2982	0.5104	0.5857
7	0.3514	0.5611	0.5703
8	0.3801	0.5632	0.5976
Average	**0.3277**	**0.4359**	**0.4245**

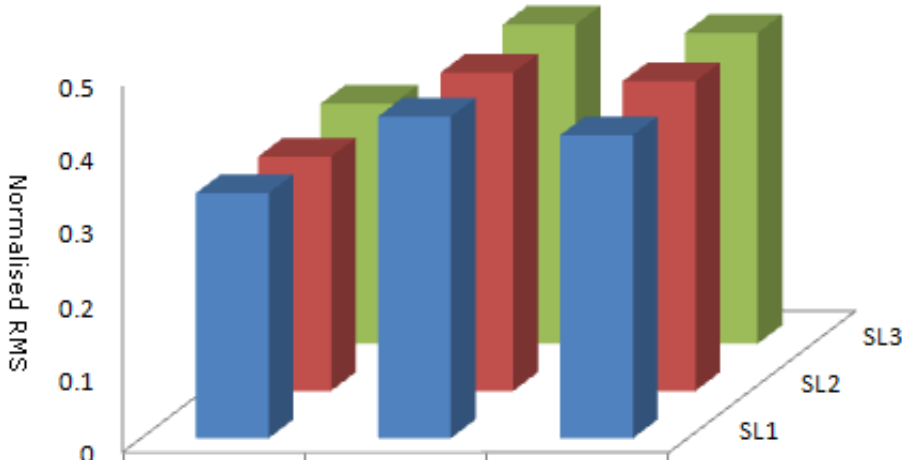

	Healthy	Offcentre	Incentre
SL1	0.3347	0.4391	0.4138
SL2	0.3202	0.4346	0.4229
SL3	0.3277	0.4359	0.4245

Figure 6.4 Average Normalised RMS values for the Experimental Velocity responses for 3 plates with 3 Shaker Locations (SL)

6.6 Numerical Validation

Numerical vibration experiments have also been conducted on the healthy and delaminated composite plates shown in Figure 6.2(a) (in-centre delaminated plate not shown) to verify experimental results. Composite plates were excited through the shaker at the first 8 modes. The steady state vibration responses (velocity and acceleration) were then collected from 169 of locations on the plates using commercial FEA software ABAQUS version 6.10. The measurement locations are shown in Figure 6.2(b). The response data were stored at the sampling frequency of 20 kHz for further analysis in MATLAB. The velocity signals were then exported to MATLAB to compute the statistical parameters (section 6.4) for all the 3 cases (healthy, off-centre and in-centre delaminated plates) and for 3 different positions (Figures 3.10-3.12) of the shaker.

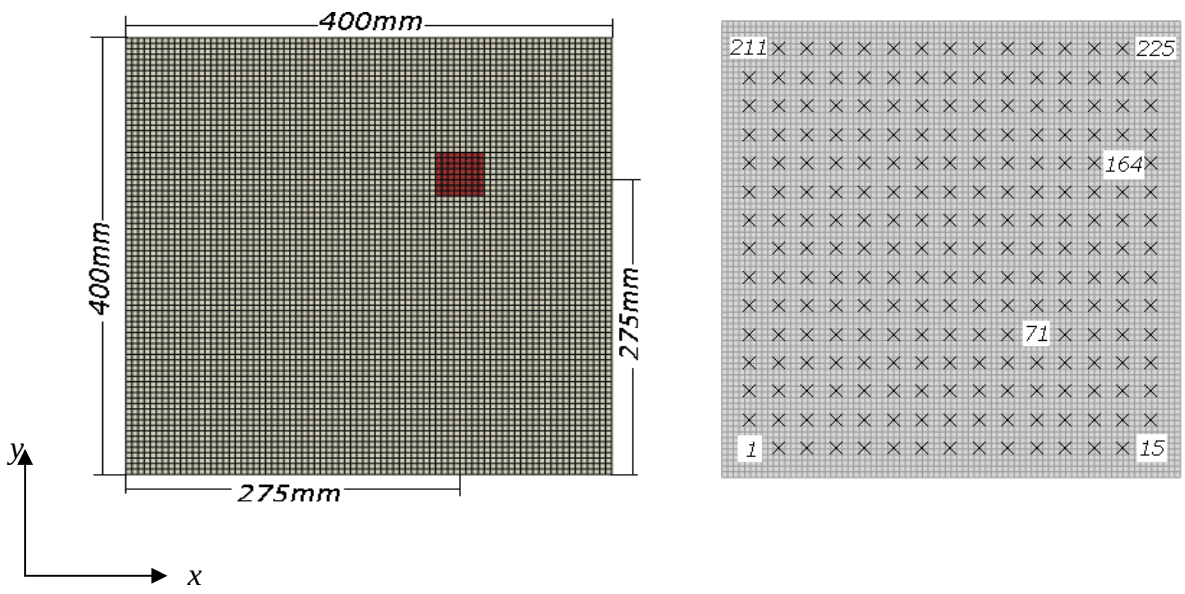

Figure 6.5 (a) An FE model of the E-glass fibre plate (also showing delamination region), (b) Measurement locations (marked as x) in FE simulation

6.6.1 Response Estimation

The amplitude spectra for the estimated acceleration responses when sinusoidal excitation was used for the first 8 modes have been computed and compared between the healthy and the delaminated plates. Few Typical acceleration spectra are shown in Figure 6.3.

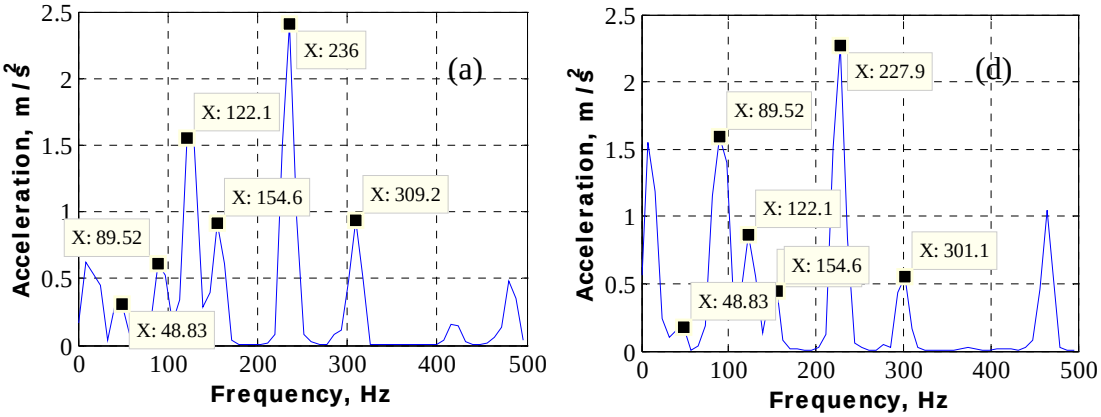

Mode 1 at the location (50mm, 100mm)

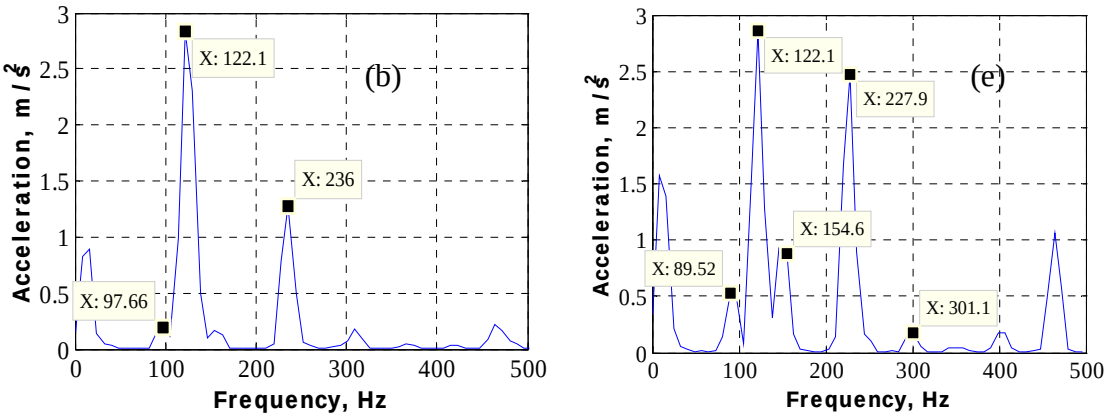

Mode 2 at the location (110mm, 80mm)

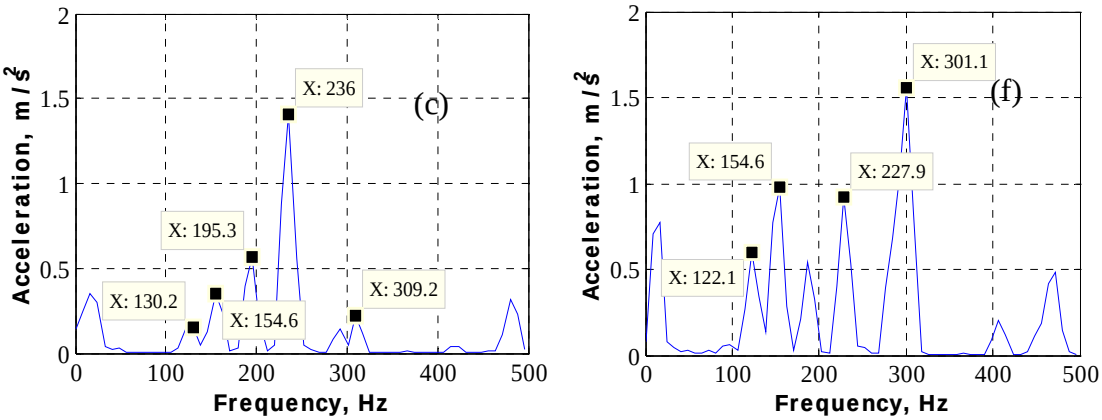

Mode 3 at the location (230mm, 110mm)

Figure 6.6 Typical acceleration amplitude spectra at first 3 modes of the FE simulations, (a) to (c) for Healthy plate, (d) to (f) for Delaminated plate

6.6.2 Delamination Detection

Similar to the experimental data processing, numerical vibration responses were also processed. Here instead of converting the accelerations signals to velocity signals, velocity response was directly outputted in ABAQUS Explicit dynamic analysis. Averaged kurtosis, averaged CF, and averaged normalised RMS were calculated for 169 measurement locations for all the three composite plates (healthy, off-centre, and in-centre delaminated) and for all the three shaker excitation positions (Figure 3.10). Results are summarised in Tables 6.10-6.12.

Table 6.10 Averaged normalised RMS values for the numerical velocity responses at each mode at shaker location 1

Mode	Healthy	Faulty(Off centre)	Faulty (In centre)
1	0.2510	0.2663	0.2495
2	0.2387	0.2697	0.2599
3	0.3059	0.3881	0.3069
4	0.2953	0.4205	0.3214
5	0.3147	0.4108	0.3891
6	0.3006	0.4604	0.4563
7	0.3113	0.5096	0.5067
8	0.3128	0.5101	0.5058
Average	**0.2913**	**0.4044**	**0.3745**

Table 6.11 Averaged normalised RMS values for the experimental velocity responses at each mode at shaker location 2

Mode #	Healthy	Faulty(Off centre)	Faulty (In centre)
1	0.3056	0.2902	0.3004
2	0.3247	0.3231	0.2964

3	0.3102	0.3992	0.3013
4	0.2897	0.4567	0.3661
5	0.3125	0.3698	0.3623
6	0.2964	0.4661	0.5991
7	0.3446	0.5950	0.5667
8	0.3781	0.5770	0.5908
Average	**0.3202**	**0.4346**	**0.4229**

Table 6.12 Averaged normalised RMS values for the numerical velocity responses at each mode at shaker location 3

Mode #	Healthy	Faulty(Off centre)	Faulty (In centre)
1	0.2298	0.2442	0.2605
2	0.2712	0.2754	0.2637
3	0.3214	0.3781	0.2996
4	0.3207	0.4136	0.3657
5	0.3211	0.3905	0.3771

6	0.3124	0.4312	0.4614
7	0.331	0.4958	0.4416
8	0.3601	0.5124	0.4996
Average	**0.3085**	**0.3927**	**0.3712**

The cumulative average for the normalised RMS upto 8 modes for the 3 plates with 3 different shaker location positions are also shown graphically in Figures 6.7. It can be observed from comparing Tables 6.7-6.9 (experimental results) and Tables 6.10-6.12 that both experimental and numerical results give same indication that averaged normalised RMS can be used for delamination detection in composite plates.

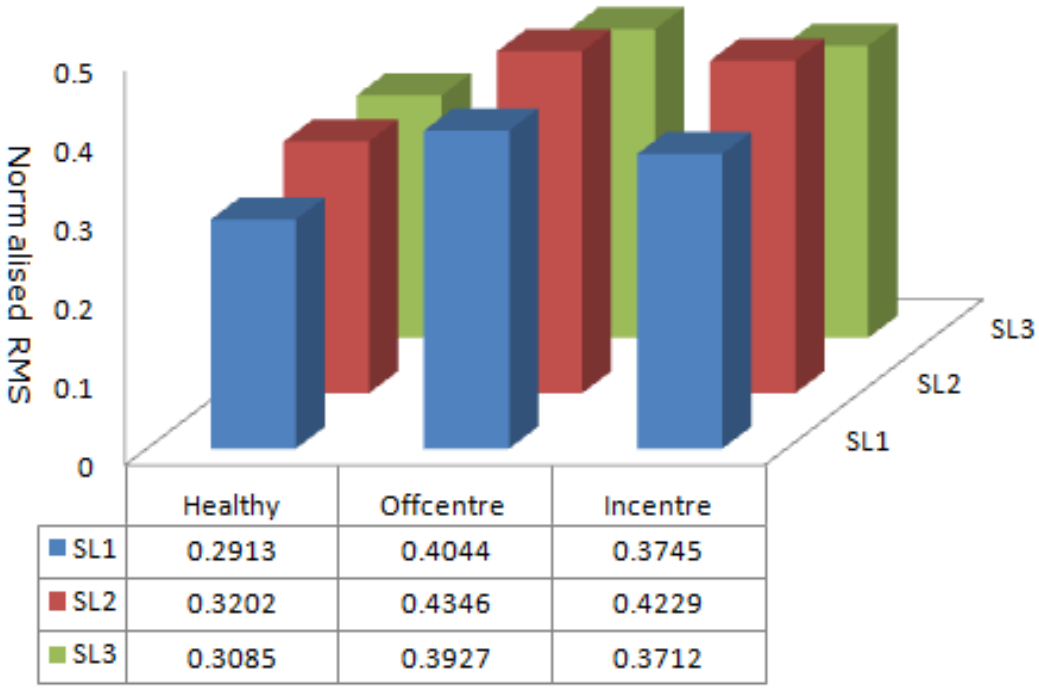

Figure 6.7 Average Normalised RMS values for the Numerical Velocity responses for 3 plates with 3 Shaker Locations (SL)

6.7 Summary

The dynamics of the three composite plates – one healthy (no delamination) and other two plates having delamination at centre and off-centre have been study when excited experimentally at few lower modes. It has been observed that the measured acceleration spectra show the appearance of other modes when excited at a mode due to anisotropic property of the composite. In addition to this observation, the plates with delamination also show some higher harmonics of the excited frequency due to the non-linear interaction between the delaminated layers. Statistical parameters like kurtosis, crest factor, skewness and RMS values were calculated for all the three plates (healthy, delaminated at centre and off-centre) and for the three different positions of excitations were calculated and it was found that only normalized RMS values were able to diagnose the damage present in the plate. It has been observed that the normalised average RMS value at each mode show increasing trend for the delaminated plates compared to the healthy composite plate. It is also observed that the normalised average RMS value for the velocity responses for all the modes more than 0.37 indicates the presence of the delamination.

CHAPTER 7
SECOND DERIVATIVE OF THE ACCELERATION RESPONSES FOR IDENTIFICATION OF DELAMINATION AND ITS LOCATION IN COMPOSITE STRUCTURES

7.1 Introduction

In this chapter, the measured responses when excited at a few lower modes using the conventional accelerometers and the shaker have been considered for the delamination location without the use of the data from the healthy condition. The proposed method has been developed initially on the finite element (FE) simulation. The nonlinear interaction between the delaminated layers has been considered in the FE simulation during the computation of the responses. It was expected that such nonlinear interaction between the delaminated layers may result in the impulsive kind of the response at the delamination location. The statistical parameter kurtosis has then been calculated for the acceleration responses and its higher derivatives. It has been observed that the 2^{nd} derivative of the acceleration response provides a good indicator for the delamination location. This has further been validated through the experiments.

7.2 Experimental Set-up and Modal Testing

The experimental setup for conducting the vibration test on the composite plates is shown in Figure 3.9. The plate was hanged by the soft elastic rope from the top 2 edges to realise the free boundary condition for all the 4 edges of the plate as shown in Figure 3(a). Modal testing was done as explained in Chapter 5 and 6.

7.3 Finite Element (FE) Modelling

The FE models for both the plates (with and without delamination) have been constructed in the ABAQUS 6.9 FE code. Based on the results from Chapter 6 element C3D8I has been used for FE modelling. An element size of 10mm x 10mm has been used for each layers resulting in 12800 elements for a plate. Modal analysis was performed and the results are summarised in Tables 5.2-5.3 and Tables 6.1-6.3.

7.4 Response Estimation

The vibration responses were also estimated from the FE models when excited at a few lower modes to understand the dynamic behaviour. It is expected that the delaminated layers in the plate will interact nonlinearly when the plate is subjected to the external excitation. Hence, this analysis has also been considered while estimating the vibration responses for the delaminated plate. The average time step chosen for this analysis was $5e-8$s based on the criteria in the ABAQUS code. It is also important to note that the response data have been stored at a step of $0.2\mu s$ for all the measurement locations indicated by 'dots' in Figure 6.1(b) for this simulated example. This means that the sampling frequency is 20MHz which is often not considered very high in the vibration measurement, hence the data have been down sampled to the sample frequency of 20kHz with the low pass filter to 9kHz for further signal processing. The computed acceleration responses at each measurement location have been polluted with noise (Signal to Noise ratio 20dB) to simulate the actual vibration measurements.

Figure 7.1(a) typically shows the out of plane displacement responses at the centre of the delamination for the delaminated layers at nodes 51093 (node number at the centre of the delamination on top of the 4th layer) and 151093 (node number at the centre of the delamination at the bottom of the 3th layer) for the top and bottom delaminated layers when excited at mode 1 (45.88Hz). In Figure 7.1(a), the displacement responses at nodes 51093 and 151093 are shown as the line with squares and circles respectively, where the displacement responses do not clearly indicates nonlinear interaction. However the difference of the responses shown in Figure 7.1(b) clearly shows the nonlinear interaction between the delaminated layers.

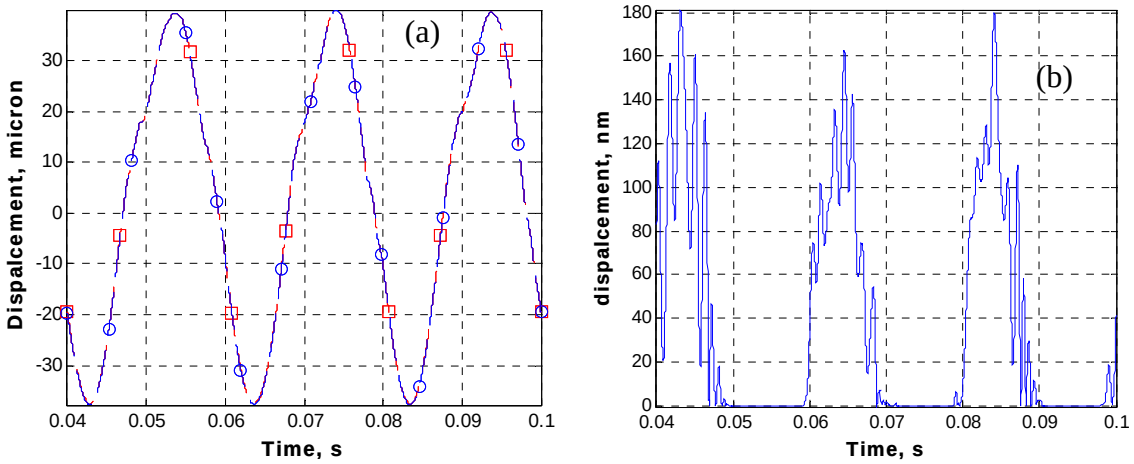

Figure 7.1 (a) Displacement responses at centre of the delamination at mode 1, (b) Difference in the responses indicating interaction between the layers

7.5 Delamination Location

The statistical parameter kurtosis (k_u) seems to be useful for detection of crack [27]. In the present study, the nonlinear interaction between the delaminated layers is also likely to produce some impulsive acceleration response which can be detected by the

parameter kurtosis. Hence the kurtosis for the following data has been computed to explore the possibility of identifying the location of delamination correctly.

(a) Acceleration responses

(b) Derivative of the acceleration responses (DA).

(c) 2nd derivative of the acceleration responses (DDA or D^2A)

(d) 3rd derivative of the acceleration responses (DDDA or D^3A)

These derivatives have been computed as

$$\text{DA, } \dot{a}_{n,m}(t_k) = \frac{a_{n,m}(t_{k+1}) - a_{n,m}(t_k)}{\Delta t} \tag{7.1}$$

$$\text{DDA, } \ddot{a}_{n,m}(t_k) = \frac{a_{n,m}(t_{k+1}) - 2a_{n,m}(t_k) + a_{n,m}(t_{k-1})}{(\Delta t)^2} \tag{7.2}$$

$$\text{DDDA, } \dddot{a}_{n,m}(t_k) = \frac{a_{n,m}(t_{k+2}) - 3a_{n,m}(t_{k+1}) + 3a_{n,m}(t_k) - a_{n,m}(t_{k-1})}{(\Delta t)^3} \tag{7.3}$$

where $\dot{a}_{n,m}(t_k)$, $\ddot{a}_{n,m}(t_k)$ and $\dddot{a}_{n,m}(t_k)$ are the 1st, 2nd and 3rd derivatives respectively for the acceleration response, $a_{n,m}(t_k)$ at the time, t_k at the measurement location, *n* for the mode, *m*, and Δt is the time step. The advantage of examining the higher derivatives of the acceleration is that if the impact energy between the delamination layers due to nonlinear interaction during vibration tests may not be sufficient to observe the impulsive nature in the acceleration responses, but it may get amplified in the higher order derivatives. Typical kurtosis plots for the acceleration responses at mode 1 to 3 are shown in Figure 7.2 for both the healthy and the delaminated plates. Here, the

calculated kurtosis values for each mode were normalised to the maximum value to keep the maximum value 1 in the plots. None of the modes show any indication for the presence and location of the delamination in the delaminated plate. The kurtosis of the 1st derivative of acceleration (DA) responses also does not indicate the location of delamination in the delaminated plate. They are typically shown in Figure 7.3 where multi-peaks observed in the plots but related to the delamination location. However, the kurtosis of the 2nd derivative (DDA or D^2A) and 3rd derivative (DDDA or D^3A) clearly indicates the location of delamination which is shown in Figures 7.4-7.5. Hence the last two derivatives are found to be useful for the delamination detection so the DDA has been considered as the optimum indicator for further study. Figure 7.6 shows few typical kurtosis plots for healthy case where there is no indication of any delamination.

However, further investigation has been made to understand why the kurtosis of the acceleration response only has not been able to detect the delamination location, but 2nd derivative (DDA) detects the location clearly. Hence the acceleration response and its derivatives at the centre of the delamination for the delaminated plate are compared with the healthy plate. A typical acceleration response and derivatives when excited at mode 1 are shown in Figure 7.7. It is evident from Figure 7.7(e) that the energy exchange during the nonlinear interaction between the delaminated layers was not sufficient to generate an impulsive nature of the acceleration response in the delaminated composite plate. This is reason why the kurtosis of the acceleration response only could not detect the delamination. But the derivatives of the acceleration response start amplifying such nonlinear behaviour as the impulsive signal and become prominent in the 2nd and 3rd derivatives in case of delaminated plate but remain absent

for the healthy plate as expected. This is typically seen in Figure 7.7 which produced the required result.

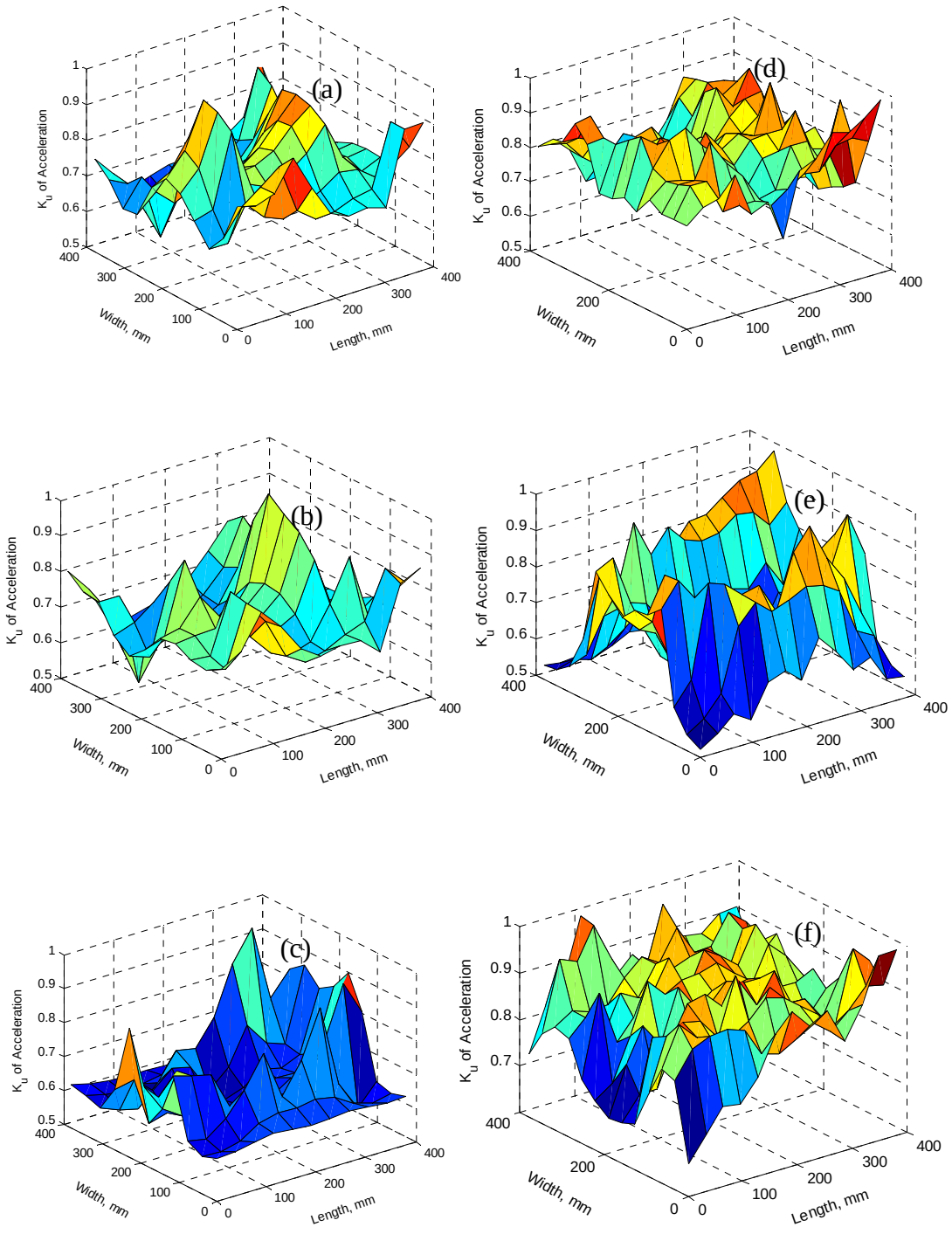

Figure 7.2 The kurtosis plots for the acceleration responses, (a) to (c) for the healthy plate from Mode 1 to 3, (d) to (f) for the delaminated plate from Mode 1 to 3

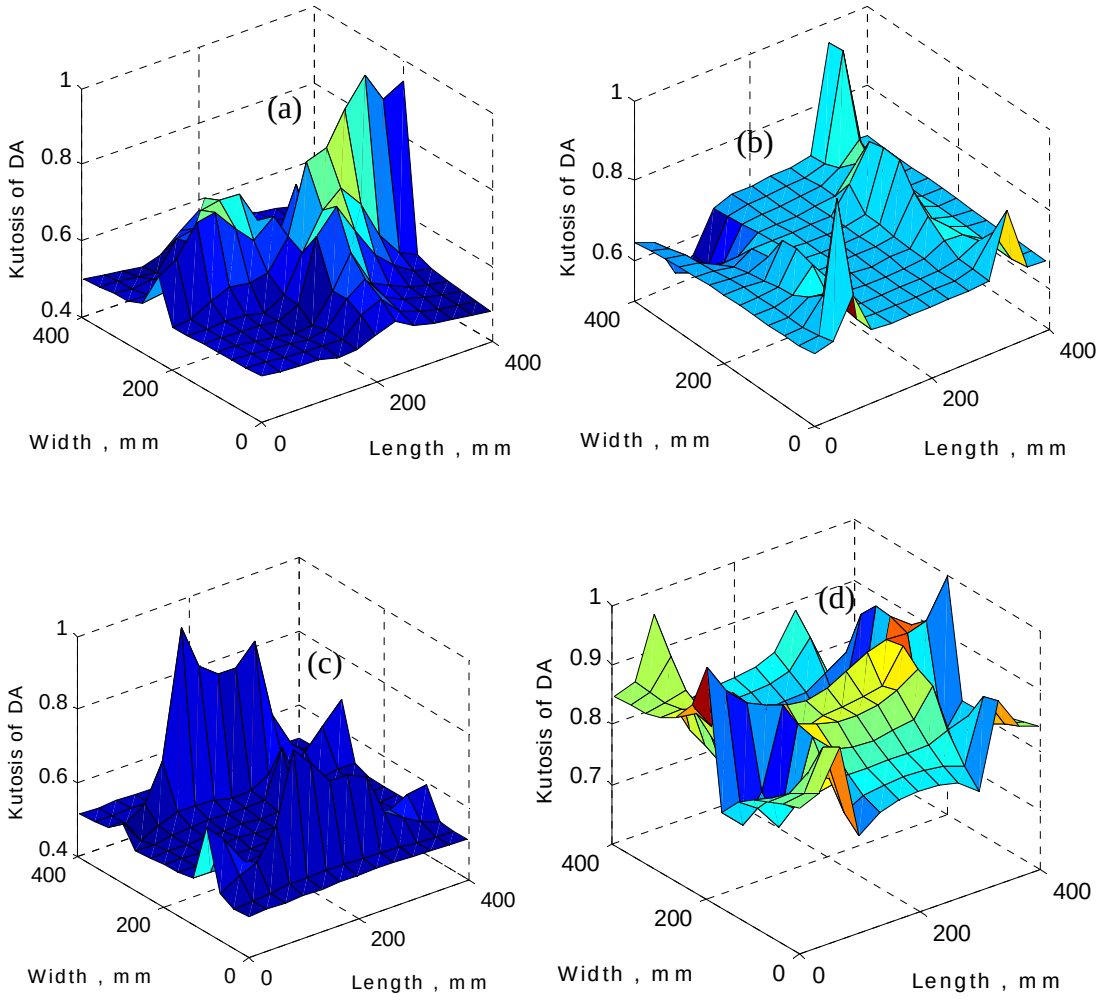

Figure 7.3 The kurtosis plots for the 1st derivative of acceleration (DA) responses for the delaminated plate, (a) Mode 1 to (d) Mode 4

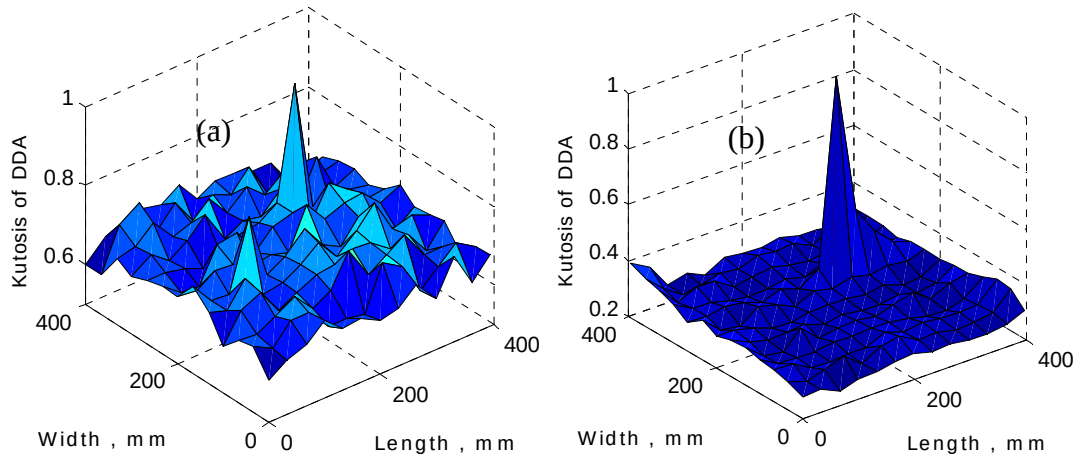

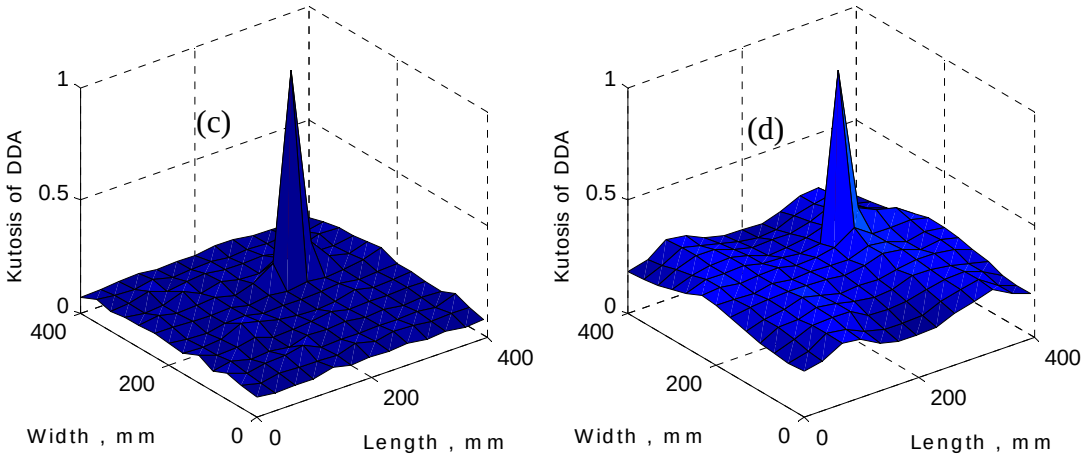

Figure 7.4 The kurtosis plots for the 2nd derivative of acceleration (DDA) responses for the delaminated plate, (a) Mode 1 to (d) Mode 4

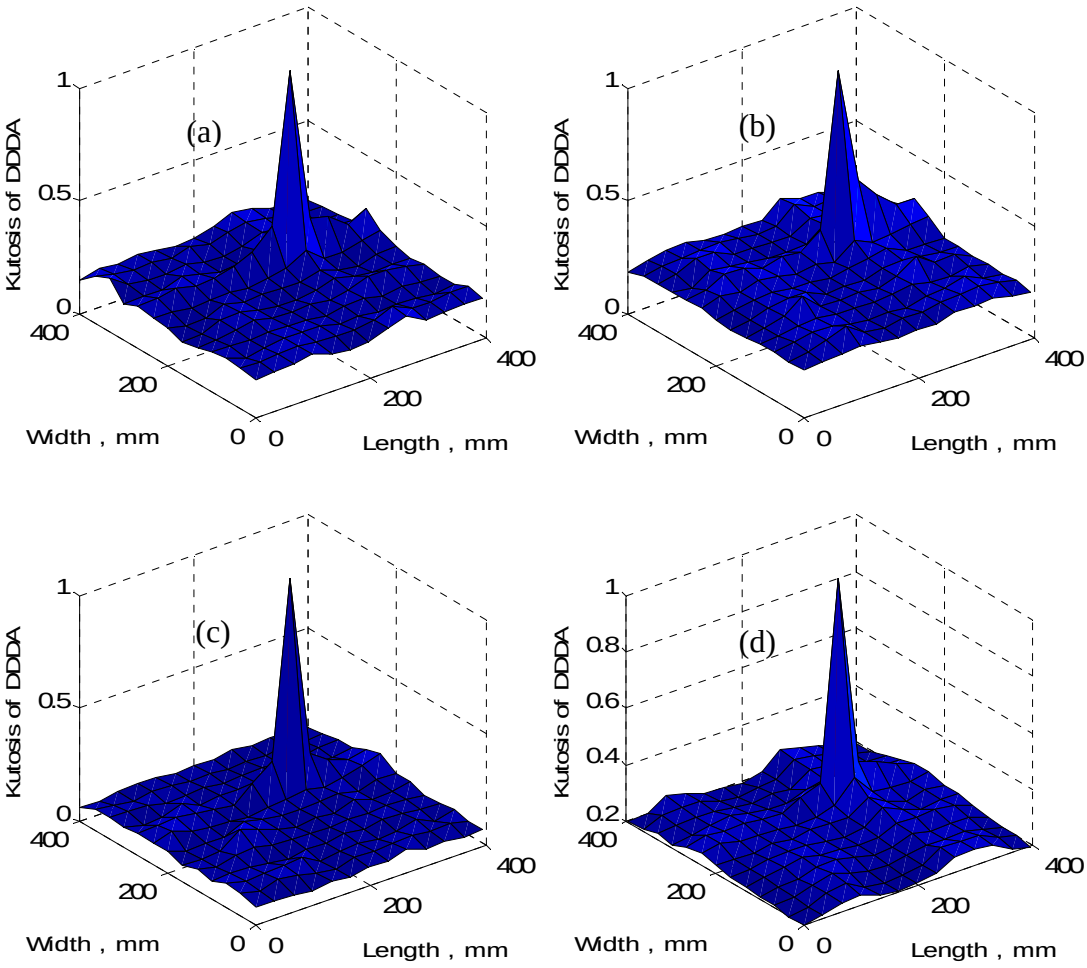

Figure 7.5 The kurtosis plots for the 3rd derivative of acceleration (DDDA) responses for the delaminated plate, (a) Mode 1 to (d) Mode 4

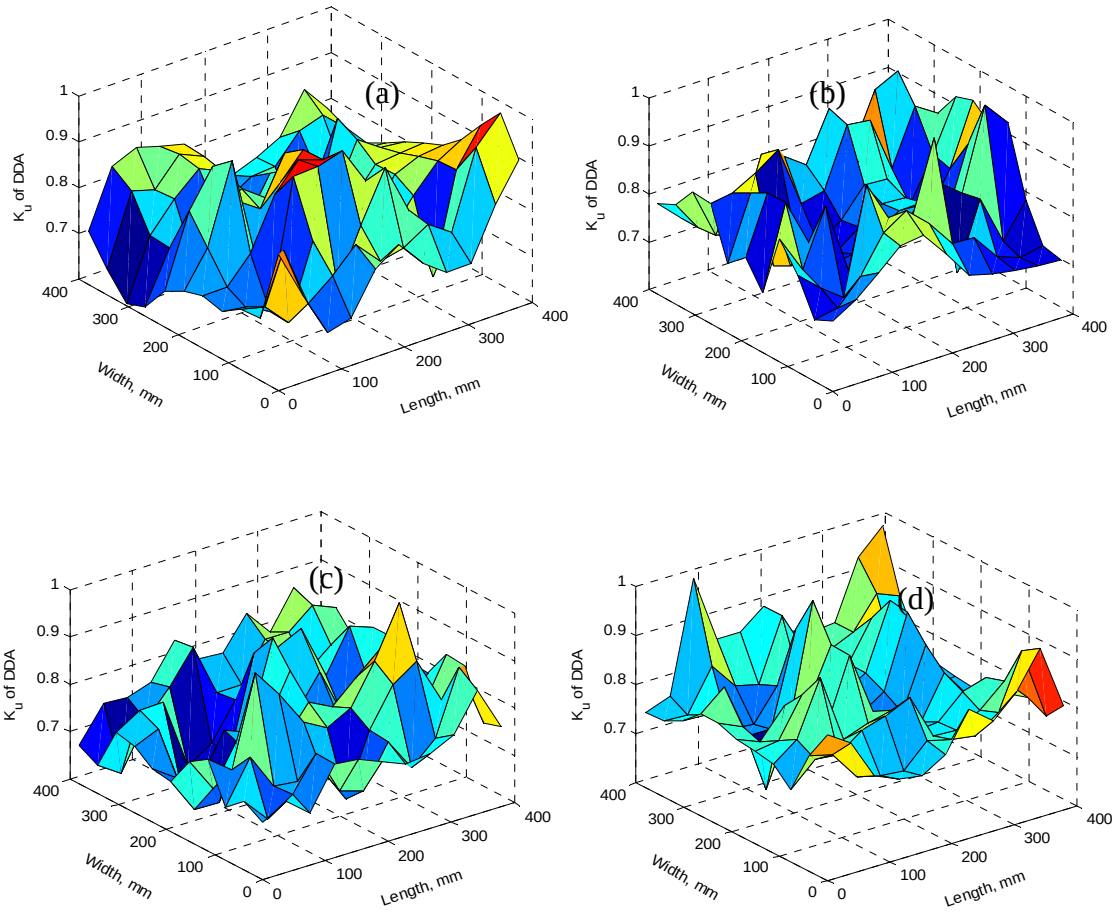

Figure 7.6 The kurtosis plots for the DDA signals for the healthy plate, (a) Mode 1 to (d) Mode 4

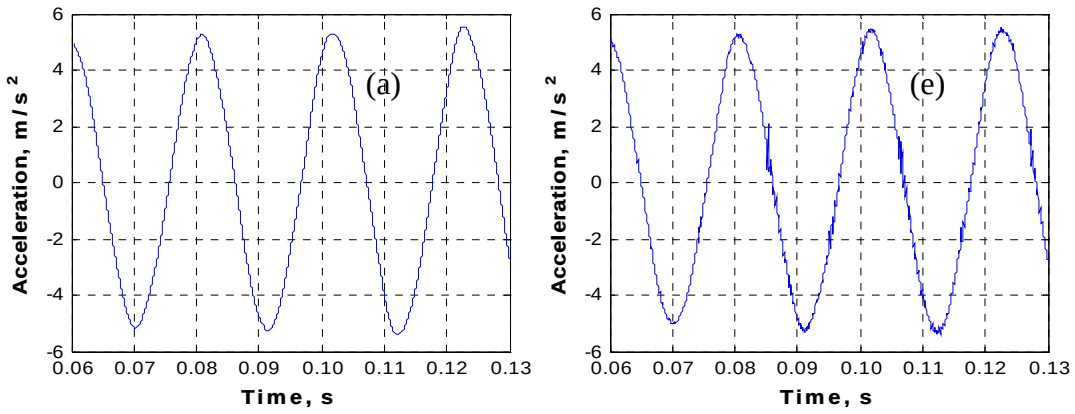

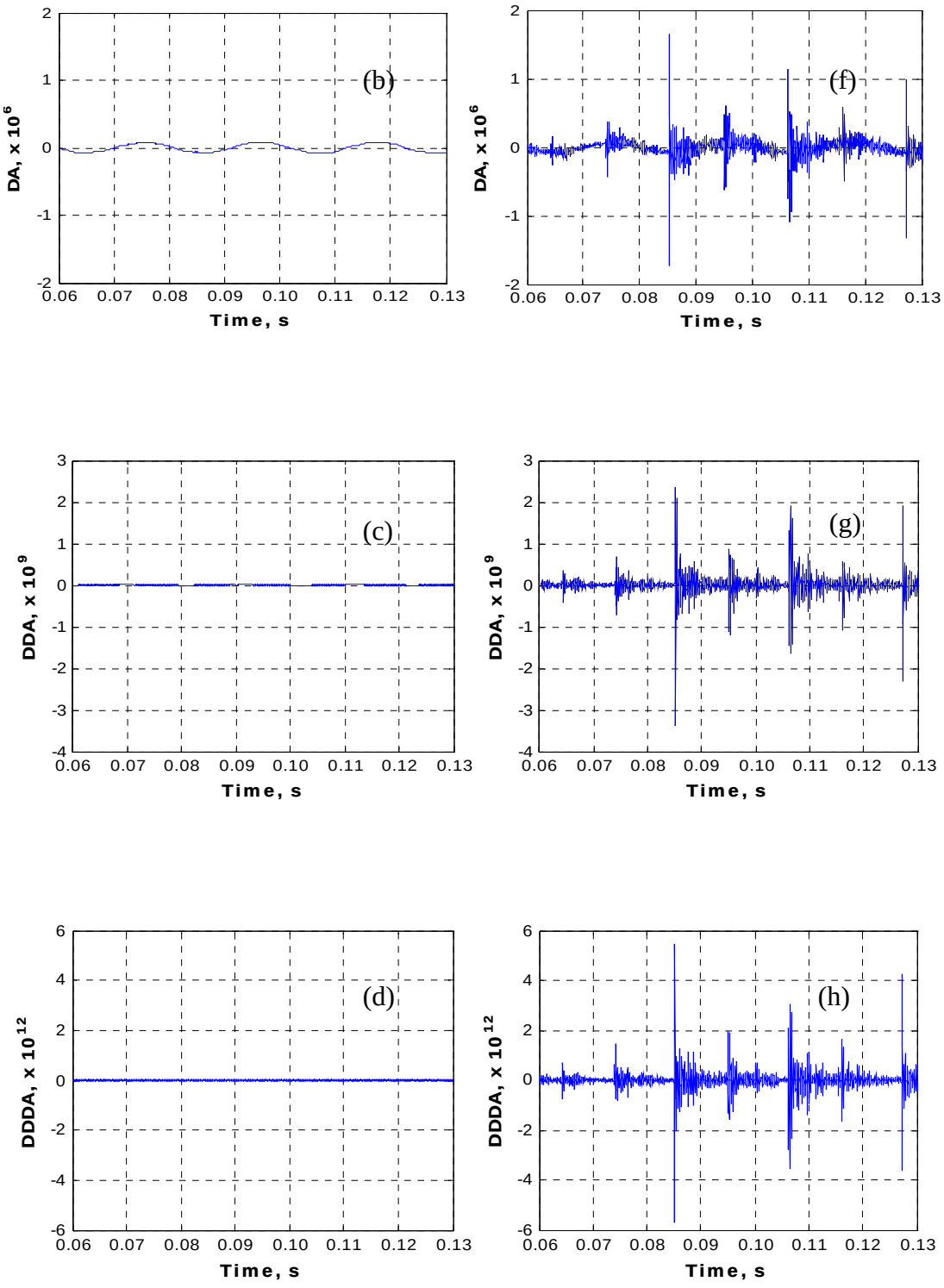

Figure 7.7 Acceleration response and its derivatives (DA, DDA, DDDA) at the centre of the delamination, (a) to (d) Healthy plate, (e) to (h) Delaminated plate

7.6 Multi-delaminations

To further examine the robustness of the 2nd derivative of acceleration response (DDA) in delamination location detection, the same simulated example with 2 delaminations of size 40mm x 40mm with their centres at (270mm, 270mm) and (140mm, 140mm) has also been considered. Once again, the kurtosis of the DDA has successfully detected the locations which are shown in Figure 7.8.

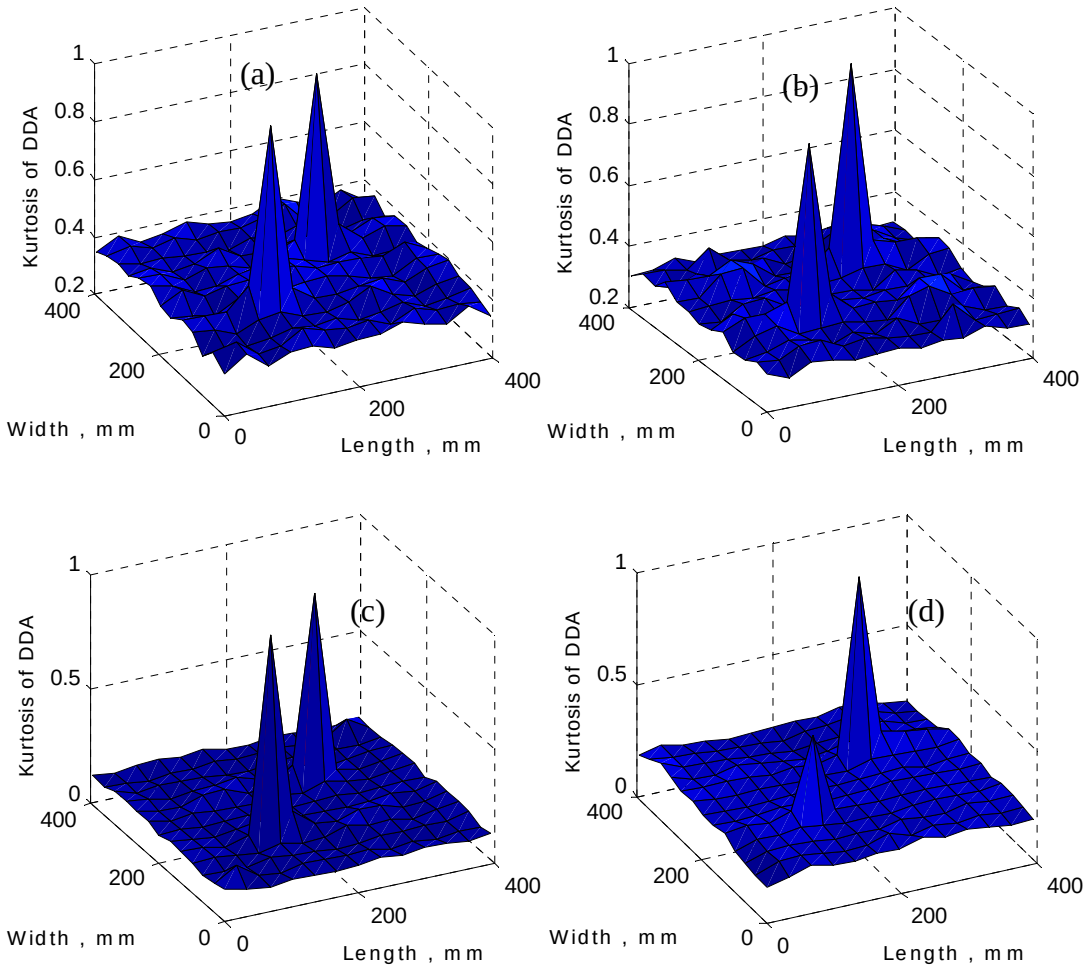

Figure 7.8 The kurtosis plots for the 2nd derivative of acceleration (DDA) responses for the plate with 2 delamination,(a) Mode 1 to (d) Mode 4

7.7 Experiments

Having observed the acceleration responses at the different modes and the usefulness of the kurtosis of the DDA in the location detection in the simulations, the vibration experiments have also been conducted on the healthy and delaminated composite plates shown in Figure 3.9. Both plates were excited through the shaker at the first 6 modes. The steady state acceleration responses were then collected from 25 locations on both the plates. The measurement locations are shown in Figure 3.10. The data were collected to the PC through the 16-bit 8-channels data acquisition device at the sampling frequency of 20 kHz. The data have then been analyzed to compute the kurtosis of the DDA signals which are typically shown in Figures 7.10. Here again, the kurtosis of the DDA signals clearly identify the location of the delamination for Modes 3 and 4. Probably the excitation used during experiment was not enough for Mode 1 and 2 to initiate the nonlinear interaction between the delaminated layers. However, the normalised cumulative kurtosis of the DDA signals for a few modes produced much better identification of the delamination location. It is typically shown in Figure 7.11 when modes 1 to 4 were used.

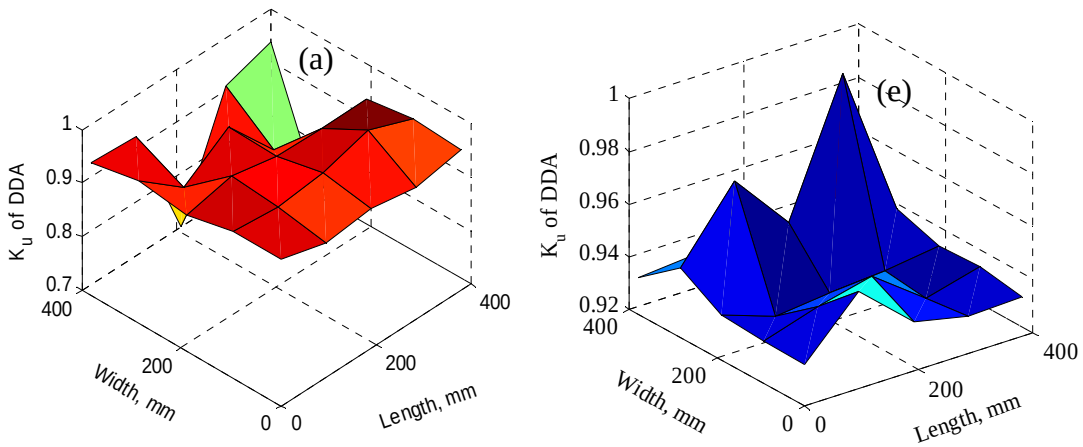

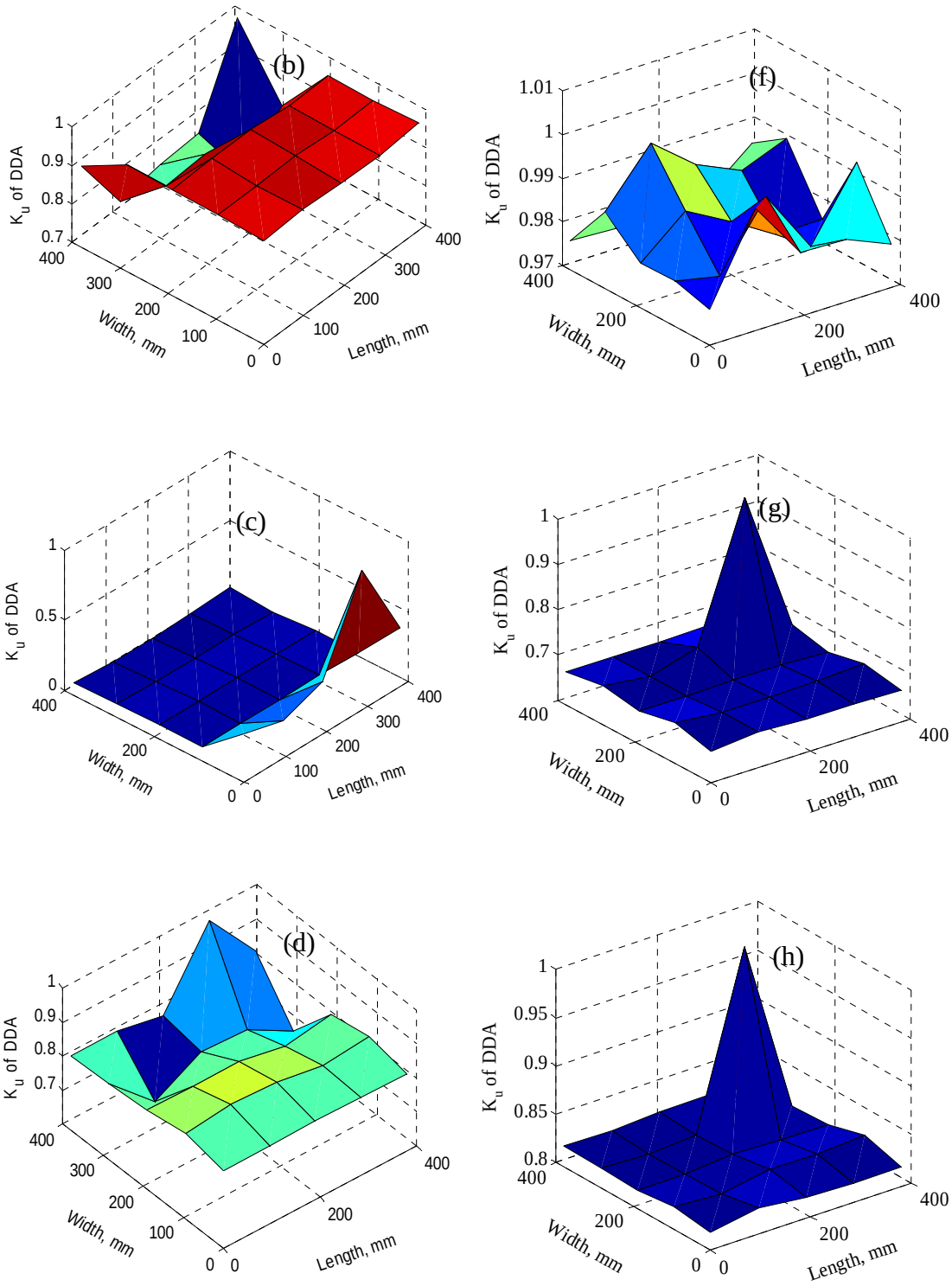

Figure 7.9 The kurtosis plots for the DDA signals for the experimental cases, (a) to (d) for the healthy plate from Mode 1 to 4, (e) to (h) for the delaminated plate from Mode 1 to 4

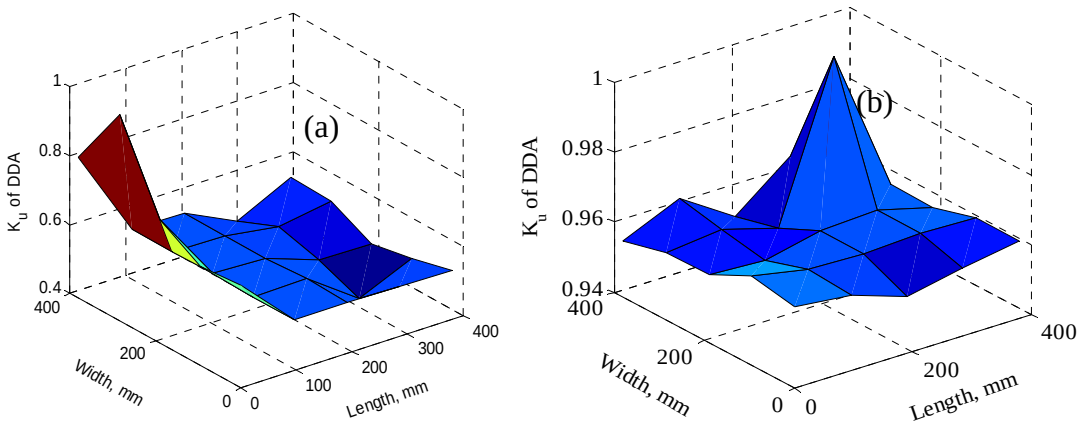

Figure 7.10 The normalised cumulative kurtosis plots for the DDA signals for the modes 1 to 4 for the experimental cases, (a) Healthy plate, (b) Delaminated plate

7.8 Summary

In the present study, a method of delamination location detection in the composite has been suggested using the kurtosis of the 2nd derivative of the acceleration responses when the composite structure is excited at a few lower modes. Initially the method has been developed in the FE simulation with one and two delaminations in a composite plate and then the method has further been qualified through the experimental examples of a composite plate with and without delamination. The advantage of the proposed method is that the small size delamination can be detected reliably even when excited just at a few lower modes where change in the natural frequencies and mode shapes are generally insignificant when compared with the healthy case. The suggested method also does not require any vibration data from the healthy condition and there is no need to do the signal processing in the frequency domain for the measured vibration data.

CHAPTER 8
A NOVEL APPROACH FOR DETECTING DELAMINATION IN COMPOSITES

8.1 Introduction

Considering the limitations of existing delamination detection methods, a simple method which may be relatively easy to implement in practice and not requiring data from the healthy state condition is needed to meet the objective. Hence it is assumed that the excitation at a few lower modes using conventional shaker is always possible and then scanning the complete composite surface through the laser vibrometer may not impose any practical limitations. With this assumption, the excitation of a composite plate with and without a delamination at a few lower modes and then the velocity responses measurements at number of points has been considered in the present study. Initially, the finite element (FE) model of a composite plate with and without delamination has been developed to simulate this experiment. In fact, it has been observed that the nonlinear interaction between the delaminated layers produce higher harmonics of the exciting frequency. These higher harmonics are then observed to be useful for the detection and location of the delamination without comparing the vibration data from the healthy state of the composite structure. This chapter presents a novel method based on the utilization of the higher harmonics which can successfully identify delamination in the composite plate with built-in delamination.

8.2 Finite Element (FE) Modelling

The FE models for both the plates (with and without delamination) have been constructed in the ABAQUS 6.10 FE code. The element C3D8I has been used for this modelling. An element size of 5mm x 5mm has been used for each layers resulting in 51200 elements for a plate.

8.3 Response Estimation

The velocity responses have been estimated using the explicitly dynamics analysis in the ABAQUS 6.10 FE code for both healthy and delaminated plates when excited at few lower modes. The non-linear interaction between the delaminated layers has also been simulated during the response estimation for the delaminated plates. Typical velocity amplitude spectra when excited at Mode 6 are shown in Figure 8.1. It has been observed that the modes other than the excited mode are also present in the spectra for both the healthy and delaminated plates, probably due to anisotropic material properties of the composite material. In addition, the prominent higher harmonics of the exciting frequency has also been observed as expected due to the nonlinear interaction between the delaminated layers for the delaminated plate compared to the healthy plate. The exciting frequency (1X) and its higher harmonics (2X, 3X, …) are marked as '**O**' in Figure 8.1 for the composite plate with off-centre delamination and shaker location 1 (shown in Figure 3.10). Similar plots have been observed for shaker location 2 (Figure 3.11) and shaker location 3(Figure 3.12). Responses were also estimated for the three locations but for the composite plate with delamination in the centre and similar behaviour like in Figure 8.1 were observed.

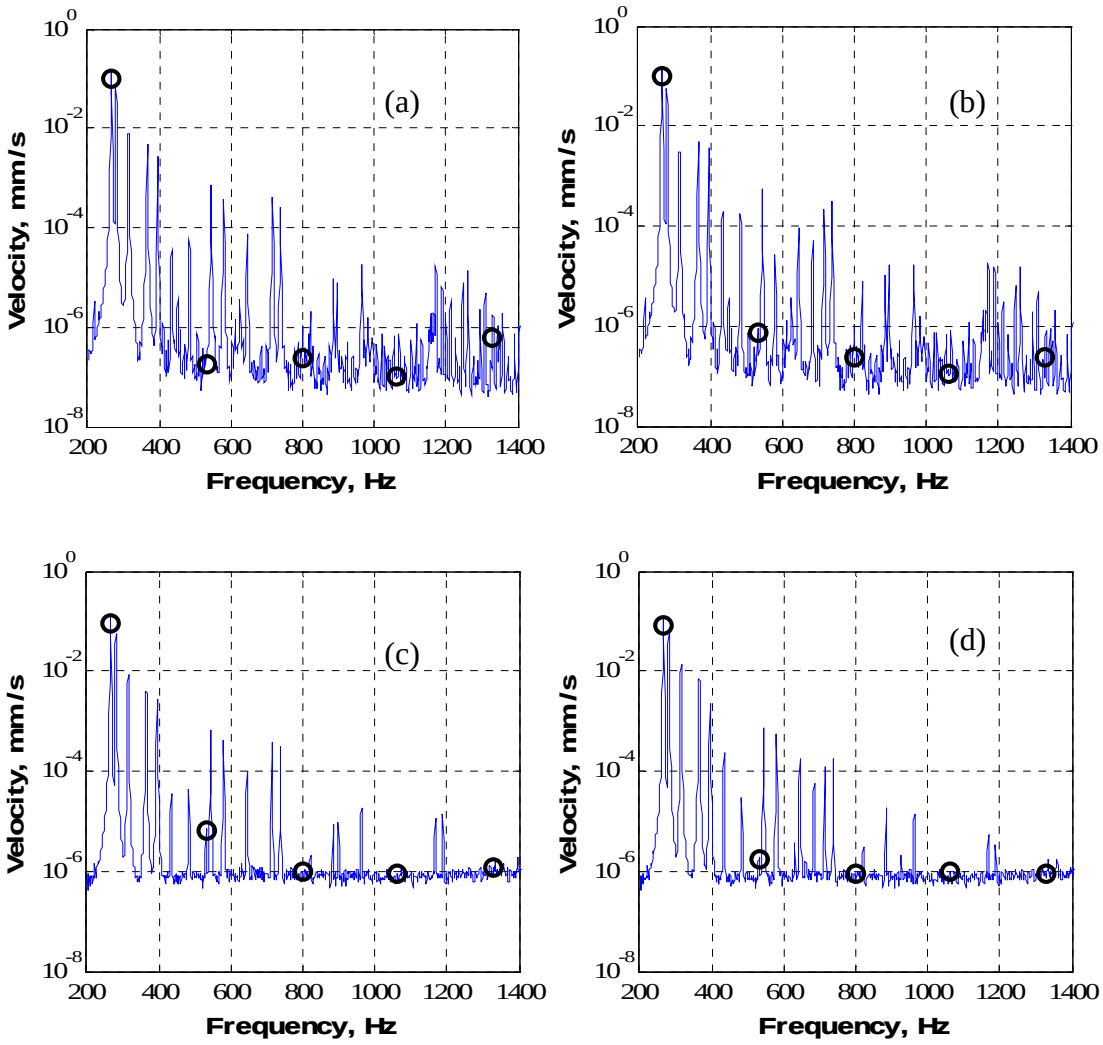

Figure 8.1 Typical FE simulated amplitude velocity response spectra at location at nodes 71, 164 for the healthy (a-b) and delaminated plates (c-d) when excited at Mode 6 respectively

8.4 Delamination Detection

Having known the presence of prominent higher harmonic components of the exciting frequency in the spectra due to the nonlinear interaction between the delaminated layers in the composite structure, a simple approach has been devised for this purpose of the

delamination detection. The term “Normalised Summation of higher Harmonics (NSH)” at each mode has been defined which is computed as

Summation of harmonics (SH) when excited at Mode *i* at location *j*,

$$SH_{ij} = \sum_{n=2}^{h} (v_{ij})_n \tag{8.1}$$

where *n* is the harmonics of the exciting frequency from 2, 3,…, *h*, $(v_{ij})_n$ is the velocity amplitude of the harmonic, *n* at the exciting mode, *i* at the measured location, *j* and then this SH_{ij} is normalised by the maximum value from all the measured location to get the normalised SH (NSH). The component 1X which is the amplitude of the exciting mode has not been included in the equation (8.1) because the operation deflection shape (ODS) at 1X generally represents the mode shape of the exciting mode. However, the amplitude of the higher harmonics definitely related to the size and location of the delamination. Finally the contribution from few lower modes has been defined as “Cumulative NSH (CNSH)” at each measured location which has been computed as

$$CNSH_j = \sum_{i=1}^{q} NSH_{ij} \tag{8.2}$$

where *q* is the number of modes used for this computation. Here the first 6 modes have been used. The plots of the CNSH of the plate with and without delamination (off-centre delamination and shaker location 1) are shown in Figure 8.2 which provides excellent indication for the location of the delamination. Figure 8.3 shows similar plots like Figure 8.2 but the healthy plate response is compared with the delaminated plate (delamination in the centre) and at shaker location 2.

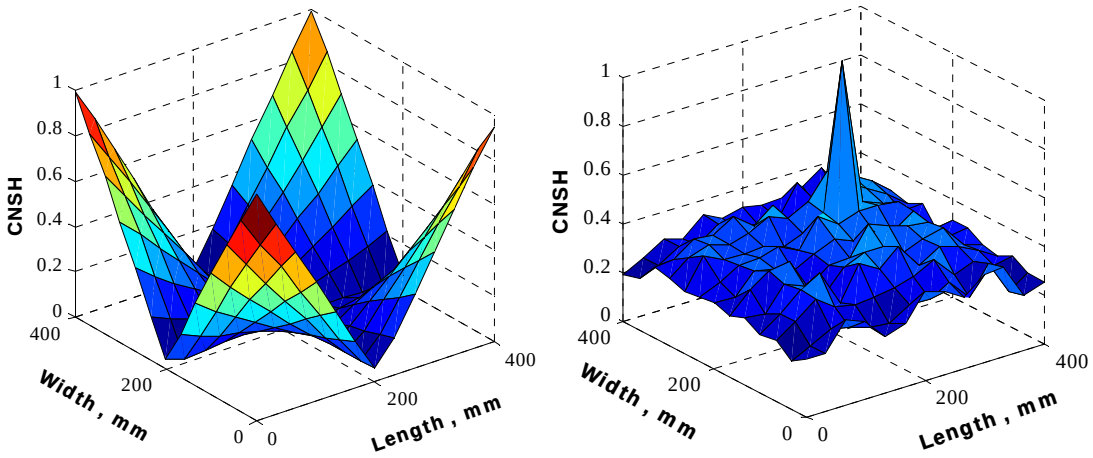

Figure 8.2 Typical CNSH plots at shaker location 1, using Modes 1 to 6 in the FE simulations, (a) Healthy plate, (b) Delaminated plate (Off-centre delamination)

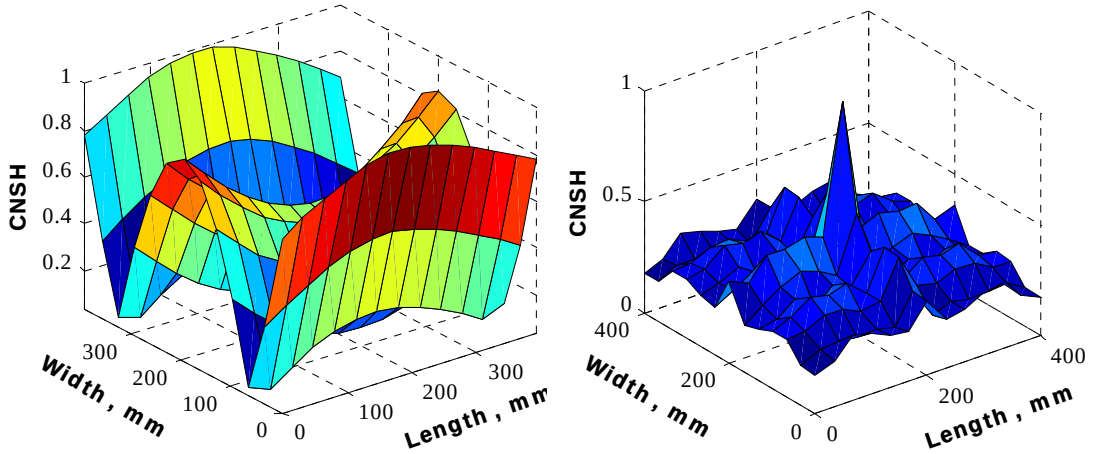

Figure 8.3 Typical CNSH plots at shaker position 2, using Modes 1 to 6 in the FE simulations, (a) Healthy plate, (b) Delaminated plate (In-centre delamination)

8.5 Delamination Size Variation

So far in this chapter delamination size (40mm x 40 mm) has been used in the numerical experiments. To see the effect of the delamination size on the location and the possibility of the measurement of the extent of the damage two different sizes 80 mm x 80 mm (twice the original size) and 120 mm x 120 mm (triple of the original damage size) were also studied. Figure 8.4 shows the comparison of the CNSH plots of the three sizes viz., 40 mm x 40 mm, 80 mm x 80 mm, and 120 mm x 120 mm.

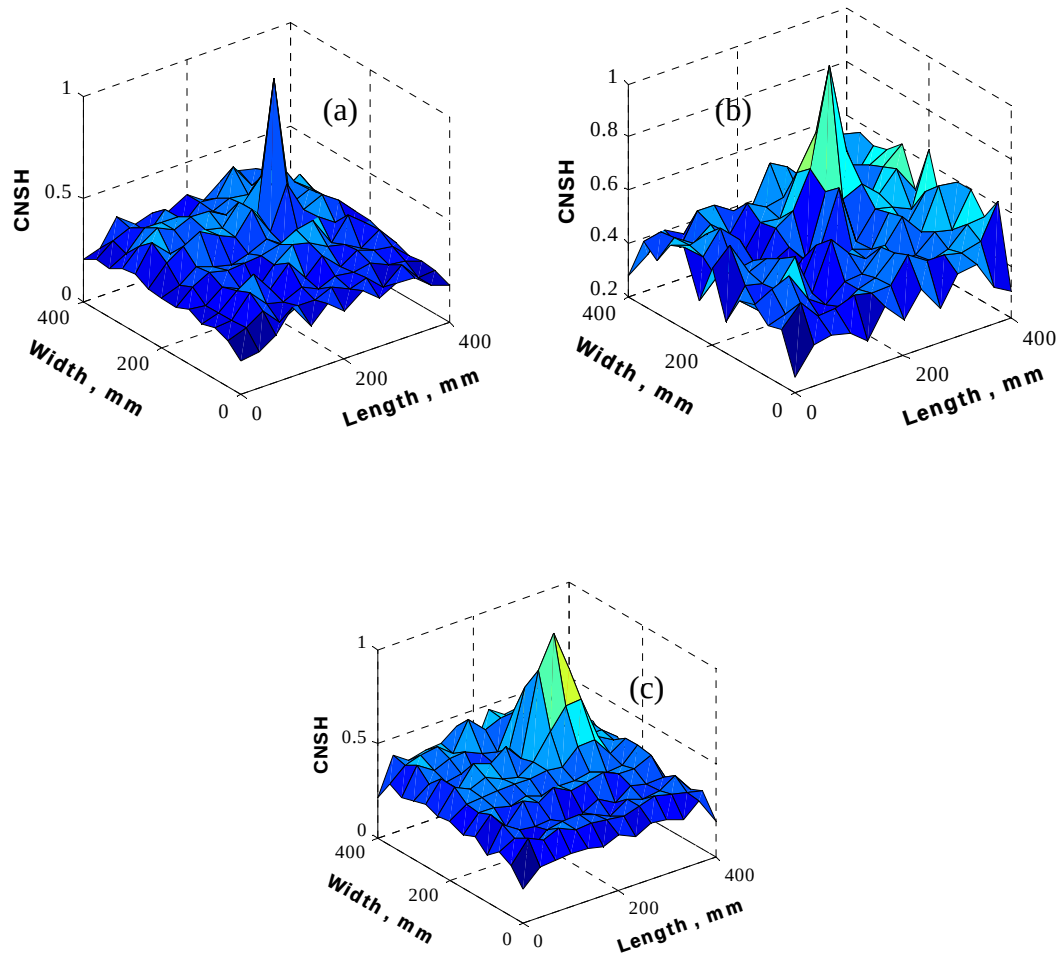

Figure 8.4 Typical CNSH plots at shaker position 1, using Modes 1 to 6 in the FE simulations of the delaminated plate (off-centre delamination) with (a) 40mm x 40mm (b) 80mm x 80mm (c) 120mm x 120mm

8.6 Experiments

The schematic of the experimental setup is shown in Figure 3.9. It consists of a composite plate shown in Figure 3.8 which was hanged by the soft elastic rope from the top 2 corners of the top edge to realise the free boundary condition for all the 4 edges of the plate. Modal analysis was performed, and the plates were excited at first 6 modes. Few typical acceleration spectra for the healthy plate and the delaminated plate (off-centre delamination) and shaker location 1 are shown in Figure 8.3 when excited at mode 6 at locations 9 and 20 (marked in Figure 3.10). The '1X' in the spectra indicates the exciting frequency and the components 2X, 3X, … represent the higher harmonics of the exciting frequency in the spectra. Once again, it has been observed from the spectra that due to anisotropic nature of the composite plate, the modes other than the exciting mode also contribute to the overall response. In addition to this effect, the nonlinear interactions between the delaminated layers in the plate with delamination also introduce the higher harmonics of the exciting frequency. Although the presence of such higher harmonics has also been observed in the healthy composite plate, probably again due to anisotropic property of the composite material, but the effect was not prominent compared to the plate with delamination.

The plots of the CNSH of the plate with (off-centre delamination) and without delamination for the experimental cases are also shown in Figure 8.4 at shaker location 1 which, once again, provides excellent indication for the location of the delamination. Hence the experimental observations are consistent with the FE simulated results. Figure 8.5 is similar plot comparison but for shaker location 2 and the delaminated plate with delamination in the centre case.

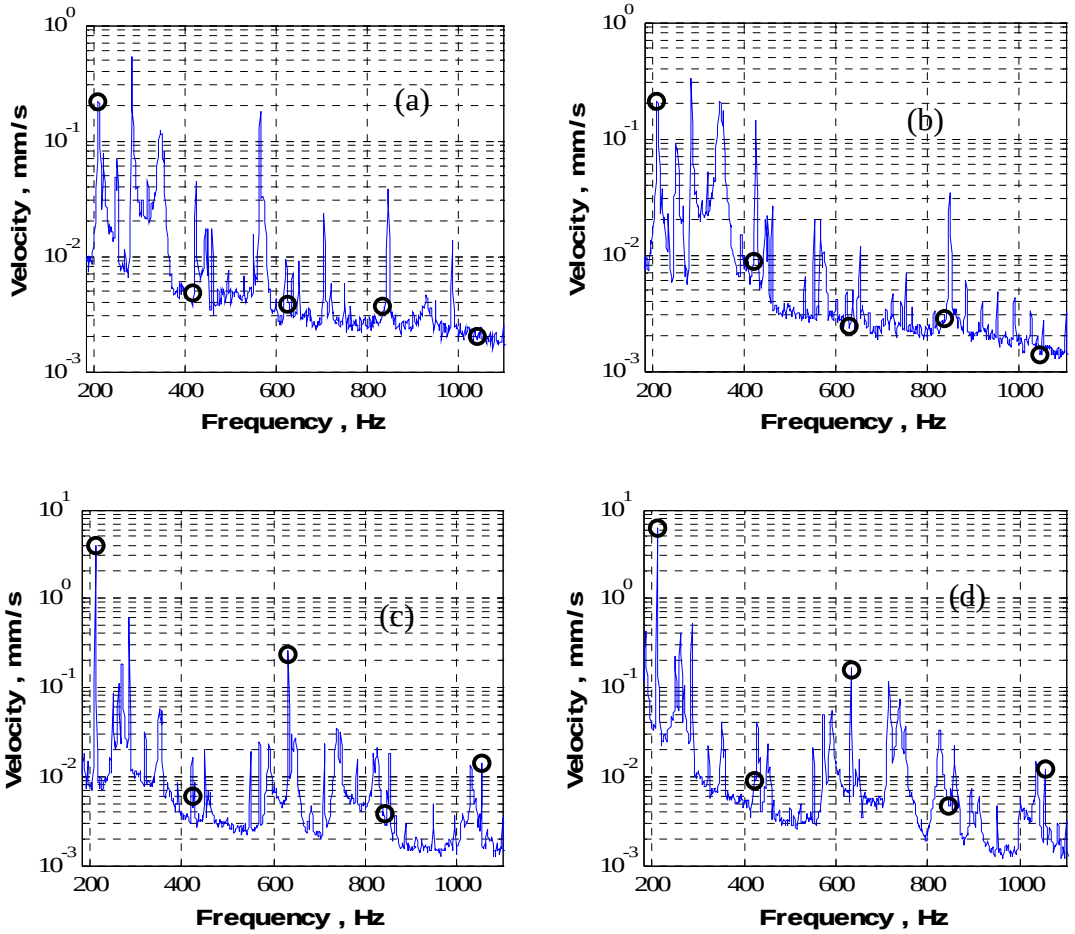

Figure 8.5 Typical measured amplitude acceleration response spectra at locations 9, 20 for the healthy (a-b) and delaminated plates (c-d) when excited at Mode 6 respectively

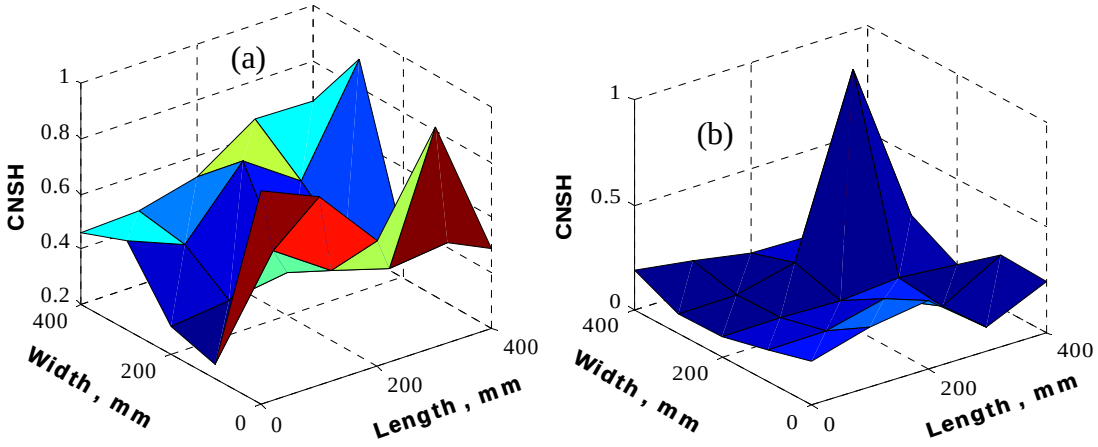

Figure 8.6 Typical CNSH plots at shaker position 1, using Modes 1 to 6 for the experimental examples, (a) Healthy plate, (b) Delaminated plate (Off-centre delamination)

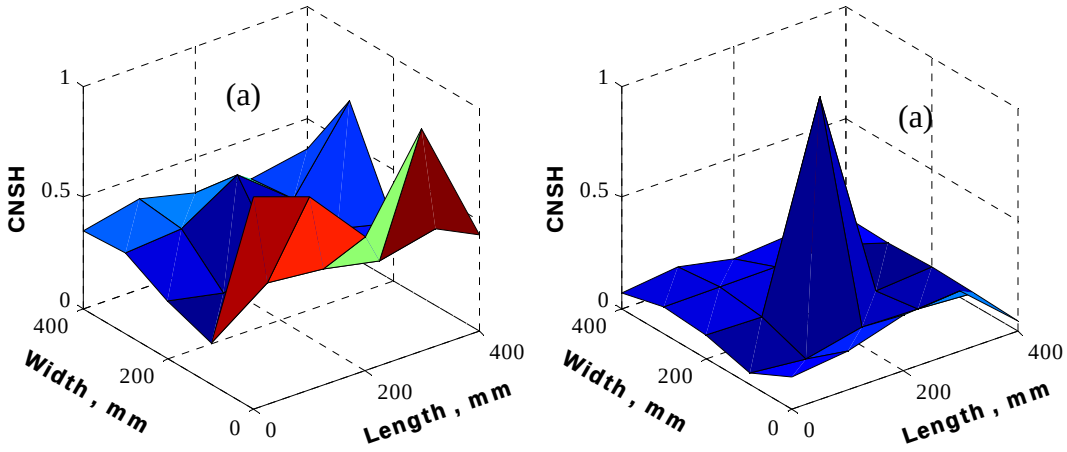

Figure 8.7 Typical CNSH plots at shaker position 2, using Modes 1 to 6 for the experimental examples, (a) Healthy plate, (b) Delaminated plate (In-centre delamination)

8.7 Summary

The nonlinear interaction between the delaminated layers in the composite plate during vibration has been considered here for the delamination detection. Initially, a typical composite plate made E-glass epoxy with and without delamination has been used in the FE simulation for the development of the detection method. As expected, the nonlinear interaction between the delaminated layers when excited at a few lower modes produced the prominent higher harmonics components of the exciting frequency. Then the normalised contribution of higher harmonic components at each mode has been defined as the "Normalised Summation of Harmonics (NSH)" and then it's cumulative for a few lower modes as CNSH. The delamination location has clearly been identified by the proposed CNSH method for the simulated examples. The method has then further been validated by the experiments conducted on the composite plates same as used in the FE simulations with and without delamination. Hence the proposed

CNSH can be deemed as a good indicator for the delamination detection. Since the development of method uses the velocity responses at just few lower modes so it is practically feasible for real structure using the conventional shaker and the laser vibrometer for this purpose.

CHAPTER 9
CONCLUSION AND FUTURE WORK

9.1 Overview

There are number of methods in the literature for the damage (cracks, debonds, and internal delaminations) detection of engineering structures. Most of these methods are using the data from the healthy structure for damage detection while some are "baseline free/reference free method" and are superior to the former methods both in terms of simplicity and accuracy. Composite structures are lightweight and strong but are more difficult to dynamically understand its behaviour as compared to linear materials like Steel and Aluminium. Due to its complex nature, very limited vibration-based methods are available in the literature for the delamination detection in composite structures. Many of these methods are kind of simulated studies without experimental validations. Conventional non-destructive techniques are not good enough to identify internal damage in composite. Hence vibration-based methods are the preferred choice for composite structures. Mainly two kinds of the vibration-based approaches have been suggested in the literature for the structural health monitoring of composite structures, one related to low frequency methods and other high frequency methods. In low frequency approaches, the change in the modal parameters (natural frequency, mode shape and damping) is compared with the healthy structure as the reference. It is believed that damages presented in composite structure cause modal parameters to change and this provides sufficient indication about the presence and location of the damage especially when the

damaged part results are compared with the identical composite part but without damage. The second type of damage detection and localisation technique is the high frequency approaches. In this approach composite structures are excited at higher modes of the order of few kHz or more (MHz's) needed with distributed sensors to map the deflection for identification of delamination. Use of high frequency methods imposes the limitations on the use of the conventional electromagnetic shaker and vibration sensors, whereas the low frequency methods may not be feasible for practical purpose because it often requires data from the healthy state which may not be available for old structures.

9.2 Summary of Present Research

The main objective of this research was to develop a novel reference-free method of (1) delamination detection and (2) delamination localisation, which can just use the vibration responses at a few lower modes using the conventional piezo-shaker and vibration sensor (accelerometer/laser vibrometer). It is believed that the delaminated layers will interact nonlinearly when excited externally by a piezo-shaker especially at the natural frequencies (exploiting the resonance phenomena). Hence this mechanism has been utilised in the numerical simulations and the number of experiments on the healthy and delaminated composite plates have been performed. In the numerical experiments different delaminated sizes and locations were used. Not only delaminated sizes and locations were studied but the data from the composite plates with multi-delaminations were also analysed. The exhaustive numerical work resulted in conclusions which were organised to develop two methods– first method (Objective 2) can quickly identify the presence of the delamination when excited at just few lower modes and the other method is capable

of identifying the location using the same method data once the presence of the delamination is confirmed. In the first approach (Delamination Detection) an averaged normalised root-mean square (RMS) has been suggested and experimentally validated for this purpose. In fact, in the method above normalised RMS are calculated for all the measurement locations and then these normalised RMS are simply averaged. It has been observed that the composite plate with internal delamination will have higher value of the averaged normalised RMS as compared to a composite plate with no delamination (healthy plate). This observation was confirmed by experiments and has been seen to be independent of the delamination location. The drawback of the method is it can't indentify multi-delaminations.

Latter the vibration data have then been analysed further to identify the location (Objective 3 as of chapter 2) of delamination and its size. Initially, the measured acceleration responses from the composite plates have been differentiated twice to amplify the nonlinear interaction clearly in case of delaminated plate and then Kurtosis was calculated at each measured location to identify the delamination location. The method has been referred to as "Kurtosis of DDA technique for delamination localisation". The method gave equally good results for different sizes of off-centre delaminations and locations. The technique also worked for multi-delaminations. The method was experimentally verified. The method could not locate the in-centre delamination from the experimental results. Since the technique is based on acceleration measurements and its difficult to measure acceleration responses, with smaller spacing between the adjacent measurement locations, as

compared to remotely operated scanning laser vibrometer which measures velocity as compared to accelerations.

To overcome the limitation mentioned above, the method has further been simplified (Objective 4 as of chapter 2) by just using the harmonics (velocity responses) in the measured responses to identify the location. To explain the method further, higher harmonics are first added for all the measurement locations (velocity data) at number of lower modes and then the results (summation of harmonics) of the first few modes are added together and then plotted against the grid points of the composite plate. A composite with delamination results in a clear peak at the delamination location when the above parameter (CNSH) is plotted. While Kurtosis of DDA techniques failed to locate delamination in the centre of the plate, the CNSH technique did succeed in identifying the damage in the centre of the plate.

9.3 Future Work Recommendations

- The effect of thickness of the plate on the delamination detection can also be seen in further research on the plates and the experiment can be performed on a tapered plate with internal delamination.

- Composite plates with multi-delaminations can be studied by experiments to see the effectiveness of the techniques developed in this research study.

- So far only one composite with built-in delaminations have been studied. The study can be extended to composite structures with joints and dis-bonds.

REFERENCES

1. Locke, S.B., *CTSB: Faulty Airbus Bond Caused Loss Of Rudder* in *The Wave*. 2007, WAVE PUBLISHING CO.: New York.

2. Kilroy, C. *www.airdisaster.com/photos/c-gpat/4.shtml*. AirDisaster.com; Available from: www.airdisaster.com.

3. Pascoe, D. *Bad News For Bertram*. Yachtsurvey.com 2009 [cited 2009 January 23, 2009]; CORES AND STRUCTURAL ISSUES]. Available from: http://www.yachtsurvey.com/bad_news_for_Bertram.htm.

4. Black, S., *Article*. High-Performance Composites 2008(Composites get smart): p. 6.

5. Mufti, A., *Guidelines for structural Health Monitoring.* ISIS Canada Carpporation, 2001. **Design Manual No. 2**: p. 127.

6. Daniel Balageas, C.-P.F., Alfredo Güemes, *Structural Health Monitoring.* ISTE Ltd, 2006: p. 496.

7. Hellier, C., *Handbook of Nondestructive Evaluation.* McGraw-Hill, New York, 2001.

8. Adams, D.E., *Health Monitoring of Structural Materials and Components: Methods with Applications.* John Wiley & Sons, 2007.

9. Freemantle, R. *Unltrsonic and acoustic techniques for non-destructive testing of composites*. WavelengthNDT [Presentation].

10. Dutton, A.G., *Flaw detection in composite materials using infra-red thermography by the method of external heating.* ARCHIVE: Proceedings of the Institution of Mechanical Engineers, Part C: Journal of Mechanical Engineering Science 1989-1996 (vols 203-210), 1996. **210**(53): p. 399-407.

11. Genest, M., et al., *Pulsed thermography for non-destructive evaluation and damage growth monitoring of bonded repairs.* Composite Structures, 2009. **88**(1): p. 112-120.

12. Avdelidis, N.P., et al., *Aircraft composites assessment by means of transient thermal NDT*. Progress in Aerospace Sciences, 2004. **40**(3): p. 143-162.

13. Meola, C., et al., *Detection of delamination in carbon-fibre-reinforced polymers with lock-in thermography*. Proceedings of the Institution of Mechanical Engineers, Part G: Journal of Aerospace Engineering, 2010. **224**(11): p. 1219-1227.

14. Tsao, C.C. and H. Hocheng, *Computerized tomography and C-Scan for measuring delamination in the drilling of composite materials using various drills.* International Journal of Machine Tools and Manufacture, 2005. **45**(11): p. 1282-1287.

15. Shin, Y.-S., Y.-H. Park, and T. Hinoki, *Nondestructive Testing of NITE-SiC Ceramics for Fusion Reactor Application*, in *Zero-Carbon Energy Kyoto 2009*, T. Yao, Editor. 2010, Springer Japan. p. 346-353.

16. De Albuquerque, V.H.C., J.M.R.S. Tavares, and L.M.P. Durão, *Evaluation of Delamination Damage on Composite Plates using an Artificial Neural Network for the Radiographic Image Analysis.* Journal of Composite Materials, 2010. **44**(9): p. 1139-1159.

17. Ueda, M. and A. Todoroki, *Delamination monitoring of CFRP laminate using the two-stage electric potential change method with equivalent electric conductivity*. Engineering Fracture Mechanics, 2008. **75**(9): p. 2737-2750.

18. Todoroki, A., *Delamination Monitoring Analysis of CFRP Structures using Multi-Probe Electrical Method.* Journal of Intelligent Material Systems and Structures, 2008. **19**(3): p. 291-298.

19. Hatta, H., et al., *Damage detection of C/C composites using ESPI and SQUID techniques.* Composites Science and Technology, 2005. **65**(7-8): p. 1098-1106.

20. M.A.U., K. *Non-destructive Testing Applications in Commercial Aircraft Maintenance*. in *Proceedings of the 7th Europian Conference on Non-Destructive Testing*. 1999.

21. Abdel-Latif, A.M., *An Overview of the Applications of NDI/NDT in Engineering Design for Structural Integrity and Damage Tolerance in Aircraft Structures*, in *Damage and Fracture Mechanics*, T. Boukharouba, M. Elboujdaini, and G. Pluvinage, Editors. 2009, Springer Netherlands. p. 93-100.

22. Chattopadhyay, A., C. Nam, and D. Dragomir-Daescu, *Delamination Modeling and Detection in Smart Composite Plates.* Journal of Reinforced Plastics and Composites, 1999. **18**(17): p. 1557-1572.

23. Tan, P. and L. Tong, *Delamination Detection of a Laminated Beam Using Magnetostrictive Composite Sensor and Actuator*. Journal of Reinforced Plastics and Composites, 2007. **26**(8): p. 831-846.

24. Barton, D.P., *Comparative Vacuum Monitoring (CVM™)*. Encyclopedia of Structural Health Monitoring. 2009: John Wiley & Sons, Ltd.

25. Seung-Seok Lee, D.-J.Y., Joon-Hyun Lee and Sekyung Lee, *Detection of Real Defects in Composite Structures by Laser Techniques.* Key Engineering Materials, 2004. **270 - 273**: p. 6.

26. Shang, S.G.J.Y., ; Qiao, Pizhong, *Delamination identification of laminated composite plates using a continuum damage mechanics model and subset selection technique.* Smart Materials and Structures, 2010. **19**: p. 55024-55036.

27. Hadjileontiadis, L.J. and E. Douka, *Kurtosis analysis for crack detection in thin isotropic rectangular plates.* Engineering Structures, 2007. **29**(9): p. 2353-2364.

28. Yang, Z., et al., *Damage detection in composite structures using vibration response under stochastic excitation.* Journal of Sound and Vibration, 2009. **325**(4-5): p. 755-768.

29. Wang, L., Z. Yang, and T.P. Waters, *Structural damage detection using cross correlation functions of vibration response.* Journal of Sound and Vibration, 2010. **329**(24): p. 5070-5086.

30. I. Mckenzie, et al., *Optical fibre sensors for health monitoring of bonded repair systems.* Composite Structures, 2000. **50**: p. 405-416.

31. Takeda, S., Y. Okabe, and N. Takeda, *Delamination detection in CFRP laminates with embedded small-diameter fiber Bragg grating sensors.* Composites Part A: Applied Science and Manufacturing, 2002. **33**(7): p. 971-980.

32. S. Takeda, et al., *Detection of edge delamination in CFRP laminates under cyclic loading using small-diameter FBG sensors.* Composite Science and Technology, 2003. **63**: p. 1885-1894.

33. Grouve, W.J.B., et al., *Delamination detection with fibre Bragg gratings based on dynamic behaviour.* Composites Science and Technology, 2008. **68**(12): p. 2418-2424.

34. Xu, Y., et al., *A New Fiber Optic Based Method for Delamination Detection in Composites.* Structural Health Monitoring, 2003. **2**(3): p. 205-223.

35. Ihn, J.-B. and F.-K. Chang, *Pitch-catch Active Sensing Methods in Structural Health Monitoring for Aircraft Structures.* Structural Health Monitoring, 2008. **7**(1): p. 5-19.

36. Mal, A., S. Banerjee, and F. Ricci, *An automated damage identification technique based on vibration and wave propagation data.* Philosophical Transactions of the Royal Society A: Mathematical,
Physical and Engineering Sciences, 2007. **365**(1851): p. 479-491.

37. Quaegebeur, N. and et al., *Structural health monitoring strategy for detection of interlaminar delamination in composite plates.* Smart Materials and Structures, 2010. **19**(8): p. 085005.

38. Su, Z. and L. Ye, *Fundamental Lamb Mode-based Delamination Detection for CF/EP Composite Laminates Using Distributed Piezoelectrics.* Structural Health Monitoring, 2004. **3**(1): p. 43-68.

39. Krishnan balasubramaniam, B.V.S.S., J. Vishu Vardan, C.V. Krishnamurthy, *Structural Health Monitoring of Composite Structures Using Guided Lamb Waves.* Key Engineering Materials 2006. **321 - 323**: p. 6.

40. Kudela, P. and W. Ostachowicz, *A Multilayer Delaminated Composite Beam and Plate Elements: Reflections of Lamb Waves at Delamination.* Mechanics of Advanced Materials and Structures, 2009. **16**(3): p. 174-187.

41. Hu, N., et al., *Optimal Excitation Frequency of Lamb Waves for Delamination Detection in CFRP Laminates.* journal of Composite Materials, 2010. **44**(13): p. 1643-1663.

42. Pohl, J. and G. Mook, *SHM of CFRP-structures with impedance spectroscopy and Lamb waves.* International Journal of Mechanics and Materials in Design, 2010. **6**(1): p. 53-62.

43. Dong Wang, et al., *Probabilistic Damage Identification Based on Correlation Analysis Using Guided Wave Signals in Aluminum Plates.* Structural Health Monitoring, 2010. **9**(2): p. 133-144.

44. Okabe, Y. and et al., *Delamination detection in composite laminates using dispersion change based on mode conversion of Lamb waves.* Smart Materials and Structures, 2010. **19**(11): p. 115013.

45. Wandowski, T., et al., *Guided wave-based detection of delamination and matrix cracking in composite laminates.* Proceedings of the Institution of Mechanical Engineers, Part C: Journal of Mechanical Engineering Science.

46. V. T. Rathod, D.R.M., *Lamb Wave Based Monitoring of Plate-Stiffener Deboding Using A Circular Array of Piezoelectric Sensors.* INTERNATIONAL JOURNAL ON SMART SENSING AND INTELLIGENT SYSTEMS 2010. **3**(1): p. 18.

47. Yun-Kyu An, H.J.L., Hoon Sohn, *Temperature Independent Delamination Detection Using Data Normalization* Advanced Materials Research 2010. **123 - 125**: p. 4.

48. Bhalla, S., C.K. Soh, and Z. Liu, *Wave propagation approach for NDE using surface bonded piezoceramics.* NDT & E International, 2005. **38**(2): p. 143-150.

49. Z. Sharif Khodaei, M.H.A., *Damage Identification Using Lamb Waves.* Key Engineering Materials 2011. **Advances in Fracture and Damage Mechanics IX** (452-453): p. 4.

50. Paolozzi, A. and I. Peroni, *Detection of Debonding Damage in a Composite Plate through Natural Frequency Variations.* Journal of Reinforced Plastics and Composites, 1990. **9**(4): p. 369-389.

51. Salawu, O.S., *Detection of structural damage through changes in frequency: a review.* Engineering Structures, 1997. **19**(9): p. 718-723.

52. Hong-ping, Z., H. Bo, and C. Xiao-qiang, *Detection of structural damage through changes in frequency.* Wuhan University Journal of Natural Sciences, 2005. **10**(6): p. 1069-1073.

53. Cerri, M.N. and F. Vestroni, *DETECTION OF DAMAGE IN BEAMS SUBJECTED TO DIFFUSED CRACKING.* Journal of Sound and Vibration, 2000. **234**(2): p. 259-276.

54. Kim, H.Y., *VIBRATION-BASED DAMAGE IDENTIFICATION USING RECONSTRUCTED FRFS IN COMPOSITE STRUCTURES.* Journal of Sound and Vibration, 2003. **259**(5): p. 1131-1146.

55. GÖRl, E. and M. Link, *DAMAGE IDENTIFICATION USING CHANGES OF EIGENFREQUENCIES AND MODE SHAPES.* Mechanical Systems and Signal Processing, 2003. **17**(1): p. 103-110.

56. Kim, H.-Y. and W. Hwang, *Effect of debonding on natural frequencies and frequency response functions of honeycomb sandwich beams.* Composite Structures, 2002. **55**(1): p. 51-62.

57. Yam, L.H., Z. Wei, and L. Cheng, *Nondestructive Detection of Internal Delamination by Vibration-based Method for Composite Plates.* Journal of Composite Materials, 2004. **38**(24): p. 2183-2198.

58. L. H. Yam, L.C., Z. Wei, Y. J. Yan, *Damage Detection of Composite Structures Using Dynamic Analysis.* Key Engineering Materials 2005. **Vols. 295-296**: p. 6.

59. Abdo, M.A.B. and M. Hori, *A NUMERICAL STUDY OF STRUCTURAL DAMAGE DETECTION USING CHANGES IN THE ROTATION OF MODE SHAPES.* Journal of Sound and Vibration, 2002. **251**(2): p. 227-239.

60. Hamey, C.S., et al., *Experimental Damage Identification of Carbon/Epoxy Composite Beams Using Curvature Mode Shapes.* Structural Health Monitoring, 2004. **3**(4): p. 333-353.

61. Araújo dos Santos, J.V., et al., *Damage localization in laminated composite plates using mode shapes measured by pulsed TV holography.* Composite Structures, 2006. **76**(3): p. 272-281.

62. Yoon, M.-K., et al., *Local Damage Detection with the Global Fitting Method Using Mode Shape Data in Notched Beams.* Journal of Nondestructive Evaluation, 2009. **28**(2): p. 63-74.

63. Minak, G., et al., *Localization of a delamination and estimation of its length in a composite laminate beam by the VSHM and pattern recognition methods.* Mechanics of Composite Materials, 2010. **46**(4): p. 387-394.

64. Yan, Y.J., et al., *Development in vibration-based structural damage detection technique.* Mechanical Systems and Signal Processing, 2007. **21**(5): p. 2198-2211.

65. P. Z. Qiao, K. Lu, and W. Lestari., *A combined static/dynamic technique for damage detection of laminated composite plates.* Experimental Mechanics, 2008. **48**: p. 17-35.

66. Gherlone, M., et al., *Novel vibration-based methods for detecting delamination damage in composite plate and shell laminates.* Damage Assessment of Structures Vi, 2005. **293-294**: p. 289-296.

67. Qiao, P., et al., *Curvature mode shape-based damage detection in composite laminated plates.* Composite Structures, 2007. **80**(3): p. 409-428.

68. Akhter, N., et al., *Location of delamination in laminated composite plates by pulsed laser holography.* Optics and Lasers in Engineering, 2009. **47**(5): p. 584-588.

69. Ghoshal, A., et al., *Experimental Investigation of Damage Detection in Composite Material Structures Using a Laser Vibrometer and Piezoelectric Actuators.* Journal of Intelligent Material Systems and Structures, 2003. **14**(8): p. 521-537.

70. Amraoui, M.Y. and N.A.J. Lieven, *Laser Vibrometry Based Detection of Delaminations in Glass/Epoxy Composites.* Journal of Vibration and Acoustics, 2004. **126**(3): p. 430-437.

71. Choi, S., et al., *Improved fault quantification for a plate structure.* Journal of Sound and Vibration, 2006. **297**(3-5): p. 865-879.

72. I. Ullah, J.K.S. *Dynamic behaviour of a delaminated composite beam.* in *Proceedings of 5th International Conference on Condition Monitoring and Machinery Failure Prevention Technologies (CM 2008 and MFPT 2008).* 2008. Edinburgh Conference Centre, Herriot-Watt University, Edinburgh.

73. I. Ullah, J.K.S., A. Pinkerton, *Vibration-based Delamination Detection in a Composite Plate.* Mechanics of Advanced Materials & Structures, 2011. **(In Press)**.

74. Sinha, J.K. and M.I. Friswell, *Simulation of the dynamic response of a cracked beam.* Computers & Structures, 2002. **80**(18-19): p. 1473-1476.

75. U. Polimeno, M.M., D.P. Almond, *Smart Nonlinear Acoustic Based Structural Health Monitoring System.* Advances in Science and Technology, 2008. **56**: p. 426-434.

76. Meo, M., U. Polimeno, and G. Zumpano, *Detecting Damage in Composite Material Using Nonlinear Elastic Wave Spectroscopy Methods.* Applied Composite Materials, 2008. **15**(3): p. 115-126.

77. Solodov, I., et al., *Nonlinear self-modulation and subharmonic acoustic spectroscopy for damage detection and location.* Applied Physics Letters, 2004. **84**(26): p. 5386-5388.

78. (DS), D.S., *ABAQUS Documentation*. Vol. 6.10.

79. I. Ullah, J.K.S., *Dynamics of Composite Plate by Experiment and Finite Element Analysis.* European Journal of Scientific Research, 2011. **55**(2).

80. Hsien-Yang, L., H. Jin-Hung, and M. Chien-Ching, *Vibration analysis of angle-ply laminated composite plates with an embedded piezoceramic layer.* Ultrasonics, Ferroelectrics and Frequency Control, IEEE Transactions on, 2003. **50**(9): p. 1084-1099.

81. Doebling, S.W., C. R. Farrar, M B. Prime, D W. Shevitz, *Damage Identification and Health Monitoring of Structural and Mechanical Systems From Changes in their Vibration Characteristics*, in *Los Alamos National Laboratory report LA-13070-MS*. 1996.

80. I. Ullah, J.K.S., *Dynamics of Composite Plate by Experiment and Finite Element Analysis.* European Journal of Scientific Research, 2011. 55(2).

81. Hsien-Yang, L., H. Jin-Hung, and M. Chien-Ching, *Vibration analysis of angle-ply laminated composite plates with an embedded piezoceramic layer.* Ultrasonics, Ferroelectrics and Frequency Control, IEEE Transactions on, 2003. 50(9): p. 1084-1099.

82. Doebling, S.W., C. R. Farrar, M B. Prime, D W. Shevitz, *Damage Identification and Health Monitoring of Structural and Mechanical Systems From Changes in their Vibration Characteristics*, in *Los Alamos National Laboratory report LA-13070-MS*. 1996.

APPENDIX (PUBLISHED WORK)

Dynamic behaviour of de-laminated composite beam

Israr Ullah, J.K. Sinha*

Dynamics Structures and Design Group, School of Mechanical, Aerospace and Civil Engineering, the University of Manchester
PO Box 88, Manchester M60 1QD

ABSTRACT

Delamination in any composite structures generates significant local modes (coupled with higher modes of structure) at significantly higher frequencies in kHz depending on the size of the delamination pocket. The local mode is generally excited to identify the presence of delamination in the vibration based approaches. However detect process map the deformation (or mode shape) over the surface area either through laser scanner or optical sensor or using closely spaced embedded sensors. Hence these methods are costly and difficult to apply if the surface area is very large. Here again, the possibility of delamination detection has been examined in a much economical manner. In the present approach, the structure response due to the nonlinear interaction between the layers in the delamination area, when the structure is excited at higher modes, has been utilised. This nonlinear response can be picked up from just few locations of the structure. The proposed method has been validated on very simplified numerically simulation and then through a simple experimental test.

Keyword: delamination, composite, modal

***Corresponding Author**

1.0 INTRODUCTION

Now-a-days, composite materials have been used in several applications, for example, aircraft structural components, because of their light weight and high strength. However the delamination which is one of the serious defects often develops and propagates due to vibration during the service of the structure. The presence of this defect warrants the design life of the structure and the safety. Hence the presence of such defect has to be detected in time to plan the remedial action well in advance.

Several research studies have been carried for the composite structures with delamination [1-20]. They are related to the modelling aspects of the delaminated structures [3-6] and on the vibration based detection of the delamination by both experiments and analysis [7-14]. Few studies suggesting the detection by change in natural frequencies [15-17] and few have used the effect of local modes in their experiments to identify the delamination either by mapping the mode shape across the surface of the composite structure [13-15] or by advance signal processing using wavelet analysis [19-20]. Often the use of such technique requires the distributed or embedded sensors at least over the surface of the composite structure which restricts the practical used in many cases.

The present study is also on the dynamics of the delaminated composite structure. Here a numerically simulated example of a steel beam has been considered for the simplification in understanding instead of a beam made of the composite material. The beam has been modelled by the finite element (FE) method. A small delamination effect has been introduced in the FE model by dividing the flexural rigidity into parts to represent the delamination effect. The modal analysis has then been carried out to know the natural frequencies and mode shapes so that the modes with the significant

delamination effect in their mode shapes can be chosen for further study. These modes were then excited externally to compute the dynamic behaviour for the delaminated beam and their results were compared with the beam without delamination. The effect of non-linearity introduced in the delaminated area has also been simulated in the study. Results and the feasibility of the delamination detection based on the observation on the simulated example and validated on a simple experimental test have been discussed here.

2.0 SIMULATED EXAMPLE

As discussed in Section 1, a cantilever steel beam of 1 meter length and 20 mm x 20 mm cross-section has been chosen to understand the delamination effects for the simulated study instead of the composite beam to ease the modelling process. The beam under study has been modelled using 2-node beam element (each node with 2 degrees of freedom-one bending deflection and other bending rotation). The beam is divided into 100 elements of equal length. The finite element (FE) model is shown in Figure 1(a). For the de-lamination effect, the flexural rigidity of the beam has been divided into the parts at the centre of the beam. The FE model with the de-lamination effect is also shown in Figure 1(b). The nodes 51 and 102 in the FE model show the modelling of the delamination.

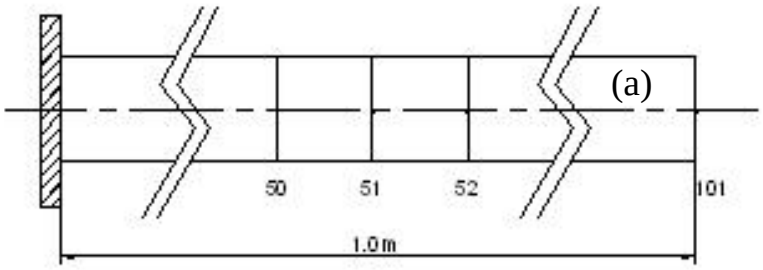

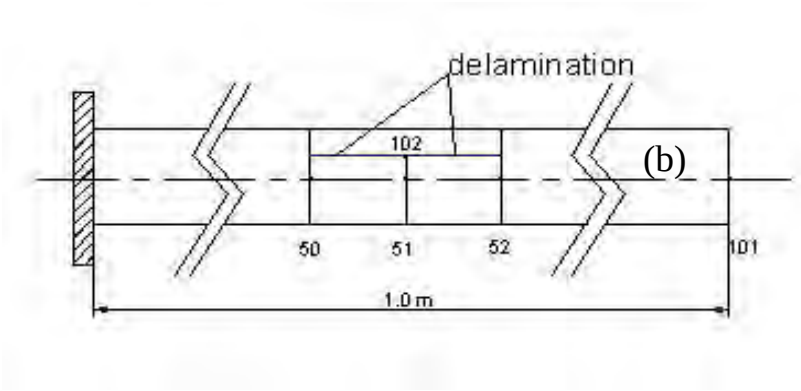

Figure 1 FE models, (a) without delamination, (b) with delamination

2.1 MODAL ANALYSIS

Modal analysis has been carried out for the beam with and without delamination. The mode shapes of first 3 natural frequencies are shown in Figure 2. Although there is small difference in natural frequencies but no change in mode shapes have been noticed. The effect of delamination can be clearly seen in the mode shapes at the much higher natural frequencies from mode 18 (14.222 kHz) onwards. Few typical mode shapes at 22, 23 and 24th modes are shown in Figure 3 for both delamination and no delamination cases.

No Delamination **Delamination**

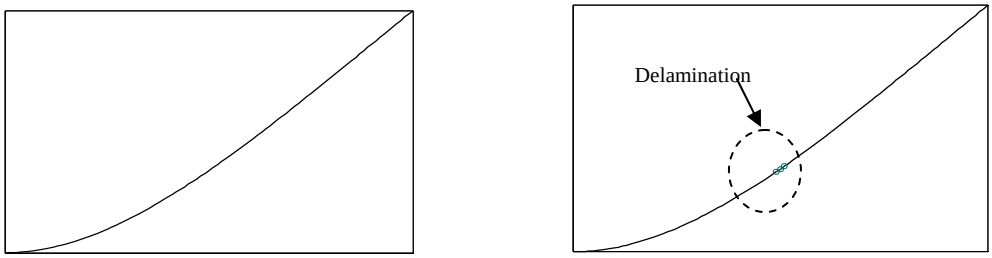

Mode 1: 16.763 Hz Mode 1: 16.692 Hz

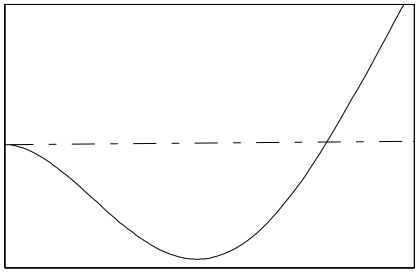

Mode 2: 105.05 Hz

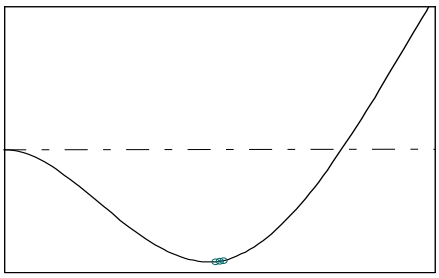

Mode 2: 103.15 Hz

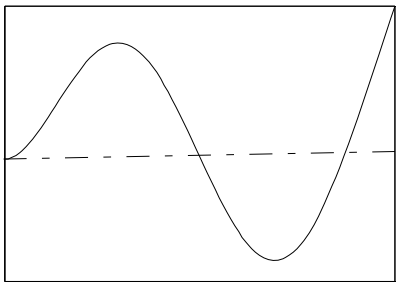

Mode 3: 294.15 Hz

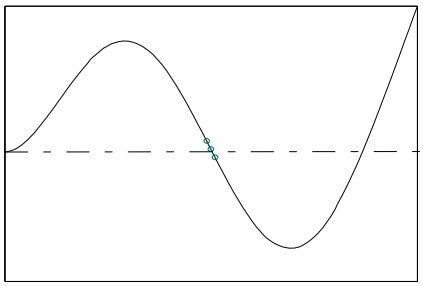

Mode 3: 294.13 Hz

Figure 2 Mode shapes at first 3 natural frequencies with & without delamination in the cantilever beam.

No delamination

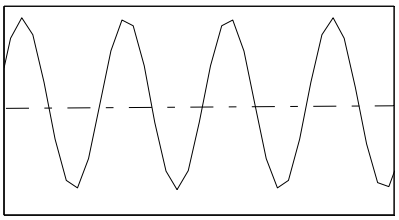

Mode 22: 21.754 kHz

Delamination

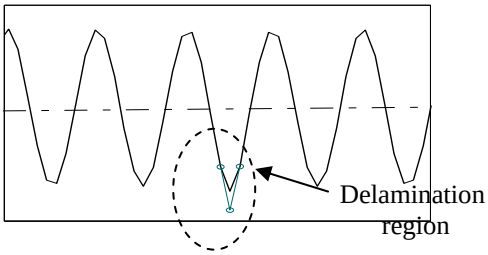

Mode 22: 21.489 kHz

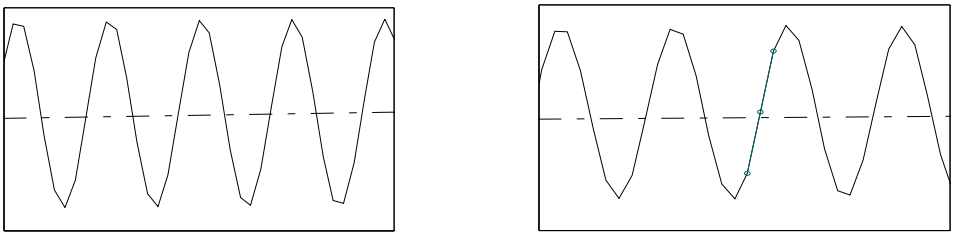

Mode 23: 23.852 kHz Mode 23: 23.758 kHz

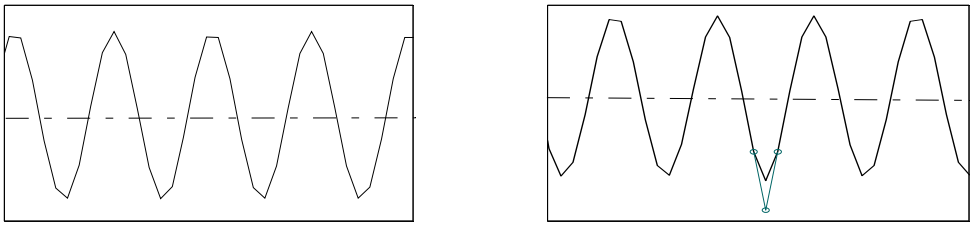

Mode 24: 25.991 kHz Mode 24: 25.685 kHz

Figure 3 Modes at 22, 23, and 24th natural frequencies with & without delamination in cantilever beam.

2.2 RESPONSE ESTIMATIONS

Having known that the delamination effect is prominent at higher frequencies, the linear chirp-sine excitation from 20 kHz to 31 kHz to include five modes has been applied at node 17 to both the models (with and without delamination). The linear chirp rate of 0.11 kHz per ms has been assumed. The Newmark–β method [21] has been used for response computations, with time step of 1e-6 s. The non-linear interaction between the nodes 51 and 102 in the delamination area has also been simulated to realise the actual behaviour in the delamination region. The displacement responses at the nodes 51 and 101 in the vertical direction at each time steps have been compared such that the beam behaves like a laminated beam when $(y_{51}(t) - y_{101}(t)) \geq 0$ (i.e., both nodes moving together), otherwise the movement of these nodes were assumed to independent like delaminated case. The acceleration responses at the free end of the cantilever beam for

both cases are shown in Figures 4 & 5 respectively. Figures 4(a) and 5(a) show the linear chirp excitation together with the natural frequencies and corresponding acceleration responses in Figures 4(b) and 5(b). The responses also indicate the presence of 5 resonance peaks in the frequency band of excitation.

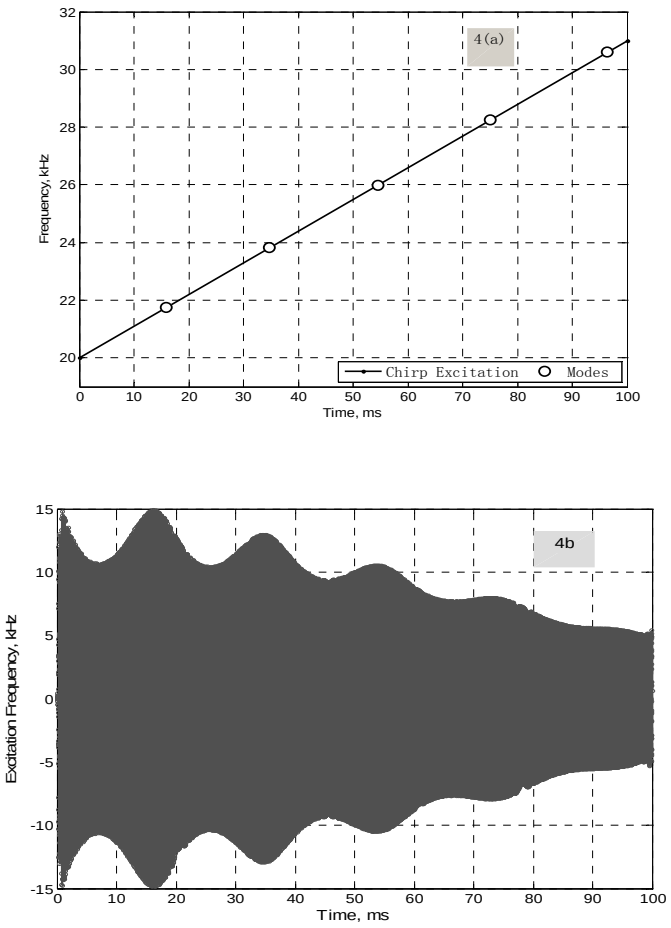

Figure 4 Excitation and Acceleration Response for the beam without delamination, (a) linear chirp excitation from 20 kHz to 31 kHz. (b). Response at the free end of the cantilever beam.

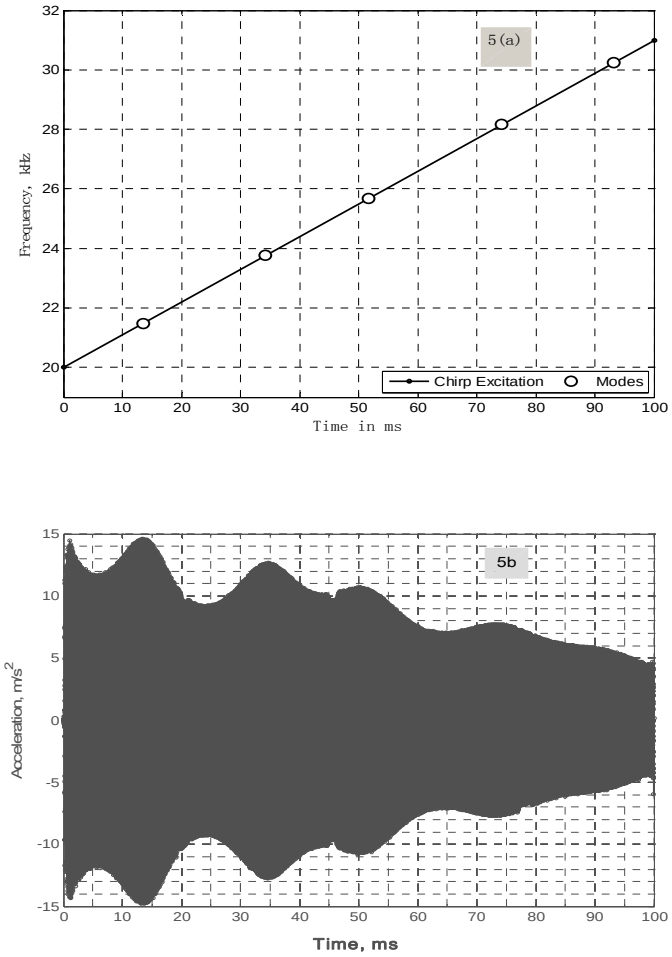

Figure 5 Excitation and Acceleration Response for the beam with delamination, (a) Linear chirp excitation from 20 kHz to 31 kHz, (b) Response at the free end of the cantilever beam.

Figure 6 shows the displacement responses at Nodes 51 and 102 near resonance peaks at modes 22, 23 and 24. Responses at modes 22 and 24 are high and non-linear interaction seems to be more compared to the 23rd mode. It is expected from the mode shapes shown in Figure 3. Although the mode shape at the 23 mode does not show significant relative deflection, however the non-linear interaction observed at this natural frequency is definitely an encouraging indication for detection of the de-lamination. Similar observations have also been made at other higher odd modes.

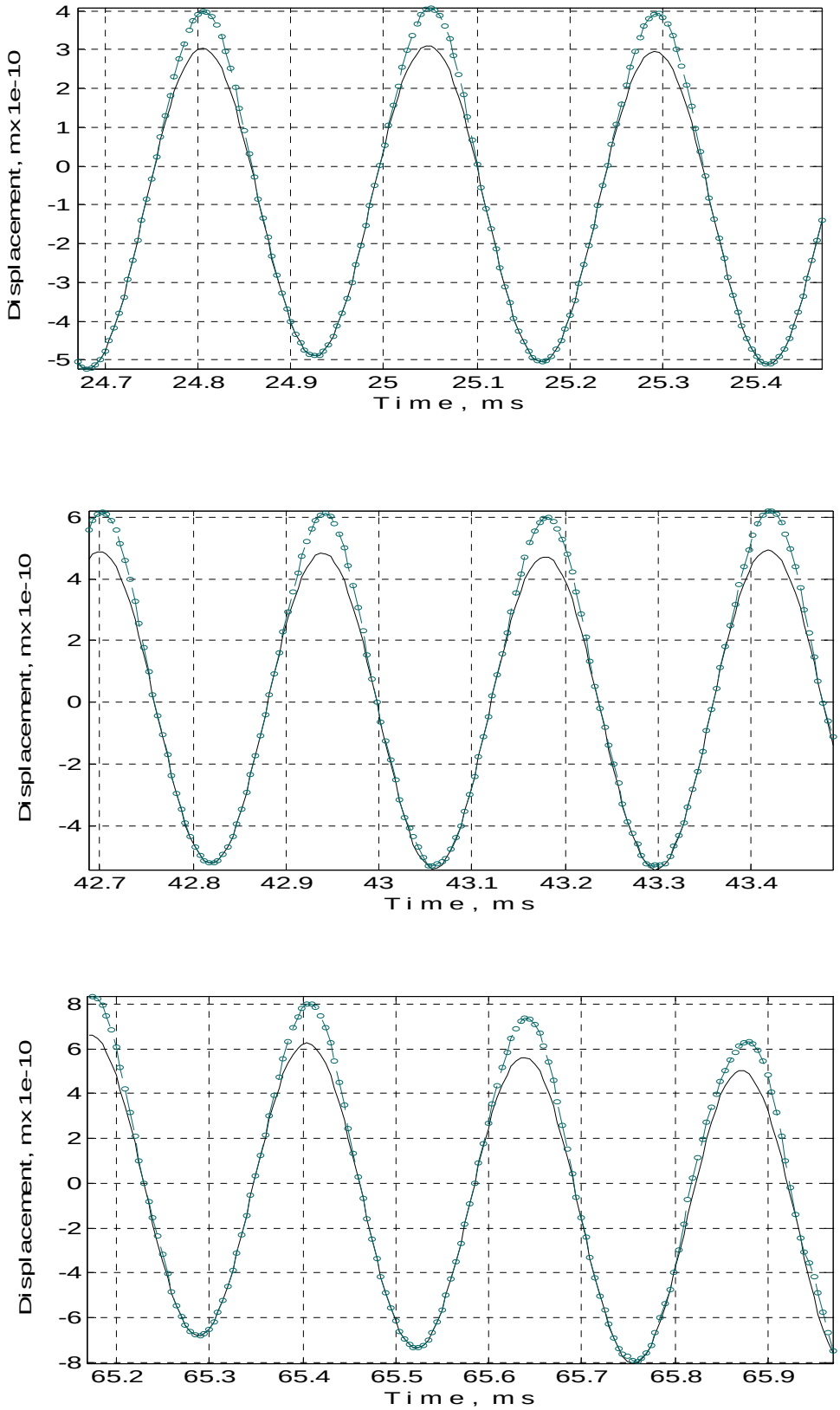

Figure 6 Displacement responses at Nodes 51 and 102 showing non-linear interaction, (a) Mode 22 – 21.486 kHz, (b) Mode 23 -23.758 kHz, (c) Mode 24 -25.685 kHz

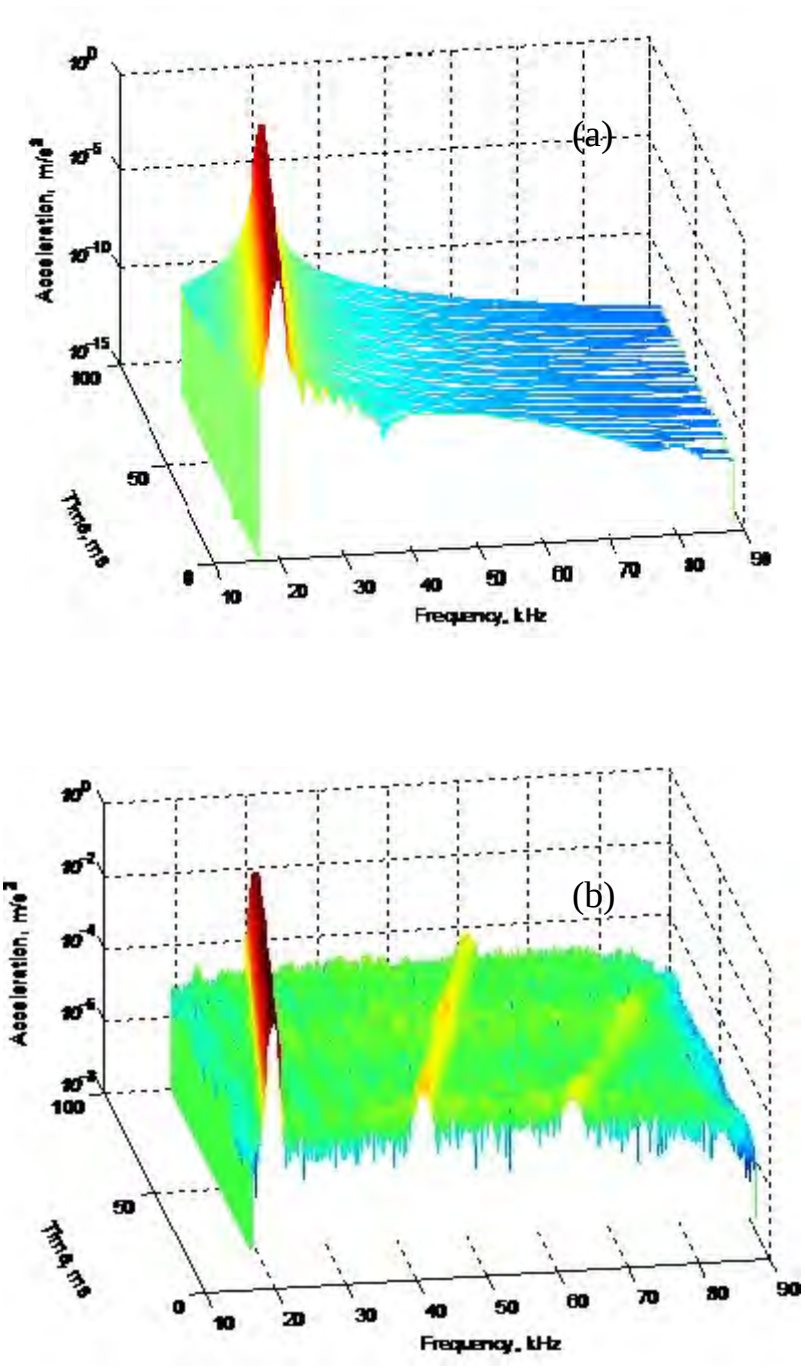

Figure 7 The waterfall plots for Acceleration spectra for the free end responses of the cantilever beam, (a) without delamination, (b) with delamination

Further analysis of the acceleration responses measured at the free end (Figures 4(b) and 5(b)) of the cantilever beam for both cases have been carried out in the frequency domain. Typical 3D waterfall plots of the short time Fourier Transformation (STFT) of

the responses for these two cases are shown in Figure 7 which show the presence of the resonance frequencies in the frequency band of the excitation and their harmonics with time for the delamination case, however the beam without delamination shows only the resonance frequency peaks without any harmonics.

3.0 CONCLUSION

The vibration behaviour of the delaminated structures has been discussed through a simple simulated and experimental study. It has been observed the excitation at the natural frequencies trigger the non-linear interaction between the layers in the delamination pocket. The acceleration response far away from the delamination location also seems to picking such non-linear behaviour, hence the present study show the possibility of delamination detection by conducting simple vibration experiments without using the embedded sensors or mapping the deformation over the area to detect the delamination. Present study has just been limited to the simple examples, however it is now plan to carry out the similar study on the composite structure with a small delamination and possibility of identifying the delamination location will also be explored.

References

[1] P.Z. Qiao, K. Lu ,W. Lestari, A combined static/dynamic technique for damage detection of laminated composite plates, *Experimental Mechanics* 48 (2008) 17–35.

[2] H. W. Park, H. Sohn, K. H. Law, C. R. Farrar, Time reversal active sensing for health monitoring of a composite plate, *Journal of Sound and Vibration* 302 (1-2) (2007) 50-66.

[3] Riccio A., Perugini P., Scaramuzzino F., Modelling compression behaviour of de-laminated composite panels, *Computers and Structures* 78 (1) (2000) 73-81.

[4] A. Gu H. Chattopadhyay, Modeling of delamination buckling in composite cylindrical shells with a new higher-order theory, *Composites Science and Technology* 54 (2) (2005) 223-232.

[5] G. Alfano, M. A. Crisfield, Finite element interface models for the delamination analysis of laminated composites, *International Journal of Numerical Methods &. Engineering* 50 (2001) 1701-1736.

[6] H. Chai, C. D. Babcock, Two-dimensional modelling of failure in laminated plates by delamination buckling, *Journal of Composite Materials* 19 (1985) 67-98.

[7] A. Todoroki, Y. Tanaka, Y. Shimamura, Delamination monitoring of graphite/epoxy laminated composite plate of electric resistance change method, *Composites Science and Technology* 62 (9) (2002) 1151-1160.

[8] A. Todoroki, M. Ueda**,** Low-cost delamination monitoring of CFRP beams using electrical resistance changes with neural networks, *Smart Material Structures* (2006) 15 (15) (2006) 75-84.

[9] J.C. Abry, S. Bochard, A. Chateauminois, M. Salvia, G. Giraud , In situ detection of damage in CFRP laminates by electric resistance measurements, *Composites Science and Technology* 59 (1999) 925–935.

[10] A. Todoroki, H. Suzuki, Health monitoring of internal delamination cracks for graphite/epoxy composites by electric potential method, *Applied Mechanics and Engineering* **51** (2000) 283–294.

[11] C.J. Jih, C.T. Sun, Prediction of Delamination in Composite Laminates Subjected to Low Velocity Impact, *Journal of Composite Materials* 27 (7) (2003) 684-701.

[12] S. Takeda, Y. Okabe, T. Yamamoto, N. Takeda, Detection of edge delamination in CFRP laminates under cyclic loading using small-diameter FBG sensors, *Composites Science and Technology* 63 (13) (2003) 1885-1894.

[13] S. Takeda, Y. Okabe, N. Takeda, Delamination detection in CFRP laminates with embedded small-diameter fibre Bragg grating sensors, *Composites Part A* 33 (2002) 971–980.

[14] S. Takeda, S. Minakuchi, Y. Okabe, N. Takeda, Delamination monitoring of laminated composites subjected to low-velocity impact using small-diameter FBG sensors, *Composites Part A* 7 (2005) 903–908.

[15] Y. Xu, C. K. Y. Leung, P. Tong, J. Yi, S. K. L. Lee, A new fiber optic based method for delamination detection in composites, *Structural Health Monitoring* 2 (3) (2003) 205-223.

[16] A. paolozzi, I. Peroni, Detection of Debonding Damage in a Composite Plate through Natural Frequency Variations, *Journal of Reinforced Plastics and Composites* 9 (4) (1990) 369-389.

[17] H. Y. Kim, W. B. Hwang, Effect of debonding on natural frequency response functions of honeycomb sandwitch beams, *Composite Structures* 55 (2002) 51-62.

[18] S. H. D. Valdes, C. Soutis, De-lamination detection in composite laminates from variations of their modal characteristics, *Journal of Sound and Vibration* 228 (8) (1999) 1-9.

[19] H. Sohn, G. Park, J. R. Wait, N.P. Limback, C.R. Farrar, Wavelet-based active sensing for delamination detection in composite structures, *Smart Material Structures* 13 (2004) 153–160.

[20] Z. Su, L. Ye, Lamb wave-based quantitative identification of delamination in CF/EP composite structures using artificial neural algorithm, *Composite Structures* 66 (4) (2004) 627-637.

[21] K.J. Bathe, Finite Element Procedures , Prentice-Hall, 1996

Paper Ref: S1145_P0506

3rd International Conference on Integrity, Reliability and Failure, Porto/Portugal, 20-24 July 2009

Dynamic Study of a composite plate with delamination

Israr Ullah, Jyoti K. Sinha

School of Mechanical, Aerospace and Civil Engineering,

The University of Manchester

PO Box 88, Manchester M60 1QD, UK

Email: Israr.Ullah@postgrad.manchester.ac.uk , Jyoti.Sinha@manchester.ac.uk

ABSTRACT

The paper is on the dynamic behaviour of a delaminated composite plate based on the numerically simulated experiment. The possibility of delamination detection using the non-linear interaction feature in the delaminated region has been explored when excited the plate through a shaker.

INTRODUCTION

Composite materials are in use in several applications, for example, aircraft structural components, because of their light weight and high strength. However the delamination which is one of the serious defects often develops and propagates due to vibration

during the service of the structure. The presence of this defect warrants the design life of the structure and the safety. Hence the presence of such defect has to be detected in time to plan the remedial action well in advance.

Several research studies have been carried for the composite structures with delamination. They are related to the modelling aspects of the composite structures with delamination **(**Kudela and Ostachowicz, 2009, Aniello *et al.*, 2008, Alnefaie, 2009, Della, 2007) and few on the vibration based detection of the delamination by both experiments and analysis (Park *et al*., 2007, Takeda *et al*., 2005, Akira, 2002, Ying *et al*., 2003, Qiao *et al*. 2008). Few studies suggesting the detection by change in natural frequencies (Wei *et al*., 2004, Ackers *et al*., 2008, Diaz, 1999, Qiao *et al*., 2007) and few have used the effect of local modes in their experiments to identify the delamination either by mapping the mode shape across the surface of the composite structure (Roseiro *et al*., 2003, Takeda *et al*., 2005, Ying, 2003) or by advance signal processing using wavelet analysis (Zhonqing and Lin, 2004, Sohn *et al*., 2004). Often the use of such technique requires the distributed or embedded sensors at least over the surface of the composite structure or the expensive experiments (Akhter *et al*., 2008, Amr and El-Dakhakhni, 2009) using the laser vibrometer and dielectrometry sensors which restricts the practical used in many cases. Now the effort is develop a method that can detect the presence of the delamination using less number of sensors. In the present approach, the structural response due to the non-linear interaction between the layers in the delamination region, when the structure is excited externally, has been utilised. It has been believed that such non-linear interaction response will travel all along the surface and can be measured at any location, hence it is expected to remove the use of the distributed sensors or the time consuming scanning of the surface with the laser

vibrometer. The proposed concept has further been demonstrated on a simple cantilever beam with delamination (Israr and Sinha, 2008). It has been observed that the delaminated beam shows number of harmonics in their acceleration responses when excited at higher modes (Israr and Sinha, 2008). Now the concept has further been extended here on a carbon fibre plate with delamination. The acceleration responses were estimated at 3 randomly selected measurement locations when excited at number of modes from 1 to mode 32. The observations have been summarised here which shows the possibility of the delamination detection in much economical way. The initial observation made on a simple experiment has also been discussed here.

FINITE ELEMENT (FE) MODELLING

A carbon fibre multi-lamina layers composite plate of 280 mm square plate and 2 mm thickness has been chosen to understand the delamination effects in the simulated study. The composite plate ply orientations are $[0^0/90^0/0^0/90^0/90^0/0^0/90^0/0^0]$ and the material properties for the lamina are; Density, ρ =1600 kg/m^3, Elastic constants, E_1=1770 GPa, E_2=14.92 GPa, Poisson ratio, μ_{12}=0.21, and Shear modulus, $G_{12} = G_{13} = 5.7$ GPa, $G_{23} = 5.63$ GPa.

The delamination has been introduced between the 3rd layer from top and 5th layer from bottom and the location is shown in Figure 1(a). The plate has been modelled using 4 node shell (S4R) shell elements using the Finite element (FE) code ABAQUS. The FE model is shown in Figure 1(b). Total of 49 elements of size 40 mm x 40 mm have been used. A small delamination area has been introduced in the plate, such that the pair of

nodes 37 shown in figure 1(b) and 65 not shown is detached and their displacements on the upper and lower surfaces within the delamination region are not connected to each other. The boundary condition has been assumed free for all the four edges.

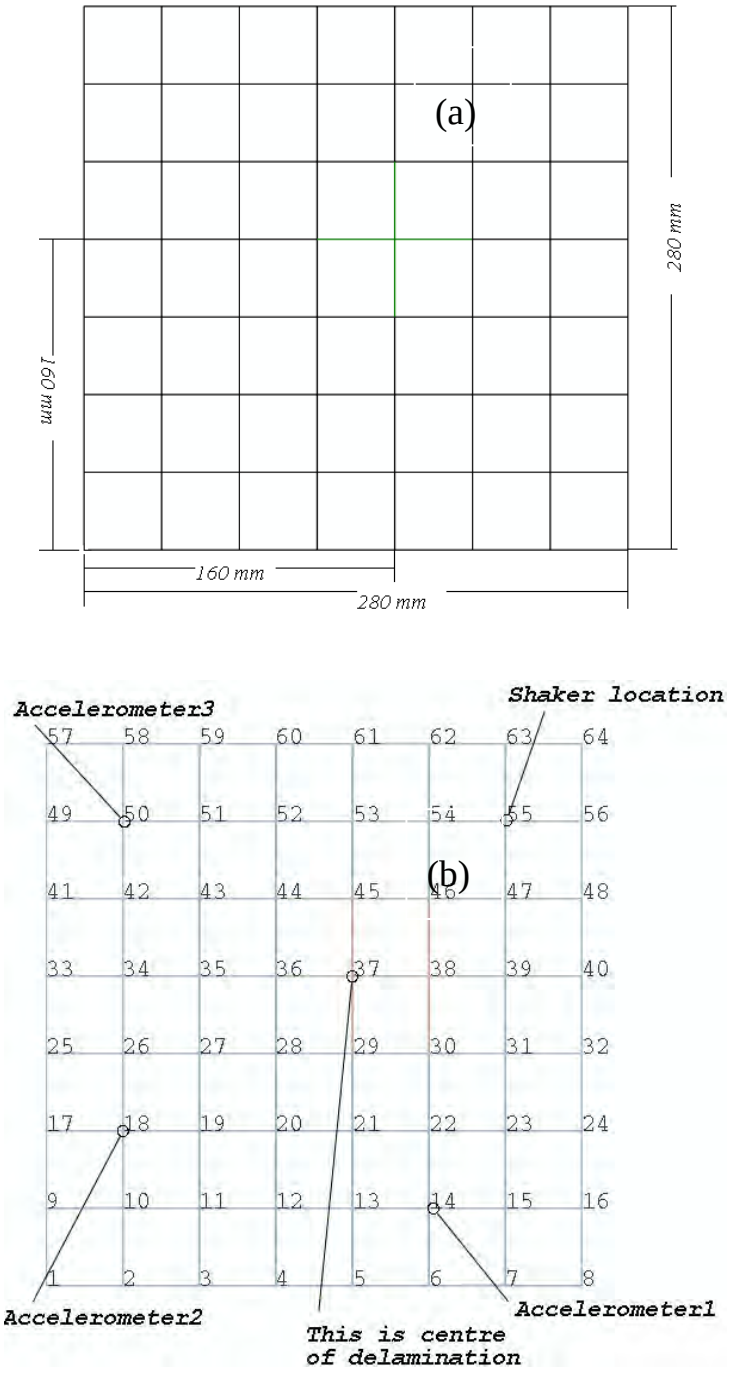

Fig. 1(a) Composite plate with size and location of delamination, (b) FE model showing delamination node, shaker location, and measurement locations used in the simulated study.

The modal analysis has been carried for this FE model to estimate the natural frequencies and the mode shapes. Few typical mode shapes and their natural frequencies are shown in Figure 2. It can be seen from Figure 2 that the modes shown do not show any visible separation between the delamination nodes 37 and 65. The deflection of the nodes 37 and 65 in the mode shapes along the thickness direction (hereafter referred to as z-direction) up to mode 30 as well as the deference between the two in the z-direction is also shown in Figure 3. The difference in the deflection between these nodes has been observed after mode 10 and becomes significant after mode 18.

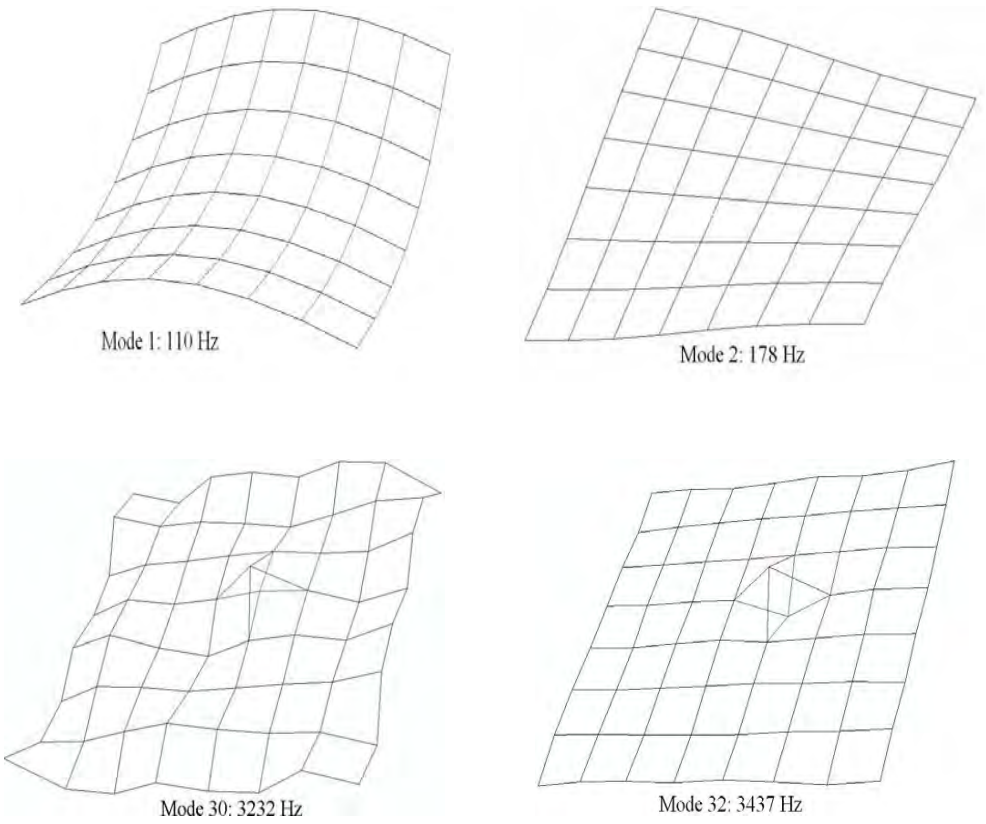

Fig. 2 few typical mode shape plots

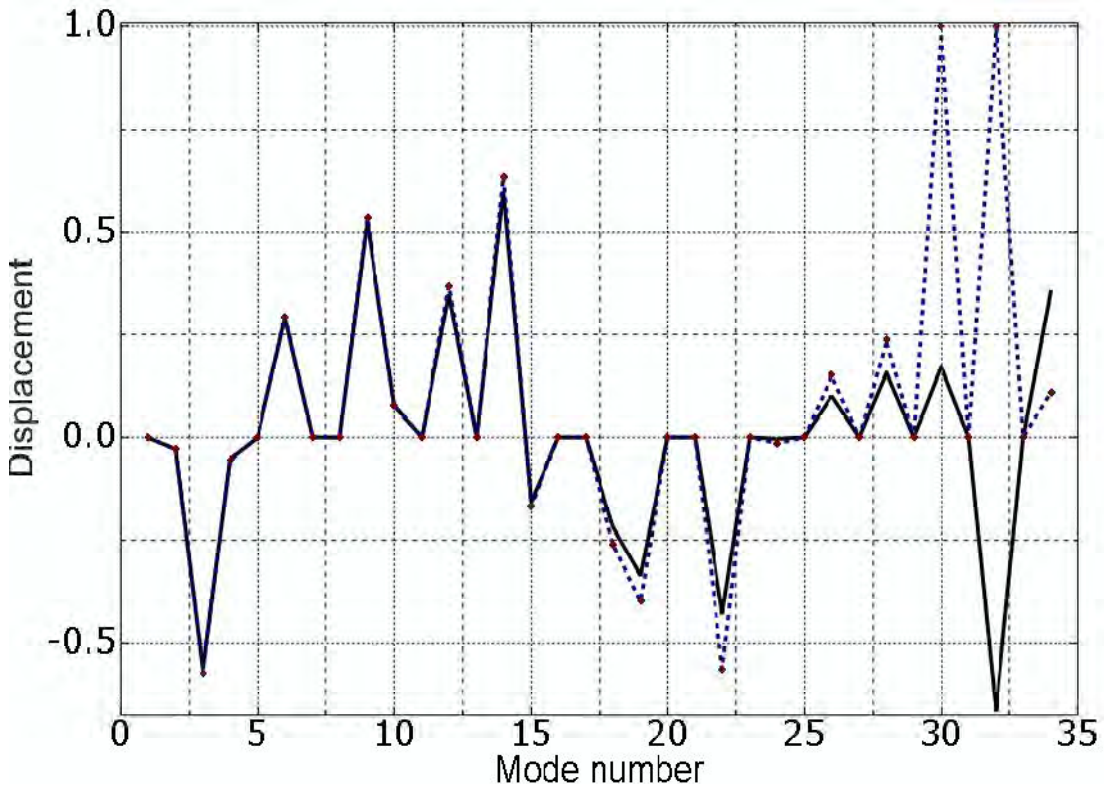

Fig. 3 Mode shape for the nodes 37 and 65 along the thickness direction with the mode number

RESPONSE ESTIMATION

The composite structure with delamination expected to show non-linear interaction in the delamination region when excited externally. Such responses may get amplified when excited at the natural frequencies. The effect is expected to be much more prominent for the mode 13 and above as the mode shapes for the mode 13 and above show significant separation in the delamination region as seen from Figure 3. Hence the acceleration responses have been computed at the randomly assumed measurement locations when the linear chirp-sine excitation were applied for the all the modes up to 18 modes. The assumed measurement locations and the shaker location for the simulated study are shown in Figure 1(b). The damping was assumed to be 0.75% for

all the modes. The linear chirp-sine excitation was given in the frequency band of $f_n \pm 10$ Hz with the chirp rate of 3.052 Hz/s for all the modes, where f_n is the *n*th natural frequency. The time step for the response computation was kept 1 μs .

It was difficult to simulate the non-linear interaction between the nodes 37 and 65 in the delamination region in the ABAQUS FE code, hence the mode-superposition method was slightly modified to allow the non-linear interaction and then responses were estimated separately which is explained here.

In the Mode-superposition method, the dynamic equation in the modal domain in Equation (1) has been used to estimate the modal responses.

$$\ddot{\mathbf{p}}_r(t) + 2\zeta_r \omega_r \dot{\mathbf{p}}_r(t) + \omega_r^2 \mathbf{p}_r(t) = \boldsymbol{\varphi}_r^T \mathbf{F}(t) \qquad (1)$$

Where ω_r is *r*th natural frequency (rad. /s), ζ_r is damping ratio at *r*th mode, $\boldsymbol{\varphi}_r$ is the vectors of the *r*th mode shape, $\mathbf{P}_r(t)$ is the modal responses at *r*th mode and $\mathbf{F}(t)$ is applied force. The responses (displacement, velocity and acceleration) have then been estimated as $\mathbf{x}(t) = \boldsymbol{\varphi}\mathbf{p}(t)$, $\mathbf{v}(t) = \boldsymbol{\varphi}\dot{\mathbf{p}}(t)$ and $\mathbf{a}(t) = \boldsymbol{\varphi}\ddot{\mathbf{p}}(t)$ respectively, where $\boldsymbol{\varphi}$ is the mode shape matrix and the modal response vectors $\mathbf{p}(t) = \left[\mathbf{p}_1(t) \quad \mathbf{p}_2(t) \quad \mathbf{p}_3(t) \quad \cdots \quad \mathbf{p}_n(t)\right]^T$. However for the present study the modal parameters - $\mathbf{f}_n$ and $\boldsymbol{\varphi}$ would not be constant with time due to the non-linear interaction. Hence the 2 sets of modal parameters have been computed, one set ($\mathbf{f}_{n\_d}$ and $\boldsymbol{\varphi}_d$) for the delamination case and another set ($\mathbf{f}_{n\_nd}$ and $\boldsymbol{\varphi}_{nd}$) for the perfectly laminated (no delamination) case. The set (1) data were used in Equation (1) and the responses estimated when the nodal displacement, $x_{37}(t) < x_{65}(t)$ in the direction of

thickness of the plate and the set (2) when $x_{37}(t) \geq x_{65}(t)$. It is because the later condition is more like the plate without delamination. Hence a computational programme has been developed based on the proposed scheme in the Matlab software code to estimate the responses using the 2 sets of the modal data from the FE model (with and without delamination) developed in the ABAQUS code. The rigid connection between the nodes 37 and 65 at all the degree of freedoms (DOFs) was assumed in the FE model with the delamination to realise the composite plate without delamination for the 2nd sets of modal data which also ensure the same number of DOFs in both the models. The Newmark-β method was used for solving Equation (1). The computed measured acceleration responses and the displacement responses at the nodes 37 and 65 were then down-sampled by 10 and low-pass filtered at 49 kHz to remove the high frequencies components likely to occur due to the time step used in the computation. The displacement responses for the nodes 37 and 65 in the thickness direction in Figure 4 show the non-linear interaction in the delamination region for the modes 4, 10, 17, and 18. The modes 17 and 18 shows significant non-linear interaction compared to the modes 1 and 10 supports the observation made in Figure 3 where the modes 17 and 18 have significant separation between the nodes 37 and 65.

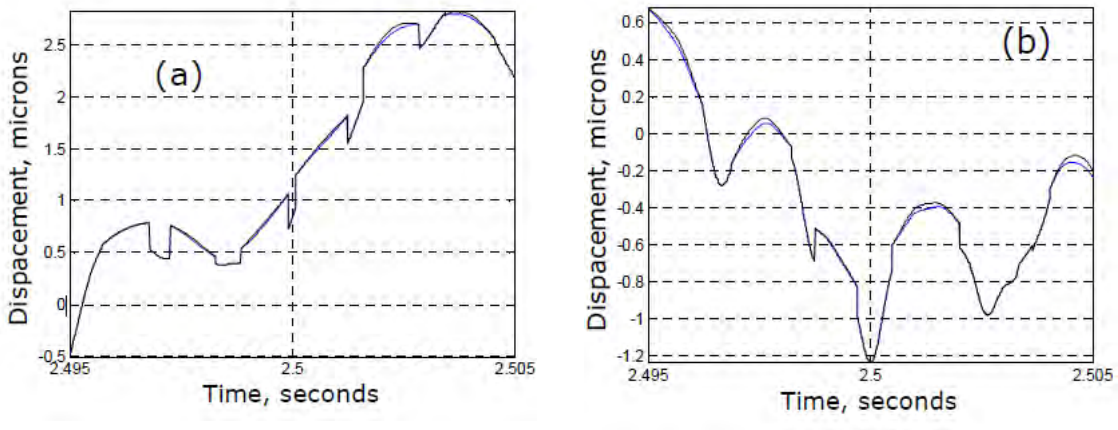

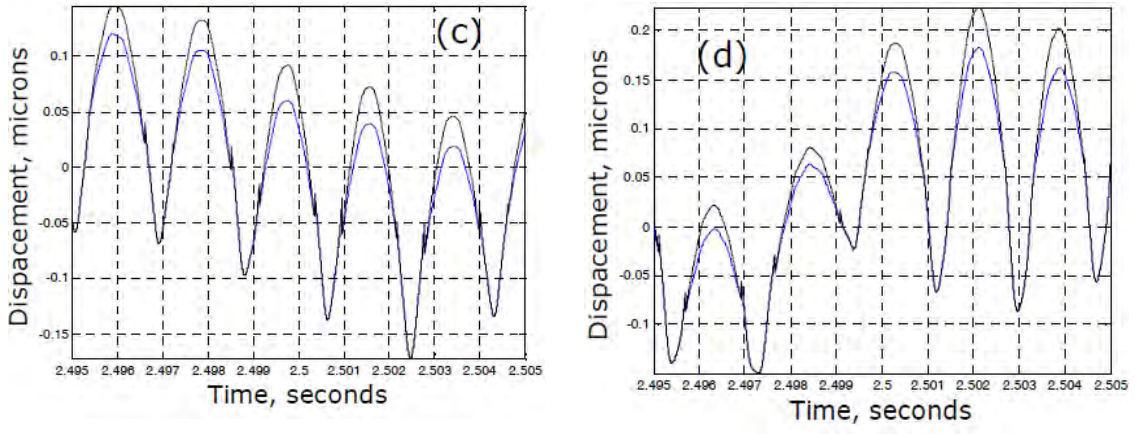

Fig. 4 The displacement responses for Nodes 37(dotted line) and 65 (solid line) showing non-linear interaction (a) Mode 1:110 Hz (b) Mode 15: 1518 Hz (c) Mode 30: 3232 Hz and (d) Mode 32: 3438 Hz

DATA ANALYSIS AND RESULTS

The data have been down sampled by 10 so that the sampling frequency now becomes equal to 100ksamples/s. The short time Fourier Transformation (STFT) has been carried out for all the data keeping the frequency resolution, Δf = 3.052 Hz and overlap of 40%. No window was used for this analysis. The averaged amplitude spectra were also plotted for all the simulated measured data. Since the excitation frequency band for each mode was the linear chirp-sine excitation, hence ordered spectra were estimated for averaging and the order axis was converted to the frequency axis by multiplying the order 1 by the excited natural frequency. Typical amplitude spectra have been shown in Figures 5-13 and the summary of the observations in Table 1. The responses were also estimated for the simulated example without delamination. Few typical acceleration spectra for the composite plate without delamination are shown in Figure 14 which shows the prominent at the excited mode only.

Table 1 Summary of the observations

Parameter used: For response calculation: Linear Chirp rate 4Hz/s, Time step, $\Delta t = 1\ \mu s$, Total time = 5sFor FFT spectrum, STFT: Sampling frequency, f_s =10 k-samples/s, Frequency resolution, Δf =3.052Hz, Overlap= 40%, No window			
Excitation	Natural Frequency (Hz)	Observation made at measured locations	Figures
1, 2, 8, 12,13	110, 178, 682, 1271,1271	Excited mode and its higher harmonics	Figures 5
3-5, 9,10, 20	244, 389, 389, 804, 906, 2377	Predominant at the excited mode only because vibration at these modes are along the plane and not along the thickness direction	Figure 6
6-7	589, 589	Response at the excited mode with multi-side bands	Figure 7
11	1179	Response at the excited mode with multi-side bands showing modulation with 110Hz and their harmonics. Peaks at Mode 6 (589Hz) and Mode 8 (682Hz)	Figure 8
14, 15,16, 19 & 21	1418, 1518, 1518, 2208, 2399	Response at the excited mode and Mode 9 (804 Hz)	Figure 9
17-18	1936, 1986	Response at the excited mode with multi-side bands showing modulation with the frequency 645Hz plus response peak at 645Hz and its harmonics	Figure 10
22-25	2551, 2551, 2787, 2787	Response at the excited mode with side bands showing	Figure 11
26-27	2874, 2874	Response at the excited mode with side band showing modulation with the frequency 635Hz plus response peak at 635Hz	Figure 12
28-32	3007, 3113, 3232,3245, 3438	Response at the excited mode with multi-side bands showing modulation with the frequency approximately	Figure 13

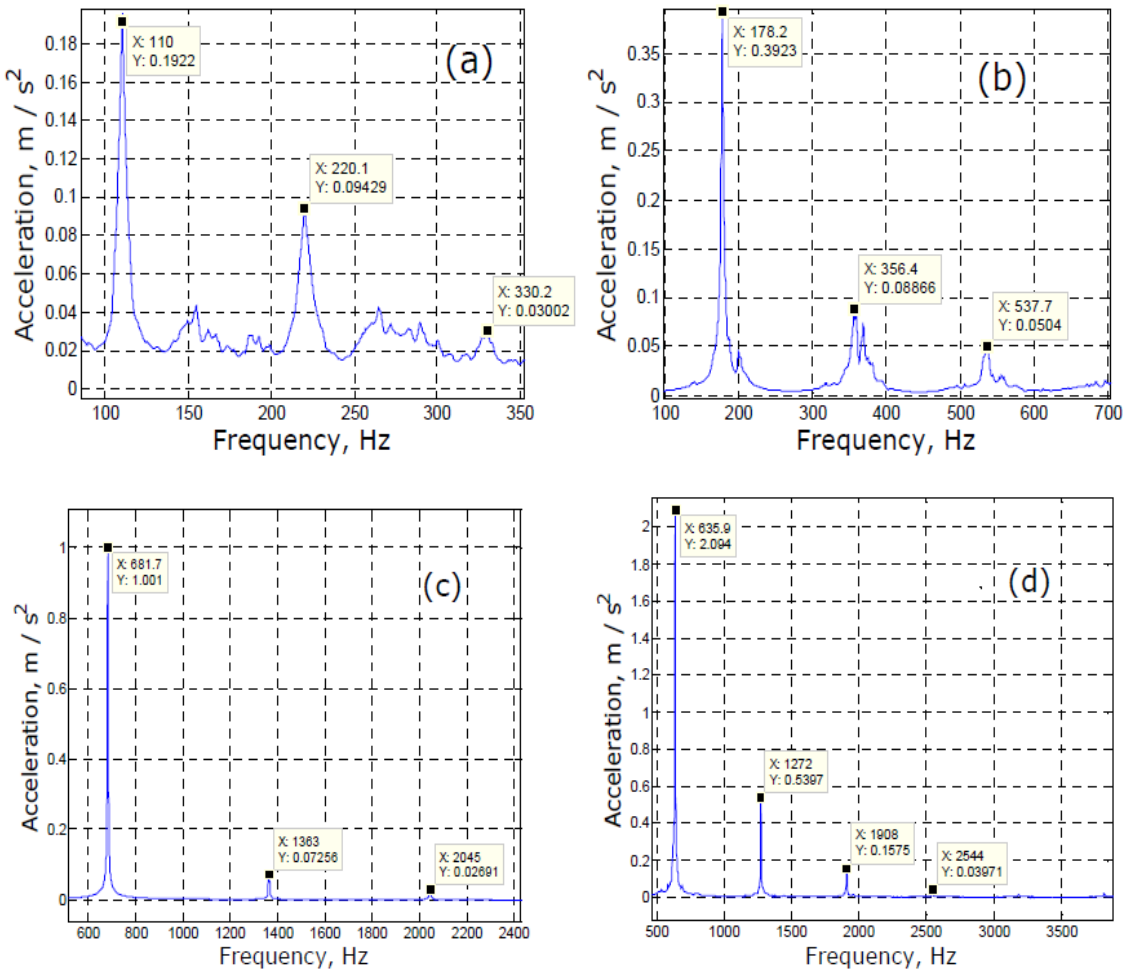

Fig. 5 Amplitude Acceleration spectra at Measurement Location 2 when excited at (a) Mode 1: 110Hz, (b) Mode 2: 178Hz, (c) Mode 8: 682Hz, (d) Mode 12: 1272Hz

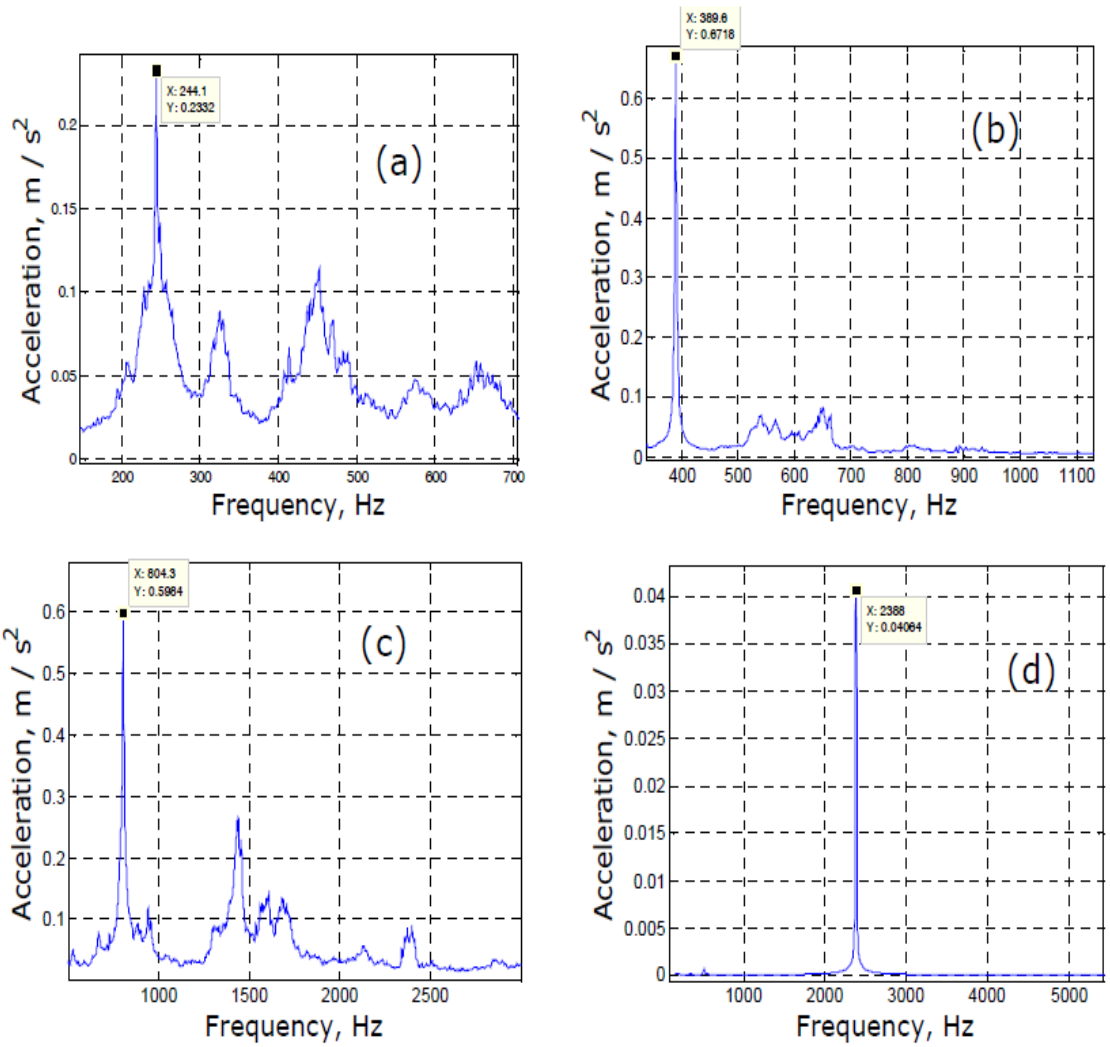

Fig. 6 Amplitude spectrum at Measurement Location 2 when excited at (a) Mode 3: 244 Hz, (b) Mode 4: 389 Hz, (c) Mode 9: 804 Hz, (d) Mode 20: 2377 Hz

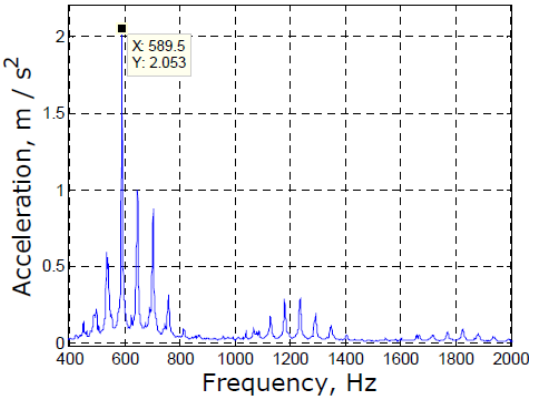

Fig. 7 Amplitude spectrum at Measurement Location 2 when excited at Mode 6: 589Hz

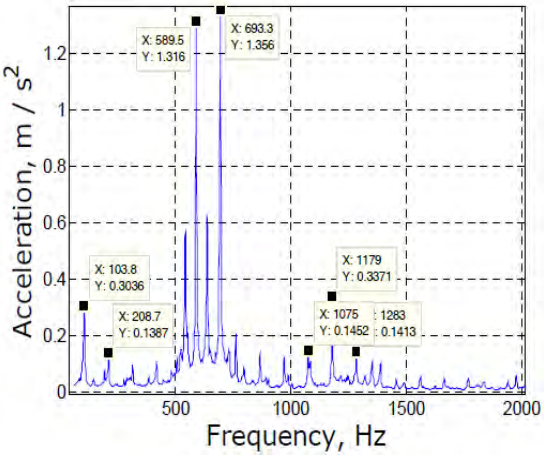

Fig. 8 Amplitude spectrum at Measurement Location 2 when excited at Mode 11: 1179Hz

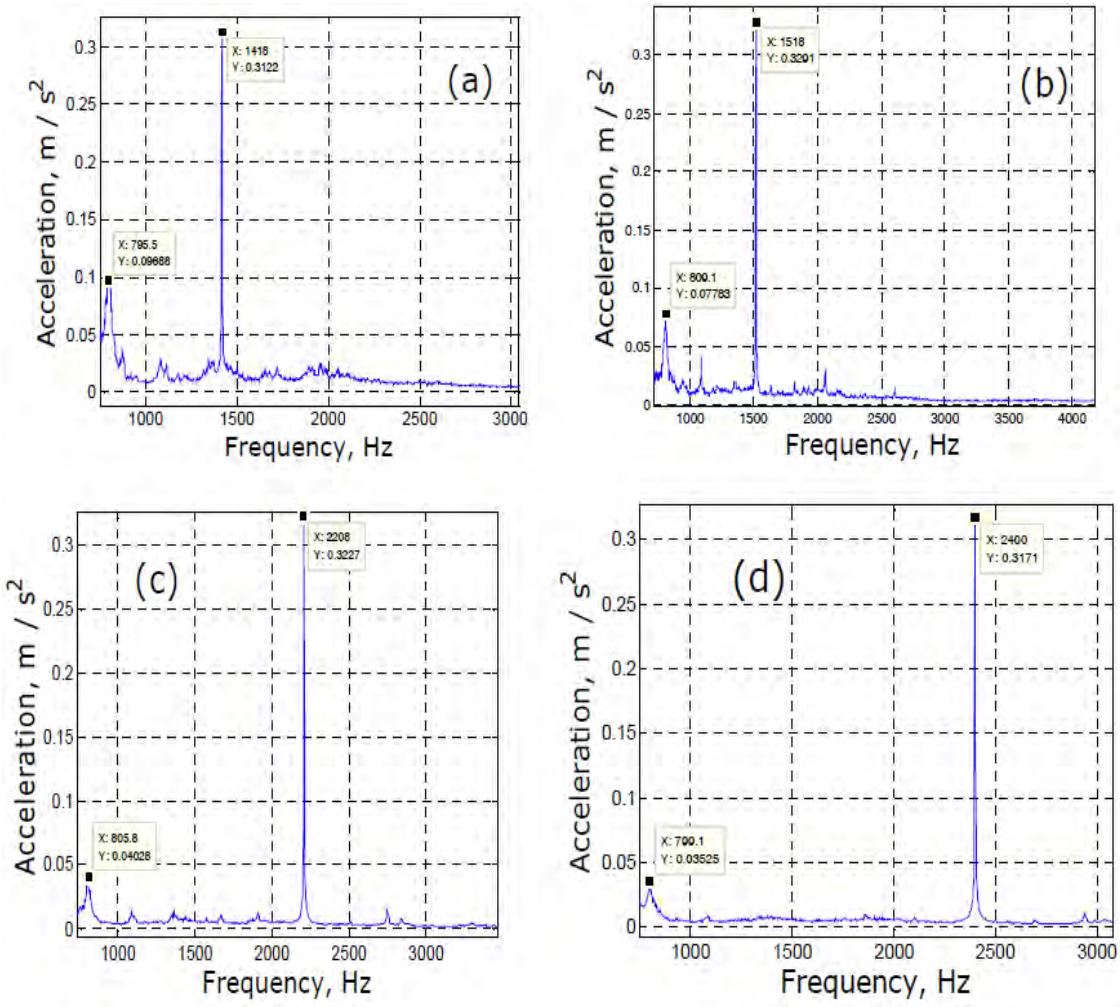

Fig. 9 Amplitude spectrums at Measurement Location 2 when excited at (a) Mode 14: 1418 Hz, (b) Mode 15: 1518 Hz, (c) Mode 19: 2208 Hz, (d) Mode 21: 2399 Hz

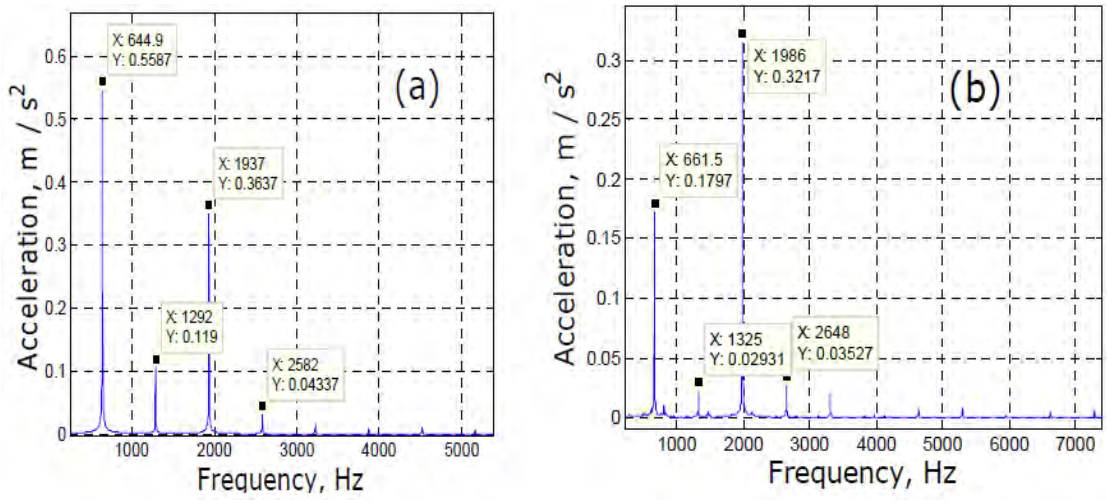

Fig. 10 Amplitude spectrum at Measurement Location 2 when excited at (a) Mode 17: 1937Hz and (b) Mode 18: 1986 Hz

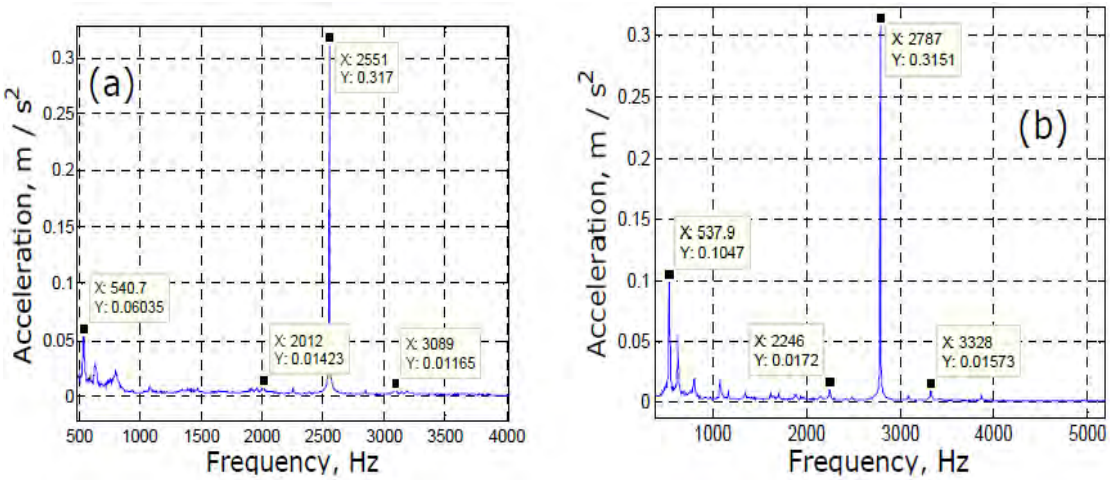

Fig. 11 Amplitude spectrum at Measurement Location 2 when excited at (a) Mode 22: 2551Hz and (b) Mode 25: 2787 Hz

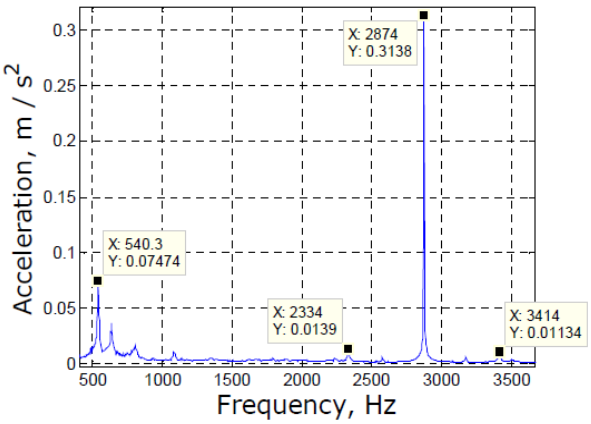

Fig. 12 Amplitude spectrum at Measurement Location 2 when excited at Mode 27: 2874Hz

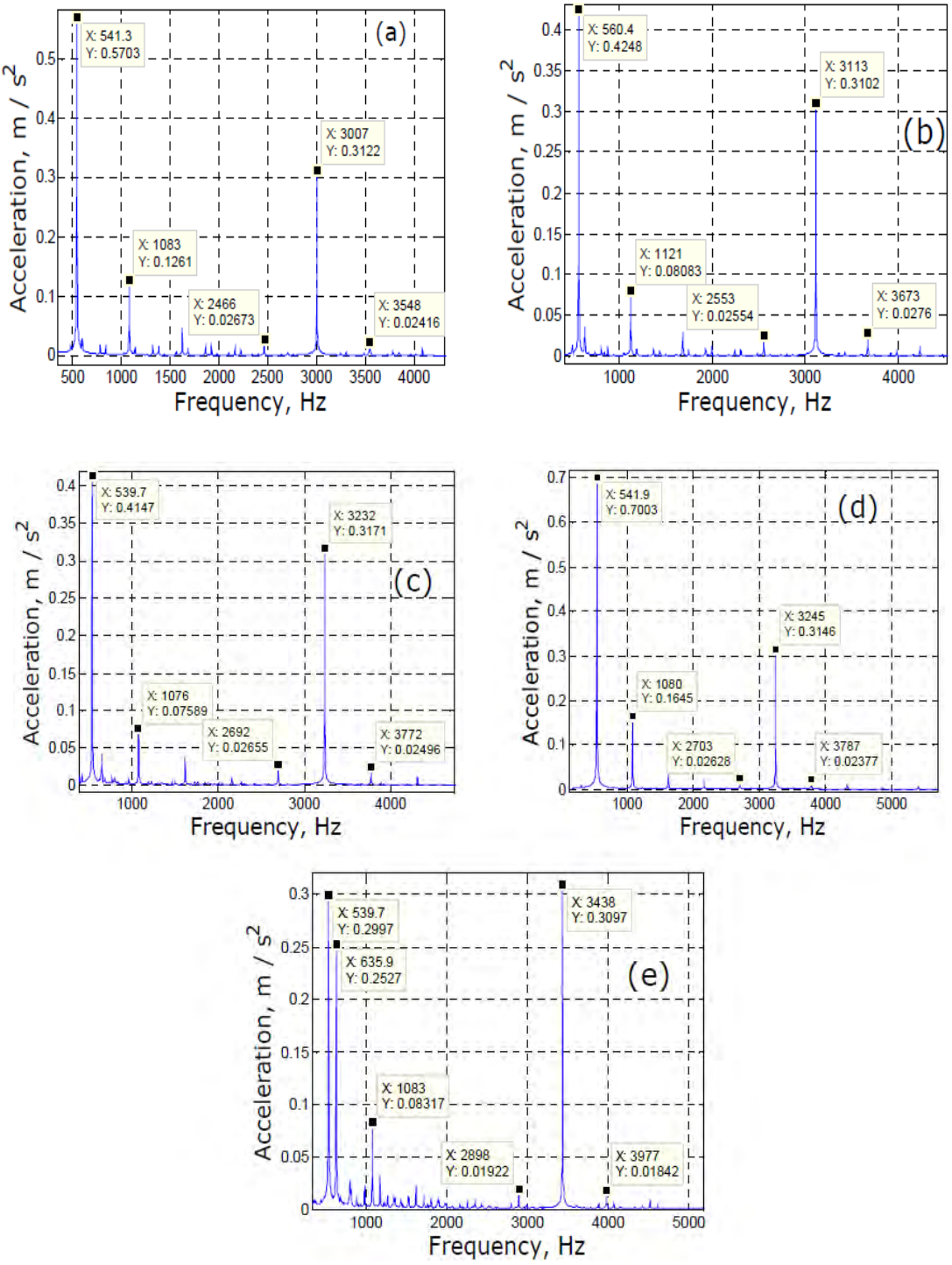

Fig. 13 Amplitude spectrum at Measurement Location 2 when excited at (a) Mode 28: 3007 Hz, (b) Mode 29:3113 Hz, (c) Mode 30: 3232 Hz, (d) Mode 31: 3245 Hz, (e) Mode 32: 3438 Hz

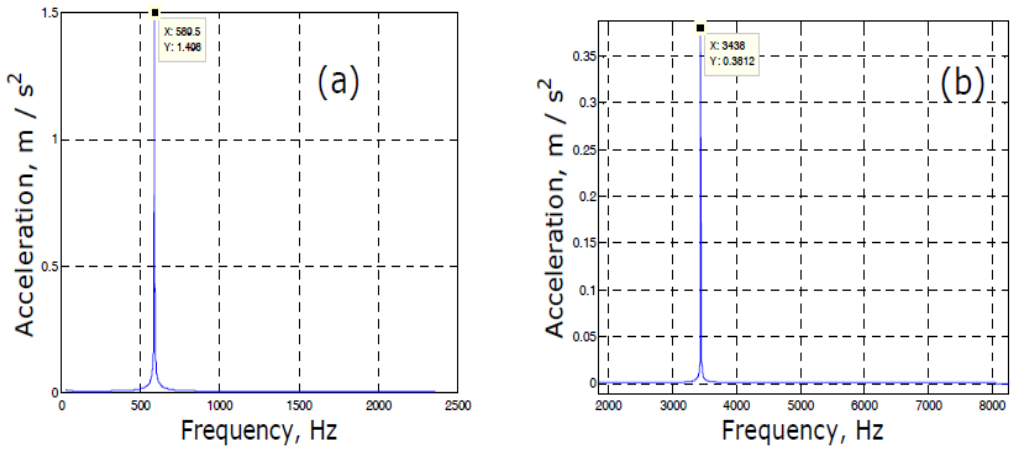

Fig. 14 Amplitude spectrum at Measurement Location 2 when excited at (a) Mode 6: 590 Hz (b) Mode 32: 3437 Hz

EXPERIMENTAL SETUP

The experimental validation of the numerical simulation has been done. Two Aluminium plates of sizes 190mm x 190mm x 1.15mm and 190mm x 190mm x 3.15mm glued together leaving a square pocket of 50 mm x 50 mm in the centre have been prepared to simulate the delamination condition. The plate is fixed on one edge as shown in Figure 15(a). Figure 15(b) shows the schematic of the experimental setup. A piezo-electric shaker (Model PS-X03, M/s ISI-SYS) has been used to excite the plate and the acceleration responses were measured using the accelerometer (Model 352C22, M/s PCB). The data were analysed online using the 2 channel FFT analyser and also recorded on the Laptop using 16-bit 8-channel data acquisition Analogy to Digital card. The data were recorded at a sampling frequency of 100ksamples/s. In the initial experiments, the impulse-response modal test (Ewins, 2000) has been carried out using the instrumented hammer (Model 086C03, M/s PCB) to find out the natural frequencies. A typical measured response both in time and frequency domain is shown in Figure 16. Then the sine excitation was given at the few identified modes. Few typical acceleration amplitude spectra are shown in Figure 17. It has been observed the higher harmonics of

the excited modes seen in the acceleration amplitude spectra even at the lower natural frequency at 75Hz confirming the nonlinear interaction in the delaminated region.

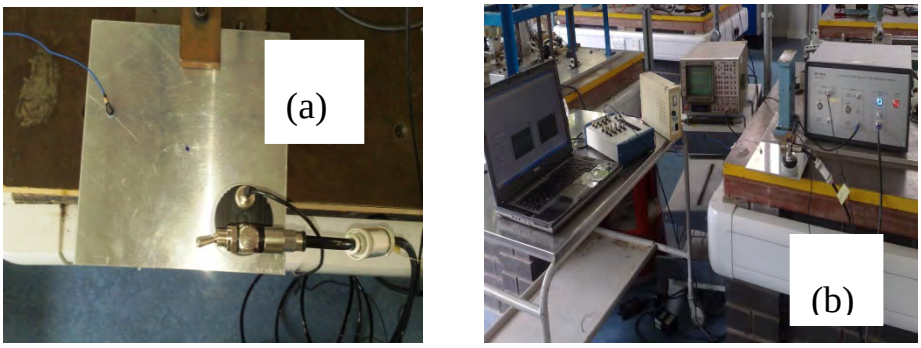

Fig. 15 Schematic of Experiments, (a) Plate with shaker and accelerometer, (b) Experimental setup

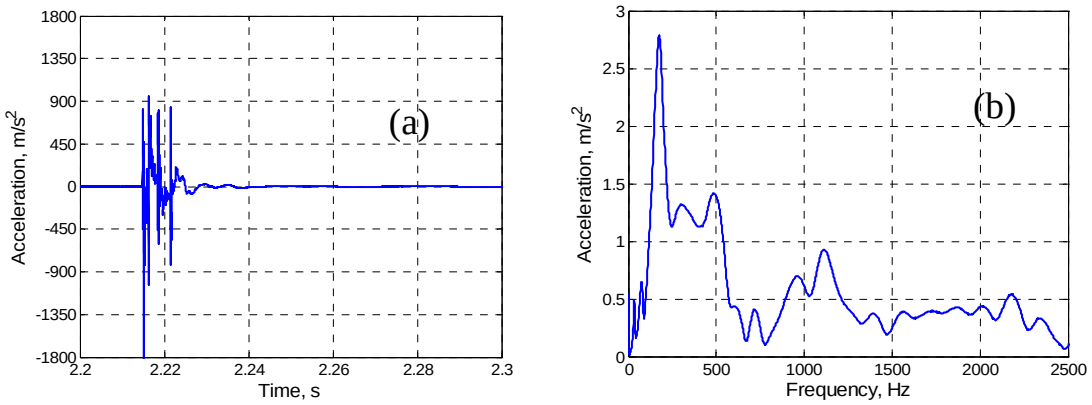

Fig. 16 A typical measured Acceleration response to the impulsive excitation, (a) time wave form, (b) Amplitude spectrum

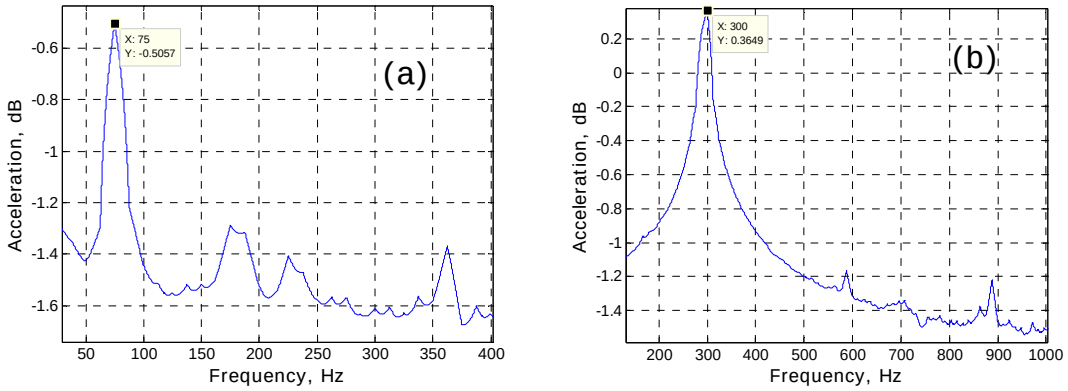

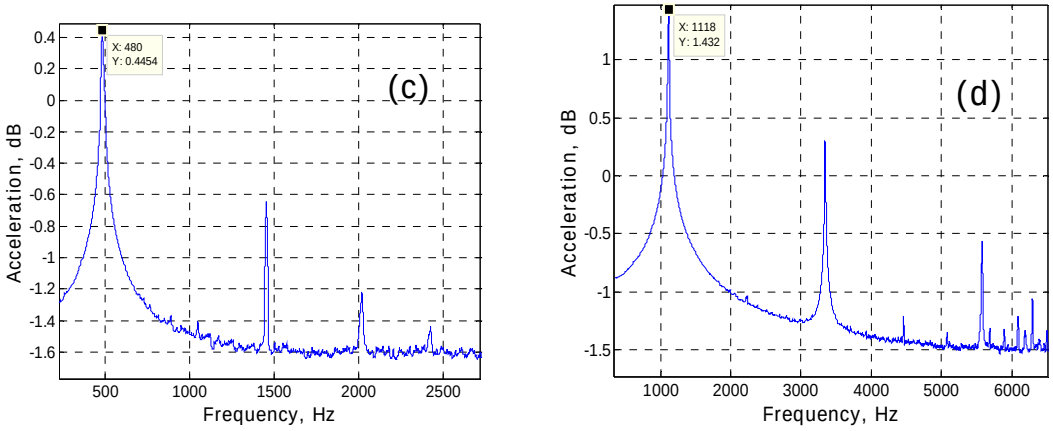

Fig. 17 Typical measured acceleration amplitude spectra when excited at modes (a) 75Hz, (b) 300 Hz, (c) 480 Hz, (d) 1118 Hz

CONCLUSIONS

The dynamics of the composite plate with delamination has been discussed. An FE model of a carbon fibre composite plate with a delamination has been developed and then the responses were estimated when excited at the number of modes using the mode-superposition method. The mode-superposition method was slightly modified to realise the nonlinear interaction between the delaminated layers. The results show the presence of harmonics and the frequency modulation appearing as side bands at the excited modes in their acceleration responses for most of the modes. Simple tests on a composite plate made of aluminium with delamination have also confirms the presence of higher harmonics when excited at number of modes. But the presence of the side bands has not been observed in the present experiments. It needs further tests to understand the nonlinear phenomena. However the presence of higher harmonics both in the simulation and then in the experiment definitely highlight the potential feature for the detection of the delamination in the composite structures in much simplified way.

REFERENCES

Ackers, S., Adams D. Crack Detection in an Embedded Spindle using Broadband Modal Excitation. Experimental Mechanics, 48; 4; 2008 p. 509-520.

Akhter N., Jung H.C., Chang H., Kim K. Location of delamination in laminated composite plates by pulsed laser holography. Optics and Lasers in Engineering, 47; 5; 2009 p.584-588.

Akira T., Yuuki T., Yoshinobu S. Delamination monitoring of graphite/epoxy laminated composite plate of electric resistance change method', Composites Science and Technology, 62; 9; 2002 p.1151-1160.

Alnefaie K. Finite element modelling of composite plates with internal delamination. Composite Structures, 90; 1; 2009, p.21-27.

Amr A. N., El-Dakhakhni W. W. Non-destructive evaluation of laminated composite plates using dielectrometry sensors. Smart Materials and Structures, 18**;** 5; 2009, 055014(8pp)

Aniello R. Modelling Damage Propagation in Composite Plates with Embedded Delamination under Compressive Load. Journal of Composite Materials, 42; 13; 2008 p.1309-1335.

Della C. N., Shu D. Vibration of beams with two overlapping delaminations in pre-buckled states, Composites Part B: Engineering 38; 2; 2007 p.09-118.

Diaz Valdes S. H., Soutis C. Delamination detection in composite laminates from variations of their modal characteristics, Journal of Sound and Vibration, 228; 18; 1999 0p.1-9

Ewins D. J. Modal Testing – Theory, Practice and Application. Research Studies Press, U.K., 2nd Edition; 2000

Park H.W., Sohn H., Law K.H., Farrar C.R. Time reversal active sensing for health monitoring of a composite plate. Journal of Sound and Vibration, 302;1-2; 2007, p. 50-66.

Israr U., Sinha J. Dynamic behaviour of a de-laminated composite beam. Proc. of 5th International Conference on Condition Monitoring and Machinery Failure Prevention Technologies (CM 2008 and MFPT 2008), the Edinburgh Conference Centre, Herriot-Watt University, Edinburgh;15-18 July 2008 p 1-10.

Kudela P., Ostachowicz W. A Multilayer Delaminated Composite Beam and Plate Elements: Reflections of Lamb Waves at Delamination. Mechanics of Advanced Materials and Structures, 16; 3; 2009, p.174-187.

Lin Y. H. Optimal Design of Delaminated Composite Plates for Maximum Buckling Load. Global Design to Gain a Competitive Edge; 2008, p. 489-498.

Qiao P., Lu K., Lestari W., Wang J. Curvature mode shape-based damage detection in composite laminated plates. Composite Structures, 80; 3; 2007 p.409-428.

Qiao. P.Z., Lu K., Lestari W. A combined static/dynamic technique for damage detection of laminated composite plates. Experimental Mechanics, 48; 2008 p. 17–35.

Roseiro L., Ramos U., Leal R. Damage detection of laminated composite plates using distributed piezoelectric sensors and neural networks. AMAS Workshop on Smart Materials and Structures SMART'03 Jadwisin, September 2-5; 2003 p. 281–290.

Sohn H., G. Park, Wait J.R., N.P. Limback, Farrar C.R. Wavelet-based active sensing for delamination detection in composite structures. Smart Mater. Struct., 13; 2004 p. 153–160.

Takeda S., Okabe Y., Takeda N. Delamination monitoring of laminated composites subjected to low-velocity impact using small-diameter FBG sensors. Composites Part A: Elsevier, 7**;** 2005 p**.** 903–908.

Wei Z., Yam L.H., Cheng L. Detection of internal delamination in multi-layer composites using wavelet packets combined with modal parameter analysis. Composite Structures, 64; 3-4; 2004 p.377-387.

Ying X., Christopher K.Y. L., Yang Z., Tong P., Stephen K.L. A new fibre-optic based method for delamination detection in composites. Structural Health Monitoring, 2; 3; 2003 p. 205-223.

Zhongqing S., Lin Y. Lamb wave-based quantitative identification of delamination in CF/EP composite structures using artificial neural algorithm. Composite Structures, 66; 4; 2004 p.627-637.

(This page is intentionally left blank)